AD_____

Award Number: W81XWH-07-1-0448

TITLE: Structural and Mechanistic Analyses of TSC1/2 and Rheb 1/2 - Mediated Regulation of the mTOR Pathway

PRINCIPAL INVESTIGATOR: Dr. David Sabatini

CONTRACTING ORGANIZATION: Whitehead Institute for Bio-Medical Research
Cambridge, MA 02142

REPORT DATE: July 2011

TYPE OF REPORT: Final

PREPARED FOR: U.S. Army Medical Research and Materiel Command
Fort Detrick, Maryland 21702-5012

REPORT DOCUMENTATION PAGE

Form Approved
OMB No. 0704-0188

1. REPORT DATE *(DD-MM-YYYY)*	**2. REPORT TYPE**	**3. DATES COVERED** *(From - To)*
01-07-2011	Final	1 JUL 2007 - 30 JUN 2011

4. TITLE AND SUBTITLE

Structural and Mechanistic Analyses of TSC1/2 and Rheb 1/2 - Mediated Regulation of the mTOR Pathway

5a. CONTRACT NUMBER

5b. GRANT NUMBER
W81XWH-07-1-0448

5c. PROGRAM ELEMENT NUMBER

6. AUTHOR(S)

Dr. David Sabatini

E-Mail: sabatini@wi.mit.edu

5d. PROJECT NUMBER

5e. TASK NUMBER

5f. WORK UNIT NUMBER

7. PERFORMING ORGANIZATION NAME(S) AND ADDRESS(ES)

Whitehead Institute for Bio-Medical Research
Cambridge, MA 02142

8. PERFORMING ORGANIZATION REPORT NUMBER

9. SPONSORING / MONITORING AGENCY NAME(S) AND ADDRESS(ES)

U.S. Army Medical Research and Materiel Command
Fort Detrick, Maryland 21702-5012

10. SPONSOR/MONITOR'S ACRONYM(S)

11. SPONSOR/MONITOR'S REPORT NUMBER(S)

12. DISTRIBUTION / AVAILABILITY STATEMENT

Approved for Public Release; Distribution Unlimited

13. SUPPLEMENTARY NOTES

14. ABSTRACT

Abstract on next page.

15. SUBJECT TERMS

mTOR, mTORC1, raptor, TSC, Rheb, Rag, Ragulator, amino acid, rapamycin, cryo-EM, phosphoproteomics, kinase, lysosome, nutrient

16. SECURITY CLASSIFICATION OF:			**17. LIMITATION OF ABSTRACT**	**18. NUMBER OF PAGES**	**19a. NAME OF RESPONSIBLE PERSON**
a. REPORT	**b. ABSTRACT**	**c. THIS PAGE**			USAMRMC
U	U	U	UU	87	**19b. TELEPHONE NUMBER** *(include area code)*

14. ABSTRACT

The multicomponent kinase mTORC1 (mammalian target of rapamycin complex 1) regulates cell growth by coordinating upstream signals from growth factors, intracellular energy levels, and amino acid availability and is deregulated in diseases such as cancer and diabetes. The TSC1 and TSC2 proteins form a tumor suppressor complex that transmits growth factor and energy signals to mTORC1 by regulating the GTP-loading state of Rheb, a Ras-related GTP-binding protein. Additionally, the Rag GTPases interact with mTORC1 and are proposed to activate it in response to amino acids by promoting mTORC1 translocation to a membrane-bound compartment that contains the mTORC1 activator, Rheb. In our recent study of the amino acid sensitivity, we showed that amino acids induce the movement of mTORC1 to lysosomal membranes, where the Rag proteins reside. A complex encoded by the MAPKSP1, ROBLD3, and c11orf59 genes, which we term Ragulator, interacts with the Rag GTPases, recruits them to lysosomes, and is essential for mTORC1 activation. Constitutive targeting of mTORC1 to the lysosomal surface is sufficient to render the mTORC1 pathway amino acid insensitive and independent of Rag and Ragulator, but not Rheb, function. Thus, Rag-Ragulator-mediated translocation of mTORC1 to lysosomal membranes is the key event in amino acid signaling to mTORC1. In a separate study, we determined the three-dimensional structure of the fully assembled human mTORC1 by cryo-electron microscopy. Our analyses reveal that mTORC1 is an obligate dimer with an overall rhomboid shape and a central cavity. The dimeric interfaces are formed by interlocking interactions between the mTOR and raptor subunits. Extended incubation with FKBP12-rapamycin compromises the structural integrity of mTORC1 in a stepwise manner, leading us to propose a model in which rapamycin inhibits mTORC1-mediated phosphorylation of 4E-BP1 and S6K1 through different mechanisms.

Table of Contents

Page

Introduction……..…….…..…..4

Body……..……..4

Key Research Accomplishments…….……..6

Reportable Outcomes……7

Conclusion……9

Appendices……...……9

INTRODUCTION

The multi-protein kinase mTORC1 (mammalian Target of Rapamycin Complex 1) regulates cell growth by coordinating upstream signals from growth factors, intracellular energy levels, and amino acid availability, and is often implicated in many human cancers, including Tuberous Sclerosis Complex (TSC). TSC is an autosomal dominant disorder characterized by benign tumors in a variety of organs, and currently affects 1 in 6000 individuals in the United States. Mutations in two evolutionarily conserved tumor suppressor genes, TSC1 and TSC2, are responsible for the disease. The TSC1 and TSC2 proteins form a tumor suppressor complex, which acts as the convergence point of many upstream regulatory signals in the mTORC1 signaling network, with the notable exception of amino acid availability**.** TSC1/2 is a GTPase activating protein (GAP) for the small GTPase Rheb, which binds directly to mTORC1 and stimulates its activity when GTP-bound. In response to growth factor withdrawal or energy stress, activation of TSC1/2 leads to the inhibition of mTORC1 by suppressing Rheb-GTP levels. In contrast to growth factor signaling, the mechanism of regulation of mTORC1 activity in response to amino acids is poorly understood. Although Rheb is necessary for mTORC1 activation, high Rheb-GTP levels achieved by TSC2 loss or Rheb overexpression have different consequences on amino acid signaling to mTORC1. While TSC2-decificient cells still respond to amino acid stimulation, Rheb overexpression makes the pathway insensitive to amino acid starvation. Prior to our proposed study, the reason for this difference was largely unknown, but we recently identified additional components of mTORC1 that are critical for amino acid signaling. Given the importance of the mTOR pathway in TSC treatment, understanding how impairment of TSC1/2 function results in the activation of mTORC1 is critical. With the long-term goal of developing cancer therapeutics based on mTORC1 regulatory mechanisms, our biochemical and structural studies attempted to address this question and find efficient means of regulating the mTOR signaling network.

BODY

<u>Aim 1: Understand the role of Rheb-mediated phosphorylation of raptor in the regulation of mTORC1</u>

One of the major aims of this project is to understand the role of raptor in mTORC1 signaling. While analyzing the raptor phosphorylation, we found, by mass spectrometry, a new Raptor-interacting protein, Rag, which interacts with mTORC1 in an amino acid–sensitive manner and is necessary for the activation of the mTORC1 pathway by amino acids. The Rag proteins are a unique family of small GTPases with a canonical Ras-like GTPase domain at the N-termini and a unique Rag A conserved region at the C-termini. In mammals, there are four Rag genes, Rag A, Rag B, Rag C and Rag D. Rag A and Rag B are very similar with 98% amino acid identity in their overlapping sequences. Rag C and RagD are 81% similar, and they differ at their N and C termini. Rag A, B, C and D were shown to interact with each other in mammalian cells and in yeast. Gain and loss of function studies of Rag proteins pointed to their specific role in amino acid signaling to mTORC1 rather than growth factor signaling. When over-expressed, a GTP-bound RagB mutant can rescue mTORC1 inactivation induced by amino acid but not serum starvation. When the Rag proteins were knocked down by RNAi, mTORC1 became insensitive to amino acid stimulation. Although we do not fully understand how the Rag proteins activate mTORC1, a critical observation prompted us to hypothesize that they may regulate mTORC1 localization within the cells. We observed that amino acid stimulation induces an mTOR localization change. Supporting our hypothesis, when Rag proteins and raptor were knocked down, mTORC1 localization change in response to amino acid availability was prevented. Similarly, when a GTP bound RagB mutant was expressed in the cells, mTORC1 localization mimics amino acid induced state in the absence of amino acids (Appendix 1)

The activation of the mTORC1 pathway by amino acids correlates with the movement of mTORC1 from an undefined location to a compartment containing Rab7, a marker of both late endosomes and lysosomes. How the Rag proteins regulate mTORC1 is unknown, but, in cells expressing a RagB mutant that is constitutively bound to GTP (RagBGTP), the mTORC1 pathway is insensitive to amino acid starvation and mTORC1 resides in the Rab7-positive compartment even in the absence of amino acids. We previously proposed that amino acids

promote the translocation of mTORC1-in a Rag-dependent fashion-to the surface of an endomembrane compartment, where mTORC1 can find its well-known activator, Rheb. In the following study, we showed that amino acids induce the movement of mTORC1 to lysosomal membranes, where the Rag proteins reside. A complex encoded by the MAPKSP1, ROBLD3, and c11orf59 genes, which we term Ragulator, interacts with the Rag GTPases, recruits them to lysosomes, and is essential for mTORC1 activation. Constitutive targeting of mTORC1 to the lysosomal surface is sufficient to render the mTORC1 pathway amino acid insensitive and independent of Rag and Ragulator, but not Rheb, function. Thus, Rag-Ragulator-mediated translocation of mTORC1 to lysosomal membranes is the key event in amino acid signaling to mTORC1 (Appendix 5).

Aim 2: Elucidate the structural features of mTORC1 and its interacting proteins via X-ray crystallography, cryo-EM and SAXS

The study of mTORC1 phosphorylation of substrate sites has been greatly aided by pharmacological inhibitors of mTORC1, in particular rapamycin. Rapamycin, in complex with its intracellular receptor FKBP12 (FK506-binding protein of 12 kDa), acutely inhibits mTORC1 by binding to the FRB domain of mTOR. Yet, the molecular mechanism of how this high-affinity interaction perturbs mTOR kinase activity and the fully assembled mTORC1 is currently unknown. Thus, a detailed knowledge of mTORC1 structure, including the organization of its components, has the potential to help understand the regulation of its kinase activity and to aid in the development of more effective mTORC1 inhibitors. Therefore, we determined the first three-dimensional (3D) structure of the fully assembled human mTORC1 in an active state by cryo-EM. To perform a cryo-EM analysis of mTORC1, microgram quantities of intact and active mTORC1 was necessary. The large size (1 MDa) and instability of mTORC1 made it difficult to obtain the purified complex for structural analysis. To address this issue, we devised a method to purify microgram quantities of intact and active human mTORC1. Keys to the successful purification of mTORC1 were the development of a human cell line stably expressing a tagged raptor subunit that incorporates into endogenous mTORC1, the identification of buffer conditions that minimize mTORC1 disintegration and/or aggregation during purification, and the implementation of tandem gel filtration chromatography steps to separate mTORC1 from other large contaminants. Purified mTORC1 consists of equimolar quantities of mTOR, raptor, and mLST8 and of PRAS40 at substoichiometric level. The kinase activity of purified mTORC1 toward S6K1 was sensitive to FKBP12-rapamycin and Torin1, an ATP-competitive inhibitor of mTOR. Negative-stain EM analysis of the purified complex revealed particles that were homogeneous in size and shape. Subsequently, we determined the three-dimensional (3D) structure of human mTORC1 by cryo-EM. This structure, together with labeling and biochemical studies, revealed the intricate organization of the components within mTORC1 and provides structural insights into the mechanism of its inhibition by FKBP12-rapamycin. In our recent publication, we reported that mTORC1 is an obligate dimer with an overall rhomboid shape and a central cavity. The dimeric interfaces are formed by interlocking interactions between the mTOR and raptor subunits. Extended incubation with FKBP12-rapamycin compromises the structural integrity of mTORC1 in a stepwise manner, leading us to propose a model in which rapamycin inhibits mTORC1-mediated phosphorylation of 4E-BP1 and S6K1 through different mechanisms. Based on these observations and our knowledge of the molecular organization of mTORC1, we proposed the following model for rapamycin-mediated inhibition of mTORC1. The initial binding of one FKBP12-rapamycin to mTORC1 causes a subtle conformational change in mTOR that weakens the mTOR-raptor interaction but does not suffice to disrupt the dimeric architecture. Moreover, the bound FKBP12-rapamycin likely occludes the binding of or blocks access to the active site for larger-sized substrates, such as S6K1. Over time, either amplified structural strain caused by the first FKBP12-rapamycin or, perhaps, the binding of a second rapamycin complex leads to a fast disintegration of the already “weakened” mTORC1 and the complete abolishment of 4E-BP1 phosphorylation. Therefore, our work suggests that in vitro rapamycin is an mTORC1 inhibitor that may work through at least two different modes. The fact that, within cells, rapamycin does not completely inhibit 4E-BP1 phosphorylation or mTORC1

stability suggests that cells contain buffering mechanisms that counter the effects of rapamycin on mTORC1 and that these are lost when mTORC1 is purified (Appendix 4).

In addition to key research accomplishments described previously, we recently published two additional manuscripts that were supported by the grant. In our first manuscript, we described that leucine deprivation causes the caspase-dependent apoptotic death of melanoma cells because it failed to appropriately activate autophagy. Hyperactivation of the RAS-MEK pathway, which is common in melanoma, prevented leucine deprivation from inhibiting mTORC1, the main repressor of autophagy under nutrient-rich conditions. In an in vivo tumor xenograft model, the combination of a leucine-free diet and an autophagy inhibitor synergistically suppressed the growth of human melanoma tumors and triggered widespread apoptosis of the cancer cells. Together, our study represents proof of principle that anticancer effects can be obtained with a combination of autophagy inhibition and strategies to deprive tumors of leucine (Appendix 6). In our second study, we defined the mTOR-regulated phosphoproteome by quantitative mass spectrometry and characterized the primary sequence motif specificity of mTOR using positional scanning peptide libraries. We found that the phosphorylation response to insulin is largely mTOR dependent and that mTOR exhibits a unique preference for proline, hydrophobic, and aromatic residues at the +1 position. The adaptor protein Grb10 was identified as an mTORC1 substrate that mediates the inhibition of phosphoinositide 3-kinase typical of cells lacking tuberous sclerosis complex 2 (TSC2), a tumor suppressor and negative regulator of mTORC1. Our work clarifies how mTORC1 inhibits growth factor signaling and opens new areas of investigation in mTOR biology (Appendix 7).

KEY RESEARCH ACCOMPLISHMENTS

- Characterized intracellular localization of mTORC1 pathway components
- Localized mTORC1 to different cellular membranes
- Identified a lysosome based signaling system that is important for amino acid signaling
- Showed that mTORC1 translocates to the lysosomal surface in response to amino acid stimulation, and the Rag GTPases constitutively reside on the lysosomal surface
- Identified the Ragulator protein complex as novel Rag GTPase interacting proteins
- Showed that the Ragulator tethers the Rag GTPases to the lysosomal surface independent of amino acid availability, and is required for amino acid-induced mTORC1 lysosomal translocation
- Constitutively localized mTORC1 to the lysosomal surface and showed that the mTORC1 pathway activity becomes insensitive to amino acid starvation when on the lysosomal membrane
- Indicated lysosomes as the site of amino acid sensing in mammals for the first time
- Developed purification methods for human mTORC1 and free raptor
- Deciphered the structures of mTORC1 and free Raptor by cryo-EM
- Analyzed the molecular architecture and subunit organization of mTORC1 based on antibody labeling and biochemical assays
- Provided structural insights into the mechanism of inhibition by rapamycin
- Developed Torin1 as a highly potent and specific mTOR inhibitor
- Showed that rapamycin does not fully inhibit 4E-BP1
- Developed a capillary isoelectric focusing technique under native conditions for the separation of mTOR complex isoforms and subcomplexes
- Showed that defective autophagy upon leucine deprivation reveals a liability of melanoma cells
- Triggered caspase activation and apoptosis of melanoma cells via leucine deprivation
- Determined mTORC1 and MAPK pathways as regulators of sensitivity to leucine deprivation
- Showed that leucine deprivation and chloroquine synergistically induce apoptosis in vivo
- Defined the mTOR-regulated phosphoproteome by quantitative mass spectrometry

- Characterized the primary sequence motif specificity of mTOR using positional scanning peptide libraries
- Identified Grb10 as an mTORC1 substrate

REPORTABLE OUTCOMES

- Publications:
  - Sancak, Y., Peterson, T.R., Shaul, Y.D., Lindquist, R.A., Thoreen, C.C., Bar-Peled, L., and Sabatini, D.M. The Rag GTPases bind raptor and mediate amino acid signaling to mTORC1. *Science* **2008,** 302 (5882), 1496-1501.
  - Thoreen, C.C., Kang, S.A., Chang, J.W., Liu, Q, Zhang, J., Gao, Y., Reichling, L.J., Sim, T. Sabatini, D.M., and Gray, N.S. An ATP-competitive mTOR inhibitor reveals rapamycin-insensitive functions of mTORC1. *J. Biol. Chem.* **2009**, 284 (12), 8023-8032.
  - Fonslow B.R., Kang S.A., Gestaut D.R., Graczyk B., Davis T.N., Sabatini D.M., Yates, J.R. Native Capillary Isoelectric Focusing for the Separation of Protein Complex Isoforms and Subcomplexes. *Anal. Chem.* **2010,** 82 (15), 6643-6651.
  - Yip, C.K., Murata, K., Walz, T., Sabatini, D.M., Kang, S.A. Structure of the human mTOR complex I and its implications for rapamycin inhibition. *Mol. Cell* **2010,** 38 (5), 768-774.
  - Sancak, Y., Bar-Peled, L., Zoncu, R., Markhard, A.L., Nada, S. and Sabatini, D.M. Ragulator-Rag Complex Targets mTORC1 to the Lysosomal Surface and Is Necessary for Its Activation by Amino Acids. *Cell* **2010,** 141 (2), 290-303.
  - Sheen, J.H., Zoncu, R., Kim, D., Sabatini, D.M. Defective Regulation of Autophagy upon Leucine Deprivation Reveals a Targetable Liability of Human Melanoma Cells In Vitro and In Vivo. *Cancer Cell* **2011** 19(5), 613-628.
  - Hsu, P. P., Kang, S. A., Rameseder, J., Zhang, Y., Ottina, K., Lim, D., Peterson, T. R., Yongmun, C., Gray, N. S., Yaffe, M. B., Marto, J. A., Sabatini, D.M., (2011) The mTOR-Regulated Phosphoproteome Reveals a Mechanism of mTORC1-Mediated Inhibition of Growth Factor Signaling. *Science* **2011** 332, 1317-1322.
- Meetings attended:

  <u>David Sabatini</u>
  - March 2008, “mTOR Signaling Pathways,” Wyeth Research Frontiers in Human Diseases Symposium, New York, New York.
  - April 2008, “mTOR1 vs mTOR2,” The LAM Foundation 2008 International Research Conference, Cincinnati, Ohio.
  - November 2008, “Regulation of growth by the mTOR pathway,” CNIO (Center for National Cancer Research) Conference on "Upstream of mTOR,” Madrid, Spain.
  - November 2008, “Regulation of growth by the mTOR pathway,” AACR Meeting on PI3K Signaling and Cancer”, Cambridge, Massachusetts.
  - April 2009, “Regulation of Growth by the mTOR pathway,” 2009 Annual Meeting of the American Association for Cancer Research, Denver, Colorado.
  - April 2009, “Crosstalk between PI3K and mTOR,” 2009 Keystone Symposia on PI 3-Kinase Signaling in Disease, Olympic Valley, California.
  - July 2009, “Protein Kinases & Protein Phosphorlaytion,” FASEB Summer Research Conference, Snowmass, Colorado.
  - August 2009, “Regulation of growth by the mTOR pathway,” 2009 EMBO meeting, Amsterdam, The Netherlands.
  - September 2009, “Identification and Clinical Assessment of Genes that Regulate the Response of Cancers to Rapamycin,” 2009 Starr Cancer Consortium Retreat, Cold Spring Harbor Laboratory, Cold Spring Harbor, New York.
  - October 2009, “Control of growth by the mTOR pathway,” AACR Frontiers in Basic Cancer Research, Boston, Massachusetts.
  - December 2009, “Growth by the mTOR Pathway,” ASCB: Regulation of Cell Growth Minisymposium, San Francisco, California. Co-organized with Duojia Pan, Johns Hopkins University School of Medicine.

- February 2010, “mTOR and the control of Growth,” AACR Special Seminar: Protein Translation and Cancer, San Diego, California.
- March 2010, “mTOR and nutrient sensing,” 2010 Keystone Symposium on Metabolism and Cancer Progression. Fairmont Hotel, Vancouver, Canada.
- April 2010, “mTOR and the control of growth,” James Watson Cancer Symposium in April 2010, Dushu Lake Conference Hotel, Cold Spring Harbor Asia, Suzhou, China.
- June 2010, “Control of growth by the mTOR pathway,” 2010 Gordon Research Conference on “Phosphorylation & G-Protein Mediated Signaling Networks,” University of New England, Biddeford, Maine.
- September 2010, “Control of growth by the mTOR pathway,” Cell Press Lab Links Symposium: Cellular Metabolism and Cancer, Broad Institute, Cambridge, Massachusetts. Co-organized with Cell Press.
- September 2010, “Growth Control by the mTOR pathway,” Cell Signaling Conference, HHMI, Janella Farm Research Campus, Ashburn, Virginia.
- February 2011, “Growth Control by the mTOR pathway,” AACR Special Conference, “Targeting P13K/mTOR Signaling in Cancer,” San Francisco, California. Co-chairperson with Lewis C. Cantley and Funda Meric-Bernstam.
- April 2011, “Regulation of Growth by the mTOR pathway,” AACR 102nd Annual Meeting, “Meet the Expert Session,” Orange county Convention Center, Orlando, FL.
- April 2011, “Regulation of Growth by the mTOR pathway,” Stony Brook University, Molecular and Cellular Biology, “4th Annual MCB/BSB Meeting,” Stony Brook, NY.
- June 2011, “Regulation of Growth by the mTOR pathway,” AFAR Grantee Conference 24th Annual Meeting, Santa Barbara, CA.
- June 2011, Keynote Speaker: “Regulation of Growth by the mTOR pathway,” 8th Annual Research and Education Day, University of Western Ontario, London, Ontario, Canada.
- June 2011, “Regulation of Growth by the mTOR pathway,” 2011 Gordon Research Conference on Cell Growth and Proliferation, Biddeford, Maine.
- July 2011, “Regulation of Growth by the mTOR pathway,” Protein Kinases and Protein Phosphorylation, FASEB Summer Research Conference, Snowmass, Colorado.

<u>Seong Woo Kang</u>

- June 2008, “Pharmacological inhibition of mTORC1 and mTORC1” 2010 Gordon Research Conference on “Phosphorylation & G-Protein Mediated Signaling Networks,” University of New England, Biddeford, Maine.
- April 2009, “Structure of the human mTOR complex I and its implications for rapamycin inhibition,” The LAM Foundation 2009 International Research Conference, Cincinnati, Ohio.
- October 2009, “Pharmacological inhibition of mTORC1 and mTORC1,” AACR Frontiers in Basic Cancer Research, Boston, Massachusetts.
- June 2010, “Structure of the human mTOR complex I and its implications for rapamycin inhibition,” “Phosphorylation & G-Protein Mediated Signaling Networks,” University of New England, Biddeford, Maine.

<u>Yasemin Sancak</u>

- June 2008, “The Rag GTPases bind raptor and mediate amino acid signaling to mTORC1” 2010 Gordon Research Conference on “Phosphorylation & G-Protein Mediated Signaling Networks,” University of New England, Biddeford, Maine.
- January 2009, “The Rag GTPases bind raptor and mediate amino acid signaling to mTORC1” Biochemical Society Meeting, Oxford, England.

- Patents applied:
    - SOLUBLE MTOR COMPLEXES AND MODULATORS THEREOF, International patent application number: PCT/US2009/005656, Based on U.S. patent application number: 61/185923, 61/196772 and 61/106411, Inventors: Nathanael Gray et al.

- Degrees awarded:
    - Yasemin Sancak, Ph.D. (May, 2010)

CONCLUSION

Our recent findings, together with previous work showing that Rheb is required for amino acids to activate the mTORC1 pathway and can localize to late endosomes/lysosomes, is consistent with a model in which amino acids induce mTORC1 to associate with the endomembrane system of the cell and thus allow it to encounter its activator Rheb. In this model, the essential role of the Ragulator-Rag complex is to serve as an amino acid-regulated docking site for mTORC1 on lysosomal membranes. Ragulator, which consists of p14, p18, and MP1, is a Rag-interacting complex that is essential for amino acid signaling to mTORC1 and represents an additional critical component of the TORC1 signaling pathway in mammals and flies. The proposed link between the Rag and Rheb GTPases in the regulation of the mTORC1 pathway provides an explanation for why activation of mTORC1 occurs only when activators of both Rheb (e.g., growth factors and energy) and the Rags (i.e., amino acids) are available. In the second part of our study, we deciphered the molecular architecture of mTORC1 via cryo-electron microscopy. For years, lack of meaningful structural information of the mTOR complexes has prevented us from answering a number of key questions concerning the mechanism of the action of the mTOR kinase, kinase-substrate interactions, and ultimately, its inhibition by FKBP12-rapamycin. Our structure of mTORC1 reveals that the holoenzyme exists as an obligate heterodimer, in which raptor provides a basis for the complex assembly in part by scaffolding mTOR through its multiple protein-protein interfaces. Even though the exact structural dynamics of mTORC1 with regard to kinase activity remain elusive, the gross conformational changes associated with rapamycin binding are critical for the substrate-specific inhibition of mTORC1.

The mTORC1 signaling pathway is a major therapeutic target for TSC. Early clinical trials of rapamycin already gave promising results in TSC patients, emphasizing the importance of understanding the structure and regulation of mTORC1. Over the past four years, we addressed two important aspects of mTOR biology: amino acid signaling and structure of mTORC1. Therefore, our work will lead to the discovery of novel signaling mechanisms that will provide a new foundation for the rational development of drugs targeting the mTOR pathway.

APPENDICES

1. Sancak, Y., Peterson, T.R., Shaul, Y.D., Lindquist, R.A., Thoreen, C.C., Bar-Peled, L., and Sabatini, D.M. The Rag GTPases bind raptor and mediate amino acid signaling to mTORC1. *Science* **2008,** 302 (5882), 1496-1501.
2. Thoreen, C.C., Kang, S.A., Chang, J.W., Liu, Q, Zhang, J., Gao, Y., Reichling, L.J., Sim, T. Sabatini, D.M., and Gray, N.S. An ATP-competitive mTOR inhibitor reveals rapamycin-insensitive functions of mTORC1. *J. Biol. Chem.* **2009**, 284 (12), 8023-8032.
3. Fonslow B.R., Kang S.A., Gestaut D.R., Graczyk B., Davis T.N., Sabatini D.M., Yates, J.R. Native Capillary Isoelectric Focusing for the Separation of Protein Complex Isoforms and Subcomplexes. *Anal. Chem.* **2010,** 82 (15), 6643-6651.
4. Yip, C.K., Murata, K., Walz, T., Sabatini, D.M., Kang, S.A. Structure of the human mTOR complex I and its implications for rapamycin inhibition. *Mol. Cell* **2010,** 38 (5), 768-774.
5. Sancak, Y., Bar-Peled, L., Zoncu, R., Markhard, A.L., Nada, S. and Sabatini, D.M. Ragulator-Rag Complex Targets mTORC1 to the Lysosomal Surface and Is Necessary for Its Activation by Amino Acids. *Cell* **2010,** 141 (2), 290-303.

6. Sheen, J.H., Zoncu, R., Kim, D., Sabatini, D.M. Defective Regulation of Autophagy upon Leucine Deprivation Reveals a Targetable Liability of Human Melanoma Cells In Vitro and In Vivo. *Cancer Cell* **2011** 19(5), 613-628.
7. Hsu, P. P., Kang, S. A., Rameseder, J., Zhang, Y., Ottina, K., Lim, D., Peterson, T. R., Yongmun, C., Gray, N. S., Yaffe, M. B., Marto, J. A., Sabatini, D.M., (2011) The mTOR-Regulated Phosphoproteome Reveals a Mechanism of mTORC1-Mediated Inhibition of Growth Factor Signaling. *Science* **2011** 332, 1317-1322.

in others, such as adult liver, it does not substantially affect protein secretory function but rather controls select transcriptional programs such as lipogenesis. Preservation of the normal hepatic lipid profile suggests that compounds that inhibit XBP1 activation in the liver may reduce serum lipids without causing hepatic steatosis in patients with dyslipidemias.

Given XBP1's known function as a key mediator of the UPR, it was surprising that its function in regulating lipogenesis was unrelated to the ER stress response. Indeed, apoB-100 folding and secretion, as well as the overall hepatocyte protein secretory function, were minimally compromised by loss of XBP1, likely because XBP1 independent basal chaperone gene expression is sufficient to accommodate moderate secretory loads. Interestingly, IRE1α, the upstream activator of XBP1, was constitutively active in the *Xbp1*Δ liver, suggesting the presence of a negative feedback loop that precisely maintains XBP1s protein levels even in the absence of ER stress. The nature of this signal, and its relationship to the ER stress response and to the activation of XBP1 in the liver by carbohydrate feeding, require further investigation.

References and Notes

1. H. N. Ginsberg, Y. L. Zhang, A. Hernandez-Ono, *Obesity* **14** (suppl. 1), 41S (2006).
2. F. Foufelle, P. Ferre, *Biochem. J.* **366**, 377 (2002).
3. D. Ron, P. Walter, *Nat. Rev. Mol. Cell Biol.* **8**, 519 (2007).
4. A. L. Shaffer *et al.*, *Immunity* **21**, 81 (2004).
5. A. H. Lee, N. N. Iwakoshi, L. H. Glimcher, *Mol. Cell. Biol.* **23**, 7448 (2003).
6. D. Acosta-Alvear *et al.*, *Mol. Cell* **27**, 53 (2007).
7. A. M. Reimold *et al.*, *Nature* **412**, 300 (2001).
8. A. H. Lee, G. C. Chu, N. N. Iwakoshi, L. H. Glimcher, *EMBO J.* **24**, 4368 (2005).
9. A. M. Reimold *et al.*, *Genes Dev.* **14**, 152 (2000).
10. R. Sriburi, S. Jackowski, K. Mori, J. W. Brewer, *J. Cell Biol.* **167**, 35 (2004).
11. N. O. Davidson, G. S. Shelness, *Annu. Rev. Nutr.* **20**, 169 (2000).
12. M. M. Hussain, J. Iqbal, K. Anwar, P. Rava, K. Dai, *Front. Biosci.* **8**, s500 (2003).
13. M. C. Schotz, A. Scanu, I. H. Page, *Am. J. Physiol.* **188**, 399 (1957).
14. S. J. Stone *et al.*, *J. Biol. Chem.* **279**, 11767 (2004).
15. X. X. Yu *et al.*, *Hepatology* **42**, 362 (2005).
16. J. M. Ntambi *et al.*, *Proc. Natl. Acad. Sci. U.S.A.* **99**, 11482 (2002).
17. P. Cohen *et al.*, *Science* **297**, 240 (2002).
18. L. Abu-Elheiga, W. Oh, P. Kordari, S. J. Wakil, *Proc. Natl. Acad. Sci. U.S.A.* **100**, 10207 (2003).
19. J. D. Horton, J. L. Goldstein, M. S. Brown, *J. Clin. Invest.* **109**, 1125 (2002).
20. H. C. Towle, E. N. Kaytor, H. M. Shih, *Annu. Rev. Nutr.* **17**, 405 (1997).
21. M. Miyazaki *et al.*, *J. Biol. Chem.* **279**, 25164 (2004).
22. H. Basciano, L. Federico, K. Adeli, *Nutr. Metab.* **2**, 5 (2005).

23. Supported by NIH grants AI32412 and P01 AI56296 (L.H.G.), NIH grants DK48873 and DK56626 (D.E.C.), and the Ellison Medical Foundation (L.H.G.). We thank K. Rajewsky for providing *Mx1-cre* mice, J. Goldstein and M. Brown for SREBP antibodies, R. Milne for apoB antibody, K. Mori for ATF6α antibody, E. Fisher for advice on pulse-chase experiments, M. Wu and J. Wei for help with FPLC analyses, D. Hu for histologic analyses, K. Heidtman for excellent technical assistance, and M. Wein and W. Garrett for critical reading of the manuscript. L.H.G. has equity in Bristol-Myers Squibb and has filed a patent regarding methods for regulating hepatic lipogenesis with XBP1.

Supporting Online Material

www.sciencemag.org/cgi/content/full/320/5882/1492/DC1
Materials and Methods
Figs. S1 to S5
Tables S1 to S4
References

19 March 2008; accepted 17 April 2008
10.1126/science.1158042

The Rag GTPases Bind Raptor and Mediate Amino Acid Signaling to mTORC1

Yasemin Sancak,[1,2] Timothy R. Peterson,[1,2] Yoav D. Shaul,[1,2] Robert A. Lindquist,[1,2] Carson C. Thoreen,[1,2] Liron Bar-Peled,[1] David M. Sabatini[1,2,3]*

The multiprotein mTORC1 protein kinase complex is the central component of a pathway that promotes growth in response to insulin, energy levels, and amino acids and is deregulated in common cancers. We find that the Rag proteins—a family of four related small guanosine triphosphatases (GTPases)—interact with mTORC1 in an amino acid–sensitive manner and are necessary for the activation of the mTORC1 pathway by amino acids. A Rag mutant that is constitutively bound to guanosine triphosphate interacted strongly with mTORC1, and its expression within cells made the mTORC1 pathway resistant to amino acid deprivation. Conversely, expression of a guanosine diphosphate–bound Rag mutant prevented stimulation of mTORC1 by amino acids. The Rag proteins do not directly stimulate the kinase activity of mTORC1, but, like amino acids, promote the intracellular localization of mTOR to a compartment that also contains its activator Rheb.

The mTOR complex 1 (mTORC1) branch of the mammalian target of rapamycin (mTOR) pathway is a major driver of cell growth in mammals and is deregulated in many common tumors (*1*). It is also the target of the drug rapamycin, which has generated considerable interest as an anticancer therapy. Diverse signals regulate the mTORC1 pathway, including insulin, hypoxia, mitochondrial function, and glucose and amino acid availability. Many of these are integrated upstream of mTORC1 by the tuberous sclerosis complex (TSC1-TSC2) tumor suppressor, which acts as an important negative regulator of mTORC1 through its role as a guanosine triphosphatase (GTPase)–activating protein (GAP) for Rheb, a small guanosine triphosphate (GTP)–binding protein that potently activates the protein kinase activity of mTORC1 (*2*). Loss of either TSC protein causes hyperactivation of mTORC1 signaling, even in the absence of many of the upstream signals that are normally required to maintain pathway activity. A notable exception is the amino acid supply, as the mTORC1 pathway remains sensitive to amino acid starvation in cells lacking either TSC1 or TSC2 (*3*–*5*).

The mechanisms through which amino acids signal to mTORC1 remain mysterious. It is a reasonable expectation that proteins that signal the availability of amino acids to mTORC1 are also likely to interact with it, but, so far, no good candidates have been identified. Because most mTORC1 purifications rely on antibodies to isolate mTORC1, we wondered if in previous work antibody heavy chains obscured, during SDS–polyacrylamide electrophoresis (SDS-PAGE) analysis of purified material, mTORC1-interacting proteins of 45 to 55 kD. Indeed, using a purification strategy that avoids this complication (*6*), we identified the 44-kD RagC protein as copurifying with overexpressed raptor, the defining component of mTORC1 (*7*–*10*).

RagC is a Ras-related small GTP-binding protein and one of four Rag proteins in mammals (RagA, RagB, RagC, and RagD). RagA and RagB are very similar to each other and are orthologs of budding yeast Gtr1p, whereas RagC and RagD are similar and are orthologs of yeast Gtr2p (*11*–*13*). In yeast and in human cells, the Rag and Gtr proteins function as heterodimers consisting of one Gtr1p-like (RagA or RagB) and one Gtr2p-like (RagC or RagD) component (*14*, *15*). The finding that RagC copurifies with raptor was intriguing to us because, in yeast, Gtr1p and Gtr2p regulate the intracellular sorting of the Gap1p amino acid permease (*16*) and microautophagy (*17*), processes modulated by amino acid levels and

[1]Whitehead Institute for Biomedical Research and Department of Biology, Massachusetts Institute of Technology (MIT), Nine Cambridge Center, Cambridge, MA 02142, USA. [2]MIT Center for Cancer Research, 77 Massachusetts Avenue, Cambridge, MA 02139, USA. [3]Broad Institute, Seven Cambridge Center, Cambridge, MA 02142, USA.

*To whom correspondence should be addressed. E-mail: sabatini@wi.mit.edu

the TOR pathway (*18*–*20*). The Gtr proteins have been proposed to act downstream or in parallel to TORC1 in yeast because their overexpression induces microautophagy even in the presence of rapamycin, which normally suppresses it (*17*).

To verify our identification of RagC as an mTORC1-interacting protein, we expressed raptor with different pairs of Rag proteins in human embryonic kidney (HEK)-293T cells. Consistent with the Rags functioning as heterodimers, raptor copurified with RagA-C or RagB-C, but not with RagA-B or the Rap2A control protein (Fig. 1A). Because the nucleotide loading state of most GTP-binding proteins regulates their functions, we generated RagB, RagC, and RagD mutants predicted (*14*, *16*, *17*) to be restricted to the GTP- or guanosine diphosphate (GDP)–bound conformations (for simplicity, we call these mutants $RagB^{GTP}$, $RagB^{GDP}$, etc.) (*6*). When expressed with mTORC1 components, Rag heterodimers containing $RagB^{GTP}$ immunoprecipitated with more raptor and mTOR than did complexes containing wild-type RagB or $RagB^{GDP}$ (Fig. 1B). The GDP-bound form of RagC increased the amount of copurifying mTORC1, so that $RagB^{GTP}$-C^{GDP} recovered the highest amount of endogenous mTORC1 of any heterodimer tested (Fig. 1C). Giving an indication of the strength of the mTORC1-$RagB^{GTP}$-C^{GDP} association, in this same assay, we could not detect coimmunoprecipitation of mTORC1 with Rheb1 (Fig. 1C), an established interactor and activator of mTORC1 (*1*). When expressed alone, raptor, but not mTOR, associated with $RagB^{GTP}$-D^{GDP}, which suggests that raptor is the key mediator of the Rag-mTORC1 interaction (Fig. 1D). Consistent with this, rictor, an mTOR-interacting protein that is only part of mTORC2 (*1*), did not copurify with any Rag heterodimer (Fig. 1C and fig. S1). Last, highly purified raptor interacted in vitro with RagB-D and, to a larger extent, with $RagB^{GTP}$-D^{GDP}, which indicates that the Rag-raptor interaction is most likely direct (Fig. 1E).

We tested whether various Rag heterodimers affected the regulation of the mTORC1 pathway within human cells. In HEK-293T cells, expression of the $RagB^{GTP}$-D^{GDP} heterodimer, which interacted strongly with mTORC1, not only activated the pathway, but also made it insensitive to deprivation for leucine or total amino acids, as judged by the phosphorylation state of the mTORC1 substrate T389 of S6K1 (Fig. 2, A and B). The wild-type RagB-C heterodimer had milder effects than $RagB^{GTP}$-C^{GDP}, making the mTORC1 pathway insensitive to leucine deprivation, but not to the stronger inhibition caused by total amino acid starvation (Fig. 2, A and B). Expression of $RagB^{GDP}$-D^{GTP}, a heterodimer that did not interact with mTORC1 (Fig. 1, C and D), had dominant-negative effects, as it eliminated S6K1 phosphorylation in the presence, as well as absence, of leucine or amino acids (Fig. 2, A and B). Expression of $RagB^{GDP}$ alone also suppressed S6K1 phosphorylation (fig. S2). These results suggest that the activity of the mTORC1 pathway

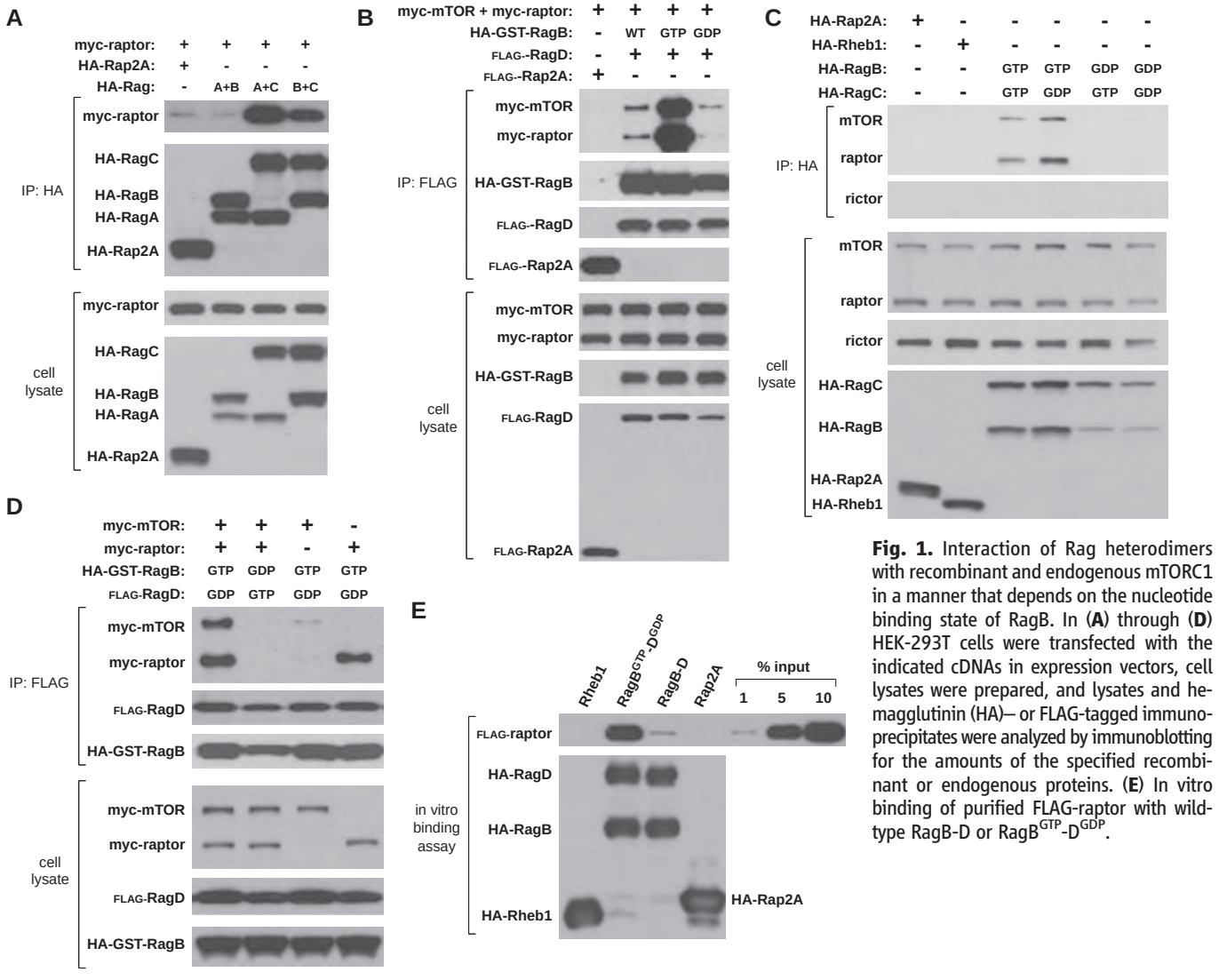

Fig. 1. Interaction of Rag heterodimers with recombinant and endogenous mTORC1 in a manner that depends on the nucleotide binding state of RagB. In (**A**) through (**D**) HEK-293T cells were transfected with the indicated cDNAs in expression vectors, cell lysates were prepared, and lysates and hemagglutinin (HA)– or FLAG-tagged immunoprecipitates were analyzed by immunoblotting for the amounts of the specified recombinant or endogenous proteins. (**E**) In vitro binding of purified FLAG-raptor with wild-type RagB-D or $RagB^{GTP}$-D^{GDP}.

under normal growth conditions depends on endogenous Rag function.

To verify the actions of the Rags in a more physiological setting than that achieved by transient cDNA transfection, we generated HEK-293T cell lines stably expressing Rheb1, RagB, or $RagB^{GTP}$ (attempts to generate lines stably expressing $RagB^{GDP}$ failed). Under normal growth conditions, these cells were larger than control cells and had higher levels of mTORC1 pathway activity (Fig. 3A). Unlike transient Rheb1 overexpression (Fig. 2, A and B), stable expression did not make the mTORC1 pathway insensitive to leucine or amino acid starvation (Fig. 3, B and C), consistent with evidence that transiently overexpressed Rheb may have nonphysiological consequences on amino acid signaling to mTORC1 (*4*, *5*). Stable expression of a $Rheb1^{GTP}$ mutant was also unable to make the mTORC1 pathway resistant to amino acid deprivation (fig. S3). In contrast, stable expression of $RagB^{GTP}$ eliminated the sensitivity of the mTORC1 pathway to leucine or total amino acid withdrawal, whereas that of wild-type RagB overcame sensitivity to leucine but not to amino acid starvation (Fig. 3, B and C). Thus, transient or stable expression of the appropriate Rag mutants is sufficient to put the mTORC1 pathway into states that mimic the presence or absence of amino acids.

To determine if the Rag mutants affect signaling to mTORC1 from inputs besides amino acids, we tested whether in $RagB^{GTP}$-expressing cells the mTORC1 pathway was resistant to other perturbations known to inhibit it. This was not the case, as oxidative stress, mitochondrial inhibition, or energy deprivation still reduced S6K1 phosphorylation in these cells (fig. S4). Moreover, in HEK-293E cells, expression of $RagB^{GTP}$-D^{GDP} did not maintain mTORC1 pathway activity in the absence of insulin (Fig. 2C). Expression of the dominant-negative $RagB^{GDP}$-D^{GTP} heterodimer did, however, block insulin-stimulated phosphorylation of S6K1 (Fig. 2C), as did amino acid starvation (Fig. 2D). Thus, although $RagB^{GTP}$ expression mimics amino acid sufficiency, it cannot substitute for other inputs that mTORC1 normally monitors.

This evidence for a primary role of the Rag proteins in amino acid signaling to mTORC1 raised the question of where, within the pathway that links amino acids to mTORC1, the Rag proteins might function. The existence of the Rag-mTORC1 interaction (Fig. 1), the effects on amino acid signaling of the Rag mutants (Figs. 2 and 3), and the sensitivity to rapamycin of the S6K1 phosphorylation induced by $RagB^{GTP}$ (fig. S4), strongly suggested that the Rag proteins function downstream of amino acids and upstream of mTORC1. To verify this, we took advantage of the established finding that cycloheximide reactivates mTORC1 signaling in cells starved for amino acids by blocking protein synthesis and thus boosting the levels of the intracellular amino acids sensed by mTORC1 (*21*–*23*). Thus, if the Rag proteins act upstream of amino acids, cycloheximide should overcome the inhibitory effects of the $RagB^{GDP}$-C^{GTP} heterodimer on mTORC1 signaling, but if they are downstream, cycloheximide should not reactivate the pathway. The results were clear: cycloheximide treatment of cells reversed the inhibition of mTORC1 signaling caused by leucine deprivation, but not that caused by expression of $RagB^{GDP}$-C^{GTP} (fig. S5). Given the place-

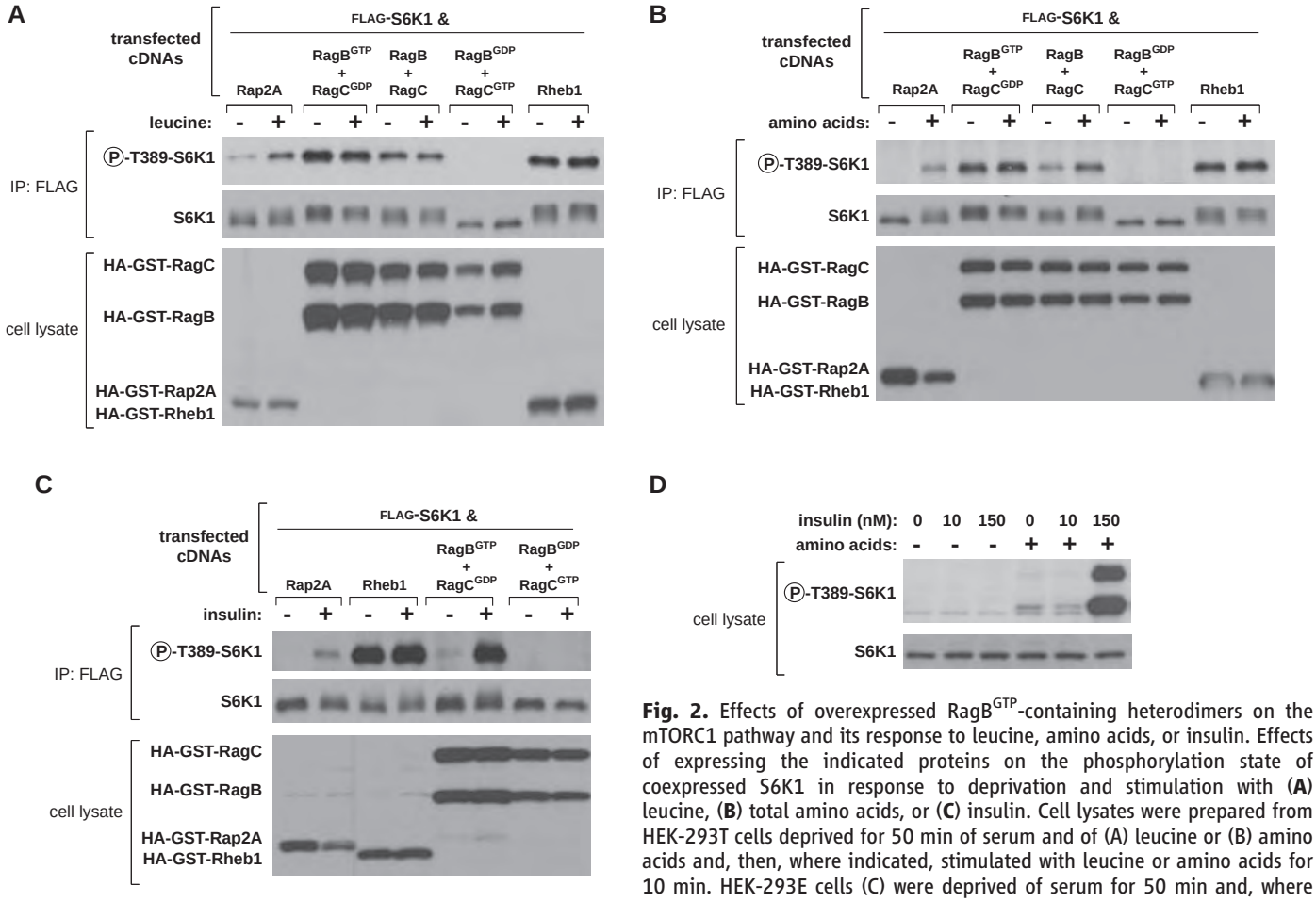

Fig. 2. Effects of overexpressed $RagB^{GTP}$-containing heterodimers on the mTORC1 pathway and its response to leucine, amino acids, or insulin. Effects of expressing the indicated proteins on the phosphorylation state of coexpressed S6K1 in response to deprivation and stimulation with (**A**) leucine, (**B**) total amino acids, or (**C**) insulin. Cell lysates were prepared from HEK-293T cells deprived for 50 min of serum and of (A) leucine or (B) amino acids and, then, where indicated, stimulated with leucine or amino acids for 10 min. HEK-293E cells (C) were deprived of serum for 50 min and, where indicated, stimulated with 150 nM insulin for 10 min. Lysates and FLAG-immunoprecipitates were analyzed for the levels of the specified proteins and the phosphorylation state of S6K1. (**D**) Effects of amino acid deprivation on insulin-mediated activation of mTORC1. HEK-293E cells were starved for serum and amino acids or just serum for 50 min, and where specified, stimulated with 10 or 150 nM insulin. Cell lysates were analyzed for the level and phosphorylation state of S6K1.

ment of the Rag proteins downstream of amino acids and upstream of mTORC1, we determined whether amino acids regulate the Rag-mTORC1 interaction within cells. Initial tests using transiently coexpressed Rag proteins and mTORC1 components did not reveal any regulation of the interaction. Because we reasoned that pronounced overexpression might overcome the normal regulatory mechanisms that operate within the cell, we developed an assay (*6*), based on a reversible chemical cross-linker, that allows us to detect the interaction of stably expressed FLAG-tagged Rag proteins with endogenous mTORC1. With this approach, we readily found that amino acids, but not insulin, promote the Rag-mTORC1 interaction when we used either FLAG-tagged RagB or RagD to isolate mTORC1 from cells (Fig. 3D and fig. S6A). As the GTP-loading state of the Rag proteins also regulates the Rag-mTORC1 interaction (Fig. 1), we determined whether amino acids modulate the amount of GTP bound to RagB. Indeed, amino acid stimulation of cells increased the GTP loading of RagB (Fig. 3E). Consistent with this, amino acids did not further augment the already high level of interaction between mTORC1 and the $RagB^{GTP}$ mutant (Fig. 3D).

To determine whether the Rag proteins are necessary for amino acids to activate the mTORC1 pathway, we used combinations of lentivirally delivered short hairpin RNAs (shRNAs) to suppress RagA and RagB or RagC and RagD at the same time. Loss of RagA and RagB also led to the loss of RagC and RagD and vice versa, which suggests that, within cells, the Rag proteins are unstable when not in heterodimers (Fig. 3F). In cells with a reduction in the expression of all the Rag proteins, leucine-stimulated phosphorylation of S6K1 was strongly reduced (Fig. 3G). The role of the Rag proteins appears to be conserved in *Drosophila* cells as double-stranded RNA–mediated suppression of the *Drosophila* orthologs of RagB or RagC eliminated amino acid–induced phosphorylation of dS6K (Fig. 3H). Consistent with amino acids being necessary for activation of mTORC1 by insulin, a reduction in Rag expression also suppressed insulin-stimulated phosphorylation of S6K1 (fig. S6B). Thus, the Rag proteins appear to be both necessary and

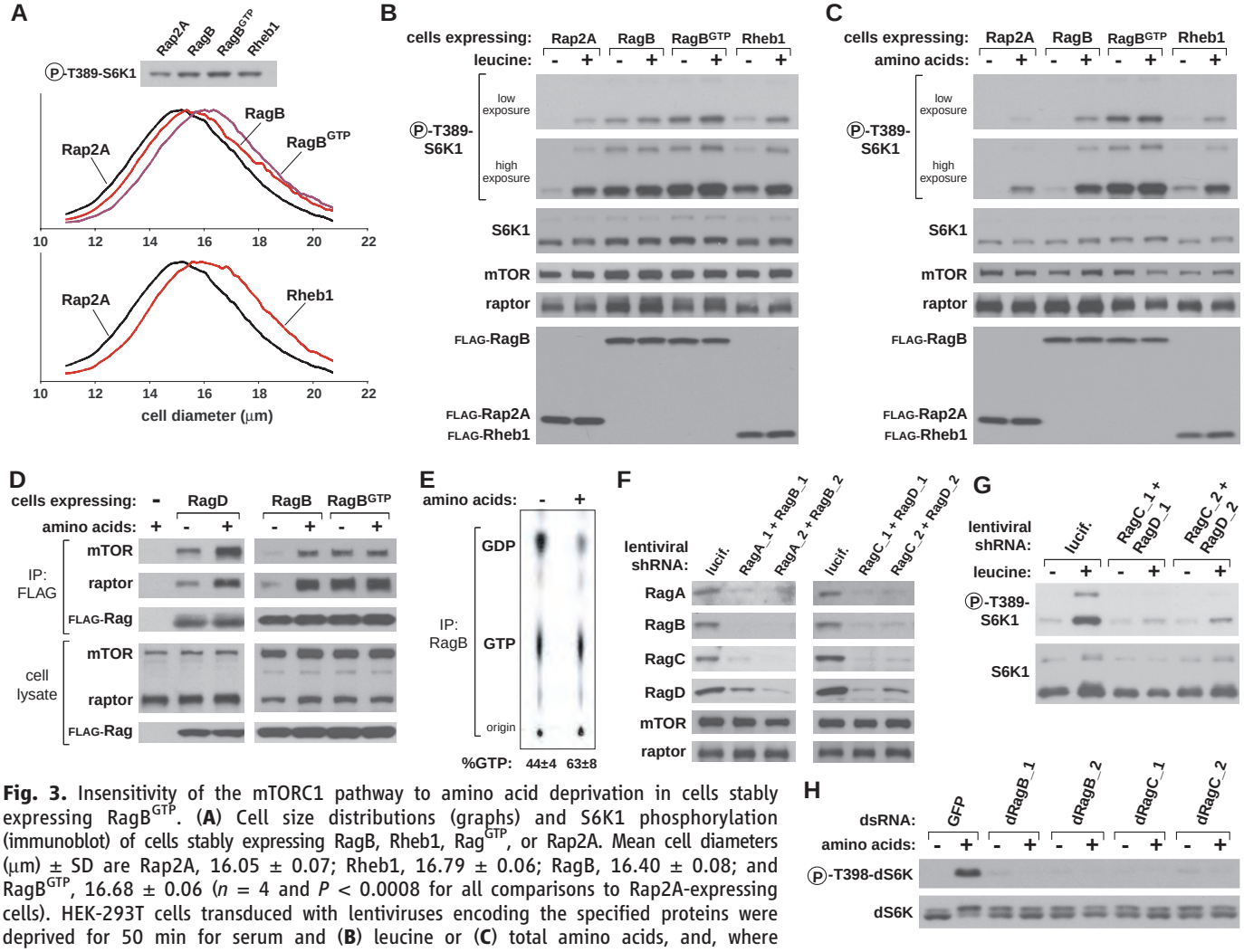

Fig. 3. Insensitivity of the mTORC1 pathway to amino acid deprivation in cells stably expressing $RagB^{GTP}$. (**A**) Cell size distributions (graphs) and S6K1 phosphorylation (immunoblot) of cells stably expressing RagB, Rheb1, Rag^{GTP}, or Rap2A. Mean cell diameters (μm) ± SD are Rap2A, 16.05 ± 0.07; Rheb1, 16.79 ± 0.06; RagB, 16.40 ± 0.08; and $RagB^{GTP}$, 16.68 ± 0.06 (n = 4 and $P < 0.0008$ for all comparisons to Rap2A-expressing cells). HEK-293T cells transduced with lentiviruses encoding the specified proteins were deprived for 50 min for serum and (**B**) leucine or (**C**) total amino acids, and, where indicated, restimulated with leucine or amino acids for 10 min. Cell lysates were analyzed for the levels of the specified proteins and the phosphorylation state of S6K1. (**D**) Amino acid–stimulated interaction of the Rag proteins with mTORC1. HEK-293T cells stably expressing FLAG-tagged RagB, RagD, or $RagB^{GTP}$ were starved for amino acids and serum for 50 min and, where indicated, restimulated with amino acids for 10 min. Cells were then processed with a chemical cross-linking assay, and cell lysates and FLAG immunoprecipitates were analyzed for the amounts of the indicated proteins. (**E**) Effects of amino acid stimulation on GTP loading of RagB. Values are means ± SD for n = 3 ($P < 0.02$ for increase in GTP loading caused by amino acid stimulation). (**F**) Abundance of RagA, RagB, RagC, and RagD in HeLa cells expressing the indicated shRNAs. (**G**) S6K1 phosphorylation in HeLa cells expressing shRNAs targeting RagC and RagD. Cells were deprived of serum and leucine for 50 min, and, where indicated, were restimulated with leucine for 10 min. (**H**) Effects of double-stranded RNA (dsRNA)–mediated knockdowns of *Drosophila* orthologs of RagB or RagC on amino acid–induced phosphorylation of dS6K.

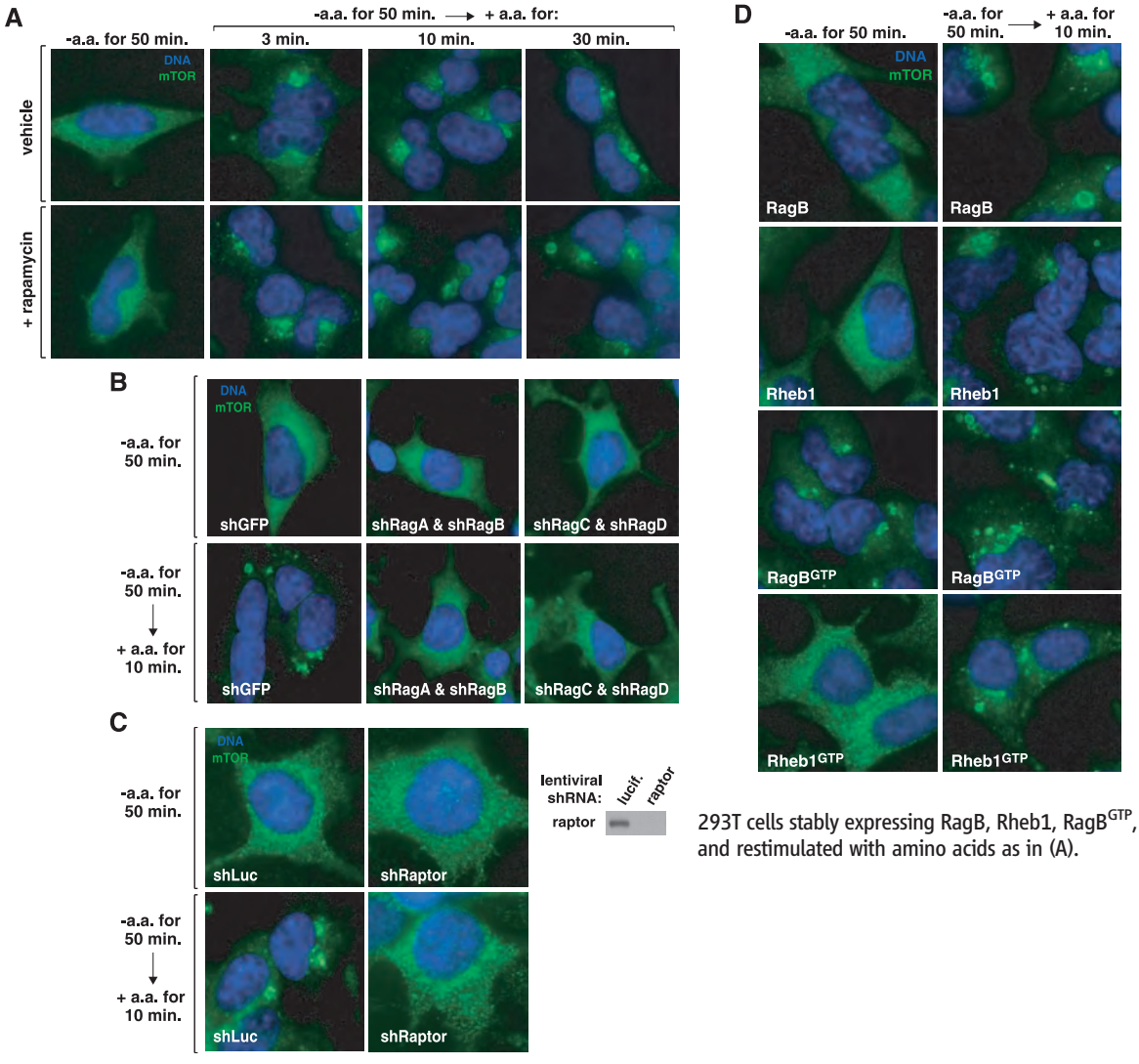

Fig. 4. Rag-dependent regulation by amino acids of the intracellular localization of mTOR. (**A**) HEK-293T cells were starved for serum and amino acids for 50 min or starved and then restimulated with amino acids for the indicated times in the presence or absence of rapamycin. Cells were then processed in an immunofluorescence assay to detect mTOR (green), costained with 4′,6′-diamidino-2-phenylindole (DAPI) for DNA content (blue), and imaged. Of these cells, 80 to 90% exhibited the mTOR localization pattern shown. (**B**) and (**C**) mTOR localization in HEK-293T cells expressing the indicated shRNAs and deprived and restimulated with amino acids as in (A). Immunoblot of raptor expression levels. (**D**) mTOR localization in HEK-293T cells stably expressing RagB, Rheb1, RagB^{GTP}, or Rheb1^{GTP} and deprived and restimulated with amino acids as in (A).

sufficient for mediating amino acid signaling to mTORC1.

Unlike Rheb (*24*, *25*), the Rag heterodimers did not directly stimulate the kinase activity of mTORC1 in vitro (fig. S7), so we considered the possibility that the Rag proteins regulate the intracellular localization of mTOR. mTOR is found on the endomembrane system of the cell, including the endoplasmic reticulum, Golgi apparatus, and endosomes (*26*, *27*). The intracellular localization of endogenous mTOR, as revealed with an antibody that we validated recognizes mTOR in immunofluorescence assays (fig. S8), was strikingly different in cells deprived of amino acids than in cells starved and briefly restimulated with amino acids (Fig. 4A and fig. S11) or growing in fresh complete media (fig. S9). In starved cells, mTOR was in tiny puncta throughout the cytoplasm, whereas in cells stimulated with amino acids for as little as 3 min, mTOR localized to the perinuclear region of the cell, to large vesicular structures, or to both (Fig. 4A). Rapamycin did not block the change in mTOR localization induced by amino acids (Fig. 4A), which indicated that it is not a consequence of mTORC1 activity but rather may be one of the mechanisms that underlies mTORC1 activation. The amino acid–induced change in mTOR localization required expression of the Rag proteins and of raptor (Fig. 4, B and C), and amino acids also regulated the localization of raptor (fig. S10).

In cells overexpressing RagB, Rheb1, or Rheb1^{GTP}, mTOR behaved as in control cells, its localization changing upon amino acid stimulation from small puncta to the perinuclear region and vesicular structures (Fig. 4D). In contrast, in cells overexpressing the RagB^{GTP} mutant that eliminates the amino acid sensitivity of the mTORC1 pathway, mTOR was already present on the perinuclear and vesicular structures in the absence of amino acids, and became even more localized to them upon the addition of amino acids (Fig. 4D). Thus, there is a correlation, under amino acid–starvation conditions, between the activity of the mTORC1 pathway and the subcellular localization of mTOR, which implies a role for Rag-mediated mTOR translocation in the activation of mTORC1 in response to amino acids.

We failed to find an established marker of the endomembrane system that colocalized with mTOR in amino acid–starved cells. However, in cells stimulated with amino acids, mTOR in the perinuclear region and on the large vesicular structures overlapped with Rab7 (Fig. 5A), which indicated that a substantial fraction of mTOR translocated to the late endosomal and lysosomal compartments in amino acid–replete cells. In cells expressing RagB^{GTP}, mTOR was present on the Rab7-positive structures even in the absence of amino acids (Fig. 5B).

The perinuclear region and vesicular structures on which mTOR appears after amino acid stimulation are similar to the Rab7-positive structures where green fluorescent protein (GFP)–tagged Rheb localizes in human cells (*28*, *29*). Unlike mTOR, however, amino acids did not appreciably affect the localization of Rheb, as GFP-Rheb1 colocalized with *Discosoma* red fluorescent protein (DsRed)–labeled Rab7 (DsRed-

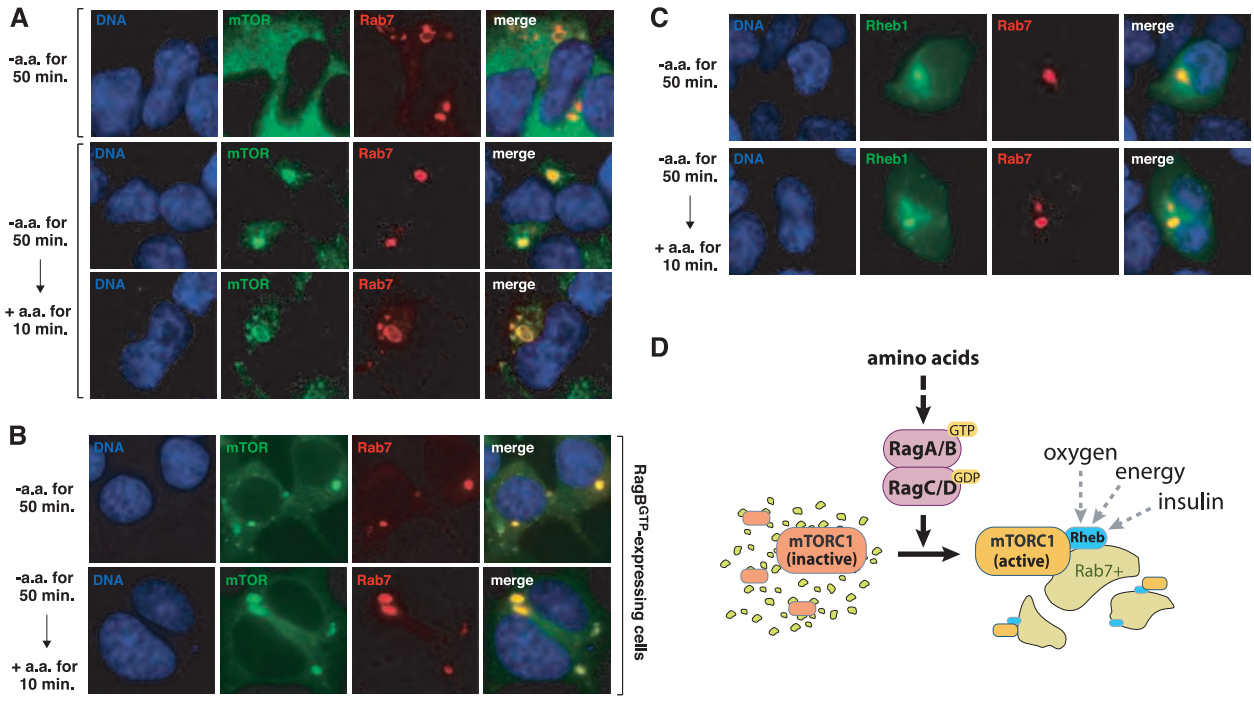

Fig. 5. Amino acids promote the localization of mTOR to a Rab7-positive compartment that also contains Rheb. (**A**) mTOR and Rab7 localization in cells deprived or stimulated with amino acids. HEK-293T cells transiently transfected with a cDNA for DsRed-Rab7 were starved for serum and amino acids for 50 min and, where indicated, stimulated with amino acids for 10 min. Cells were then processed to detect mTOR (green), Rab7 (red), and DNA content (blue), and imaged. Two examples are shown of mTOR localization in the presence of amino acids. (**B**) HEK-293T cells stably expressing $RagB^{GTP}$ and transiently transfected with a cDNA for DsRed-Rab7 were treated and processed as in (A). (**C**) Rheb1 and Rab7 localization in cells deprived or stimulated with amino acids. HEK-293T cells transiently transfected with 1 to 2 ng of cDNAs for GFP-Rheb1 and DsRed-Rab7 were treated as in (A), processed to detect Rheb1 (green), Rab7 (red), and DNA content (blue), and imaged. (**D**) Model for role of Rag GTPases in signaling amino acid availability to mTORC1.

Rab7) in the presence or absence of amino acids (Fig. 5C). Unfortunately, it is currently not possible to compare, in the same cells, the localization of endogenous mTOR with that of Rheb, because the signal for GFP-Rheb or endogenous Rheb is lost after fixed cells are permeabilized to allow access to intracellular antigens (*28*, *29*). Nevertheless, given that both mTOR and Rheb are present in Rab7-positive structures after amino acid stimulation, we propose that amino acids might control the activity of the mTORC1 pathway by regulating, through the Rag proteins, the movement of mTORC1 to the same intracellular compartment that contains its activator Rheb (see model in Fig. 5D). This would explain why activators of Rheb, like insulin, do not stimulate the mTORC1 pathway when cells are deprived of amino acids and why Rheb is necessary for amino acid–dependent mTORC1 activation (*4*) (fig. S12). When Rheb is highly overexpressed, some might become mislocalized and inappropriately encounter and activate mTORC1, which could explain why Rheb overexpression, but not loss of TSC1 or TSC2, makes the mTORC1 pathway insensitive to amino acids (*4*, *5*).

In conclusion, the Rag GTPases bind raptor, are necessary and sufficient to mediate amino acid signaling to mTORC1, and mediate the amino acid–induced relocalization of mTOR within the endomembrane system of the cell. Given the prevalence of cancer-linked mutations in the pathways that control mTORC1 (*1*), it is possible that Rag function is also deregulated in human tumors.

References and Notes

1. D. A. Guertin, D. M. Sabatini, *Cancer Cell* **12**, 9 (2007).
2. D. D. Sarbassov, S. M. Ali, D. M. Sabatini, *Curr. Opin. Cell Biol.* **17**, 596 (2005).
3. M. P. Byfield, J. T. Murray, J. M. Backer, *J. Biol. Chem.* **280**, 33076 (2005).
4. T. Nobukuni *et al.*, *Proc. Natl. Acad. Sci. U.S.A.* **102**, 14238 (2005).
5. E. M. Smith, S. G. Finn, A. R. Tee, G. J. Browne, C. G. Proud, *J. Biol. Chem.* **280**, 18717 (2005).
6. Materials and methods are available as supporting material on *Science* Online.
7. D.-H. Kim *et al.*, *Cell* **110**, 163 (2002).
8. R. Loewith *et al.*, *Mol. Cell* **10**, 457 (2002).
9. K. P. Wedaman *et al.*, *Mol. Biol. Cell* **14**, 1204 (2003).
10. K. Hara *et al.*, *Cell* **110**, 177 (2002).
11. M. Bun-Ya, S. Harashima, Y. Oshima, *Mol. Cell. Biol.* **12**, 2958 (1992).
12. A. Schurmann, A. Brauers, S. Massmann, W. Becker, H. G. Joost, *J. Biol. Chem.* **270**, 28982 (1995).
13. E. Hirose, N. Nakashima, T. Sekiguchi, T. Nishimoto, *J. Cell Sci.* **111**, 11 (1998).
14. N. Nakashima, E. Noguchi, T. Nishimoto, *Genetics* **152**, 853 (1999).
15. T. Sekiguchi, E. Hirose, N. Nakashima, M. Ii, T. Nishimoto, *J. Biol. Chem.* **276**, 7246 (2001).
16. M. Gao, C. A. Kaiser, *Nat. Cell Biol.* **8**, 657 (2006).
17. F. Dubouloz, O. Deloche, V. Wanke, E. Cameroni, C. De Virgilio, *Mol. Cell* **19**, 15 (2005).
18. J. B. Kunz, H. Schwarz, A. Mayer, *J. Biol. Chem.* **279**, 9987 (2004).
19. K. J. Roberg, N. Rowley, C. A. Kaiser, *J. Cell Biol.* **137**, 1469 (1997).
20. E. J. Chen, C. A. Kaiser, *J. Cell Biol.* **161**, 333 (2003).
21. A. Beugnet, A. R. Tee, P. M. Taylor, C. G. Proud, *Biochem. J.* **372**, 555 (2003).
22. G. R. Christie, E. Hajduch, H. S. Hundal, C. G. Proud, P. M. Taylor, *J. Biol. Chem.* **277**, 9952 (2002).
23. D. J. Price, R. A. Nemenoff, J. Avruch, *J. Biol. Chem.* **264**, 13825 (1989).
24. Y. Sancak *et al.*, *Mol. Cell* **25**, 903 (2007).
25. X. Long, Y. Lin, S. Ortiz-Vega, K. Yonezawa, J. Avruch, *Curr. Biol.* **15**, 702 (2005).
26. R. M. Drenan, X. Liu, P. G. Bertram, X. F. Zheng, *J. Biol. Chem.* **279**, 772 (2004).
27. M. Mavrakis, J. Lippincott-Schwartz, C. A. Stratakis, I. Bossis, *Autophagy* **3**, 151 (2007).
28. K. Saito, Y. Araki, K. Kontani, H. Nishina, T. Katada, *J. Biochem.* **137**, 423 (2005).
29. C. Buerger, B. DeVries, V. Stambolic, *Biochem. Biophys. Res. Commun.* **344**, 869 (2006).

30. Supported by grants from the NIH (R01 CA103866 and AI47389), Department of Defense (W81XWH-07-0448), and W.M. Keck Foundation to D.M.S. as well as an EMBO fellowship to Y.D.S. We thank T. Kang for the preparation of FLAG-raptor and members of the Sabatini lab for helpful suggestions.

Supporting Online Material

www.sciencemag.org/cgi/content/full/1157535/DC1
Materials and Methods
Figs. S1 to S12
References

10 March 2008; accepted 13 May 2008
Published online 22 May 2008;
10.1126/science.1157535
Include this information when citing this paper.

THE JOURNAL OF BIOLOGICAL CHEMISTRY VOL. 284, NO. 12, pp. 8023–8032, March 20, 2009

An ATP-competitive Mammalian Target of Rapamycin Inhibitor Reveals Rapamycin-resistant Functions of mTORC1*[S]

Received for publication, January 15, 2009 Published, JBC Papers in Press, January 15, 2009, DOI 10.1074/jbc.M900301200

Carson C. Thoreen[‡§], Seong A. Kang[‡§], Jae Won Chang[¶], Qingsong Liu[¶], Jianming Zhang[¶], Yi Gao[‖], Laurie J. Reichling[‖], Taebo Sim[¶], David M. Sabatini[‡§1], and Nathanael S. Gray[¶2]**

*From the [‡]Whitehead Institute for Biomedical Research, Cambridge, Massachusetts 02142, [§]Howard Hughes Medical Institute, Department of Biology and **Koch Center for Integrative Cancer Research, Massachusetts Institute of Technology, Cambridge, Massachusetts 02139, [¶]Department of Cancer Biology, Dana Farber Cancer Institute, Department of Biological Chemistry and Molecular Pharmacology, Harvard Medical School, Boston, Massachusetts 02115, and [‖]Invitrogen Corporation, Madison, Wisconsin 53719*

The mammalian target of rapamycin (mTOR) kinase is the catalytic subunit of two functionally distinct complexes, mTORC1 and mTORC2, that coordinately promote cell growth, proliferation, and survival. Rapamycin is a potent allosteric mTORC1 inhibitor with clinical applications as an immunosuppressant and anti-cancer agent. Here we find that Torin1, a highly potent and selective ATP-competitive mTOR inhibitor that directly inhibits both complexes, impairs cell growth and proliferation to a far greater degree than rapamycin. Surprisingly, these effects are independent of mTORC2 inhibition and are instead because of suppression of rapamycin-resistant functions of mTORC1 that are necessary for cap-dependent translation and suppression of autophagy. These effects are at least partly mediated by mTORC1-dependent and rapamycin-resistant phosphorylation of 4E-BP1. Our findings challenge the assumption that rapamycin completely inhibits mTORC1 and indicate that direct inhibitors of mTORC1 kinase activity may be more successful than rapamycin at inhibiting tumors that depend on mTORC1.

The mammalian target of rapamycin (mTOR)[3] pathway is considered a major regulator of cell growth. The mTOR serine/threonine kinase is the founding component of the pathway and the catalytic subunit of two functionally distinct protein complexes, mTORC1 and mTORC2. mTORC1 contains the large protein Raptor, as well as mLST8/GβL and PRAS40, whereas mTORC2 is defined by the protein Rictor and also includes Sin1, Protor, and mLST8/GβL (1). Growth factors, such as insulin and IGF, activate both complexes, and they are important downstream effectors of the PI3K/PTEN signaling network (2). Additionally, the availability of nutrients, like amino acids and glucose, regulates mTORC1.

Many insights into mTOR signaling have come from investigations into the mechanism of action of rapamycin, a bacterially produced macrolide inhibitor of mTOR that has diverse clinical applications as an anti-fungal, immunosuppressant, and anti-cancer drug (3). Rapamycin acts through an unusual allosteric mechanism that requires binding to its intracellular receptor, FKBP12, for inhibition of its target. Under acute treatment, rapamycin is thought to selectively inhibit mTORC1, which is often referred to as the rapamycin-sensitive complex. Conversely, mTORC2 is considered rapamycin-insensitive, although its assembly can be inhibited by prolonged rapamycin treatment in some cell types (4). Because of its perceived potency and selectivity, rapamycin is commonly used in research experiments as a test of the involvement of mTORC1 in a particular process.

Two downstream mTORC1 substrates that were identified, in part, by their sensitivity to rapamycin are the S6 kinases (S6K1 and S6K2) and the translational inhibitor 4E-BP1. Both proteins mediate important links between mTORC1 and the cell growth machinery, largely through their influence on cap-dependent translation (reviewed in Ref. 5). All nuclear-encoded mRNAs possess a 5′,7-methyl guanosine cap, which is recognized and bound by the small protein eIF-4E. Under growth-promoting conditions, eIF-4E also associates with the large

* This work was supported, in whole or in part, by National Institutes of Health Grants R01 AI47389 and R01 CA103866. This work was also supported by start-up funding from the Dana Farber Cancer Institute, the Barr Foundation, and the Damon Runyon Cancer Research Foundation (to N. S. G.), Keck Foundation, LAM Foundation, and Department of Defense Grant W81XWH-07-1-0448 (to D. M. S.), and a fellowship from the American Cancer Society (to S. A. K.). The costs of publication of this article were defrayed in part by the payment of page charges. This article must therefore be hereby marked "*advertisement*" in accordance with 18 U.S.C. Section 1734 solely to indicate this fact.

[S] The on-line version of this article (available at http://www.jbc.org) contains supplemental Experimental Procedures, Figs. S1–S5, and an additional reference.

[1] To whom correspondence may be addressed: Whitehead Institute, 9 Cambridge Center, Cambridge, MA 02142. Tel.: 617-258-6407; Fax: 617-258-5213; E-mail: sabatini@wi.mit.edu.

[2] To whom correspondence may be addressed: Dept. of Biological Chemistry and Molecular Pharmacology, Harvard Medical School, 250 Longwood Ave., Boston, MA 02115. Tel.: 617-582-8590; Fax: 617-582-8615; E-mail: Nathanael_Gray@dfci.harvard.edu.

[3] The abbreviations used are: mTOR, mammalian target of rapamycin; Raptor, regulatory associated protein of mTOR; Rictor, rapamycin-insensitive companion of mTOR; PI3K, phosphatidylinositol 3-kinase; LC3, light chain 3; 4E-BP1, eIF4E-binding protein 1; eIF4E, eukaryotic initiation factor 4E; GβL, G-β subunit-like; MEF, mouse embryonic fibroblast; mTORC1, mTOR complex 1; mTORC2, mTOR complex 2; HEK, human embryonic kidney; DMSO, dimethyl sulfoxide; CHAPS, 3-[(3-cholamidopropyl)dimethylammonio]-1-propanesulfonic acid; ATM, ataxia telangiectasia, mutated; PI, phosphatidylinositol; BSA, bovine serum albumin; PBS, phosphate-buffered saline; shRNA, short hairpin RNA.

scaffolding protein eIF-4G, the eIF-4A helicase, and the eIF-4B regulatory protein, together forming the eIF-4F complex. This complex, in conjunction with the eIF3 preinitiation complex, delivers the mRNA to the 40 S ribosomal subunit and primes the translational apparatus. 4E-BP1 interferes with this process by binding to eIF-4E and preventing the formation of a functional eIF-4F complex. However, its ability to do this is blocked by phosphorylation at four sites, two of which are considered rapamycin-sensitive. S6K1 also plays a role in regulating translational initiation by phosphorylating the S6 protein of the 40 S ribosomal subunit and by stimulating eIF-4A helicase activity (6–8).

Despite the connections of mTORC1 to the translational machinery, the effects of rapamycin on mammalian cell growth and proliferation are, oddly, less severe than its effects in yeast. In *Saccharomyces cerevisiae*, rapamycin treatment induces a starvation-like state that includes a severe G_1/S cell cycle arrest and suppression of translation initiation to levels below 20% of nontreated cells (9). Moreover, in yeast rapamycin strongly promotes induction of autophagy (self-eating), a process by which cells consume cytoplasmic proteins, ribosomes, and organelles, such as mitochondria, to maintain a sufficient supply of amino acids and other nutrients (10).

The effects of rapamycin in mammalian cells are similar to those in yeast, but typically much less dramatic and highly dependent on cell type. For instance, rapamycin only causes cell cycle arrest in a limited number of cell types and has modest effects on protein synthesis (11–13). Moreover, rapamycin is a relatively poor inducer of autophagy, and it is often used in combination with LY294002, an inhibitor of PI3K and mTOR (14). These inconsistent effects may explain why, despite high expectations, rapamycin has had only limited success as a clinical anti-cancer therapeutic. We have hypothesized that the effectiveness of rapamycin against a particular cancer might be determined by its ability to inhibit mTORC2 in addition to mTORC1 (15). To test this hypothesis, we developed the ATP-competitive inhibitor Torin1 that suppresses both complexes. In contrast to rapamycin, Torin1 treatment recapitulates in mammalian cells many of the phenotypes caused by TOR inhibition in yeast. Surprisingly, however, we find that these effects are independent of mTORC2 and are instead caused by inhibition of rapamycin-resistant functions of mTORC1.

EXPERIMENTAL PROCEDURES

Materials—Reagents were obtained from the following sources: antibodies to phospho-Thr-389 S6K, phospho-Ser-473 Akt, phospho-Thr-308 Akt, pan-Akt, phospho-Thr-36/47 4E-BP1, phospho-Ser-65 4E-BP1, phospho-Thr-70 4E-BP1, 4E-BP1, α-tubulin, Raptor, eIF-4E, phospho-S51 eIF2α, cyclin D1, cyclin D3 and p27/Kip1 from Cell Signaling Technology (note: we have not confirmed that the phospho-Thr-70 4E-BP1 antibody does not detect unphosphorylated 4E-BP1); antibodies to mTOR, S6K, and horseradish peroxidase-labeled anti-mouse, anti-goat, and anti-rabbit secondary antibodies from Santa Cruz Biotechnology; anti-Rictor antibodies from Bethyl Laboratories; FuGENE 6 and Complete Protease Mixture from Roche Applied Science; FLAG M2 antibody, FLAG M2-agarose, and ATP from Sigma; 7-methyl-GTP-Sepharose from GE Healthcare; PI-103 from Calbiochem; NVP-BEZ235 from Axon Medchem; rapamycin from LC Laboratories; PI3K-α from Millipore/Upstate; CellTiter-Glo, DNA-PK, and DNA-PK peptide substrate from Promega; phosphatidylinositol and phosphatidylserine from Avanti Polar Lipids; EasyTag^{TM} EXPRESS ^{35}S protein labeling mix and ATP [γ-^{32}P] EasyTide from PerkinElmer Life Sciences; Dulbecco's modified Eagle's medium from SAFC Biosciences; inactivated fetal calf serum from Invitrogen. p53$^{-/-}$/TSC2$^{-/-}$ MEFs as well as p53$^{-/-}$/TSC2$^{+/+}$ MEFs were kindly provided by David Kwiatkowski (Harvard Medical School) and cultured in Dulbecco's modified Eagle's medium with 10% inactivated fetal calf serum. p53$^{-/-}$/mLST8$^{-/-}$ and p53$^{-/-}$/Rictor$^{-/-}$ MEFs have been described (16). Torin1 was synthesized and purified in the Gray Laboratory and is available upon request.

Cell Lysis—Cells rinsed once with ice-cold PBS were lysed in ice-cold lysis buffer (40 mM HEPES, pH 7.4, 2 mM EDTA, 10 mM pyrophosphate, 10 mM glycerophosphate, and 0.3% CHAPS or 1% Triton X-100, and 1 tablet of EDTA-free protease inhibitors per 25 ml). The soluble fractions of cell lysates were isolated by centrifugation at 13,000 rpm for 10 min in a microcentrifuge.

Mammalian Lentiviral shRNAs—All shRNA vectors were obtained from the collection of The RNAi Consortium at the Broad Institute (17). These shRNAs are named with the numbers found at the RNAi Consortium public website: mouse Raptor shRNA, TRCN0000077472, NM_028898.1-3729s1c1; and mouse Rictor shRNA, TRCT0000037708, NM_030168.2-867s1c1. shRNA-encoding plasmids were co-transfected with the Δ VPR envelope and vesicular stomatitis virus G packaging plasmids into actively growing HEK-293T using FuGENE 6 transfection reagent as described previously (18, 19). Virus-containing supernatants were collected at 48 h after transfection and filtered to eliminate cells, and target cells were infected in the presence of 8 μg/ml Polybrene. 24 h later, cells were selected with puromycin and analyzed on the 4th day after infection.

Metabolic Labeling—Cells were seeded in 6-well plates and grown overnight. Cells were then treated with appropriate compounds for 2.5 h, washed one time with cysteine/methionine-free Dulbecco's modified Eagle's medium, and then incubated in 2 ml of cysteine/methionine-free Dulbecco's modified Eagle's medium, 10% dialyzed inactivated fetal calf serum, compound, and 165 μCi (15 μl, 11 mCi/μl) of EasyTag^{TM} EXPRESS ^{35}S protein labeling mix. After 30 min, cells were lysed, and soluble fractions were isolated by centrifugation at 13,000 rpm for 10 min. To precipitate protein, lysates were spotted on Whatman filter paper, precipitated with 5% trichloroacetic acid, washed two times for 5 min in cold 10% trichloroacetic acid, washed two times for 2 min in cold ethanol, washed one time for 2 min in acetone, and air-dried at room temperature. The amount of ^{35}S incorporated into protein was measured using a Beckman LS6500 Scintillation Counter.

mTORC1 and mTORC2 in Vitro Kinase Assays—To produce soluble mTORC1, we generated HEK-293T cell lines that stably express N-terminally FLAG-tagged Raptor using vesicular stomatitis virus G-pseudotyped MSCV retrovirus. For mTORC2, we similarly generated HeLa cells that stably express N-terminally FLAG-tagged Protor-1. Both complexes were purified by

lysing cells in 50 mM HEPES, pH 7.4, 10 mM sodium pyrophosphate, 10 mM sodium β-glycerophosphate, 100 mM NaCl, 2 mM EDTA, 0.3% CHAPS. Cells were lysed at 4 °C for 30 min, and the insoluble fraction was removed by microcentrifugation at 13,000 rpm for 10 min. Supernatants were incubated with FLAG-M2 monoclonal antibody-agarose for 1 h and then washed three times with lysis buffer and once with lysis buffer containing a final concentration of 0.5 M NaCl. Purified mTORC1 was eluted with 100 μg/ml 3× FLAG peptide in 50 mM HEPES, pH 7.4, 100 mM NaCl. Eluate can be aliquoted and stored at −80 °C. Substrates S6K1 and Akt1 were purified as described previously (16, 20). Kinase assays were performed for 20 min at 30 °C in a final volume of 20 μl consisting of the kinase buffer (25 mM HEPES, pH 7.4, 50 mM KCl, 10 mM $MgCl_2$, 500 μM ATP) and 150 ng of inactive S6K1 or Akt1 as substrates. Reactions were stopped by the addition of 80 μl of sample buffer and boiled for 5 min. Samples were subsequently analyzed by SDS-PAGE and immunoblotting.

PI3K and hVps34 Assays—Cellular IC_{50} values for PI3Kα were determined using $p53^{-/-}$/$mLST8^{-/-}$ MEFs. Cells were treated with vehicle or increasing concentrations of compound for 1 h and then lysed. Phosphorylation of Akt Thr-308 was monitored by immunoblotting using a phospho-specific antibody. *In vitro* IC_{50} values for PI3Kα were determined as described previously (21). Briefly, chloroform stocks of phosphatidylinositol (PI) and phosphatidylserine were combined in equimolar ratios, dried under nitrogen gas, resuspended in 50 mM HEPES, pH 7.4, 100 mM KCl, sonicated to clarity using a bath sonicator, and aliquoted and stored at −80 °C. For kinase assays, purified PI3Kα was combined with 100 μM phosphatidylserine/phosphatidylinositol, compound, and 10 μCi of [γ-^{32}P]ATP (100 μM final concentration) in kinase buffer and incubated at 37 °C for 20 min. Reactions were stopped with 1 N HCl. Lipid was extracted with a 1:1 mixture of chloroform: methanol and separated on silica TLC plates. ^{32}P-Labeled phosphatidylinositol 3-phosphate was quantitated by PhosphorImager. hVps34 was purified as a glutathione *S*-transferase fusion protein from HEK-293T cells(22) and assayed using the same procedure.

ATM and DNA-PK—For DNA-PK kinase assays, purified DNA-PK was combined with DNA-PK peptide substrate (derived from the N-terminal sequence of p53), compound, and 10 μCi/reaction [γ-^{32}P]ATP (100 μM final concentration) in kinase buffer and incubated for 10 min at 37 °C. Reactions were stopped with 1 N HCl and spotted onto P81 phosphocellulose squares. P81 squares were washed three times for 5 min in 0.75% phosphoric acid, and one time for 5 min in acetone, dried, and measured by scintillation counter. ATM *in vitro* kinase assays were performed according to previously published protocols (21).

Cell Size Determinations—Cells were seeded in 10-cm culture dishes, grown overnight, and subjected to appropriate treatment. 24 h later, cells were harvested by trypsinization in a 5-ml volume, diluted 1:20 with counting solution (Isoton II Diluent, Beckman Coulter), and cell diameters determined using a particle size counter (Coulter Z2, Beckman Coulter) with Coulter Z2 AccuComp software.

Cell Proliferation/Viability Assay—Cell viability was assessed with the CellTiter-Glo Luminescent Cell Viability Assay. On Day 0, 96-well plates were seeded with 500 cells per well and grown overnight. On Day 1, cells were treated with the appropriate compounds and subsequently analyzed on Days 3–5. For analysis, plates were incubated for 60 min at room temperature; 50 μl of CellTiter-Glo reagent was added to each well, and plates were mixed on an orbital shaker for 12 min. Luminescence was quantified on a standard plate luminometer.

Cell Cycle Analysis—Cells were seeded in 15-cm plates and grown overnight. Cells were then subjected to the appropriate treatment for 48 h and then trypsinized, washed twice in PBS + 2% FBS, and then fixed overnight at 4 °C in ethanol. Cells were then washed three times in PBS + 1% BSA and incubated in PBS, 1% BSA, 50 μg/ml propidium iodide, and 100 μg/ml RNase at 37 °C for 30 min. Cells were then washed 1× in PBS + 1% BSA, resuspended in 1 ml PBS, and analyzed using a FACSCalibur flow cytometer (BD Biosciences). Cell cycle distribution was determined using the ModFit LT software package.

RESULTS

Torin1 Is a Potent and Selective mTOR Inhibitor—To identify small molecule ATP-competitive inhibitors of mTOR, we conducted a biochemical screen for inhibitors of mTOR kinase activity in a library of heterocyclic chemical compounds. From this screen, we identified a lead compound that was further elaborated through a medicinal chemistry effort to produce Torin1, a member of the pyridinonequinoline class of kinase inhibitors.[4] In *in vitro* kinase assays using immuno-purified mTORC1 or mTORC2, Torin1 inhibits both mTOR-containing complexes with IC_{50} values between 2 and 10 nM (Fig. 1*A*) and acts through an ATP-competitive mechanism (Fig. 1*B*). We also measured the potency of Torin1 in cells. MEFs were treated with increasing amounts of Torin1 or the dual mTOR/PI3K inhibitors PI-103 and NVP-BEZ235, and the activity of each complex was determined by monitoring the phosphorylation status of S6K at Thr-389 and Akt at Ser-473, mTORC1 and mTORC2 substrates, respectively (Fig. 1*C*). As *in vitro*, the IC_{50} for Torin1 in cells is also between 2 and 10 nM. Unlike rapamycin, Torin1 had no effect on the stability of either mTORC1 or mTORC2.

We next determined the selectivity of Torin1 for mTOR over other kinases. Because mTOR belongs to the PI3K-like kinase family, a family of protein kinases that is defined by a high degree of homology to PI3K within the catalytic domain, many inhibitors of PI3K, such as wortmannin, LY294002, PI-103, and BEZ-235, are also reasonable mTOR inhibitors (21, 23, 24). To measure PI3K inhibition in cells, we made use of the observation that the phosphorylation of Akt at Thr-308 depends on two processes that directly reflect PI3K activity: phosphatidylinositol 3,4,5-triphosphate-dependent targeting of Akt to the plasma membrane and activation of PDK1, the kinase that directly phosphorylates this site. In wild-type cells, phosphorylation of Thr-308 is also influenced by phosphorylation at Ser-473 (19, 25, 26). To remove this latter variable, we tested compounds in MEFs where mLST8, an essential mTORC2

[4] N. S. Gray, manuscript in preparation.

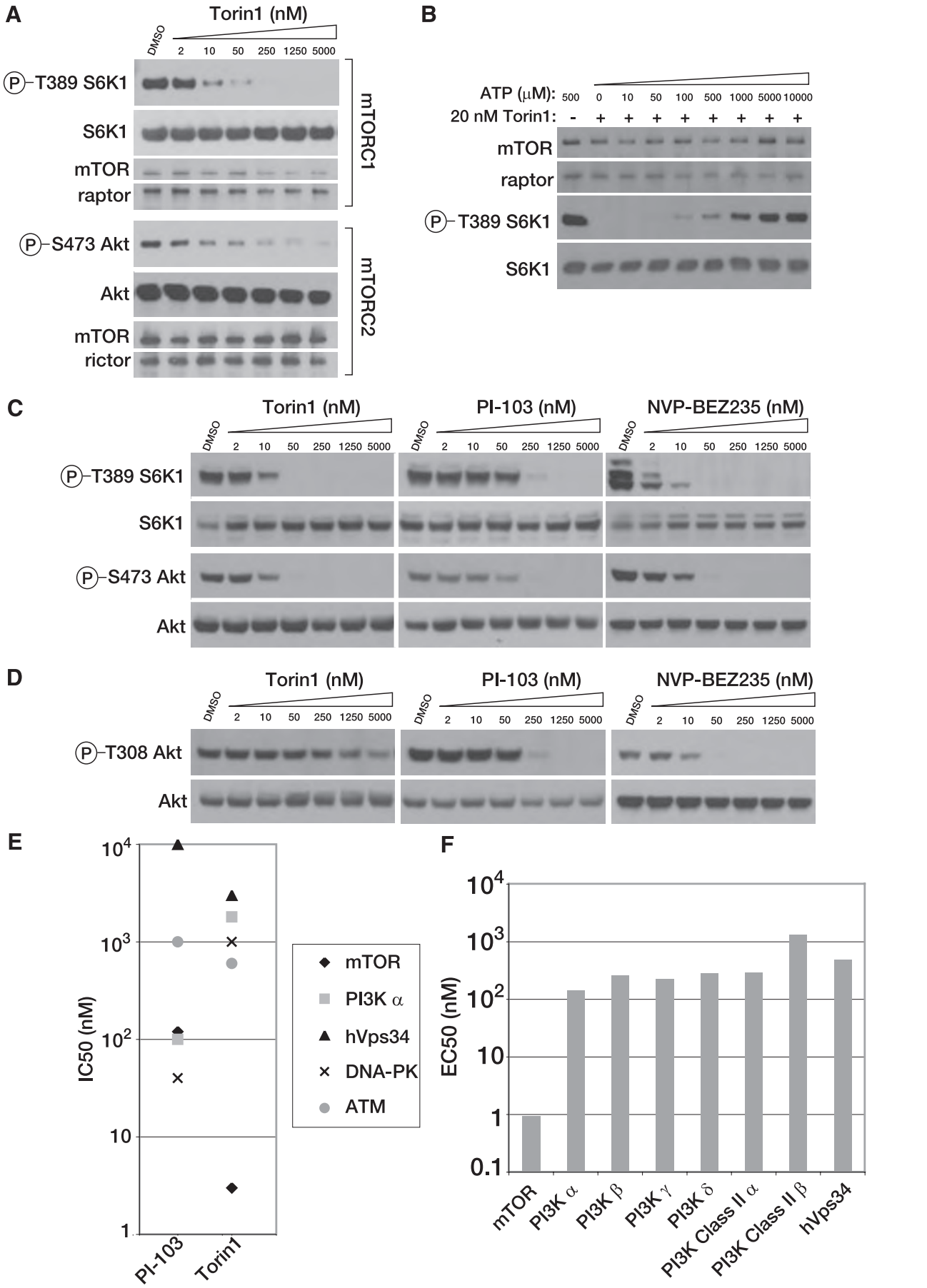

component, is deleted and Akt Ser-473 is constitutively dephosphorylated. Because Ser-473 is fixed in a single state in these cell lines, phosphorylation at Thr-308 only reflects PI3K activity. Using this system, we determined the cellular IC_{50} of Torin1 for PI3K to be ~1.8 μM (Fig. 1*D*), nearly identical to our *in vitro* measurement of the IC_{50} for PI3Kα (Fig. 1*E*). We also profiled our compound against other PI3K isoforms using the Adapta *in vitro* assay method, which confirmed a high degree of selectivity for mTOR (Fig. 1*F*).

Compounds that inhibit PI3K and mTOR also have the potential to inhibit other PI3K-like kinases, including the DNA-damage response kinases ATM and DNA-PK. For DNA-PK and ATM, we measured the IC_{50} of Torin1 using *in vitro* assays (Fig. 1*E*). We also measured inhibition of the Class III PI3K hVps34. Some reports have proposed that hVps34 acts upstream of mTORC1, and we wanted to be sure that cross-reactivity with this kinase was not indirectly influencing mTORC1 activity in cells (22). Torin1 was at least 200-fold selective for mTOR over each of these kinases. Finally, we screened Torin1 at a concentration of 10 μM against a panel of 353 diverse kinases using the Ambit Biosciences KinomeScan screening platform, which measures the relative binding of the target molecule to each kinase, and we found no indication of significant off-target effects (data shown in supplemental material). These results suggest that Torin1 is a highly selective inhibitor of mTOR when profiled against an extensive panel of serine/threonine, tyrosine, and lipid kinases.

Torin1 Causes Cell Cycle Arrest through a Rapamycin-resistant Mechanism That Is Also Independent of mTORC2—Our next goal was to test the role of mTOR signaling in normally growing cells. Rapamycin-mediated mTORC1 inhibition slows cell proliferation and reduces cell size, and so we suspected that dual mTORC1/2 inhibition would have similar but more severe effects (22). Indeed, wild-type MEFs treated with up to 500 nM rapamycin continued to proliferate, albeit at a reduced rate (Fig. 2*A* and supplemental Fig. S2). In contrast, 250 nM Torin1 completely inhibited proliferation (Fig. 2*A* and supplemental Fig. S2) and caused a G_1/S cell cycle arrest (Fig. 2*B*). Moreover, 250 nM Torin1 decreased cell size to a greater degree than 50 nM rapamycin (Fig. 2*C*). Based on the assumption that rapamycin completely disables mTORC1 kinase activity, we hypothesized that the enhanced effect of Torin1 was because of mTORC2 inhibition.

To test this hypothesis, we conducted identical experiments using MEFs that lack mTORC2 activity because Rictor has been deleted (16). We reasoned that Torin1 should have the same effect as rapamycin on the proliferation and growth of these cells because mTORC2 is already inhibited. As in wild-type MEFs, rapamycin reduced but did not prevent proliferation (Fig. 2*D*). However, we were surprised to find that Torin1 continued to dramatically suppress proliferation and diminish cell size (Fig. 2, *D–F*), indicating that the differential effects of this compound with respect to rapamycin were not due to mTORC2 inhibition. Thus, mTOR has functions that are absolutely required for cell growth and proliferation and that are kinase-dependent, rapamycin-resistant, and independent of mTORC2.

Torin1 Disrupts mTORC1-dependent Phenotypes More Completely than Rapamycin—Despite the widely held assumption to the contrary, one explanation for our results is that rapamycin inhibits some but not all of the functions of mTORC1. To explore this possibility, we examined the effects of Torin1 on other processes besides growth and proliferation that are commonly associated with mTORC1 signaling. One such process is macroautophagy, often referred to simply as autophagy. Normally considered a response to starvation conditions, autophagy involves the formation of large double-membrane enclosed vesicles that engulf cytoplasmic contents, including both proteins and organelles (reviewed in Ref. 27). These vesicles then fuse with lysosomes to form autophagosomes that digest their contents, providing the cell with a source of amino acids and other nutrients when these are not available from the environment.

In yeast, rapamycin is a potent activator of autophagy (10). The situation is less clear in mammalian systems, where rapamycin alone is, at best, an inconsistent activator of autophagy and frequently requires combination with other PI3K/mTOR inhibitors, such as LY294002, or concomitant starvation for nutrients. We suspected that autophagy might also be regulated in part by rapamycin-resistant functions of mTORC1. A commonly used marker of autophagy is the protein light chain 3 (LC3), which translocates from the cytoplasm to autophagosomes where it is degraded when autophagy is induced (28). Using a green fluorescent protein-tagged LC3 construct, we found that Torin1 causes a strong re-localization of LC3 from the cytoplasm to autophagosomes in both wild-type and Rictor$^{-/-}$ MEFs, whereas rapamycin caused only a minor change (Fig. 3*A*). Furthermore, we found that Torin1 treatment, like amino acid starvation, causes degradation of LC3B (LC3B-I) and transient accumulation of the faster running lipidated form (LC3B-II) in both MEFs and HeLa cells (Fig. 3*B* and supplemental Fig. S4*A*). An RNA interference-induced decrease in Raptor

FIGURE 1. **Torin1 is a potent and selective mTOR inhibitor.** *A,* Torin1 inhibits mTORC1 and mTORC2 *in vitro*. mTORC1 and mTORC2 were purified from HEK-293T stably expressing FLAG-Raptor and HeLa cells expressing FLAG-Protor-1, respectively. Following FLAG purification, each complex was subjected to *in vitro* kinase assays using S6K1 as a substrate for mTORC1 and Akt1 as a substrate for mTORC2. Assays were then analyzed by immunoblotting for the indicated proteins and phosphorylation states. *B,* Torin1 is an ATP-competitive inhibitor. The *in vitro* kinase activity of purified mTORC1 toward S6K1 was assayed in the presence of 20 nM Torin1 and increasing concentrations of ATP, as indicated. Assays were then analyzed by immunoblotting for the indicated proteins and phosphorylation states. *C,* Torin1 is a potent mTORC1 and mTORC2 inhibitor in cells. MEFs (p53$^{-/-}$) were treated with increasing concentrations of Torin1 or dual mTOR/PI3K inhibitors PI-103 and BEZ-235 for 1 h and then analyzed by immunoblotting for the indicated proteins and phosphorylation states. *D,* Torin1 has little effect on PI3K at concentrations where mTOR is completely inhibited. The experiment was performed as in *C* using mLST8-null MEFs and phosphorylation of Akt at Thr-308 was determined by immunoblotting. In mLST8-null MEFs, mTORC2 is inactive and Akt Ser-473 is constitutively dephosphorylated and so PDK1-mediated phosphorylation of Thr-308 only reflects PI3K activity. *E,* Torin1 is selective for mTOR over related kinases. IC_{50} values for Torin1 were determined using *in vitro* kinase assays for mTOR (3 nM), hVps34 (3 μM), PI3K-α (1.8 μM), DNA-PK (1.0 μM), and ATM (0.6 μM). IC_{50} values for PI-103 for mTOR (120 nM), PI3K-α (100 nM), DNA-PK (40 nM) were determined by the same assays. IC_{50} values for PI-103 for hVps34 (10 μM) and ATM (1.0 μM) were determined previously (21). *F,* Torin1 is selective for mTOR over other PI3K isoforms. EC_{50} values were determined for the indicated PI3K isoforms using the Invitrogen Adapta platform. The EC_{50} for mTOR was determined using the cell-based LanthaScreen platform.

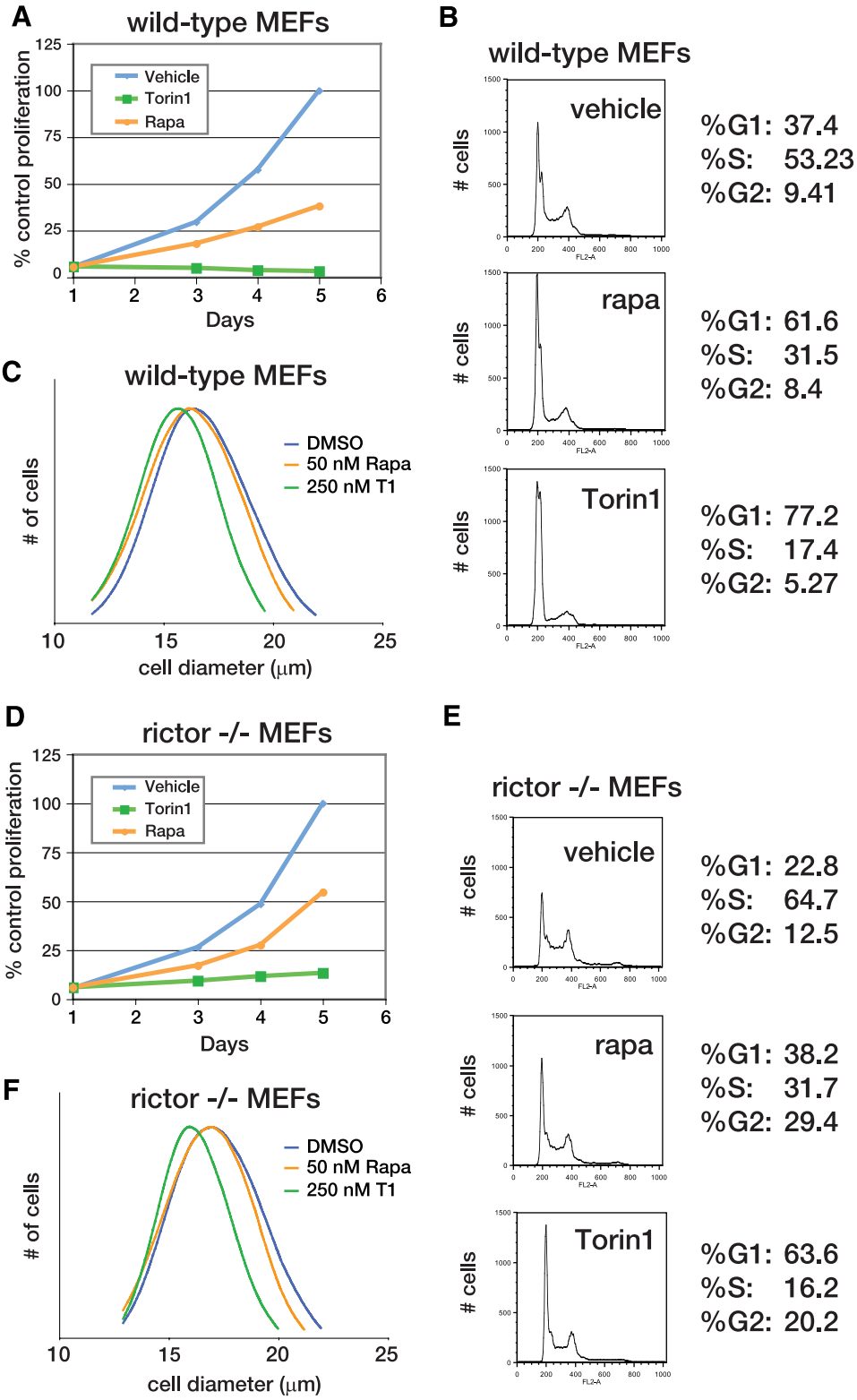

FIGURE 2. **mTOR inhibition prevents cell growth and proliferation through an mTORC2-independent mechanism.** *A*, mTOR inhibition by Torin1 but not rapamycin prevents the proliferation of wild-type MEFs. MEF ($p53^{-/-}$) cells were grown in the presence of vehicle (*blue*), 50 nM rapamycin (*orange*), or 250 nM Torin1 (*green*) for 4 days. Cell proliferation was measured in triplicate at indicated time points using the CellTiterGlo viability assay. *B*, Torin1 causes a G_1/S cell cycle arrest in wild-type MEFs. MEF ($p53^{-/-}$) cells were treated with vehicle (DMSO), 50 nM rapamycin (*rapa*), or 250 nM Torin1 for 48 h. Cells were then harvested, stained with propidium iodide, and analyzed by flow cytometry. *C*, normalized cell size distributions for Torin1 and rapamycin-treated wild-type MEFs. MEF ($p53^{-/-}$) cells were treated with vehicle (*blue*, mean 17.81 μm), 50 nM rapamycin (*orange*, mean 17.58), or 250 nM Torin1 (*green*, mean 16.46 μm) for 24 h. Cell sizes were measured using a particle counter and are displayed as a histogram. *D*, experiment was performed as in *A* using $Rictor^{-/-}$, $p53^{-/-}$ MEFs. *E*, experiment was performed as in *B* using $Rictor^{-/-}$, $p53^{-/-}$ MEFs. *F*, experiment was performed as in *C* using $Rictor^{-/-}$, $p53^{-/-}$ MEFs. Cells were treated with vehicle (*blue*, mean diameter 17.85 μm), 50 nM rapamycin (*orange*, mean diameter 17.33 μm), or 250 nM Torin1 (*green*, mean diameter 16.24 μm).

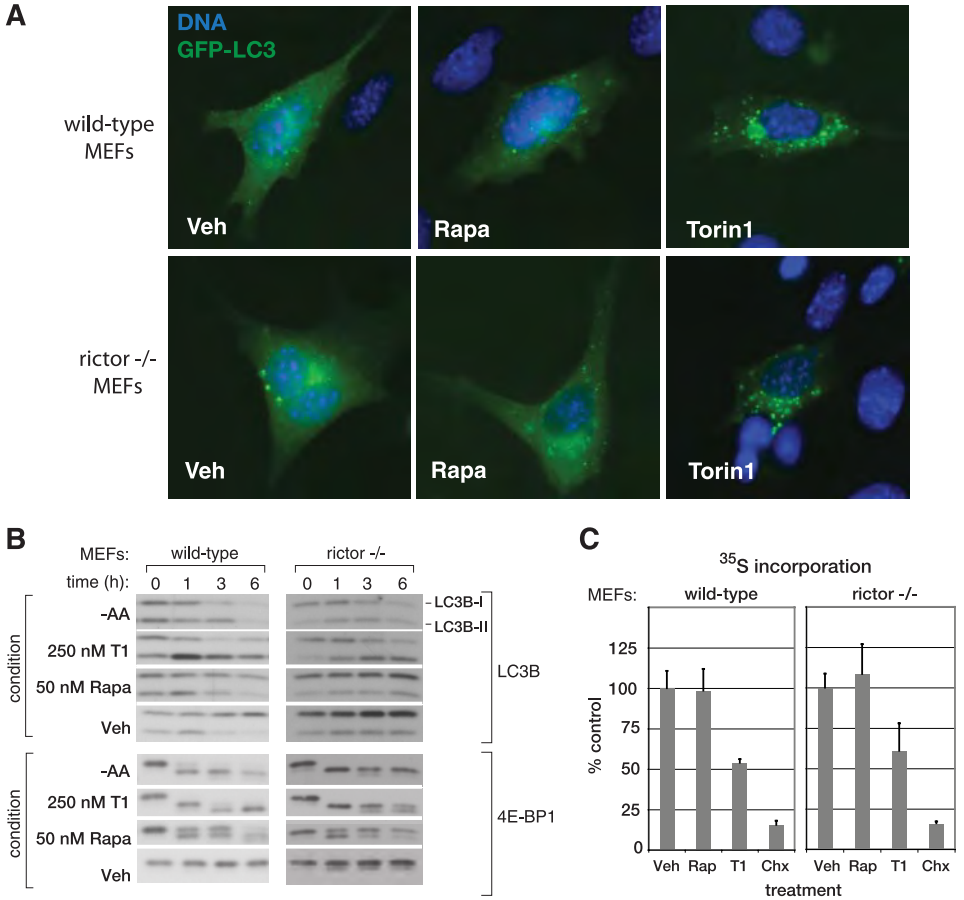

FIGURE 3. **Torin1 inhibits mTORC1-dependent processes that are resistant to rapamycin.** *A*, Torin1 but not rapamycin (*Rapa*) causes LC3 to relocalize from the cytoplasm to autophagosomes. Wild-type ($p53^{-/-}$) or Rictor-null ($p53^{-/-}$) MEFs were transiently transfected with GFP-LC3 and treated with vehicle (*Veh*) (DMSO), 50 nM rapamycin, or 250 nM Torin1 for 3 h before being fixed and processed. Cells were also stained with Hoechst to visualize nuclei and imaged at ×63. *B*, amino acid starvation and Torin1, but not rapamycin, cause LC3 degradation. Wild-type ($p53^{-/-}$) and Rictor-null ($p53^{-/-}$) MEFs were treated with vehicle (DMSO), 50 nM rapamycin, 250 nM Torin1 or grown in amino acid (*AA*)-free conditions for 0, 1, 3, or 6 h. Cells were lysed at the indicated time points and analyzed by immunoblotting. Induction of autophagy causes the degradation of the native LC3B (*LC3B-I*) protein and the transient accumulation of the faster running lipidated version (*LC3B-II*). *C*, Torin1 suppresses global protein synthesis through a rapamycin-resistant and mTORC2-independent process. Wild-type ($p53^{-/-}$) and Rictor-null ($p53^{-/-}$) MEFs were treated with vehicle (DMSO), 50 nM rapamycin (*Rap*), 250 nM Torin1, or 10 μg/ml cycloheximide (*Chx*) for 2.5 h and then pulsed with ^{35}S-labeled methionine and cysteine for 30 min. The amount of ^{35}S incorporation was determined by scintillation counting. Measurements were made in triplicate, and *error bars* indicate standard deviation.

expression affected LC3 in a similar fashion as Torin1 treatment (supplemental Fig. S4*B*). Collectively, these results suggest that mTORC1 inhibition is sufficient to induce autophagy. Although the signaling mechanisms that connect mTORC1 to autophagy are currently unclear, ATP-competitive inhibitors, like Torin1, will likely reveal specific roles for mTORC1 that have been missed because of their insensitivity to rapamycin.

The mTORC1 pathway also has many connections to the regulation of cap-dependent translation. However, rapamycin often has only modest effects on rates of protein synthesis. To test whether Torin1 might inhibit protein synthesis more completely, we metabolically labeled cells using ^{35}S methionine/cysteine in the presence of either Torin1 or rapamycin. Surprisingly, whereas rapamycin had very little effect, Torin1 caused a nearly 50% decline in total protein synthesis in both wild-type and Rictor$^{-/-}$ MEFs (Fig. 3*C*). As with autophagy, these results indicate that mTORC1 is a far more important regulator of protein synthesis than experiments with rapamycin have indicated.

Rapamycin-resistant Functions of mTORC1 Are Required for Cap-dependent Translation—Because known mTORC1 substrates, S6K and 4E-BP1, are important regulators of mRNA translation, we next considered whether either is involved in the transduction of mTORC1-dependent but rapamycin-resistant functions. S6K activity has been shown to be completely inhibited by rapamycin treatment, and therefore we considered it unlikely to be the target of any rapamycin-resistant activity of mTORC1. 4E-BP1, however, is subject to a more complex regulatory process. The ability of 4E-BP1 to bind and inhibit eIF-4E is primarily regulated by the phosphorylation of four residues: Thr-37, Thr-46, Ser-65, and Thr-70. Phosphorylation of Thr-37 and Thr-46 is thought to be a priming event that permits the phosphorylation of the other two, thereby promoting dissociation from eIF-4E and permitting the formation of a functional eIF-4F complex (29). mTORC1 has been implicated in the regulation of 4E-BP1, but there are conflicting accounts of the importance of this connection as well as the underlying mechanism. For instance, mTORC1 phosphorylates the Thr-37 and Thr-46 sites *in vitro*, but these sites are considered rapamycin-insensitive in cells (30–32). Conversely, mTORC1 has little effect *in vitro* on the phosphorylation of sites that are considered rapamycin-sensitive, Ser-65 and Thr-70. Moreover, a C-terminal motif in 4E-BP1, known as the TOR signaling motif and believed to mediate binding to mTORC1, and the N-terminal RAIP motif are required for phosphorylation of all sites (33–35). Finally, although rapamycin causes a substantial decrease in overall protein translation in some cell types (36), it has very little effect in others (13). A possible explanation is simply that rapamycin cannot completely inhibit mTORC1-dependent phosphorylation of 4E-BP1.

To test this hypothesis, we treated MEFs with increasing concentrations of either Torin1 or rapamycin and assessed the phosphorylation status of Thr-36, Thr-47, Ser-65, and Thr-70 by immunoblotting (Fig. 4*A*). Rapamycin completely prevented phosphorylation of S6K1 and caused a slight decrease in the phosphorylation of Ser-65 of 4E-BP1, but it had little effect on the phosphorylation of either Thr-37/46 or Thr-70 even at con-

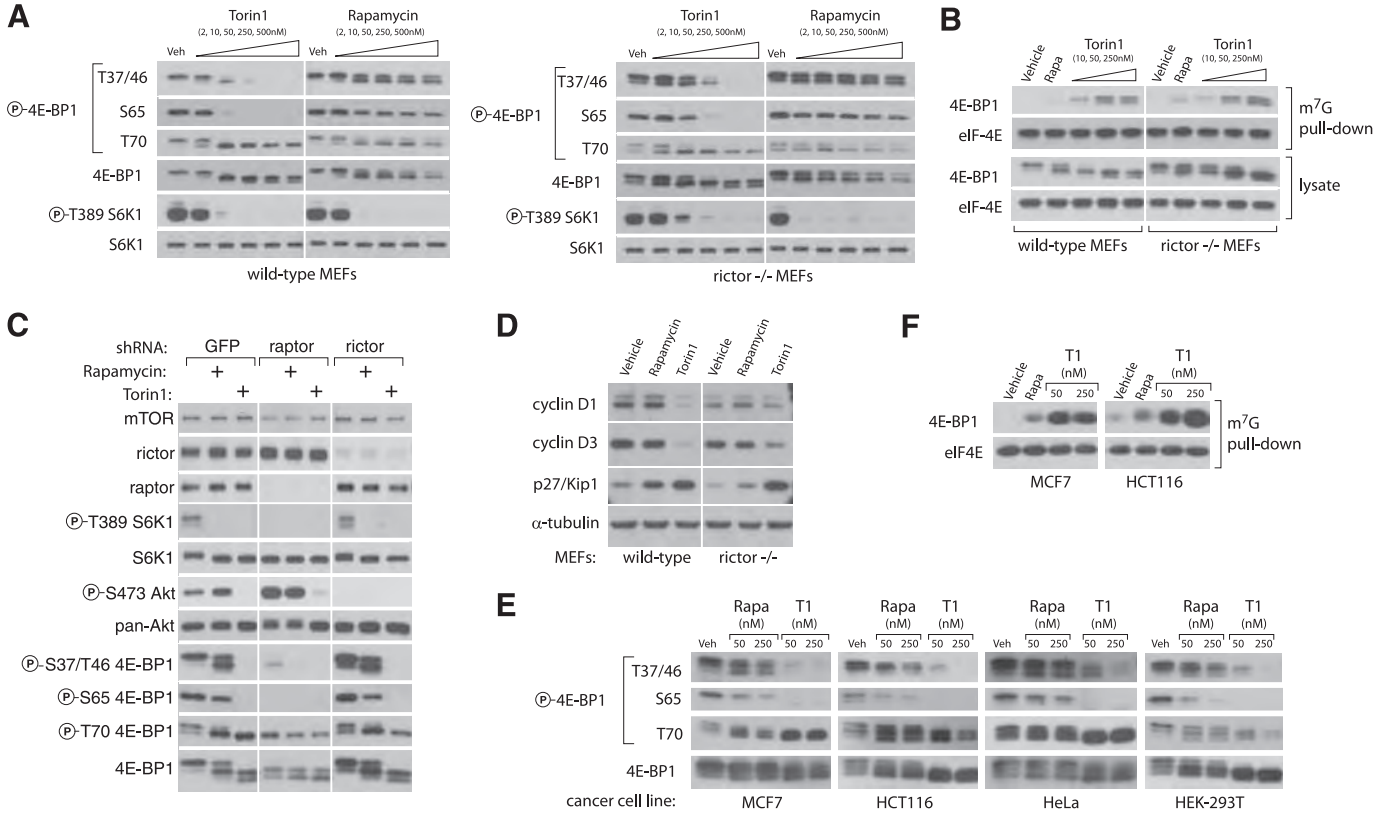

FIGURE 4. **mTORC1 regulation of 4E-BP1 phosphorylation and binding to eIF-4E reveals rapamycin-resistant functions.** *A,* phosphorylation of 4E-BP1 at Thr-37/46 and Ser-65 is dependent on mTORC1 but resistant to rapamycin. Wild-type ($p53^{-/-}$) and Rictor-null ($p53^{-/-}$) MEFs were treated with the indicated concentrations of Torin1 or rapamycin for 1 h and then lysed. Cell lysates were analyzed by immunoblot using antibodies specific for the indicated proteins or phosphorylation states. *B,* Torin1 increases the amount of 4E-BP1 bound to eIF-4E to a degree that far exceeds the effects of rapamycin. Wild-type ($p53^{-/-}$) and Rictor-null ($p53^{-/-}$) MEFs were treated with vehicle (DMSO), 50 nM rapamycin, or 250 nM Torin1 for 1 h before lysis. eIF-4E was purified from lysates using 7-methyl-GTP-Sepharose and analyzed by immunoblotting for the indicated proteins. *C,* phosphorylation of Thr-36/47 on 4E-BP1 requires Raptor but not Rictor. MEFs ($p53^{-/-}$) were infected with lentivirus expressing either control, Raptor-specific, or Rictor-specific shRNAs. Cells were grown for 4 days and then treated with vehicle (DMSO), 50 nM rapamycin, or 250 nM Torin1 for 1 h. Cell lysates were then analyzed by immunoblot using antibodies specific for the indicated proteins or phosphorylation states. *D,* prolonged mTOR inhibition alters the expression of key cell cycle regulators. Wild-type ($p53^{-/-}$) and Rictor-null ($p53^{-/-}$) MEFs were treated with vehicle (DMSO), 50 nM rapamycin, or 250 nM Torin1 for 48 h. Cell lysates were then analyzed by immunoblotting using antibodies specific for the indicated proteins. *E,* Torin1 prevents phosphorylation of rapamycin-resistant sites in human cancer cell lines. MCF7, HCT116, HeLa, and HEK-293T cell lines were treated with vehicle (*Veh*), rapamycin (*Rap*) (50 or 250 nM), or Torin1 (50 or 250 nM) for 1 h and then analyzed by immunoblotting for the indicated proteins and phosphorylation states. *F,* Torin1 increases the amount of 4E-BP1 bound to eIF-4E in human cancer cell lines. MCF7 and HCT116 cells were treated with vehicle (DMSO), 50 nM rapamycin, 50 nM Torin1, or 250 nM Torin1 for 48 h before lysis. eIF-4E was purified from lysates using 7-methyl-GTP-Sepharose and analyzed by immunoblotting for the indicated proteins.

centrations as high as 500 nM, over 500 times greater than its IC_{50} value for inhibition of mTORC1 (Fig. 4*A*). In striking contrast, Torin1 substantially suppressed phosphorylation of Thr-37/46 and Ser-65 at concentrations as low as 10 nM and abolished it completely at 250 nM (Fig. 4*A*). Torin1 had nearly identical effects in Rictor-null MEFs, consistent with the hypothesis that these effects are because of inhibition of mTORC1 (Fig. 4*A*). Surprisingly, Thr-70 was unaffected by either Torin1 or rapamycin, supporting earlier predictions that it may be the target of a different kinase, such as Erk2 (37). Alternatively, it is possible that the Thr-70 4E-BP1 antibody is not phospho-specific. The dual-PI3K/mTOR inhibitors PI-103 and NVP-BEZ235 caused similar effects as Torin1 on 4E-BP1 phosphorylation (supplemental Fig. S3). Additionally, Torin1 had much greater effects than rapamycin on 4E-BP1 phosphorylation in a variety of human tumor cell lines, indicating that rapamycin resistance of mTORC1 is likely a general feature of most if not all mammalian systems (Fig. 4*E*). We next asked whether the increased dephosphorylation of 4E-BP1 by Torin1 led to increased association with eIF-4E. Using 7-methyl-GTP-Sepharose to purify eIF-4E from cell lysates, we found that Torin1 causes substantially more binding of 4E-BP1 to eIF-4E than does rapamycin (Fig. 4, *B* and *F*). Torin1 did not affect the phosphorylation of eIF2 (supplemental Fig. S5).

Because the effects of Torin1 were nearly equivalent in wild-type and Rictor-null MEFs, we concluded that they could not be dependent on mTORC2. However, it remained possible that mTOR alone or an unidentified mTORC3 were responsible. To show that mTORC1 inhibition is sufficient to explain the effects of Torin1 on 4E-BP1 phosphorylation, we used RNA interference to knock down Raptor, an obligatory mTORC1 component, in wild-type MEFs (Fig. 4*C*). Depletion of Raptor in these cells suppressed Thr-37/46 and Ser-65 phosphorylation and 4E-BP1 mobility to a degree that equaled the effects of Torin1 and exceeded those of rapamycin, thereby supporting the conclusion that mTORC1, or at least a Raptor-containing mTOR complex, regulates 4E-BP1 phosphorylation through a rapamycin-insensitive kinase-dependent mechanism.

Defects in cap-dependent translation are also known to cause cell cycle arrest. This is thought to occur primarily through

decreased translation of cap-dependent mRNAs that encode factors that promote cell cycle progression, such as cyclin D1 and cyclin D3, and increased translation of cap-independent mRNAs that encode factors that suppress it, such as p27Kip1 (38–40). Moreover, recent work has shown that the depletion of cyclin D1 that is caused by amino acid starvation and rapamycin treated is mediated by 4E-BP1 (41). We suspected that the cell cycle arrest caused by Torin1 might be explained by changes in the abundance of these factors. Consistent with this, both wild-type and Rictor-null MEFs treated for 48 h with Torin1, but not rapamycin, had greatly depleted levels of cyclin D1 and D3, and a strong induction of p27/Kip1 (Fig. 4*D*). The ability of cells to recover from this arrest upon the removal of Torin1 was highly dependent on cell type (data not shown).

DISCUSSION

Rapamycin has been an indispensable tool throughout the history of TOR research and remains widely employed as a "complete" mTORC1 inhibitor in both research and clinical settings. Indeed, in yeast, it is a convincing mimic of the genetic inactivation of TORC1. In mammalian systems, most known mTOR substrates were discovered and validated using rapamycin as a pharmacological probe. Rapamycin forms a complex with the intracellular protein FKBP12, which then binds to the FRB domain of mTOR and inhibits phosphorylation of substrates through a poorly characterized mechanism. Although structural information is available for rapamycin in a complex with FKBP12 and the FRB domain of mTOR, it remains unclear how this prevents phosphorylation of direct mTOR kinase substrates (42). A model to explain our findings is that rapamycin blocks access to only a specific subset of mTORC1 substrates, whereas Torin1, because of its ATP-competitive mode of action, blocks phosphorylation of all. Additionally, as Torin1 is much smaller than FKBP12-rapamycin, it likely accesses its target site in mTOR-containing complexes more easily than FKBP12-rapamycin.

Re-interpretations of several recent studies support the notion that considerable mTORC1 functionality is resistant to rapamycin. Shor *et al.* (13) found that high concentrations (10 μM) of rapamycin inhibit mTOR directly through an FKBP12-independent mechanism, suppressing both mTORC1 and mTORC2. Unlike the commonly used "low dose" (10–50 nM) and similarly to Torin1, "high-dose" rapamycin potently suppresses cap-dependent translation and inhibits proliferation in a wide variety of tumor cell lines. Although these authors concluded that these effects are because of mTORC2 inhibition, our findings indicate that they are more likely because of inhibition of rapamycin-resistant mTORC1-dependent functions. A study from Averous *et al.* (41) found that amino acid starvation caused a more complete depletion of cyclin D1 than rapamycin treatment and that this effect was mediated through 4E-BP1. Based on the assumption that rapamycin completely disables mTORC1, these authors concluded that amino acid starvation signals to 4E-BP1 through additional pathways besides mTORC1. We would suggest that it is more likely that amino acid starvation leads to a more complete inhibition of mTORC1 functions than does rapamycin. Finally, Choo *et al.* (43) found that phosphorylation sites on 4E-BP1 that are acutely sensitive to rapamycin become re-phosphorylated in some cell lines after long periods of rapamycin treatment. Moreover, the recovery of 4E-BP1 phosphorylation depends on the mTORC1 component Raptor, leading the authors to conclude that prolonged rapamycin treatment confers on mTORC1 the capacity to phosphorylate 4E-BP1 in a rapamycin-resistant fashion. We find that mTORC1 likely has rapamycin-resistant functions in all cell lines (Fig. 4*E*). Because prolonged rapamycin treatment is known to hyperactivate the PI3K pathway, which is upstream of mTORC1, one possible explanation for the results of Choo *et al.* (43) is that rapamycin leads to the hyperactivation of the rapamycin-resistant functionality of mTORC1, effectively overcoming the partial inhibition caused by rapamycin.

Because many important features of TOR signaling are conserved between yeast and mammals, our finding that mTORC1 possesses cell-essential but rapamycin-resistant functions is unexpected. At the same time, our results indicate that the requirements for TORC1 signaling in maintaining protein synthesis and promoting cell division are more similar between yeast and mammalian systems than had been appreciated. Although we have focused on the rapamycin-insensitive regulation of 4E-BP1, we consider it likely that other similar mTORC1 substrates exist, particularly among the regulators of autophagy. The future combined use of Torin1 and phosphoproteomics will likely permit a more comprehensive assessment of all mTOR substrates. Given the current enthusiasm for rapamycin as a potential therapeutic, it is likely that ATP-competitive inhibitors of mTOR will have clinical utility as well.

Acknowledgments—We thank D. Kwiatowski (Harvard Medical School) for p53$^{-/-}$/TSC2$^{-/-}$ and p53$^{-/-}$/TSC2$^{+/+}$ MEFs; Christian Reinhardt (Massachusetts Institute of Technology) for p53 reagents; and Chris Armstong (Invitrogen) for kinase profiling assistance. We also thank members of the Sabatini and Gray laboratories for helpful discussions and Ambit Biosciences for performing KinomeScan profiling.

REFERENCES

1. Guertin, D. A., and Sabatini, D. M. (2007) *Cancer Cell* **12,** 9–22
2. Manning, B. D., and Cantley, L. C. (2007) *Cell* **129,** 1261–1274
3. Sehgal, S. N. (2003) *Transplant. Proc.* **35,** S7–S14
4. Sarbassov, D. D., Ali, S. M., Sengupta, S., Sheen, J. H., Hsu, P. P., Bagley, A. F., Markhard, A. L., and Sabatini, D. M. (2006) *Mol. Cell* **22,** 159–168
5. Richter, J. D., and Sonenberg, N. (2005) *Nature* **433,** 477–480
6. Holz, M. K., Ballif, B. A., Gygi, S. P., and Blenis, J. (2005) *Cell* **123,** 569–580
7. Raught, B., Peiretti, F., Gingras, A. C., Livingstone, M., Shahbazian, D., Mayeur, G. L., Polakiewicz, R. D., Sonenberg, N., and Hershey, J. W. (2004) *EMBO J.* **23,** 1761–1769
8. Shahbazian, D., Roux, P. P., Mieulet, V., Cohen, M. S., Raught, B., Taunton, J., Hershey, J. W., Blenis, J., Pende, M., and Sonenberg, N. (2006) *EMBO J.* **25,** 2781–2791
9. Barbet, N. C., Schneider, U., Helliwell, S. B., Stansfield, I., Tuite, M. F., and Hall, M. N. (1996) *Mol. Biol. Cell* **7,** 25–42
10. Noda, T., and Ohsumi, Y. (1998) *J. Biol. Chem.* **273,** 3963–3966
11. Neshat, M. S., Mellinghoff, I. K., Tran, C., Stiles, B., Thomas, G., Petersen, R., Frost, P., Gibbons, J. J., Wu, H., and Sawyers, C. L. (2001) *Proc. Natl. Acad. Sci. U. S. A.* **98,** 10314–10319
12. Pedersen, S., Celis, J. E., Nielsen, J., Christiansen, J., and Nielsen, F. C. (1997) *Eur. J. Biochem.* **247,** 449–456
13. Shor, B., Zhang, W. G., Toral-Barza, L., Lucas, J., Abraham, R. T., Gibbons,

J. J., and Yu, K. (2008) *Cancer Res.* **68,** 2934–2943
14. Takeuchi, H., Kondo, Y., Fujiwara, K., Kanzawa, T., Aoki, H., Mills, G. B., and Kondo, S. (2005) *Cancer Res.* **65,** 3336–3346
15. Sabatini, D. M. (2006) *Nat. Rev. Cancer* **6,** 729–734
16. Guertin, D. A., Stevens, D. M., Thoreen, C. C., Burds, A. A., Kalaany, N. Y., Moffat, J., Brown, M., Fitzgerald, K. J., and Sabatini, D. M. (2006) *Dev. Cell* **11,** 859–871
17. Moffat, J., Grueneberg, D. A., Yang, X., Kim, S. Y., Kloepfer, A. M., Hinkle, G., Piqani, B., Eisenhaure, T. M., Luo, B., Grenier, J. K., Carpenter, A. E., Foo, S. Y., Stewart, S. A., Stockwell, B. R., Hacohen, N., Hahn, W. C., Lander, E. S., Sabatini, D. M., and Root, D. E. (2006) *Cell* **124,** 1283–1298
18. Ali, S. M., and Sabatini, D. M. (2005) *J. Biol. Chem.* **280,** 19445–19448
19. Sarbassov, D. D., Guertin, D. A., Ali, S. M., and Sabatini, D. M. (2005) *Science* **307,** 1098–1101
20. Sancak, Y., Thoreen, C. C., Peterson, T. R., Lindquist, R. A., Kang, S. A., Spooner, E., Carr, S. A., and Sabatini, D. M. (2007) *Mol. Cell* **25,** 903–915
21. Knight, Z. A., Gonzalez, B., Feldman, M. E., Zunder, E. R., Goldenberg, D. D., Williams, O., Loewith, R., Stokoe, D., Balla, A., Toth, B., Balla, T., Weiss, W. A., Williams, R. L., and Shokat, K. M. (2006) *Cell* **125,** 733–747
22. Nobukuni, T., Joaquin, M., Roccio, M., Dann, S. G., Kim, S. Y., Gulati, P., Byfield, M. P., Backer, J. M., Natt, F., Bos, J. L., Zwartkruis, F. J., and Thomas, G. (2005) *Proc. Natl. Acad. Sci. U. S. A.* **102,** 14238–14243
23. Brunn, G. J., Williams, J., Sabers, C., Wiederrecht, G., Lawrence, J. C., Jr., and Abraham, R. T. (1996) *EMBO J.* **15,** 5256–5267
24. Maira, S. M., Stauffer, F., Brueggen, J., Furet, P., Schnell, C., Fritsch, C., Brachmann, S., Chene, P., De Pover, A., Schoemaker, K., Fabbro, D., Gabriel, D., Simonen, M., Murphy, L., Finan, P., Sellers, W., and Garcia-Echeverria, C. (2008) *Mol. Cancer Ther.* **7,** 1851–1863
25. Biondi, R. M., Kieloch, A., Currie, R. A., Deak, M., and Alessi, D. R. (2001) *EMBO J.* **20,** 4380–4390
26. Scheid, M. P., Marignani, P. A., and Woodgett, J. R. (2002) *Mol. Cell. Biol.* **22,** 6247–6260
27. Mizushima, N., Levine, B., Cuervo, A. M., and Klionsky, D. J. (2008) *Nature* **451,** 1069–1075
28. Kabeya, Y., Mizushima, N., Ueno, T., Yamamoto, A., Kirisako, T., Noda, T., Kominami, E., Ohsumi, Y., and Yoshimori, T. (2000) *EMBO J.* **19,** 5720–5728
29. Gingras, A. C., Gygi, S. P., Raught, B., Polakiewicz, R. D., Abraham, R. T., Hoekstra, M. F., Aebersold, R., and Sonenberg, N. (1999) *Genes Dev.* **13,** 1422–1437
30. Burnett, P. E., Barrow, R. K., Cohen, N. A., Snyder, S. H., and Sabatini, D. M. (1998) *Proc. Natl. Acad. Sci. U. S. A.* **95,** 1432–1437
31. Fingar, D. C., Richardson, C. J., Tee, A. R., Cheatham, L., Tsou, C., and Blenis, J. (2004) *Mol. Cell. Biol.* **24,** 200–216
32. Wang, X., Beugnet, A., Murakami, M., Yamanaka, S., and Proud, C. G. (2005) *Mol. Cell. Biol.* **25,** 2558–2572
33. Choi, K. M., McMahon, L. P., and Lawrence, J. C., Jr. (2003) *J. Biol. Chem.* **278,** 19667–19673
34. Schalm, S. S., Fingar, D. C., Sabatini, D. M., and Blenis, J. (2003) *Curr. Biol.* **13,** 797–806
35. Tee, A. R., and Proud, C. G. (2002) *Mol. Cell. Biol.* **22,** 1674–1683
36. Beretta, L., Gingras, A. C., Svitkin, Y. V., Hall, M. N., and Sonenberg, N. (1996) *EMBO J.* **15,** 658–664
37. Herbert, T. P., Tee, A. R., and Proud, C. G. (2002) *J. Biol. Chem.* **277,** 11591–11596
38. Albers, M. W., Williams, R. T., Brown, E. J., Tanaka, A., Hall, F. L., and Schreiber, S. L. (1993) *J. Biol. Chem.* **268,** 22825–22829
39. Jiang, H., Coleman, J., Miskimins, R., and Miskimins, W. K. (2003) *Cancer Cell Int.* **3,** 2
40. Rosenwald, I. B., Lazaris-Karatzas, A., Sonenberg, N., and Schmidt, E. V. (1993) *Mol. Cell. Biol.* **13,** 7358–7363
41. Averous, J., Fonseca, B. D., and Proud, C. G. (2008) *Oncogene* **27,** 1106–1113
42. Choi, J., Chen, J., Schreiber, S. L., and Clardy, J. (1996) *Science* **273,** 239–242
43. Choo, A. Y., Yoon, S. O., Kim, S. G., Roux, P. P., and Blenis, J. (2008) *Proc. Natl. Acad. Sci. U. S. A.* **105,** 17414–17419

Anal. Chem. **2010,** *82,* 6643–6651

Native Capillary Isoelectric Focusing for the Separation of Protein Complex Isoforms and Subcomplexes

Bryan R. Fonslow,[†] Seong A. Kang,[‡] Daniel R. Gestaut,[||] Beth Graczyk,[||] Trisha N. Davis,[||] David M. Sabatini,[‡,§] and John R. Yates III*[,†]

Department of Chemical Physiology, The Scripps Research Institute, 10550 N. Torrey Pines Rd. La Jolla, California 92037, Whitehead Institute for Biomedical Research, Nine Cambridge Center, Cambridge, Massachusetts 02142, Howard Hughes Medical Institute, Department of Biology, Massachusetts Institute of Technology, Cambridge, Massachusetts 02139, Department of Biochemistry, University of Washington, Seattle, Washington 98195

Here we report the use of capillary isoelectric focusing under native conditions for the separation of protein complex isoforms and subcomplexes. Using biologically relevant HIS-tag and FLAG-tag purified protein complexes, we demonstrate the separations of protein complex isoforms of the mammalian target of rapamycin complex (mTORC1 and 2) and the subcomplexes and different phosphorylation states of the Dam1 complex. The high efficiency capillary isoelectric focusing separation allowed for resolution of protein complexes and subcomplexes similar in size and biochemical composition. By performing separations with native buffers and reduced temperature (15 °C) we were able to maintain the complex integrity of the more thermolabile mTORC2 during isoelectric focusing and detection (<45 min). Increasing the separation temperature allowed us to monitor dissociation of the Dam1 complex into its subcomplexes (25 °C) and eventually its individual protein components (30 °C). The separation of two different phosphorylation states of the Dam1 complex, generated from an in vitro kinase assay with Mps1 kinase, was straightforward due to the large pI shift upon multiple phosphorylation events. The separation of the protein complex isoforms of mTORC, on the other hand, required the addition of a small pI range (4−6.5) of ampholytes to improve resolution and stability of the complexes. We show that native capillary isoelectric focusing is a powerful method for the difficult separations of large, similar, unstable protein complexes. This method shows potential for differentiation of protein complex isoform and subcomplex compositions, post-translational modifications, architectures, stabilities, equilibria, and relative abundances under biologically relevant conditions.

Protein assemblies are well-known to make up the functional machinery of the cell.[1] What is less well understood is the dynamic nature of the protein interactions necessary for the biological machinery to function properly. Many diseases have been found to be caused by aberrant protein−protein interactions.[2] New techniques, and even fields, are emerging to better probe and understand protein−protein interactions within the context of a cell. Interactomics is a recently introduced subset of systems biology which focuses on the interactions of proteins and other molecules.[3] For example, yeast two hybrid (Y2H) screens have generated binary protein interaction data for *S. cerevisiae*[4,5] and *C. elegans.*[6,7] Two global tandem-affinity purification (TAP) efforts in *S. cerevisiae* used mass spectrometry to identify proteins within purified complexes. The results increased the known curated complexes (217) from the Munich Information Center for Protein Sequences (MIPS) by 257[8] and 275.[9] Other efforts to investigate protein−protein interactions use native variations of common orthogonal biochemical separations of cell lysates to fractionate protein complexes for mass spectrometry (MS)-based analysis.

* To whom correspondence should be addressed. Phone: 858-784-8862; Fax: 858-784-8883; E-mail: jyates@scripps.edu.

[†] The Scripps Research Institute.

[‡] Whitehead Institute for Biomedical Research.

[||] University of Washington.

[§] Howard Hughes Medical Institute.

(1) Alberts, B. *Cell* **1998**, *92*, 291–294.
(2) Ryan, D. P.; Matthews, J. M. *Curr. Opin. Struct. Biol.* **2005**, *15*, 441–446.
(3) Figeys, D. *Cell Res.* **2008**, *18*, 716–724.
(4) Schwikowski, B.; Uetz, P.; Fields, S. *Nat. Biotechnol.* **2000**, *18*, 1257–1261.
(5) Uetz, P.; Giot, L.; Cagney, G.; Mansfield, T. A.; Judson, R. S.; Knight, J. R.; Lockshon, D.; Narayan, V.; Srinivasan, M.; Pochart, P.; Qureshi-Emili, A.; Li, Y.; Godwin, B.; Conover, D.; Kalbfleisch, T.; Vijayadamodar, G.; Yang, M.; Johnston, M.; Fields, S.; Rothberg, J. M. *Nature* **2000**, *403*, 623–627.
(6) Li, S.; Armstrong, C. M.; Bertin, N.; Ge, H.; Milstein, S.; Boxem, M.; Vidalain, P. O.; Han, J. D.; Chesneau, A.; Hao, T.; Goldberg, D. S.; Li, N.; Martinez, M.; Rual, J. F.; Lamesch, P.; Xu, L.; Tewari, M.; Wong, S. L.; Zhang, L. V.; Berriz, G. F.; Jacotot, L.; Vaglio, P.; Reboul, J.; Hirozane-Kishikawa, T.; Li, Q.; Gabel, H. W.; Elewa, A.; Baumgartner, B.; Rose, D. J.; Yu, H.; Bosak, S.; Sequerra, R.; Fraser, A.; Mango, S. E.; Saxton, W. M.; Strome, S.; Van Den Heuvel, S.; Piano, F.; Vandenhaute, J.; Sardet, C.; Gerstein, M.; Doucette-Stamm, L.; Gunsalus, K. C.; Harper, J. W.; Cusick, M. E.; Roth, F. P.; Hill, D. E.; Vidal, M. *Science* **2004**, *303*, 540–543.
(7) Simonis, N.; Rual, J. F.; Carvunis, A. R.; Tasan, M.; Lemmens, I.; Hirozane-Kishikawa, T.; Hao, T.; Sahalie, J. M.; Venkatesan, K.; Gebreab, F.; Cevik, S.; Klitgord, N.; Fan, C.; Braun, P.; Li, N.; Ayivi-Guedehoussou, N.; Dann, E.; Bertin, N.; Szeto, D.; Dricot, A.; Yildirim, M. A.; Lin, C.; de Smet, A. S.; Kao, H. L.; Simon, C.; Smolyar, A.; Ahn, J. S.; Tewari, M.; Boxem, M.; Milstein, S.; Yu, H.; Dreze, M.; Vandenhaute, J.; Gunsalus, K. C.; Cusick, M. E.; Hill, D. E.; Tavernier, J.; Roth, F. P.; Vidal, M. *Nat. Methods* **2009**, *6*, 47–54.
(8) Gavin, A. C.; Aloy, P.; Grandi, P.; Krause, R.; Boesche, M.; Marzioch, M.; Rau, C.; Jensen, L. J.; Bastuck, S.; Dumpelfeld, B.; Edelmann, A.; Heurtier, M. A.; Hoffman, V.; Hoefert, C.; Klein, K.; Hudak, M.; Michon, A. M.; Schelder, M.; Schirle, M.; Remor, M.; Rudi, T.; Hooper, S.; Bauer, A.; Bouwmeester, T.; Casari, G.; Drewes, G.; Neubauer, G.; Rick, J. M.; Kuster, B.; Bork, P.; Russell, R. B.; Superti-Furga, G. *Nature* **2006**, *440*, 631–636.

10.1021/ac101235k
Published on Web 07/08/2010

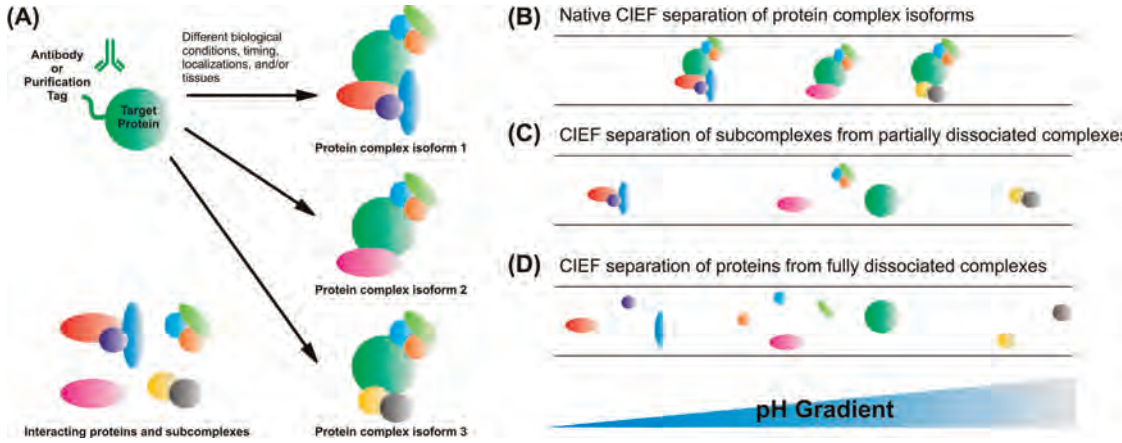

Figure 1. Schematic of protein complex isoforms and subcomplexes and their CIEF separations. (A) The composition of protein complexes are often elucidated through purification of a target protein, and all proteins associated with it, using an antibody or purification tag. The purification creates a heterogeneous mixture of protein complexes, called protein complex isoforms. Three examples are shown here. Each protein complex isoform can be composed of different proteins or subcomplexes depending on its specific function under certain biological condition. (B) A theoretical native CIEF separation of the three protein complex isoforms. Although many proteins are similar in each protein complex isoform, the proteins or subcomplexes which are different shift the isoelectric point of the protein complex isoform. This inherent pI shift allows for separation within the pH gradient generated using CIEF. (C) Dissociated protein complexes are known to maintain more thermodynamically stable subcomplexes. These subcomplexes can also be separated based on their isoelectric points using native CIEF. (D) A traditional CIEF separation of individual proteins from fully dissociated protein complexes isoforms and subcomplexes using denaturants or thermal dissociation. Note that the pIs of the separated proteins contribute, likely as a weighted average, to the pIs of the subcomplexes they are associated with in the separation above. Likewise, comparison of the subcomplex separation in (B) to the complex isoform separation in (A) illustrates how the pIs of proteins and subcomplexes contribute to the pI of the complex isoform.

Two-dimensional blue native polyacrylamide gel electrophoresis (BN-PAGE) allows for the elucidation of membrane bound protein complexes.[10] More recently, successive preparative liquid chromatography separations facilitated unbiased identification of 13 known *E. coli* complexes[11] and 20 known *P. furiosus* complexes.[12] On the analytical scale, capillary electrophoresis (CE)-MS permitted separation and detection of three protein complexes directly from a cell lysate with a concentration dynamic range of ~3.[13] Direct analysis of large (~50−700 kD), purified protein complexes in the gas phase is also progressing through instrumental and operational modifications to mass spectrometers.[14−17] As a result, native mass spectrometry is quickly advancing as a method to elucidate protein complex composition,[18−20] structure,[21] and dynamics[22] of purified protein complexes.

Experiments studying protein−protein interactions globally within the cell indicate the growing need for methods to address dynamic and versatile protein−protein interactions through direct physical or chemical analyses. Protein interactions are highly dependent on developmental, environmental, and genetic conditions,[23] making many proteins versatile in function, yet still highly specific. For instance, a single protein can differentiate cellular functions through participation in multiple protein complexes with distinct binding partners as shown in Figure 1A. Protein complexes of this nature have been deemed protein complex isoforms.[8] Further promiscuity of proteins is possible through participation in protein subcomplexes.[24] Subcomplexes are stable protein complexes within a larger protein complex as shown in Figure 1A. Elucidation of protein complex isoforms and subcomplexes can be convoluted and arduous using conventional methods. Identification of protein complexes and differentiation of their isoforms and subcomplexes usually begins with copurifications of known and suspected binding partners under native conditions. Potential binding partners are validated by identification via mass spectrometry-based proteomics[25] or Western blotting.[26] An auto-

(9) Krogan, N. J.; Cagney, G.; Yu, H.; Zhong, G.; Guo, X.; Ignatchenko, A.; Li, J.; Pu, S.; Datta, N.; Tikuisis, A. P.; Punna, T.; Peregrin-Alvarez, J. M.; Shales, M.; Zhang, X.; Davey, M.; Robinson, M. D.; Paccanaro, A.; Bray, J. E.; Sheung, A.; Beattie, B.; Richards, D. P.; Canadien, V.; Lalev, A.; Mena, F.; Wong, P.; Starostine, A.; Canete, M. M.; Vlasblom, J.; Wu, S.; Orsi, C.; Collins, S. R.; Chandran, S.; Haw, R.; Rilstone, J. J.; Gandi, K.; Thompson, N. J.; Musso, G.; St Onge, P.; Ghanny, S.; Lam, M. H.; Butland, G.; Altaf-Ul, A. M.; Kanaya, S.; Shilatifard, A.; O'Shea, E.; Weissman, J. S.; Ingles, C. J.; Hughes, T. R.; Parkinson, J.; Gerstein, M.; Wodak, S. J.; Emili, A.; Greenblatt, J. F. *Nature* **2006**, *440*, 637–643.
(10) Krause, F. *Electrophoresis* **2006**, *27*, 2759–2781.
(11) Dong, M.; Yang, L. L.; Williams, K.; Fisher, S. J.; Hall, S. C.; Biggin, M. D.; Jin, J.; Witkowska, H. E. *J. Proteome Res.* **2008**, *7*, 1836–1849.
(12) Menon, A. L.; Poole, F. L., 2nd; Cvetkovic, A.; Trauger, S. A.; Kalisiak, E.; Scott, J. W.; Shanmukh, S.; Praissman, J.; Jenney, F. E., Jr.; Wikoff, W. R.; Apon, J. V.; Siuzdak, G.; Adams, M. W. *Mol Cell Proteomics* **2009**, *8*, 735–751.
(13) Nguyen, A.; Moini, M. *Anal. Chem.* **2008**, *80*, 7169–7173.
(14) Sobott, F.; Hernandez, H.; McCammon, M. G.; Tito, M. A.; Robinson, C. V. *Anal. Chem.* **2002**, *74*, 1402–1407.
(15) Chernushevich, I. V.; Thomson, B. A. *Anal. Chem.* **2004**, *76*, 1754–1760.
(16) van den Heuvel, R. H.; van Duijn, E.; Mazon, H.; Synowsky, S. A.; Lorenzen, K.; Versluis, C.; Brouns, S. J.; Langridge, D.; van der Oost, J.; Hoyes, J.; Heck, A. *J. Anal. Chem.* **2006**, *78*, 7473–7483.
(17) Sun, J.; Kitova, E. N.; Klassen, J. S. *Anal. Chem.* **2007**, *79*, 416–425.
(18) Sun, J.; Kitova, E. N.; Sun, N.; Klassen, J. S. *Anal. Chem.* **2007**, *79*, 8301–8311.
(19) Benesch, J. L.; Ruotolo, B. T.; Sobott, F.; Wildgoose, J.; Gilbert, A.; Bateman, R.; Robinson, C. V. *Anal. Chem.* **2009**, *81*, 1270–1274.
(20) Beardsley, R. L.; Jones, C. M.; Galhena, A. S.; Wysocki, V. H. *Anal. Chem.* **2009**, *81*, 1347–1356.
(21) Lorenzen, K.; Vannini, A.; Cramer, P.; Heck, A. J. *Structure* **2007**, *15*, 1237–1245.
(22) Benesch, J. L.; Sobott, F.; Robinson, C. V. *Anal. Chem.* **2003**, *75*, 2208–2214.
(23) Levy, E. D.; Pereira-Leal, J. B. *Curr. Opin. Struct. Biol.* **2008**, *18*, 349–357.
(24) Hollunder, J.; Beyer, A.; Wilhelm, T. *Proteomics* **2005**, *5*, 2082–2089.

mated method for distinguishing these subtle differences would be highly beneficial to identify complex isoforms and subcomplexes directly.

From the separation science perspective, resolving protein complex isoforms and subcomplexes is challenging. Efficient protein separations are already difficult due to the inherent hydrophobicity and large size of proteins[27] and can suffer from recovery problems on the analytical scale.[28−31] Well-studied protein complexes were found to contain 10 or more interacting proteins[1] and a global study in yeast confirmed an average of 12 proteins per complex.[32] Larger protein complex assemblies only magnify the challenges associated with protein separations. A factor of 10 increase in analyte size results in an approximate order of magnitude reduction in diffusion coefficient and electrophoretic mobility; these are respectively detrimental to efficient separations using either liquid chromatography or electrophoretic separation methods. Additionally, by definition protein complex isoform compositions may only differ by a few proteins.[8] With a majority of the proteins conserved between complex isoforms, the size, shape, charge, chemical composition, and thermodynamic character of complex isoforms may be relatively similar. A specific protein complex isoform comparison, based on size and isoelectric point, is illustrated in Table 3. To separate complex isoforms, an extremely efficient, high resolution separation technique is required that can accentuate their subtle physical or chemical differences. Finally and most importantly, the technique must use conditions that can maintain biochemical and thermodynamic stability of the complexes.

Capillary isoelectric focusing (CIEF) has proven to be the best method for the analysis of protein isoforms, with the capability to distinguish proteins differing by as few as 0.005 pH units.[33] Proteins are focused to their isoelectric point in a capillary with a pH gradient generated by zwitterionic ampholytes and the opposing migration of an acid and base across an electric field.[34] The parallel between the subtle chemical differences of protein isoforms and protein complex isoforms made it likely that exploiting isoelectric point differences would also prove useful for separation of protein complex isoforms and subcomplexes. CIEF has become increasingly used for analysis of biochemical interactions such as protein-antibody,[35−37] protein−ligand,[38,39] protein−DNA,[40] protein-phospholipid,[41] and protein-drug[42−45] complexes indicating the potential for elucidation of biologically relevant protein complexes. Identification of protein complex standards by Fourier transform ion cyclotron resonance mass spectrometry (FTICR-MS)[46] and molecular weight profiling of *E. coli* protein complexes[47] has also been previously demonstrated using CIEF. We will demonstrate herein that performing CIEF under native conditions allows for the separation and relative quantitation of protein complex isoforms and subcomplexes.

METHODS AND MATERIALS

Reagents and Chemicals. Unless otherwise noted all chemicals were purchased from Thermo Fisher Scientific (Waltham, MA). Deionized water (18.2 MΩ, Barnstead, Dubuque, IA) was used for all preparations. The CIEF kit containing coated capillaries, pI 3−10 ampholytes, focusing acid and base, mobilization acid, anodic and cathodic stabilizers, and pI markers was obtained from Beckman Coulter (Brea, CA). Pharmalyte pI 4 − 6.5 ampholytes were purchased from GE Healthcare (Piscataway, NJ).

Dam1 Complex Preparation. *Saccharomyces cerevisiae* Dam1 complex was expressed in and purified from *E. coli* as described previously.[48] Dam1 complex polycistronic vector was transformed into BL21 Rosetta (Novagen, Madison, WI). Cultures were grown to about 30 Klett units, and the cultures were induced overnight at 23 °C. Pellets were lysed using a French press in 50 mM sodium phosphate buffer (pH 6.9) containing 350 mM NaCl and protease inhibitors (0.01 mg mL−1 chymostatin, 0.01 mg mL−1 aprotinin, 0.01 mg mL−1 leupeptin, 0.01 mg mL−1 pepstatin, 0.002 mg mL−1 benzamadine, and 1 mM phenylmethylsulfonyl fluoride). The Dam1 complex was purified by affinity chromatography using talon resin, according to the manufacturer's instructions (BD Biosciences, San Jose, CA). Peak elutions were concentrated to approximately 1 mL using a 50 kDa molecular weight cutoff Amicon Ultra centrifugal filter (Millipore, Billerica, MA) and then subjected to gel filtration chromatography on an SD × 200 16/60 column (GE Healthcare). Peak fractions were concentrated and cleared at 13 000*g*. Glycerol (10%, final concentration) was added and aliquots were snap frozen and stored at −80 °C.

(25) Link, A. J.; Eng, J.; Schieltz, D. M.; Carmack, E.; Mize, G. J.; Morris, D. R.; Garvik, B. M.; Yates, J. R. *Nat. Biotechnol.* **1999**, *17*, 676–682, 3rd.
(26) Golemis, E.; Adams, P. D. *Protein−Protein Interactions: A Molecular Cloning Manual*, 2nd ed.; Cold Spring Harbor Laboratory Press: Cold Spring Harbor, NY, 2005.
(27) Kastner, M. *Protein Liquid Chromatography*, 1st ed.; Elsevier: New York, 2000.
(28) Goheen, S. C.; Gibbins, B. M. *J Chromatogr., A* **2000**, *890*, 73–80.
(29) Greibrokk, T.; Pepaj, M.; Lundanes, E.; Andersen, T.; Novotna, K. *LC-GC Eur.* **2005**, *18*, 355−356; 358−360.
(30) Eschelbach, J. W.; Jorgenson, J. W. *Anal. Chem.* **2006**, *78*, 1697–1706.
(31) Lucy, C. A.; MacDonald, A. M.; Gulcev, M. D. *J Chromatogr., A* **2008**, *1184*, 81–105.
(32) Gavin, A. C.; Bosche, M.; Krause, R.; Grandi, P.; Marzioch, M.; Bauer, A.; Schultz, J.; Rick, J. M.; Michon, A. M.; Cruciat, C. M.; Remor, M.; Hofert, C.; Schelder, M.; Brajenovic, M.; Ruffner, H.; Merino, A.; Klein, K.; Hudak, M.; Dickson, D.; Rudi, T.; Gnau, V.; Bauch, A.; Bastuck, S.; Huhse, B.; Leutwein, C.; Heurtier, M. A.; Copley, R. R.; Edelmann, A.; Querfurth, E.; Rybin, V.; Drewes, G.; Raida, M.; Bouwmeester, T.; Bork, P.; Seraphin, B.; Kuster, B.; Neubauer, G.; Superti-Furga, G. *Nature* **2002**, *415*, 141–147.
(33) Shen, Y.; Xiang, F.; Veenstra, T. D.; Fung, E. N.; Smith, R. D. *Anal. Chem.* **1999**, *71*, 5348–5353.
(34) Hjerten, S.; Zhu, M. D. *J. Chromatogr.* **1985**, *346*, 265–270.
(35) Tan, W.; Fan, Z. H.; Qiu, C. X.; Ricco, A. J.; Gibbons, I. *Electrophoresis* **2002**, *23*, 3638–3645.
(36) Shimura, K.; Hoshino, M.; Kamiya, K.; Katoh, K.; Hisada, S.; Matsumoto, H.; Kasai, K. *Electrophoresis* **2002**, *23*, 909–917.
(37) Li, G.; Zhou, X.; Wang, Y.; El-Shafey, A.; Chiu, N. H.; Krull, I. S. *J Chromatogr., A* **2004**, *1053*, 253–262.
(38) Cunliffe, J. M.; Liu, Z.; Pawliszyn, J.; Kennedy, R. T. *Electrophoresis* **2004**, *25*, 2319–2325.
(39) Lyubarskaya, Y. V.; Carr, S. A.; Dunnington, D.; Prichett, W. P.; Fisher, S. M.; Appelbaum, E. R.; Jones, C. S.; Karger, B. L. *Anal. Chem.* **1998**, *70*, 4761–4770.
(40) Liu, Z.; Drabovich, A. P.; Krylov, S. N.; Pawliszyn, *J. Anal. Chem.* **2007**, *79*, 1097–1100.
(41) Bo, T.; Pawliszyn, J. *Anal. Biochem.* **2006**, *350*, 91–98.
(42) Bo, T.; Pawliszyn, J. *J Chromatogr., A* **2006**, *1105*, 25–32.
(43) Lemma, T.; Mandal, R.; Li, X. F.; Pawliszyn, J. *J. Sep. Sci.* **2008**, *31*, 1803–1809.
(44) Lemma, T.; Pawliszyn, J. *J. Pharm. Biomed. Anal.* **2009**, *50*, 570–575.
(45) Montgomery, R.; Shay, H.; McCarroll, M.; Tolley, L. *J. Proteome Res.* **2008**, *7*, 4594–4597.
(46) Martinovic, S.; Berger, S. J.; Pasa-Tolic, L.; Smith, R. D. *Anal. Chem.* **2000**, *72*, 5356–5360.
(47) Shen, Y.; Berger, S. J.; Smith, R. D. *J Chromatogr., A* **2001**, *914*, 257–264.
(48) Gestaut, D. R.; Graczyk, B.; Cooper, J.; Widlund, P. O.; Zelter, A.; Wordeman, L.; Asbury, C. L.; Davis, T. N. *Nat. Cell Biol.* **2008**, *10*, 407–414.

Mps1 Preparation and Kinase Assay. *Saccharomyces cerevisiae* Mps1 kinase was expressed in *E. coli* with a GST tag on the N-terminus and a 6XHis tag on the C-terminus from plasmid pDG54, (derived from plasmid pGEX6p-MPS1).[49] Expression was induced in 1 L of cells by addition of 40 mg IPTG, and cells were grown overnight at 18 °C. Mps1 was purified by the 6XHis tag using talon resin according to the manufacturer's instructions with the following exceptions. The cells were resuspended in 20 mM HEPES buffer, pH 7.2, containing 150 mM NaCl, 2% Triton X-100, and protease inhibitors and lysed using a French press. The protein was eluted from the column in 1.5 mL of 20 mM HEPES buffer, pH 7.2, containing 150 mM NaCl and 400 mM imidazole.

Dam1 complex was phosphorylated in 50 mM HEPES buffer, pH 7.2, containing 25 mM $MgCl_2$, 10 mM ATP, 150 mM NaCl, 4 μM Dam1 complex and 15 μL Mps1 kinase in a 25 μL reaction volume. The reaction was incubated at 30 °C for 90 min. The stoichiometry of phosphorylation was determined under the same assay conditions except that gamma-^{32}P ATP (3000 Ci/mmol) was included at 0.5 μCi/μL.

mTOR Complex Preparation. To produce a soluble mixture of mTORC1 and mTORC2, we generated a HEK-293T cell line that stably expresses N-terminally FLAG-tagged mLST8 using vesicular stomatitis virus G-pseudotyped MSCV retrovirus. mTOR complexes were purified by lysing cells in 50 mM HEPES, pH 7.4, 200 mM NaCl, and 0.4% CHAPS. Cells were lysed at 4 °C for 30 min, and the insoluble fraction was removed by centrifugation at 18 000 rpm for 30 min. Supernatants were incubated with FLAG-M2 monoclonal antibody-agarose for 1 h and then washed with three column volumes of wash buffer (50 mM HEPES, pH 7.4, 200 mM NaCl, 2 mM DTT, and 2 mM ATP and 0.1% CHAPS). Purified mTOR complexes were eluted with 100 μg/mL 3x FLAG peptide in 50 mM HEPES, pH 7.4, 500 mM NaCl and 0.1% CHAPS. Eluted fractions were pooled and concentrated by centrifugation prior to CIEF separation. Samples were subsequently analyzed by SDS-PAGE and immunoblotting to confirm the purification of the complexes.

CIEF Separations. Separations were performed on a PA800 Capillary Electrophoresis System (Beckman Coulter, Brea, CA) using a 50 μm ID/360 μm OD neutral coated capillary or a 100 μm ID/360 μm OD in-house hydroxypropyl cellulose (average molecular weight 100 000 g/mol) coated capillary[50] cut to 32 cm (20.2 cm to detector). The capillary was rinsed with DI water before and after runs at 50 psi for 2 min. All samples were prepared on ice and stored at 4 °C prior to loading onto the capillary. The CIEF buffer was prepared to contain 1.7% w/v Pharmalyte pI 3−10 carrier ampholytes, 2.1% w/v Pharmalyte pI 4−6.5 carrier ampholytes (for mTORC separation only), 42 mM arginine, and 1.7 mM iminodiacetic acid.[51] Protein complexes were added to the prepared CIEF buffer immediately before analysis unless otherwise stated. The CIEF capillary was thermostatted to 15 °C except for protein complex stability experiments with Dam1 where separation temperatures of 20, 25, and 30 °C were also used. Samples were loaded onto the capillary for 1 min at 50 psi. Isoelectric focusing was performed for 10 or 15 min at 25 kV with a maximum current of 50 μA using 200 mM H_3PO_4 and 300 mM NaOH at the anode (inlet) and cathode (outlet), respectively. High efficiency isotachophoretic mobilization of protein complexes past the detector after focusing was performed by substitution of 300 mM NaOH with 350 mM acetic acid at the cathode. Detection of mobilized protein complexes was performed at 4 Hz using a UV detector at 280 nm through a 200 μm aperture.

Viscosity Correction for Native CIEF Separations at Varying Temperatures. To clarify the appearance or disappearance of peaks at different separation temperatures, we normalized the mobilization time of the higher temperature separations to the lowest separation temperature (15 °C) using a viscosity correction. The correction was necessary since the viscosity of the CIEF buffer decreased with increasing temperature and caused a systematic decrease in the mobilization times of focused protein complexes illustrated in Figure 3A. Corrections for viscosity-induced mobility shifts from buffer additives in capillary electrophoresis have been made using a viscosity correction factor based on absolute[52] and relative viscosity measurements and separation currents.[53] We extended this to temperature-induced viscosity changes during CIEF. The viscosity correction based on migration time was possible since one large peak remained relatively constant throughout the separations, marked with an (*) in all separations in Figure 3. These peaks were used as a mobilization time marker for measurement of relative viscosity. Since the peak used for correction was not a spiked standard we also investigated mobilization current as a measure of relative viscosity. The equation used to calculate the viscosity correction factor based on mobilization time (ν_t) is as follows:

$$\nu_t = \frac{t_{15^\circ C}}{t_{^\circ C}} \tag{1}$$

and based on current (ν_I) is

$$\nu_I = \frac{I_{15^\circ C}}{I_{^\circ C}} \tag{2}$$

where t is the mobilization time of the peak and I is the average mobilization current at 15 °C and the higher temperatures, respectively. The mobilization time and current corrections are listed in Table 2. There was close agreement between the values from the two correction methods, but we used ν_t values since there is greater variability in the CIEF current relative to CE. The corrections were performed by multiplying the original mobilization times of the 20, 25, and 30 °C separations by their corresponding viscosity correction factor. The viscosity-corrected separations are shown in Figure 3B. Aligned peaks at different separation temperatures resulting from the viscosity correction are highlighted with red, blue, and black boxes.

Ω Plot Generation. For measurement of currents during the focusing step, CIEF buffer was loaded, voltage was applied for 1 min, the maximum current was measured, and the process was

(49) Holinger, E. P.; Old, W. M.; Giddings, T. H., Jr.; Wong, C.; Yates, J. R., 3rd; Winey, M. *J. Biol. Chem.* **2009**, *284*, 12949–12955.
(50) Shen, Y. F.; Smith, R. D. *J. Microcolumn Sep.* **2000**, *12*, 135–141.
(51) Mack, S.; Cruzado-Park, I.; Chapman, J.; Ratnayake, C.; Vigh, G. *Electrophoresis* **2009**, *30*, 4049–4058.
(52) Peng, X.; Bebault, G. M.; Sacks, S. L.; Chen, D. D. Y. *Can. J. Chem.* **1997**, *75*, 507–517.
(53) Shibukawa, A.; Lloyd, D. K.; Wainer, I. W. *Chromatographia* **1993**, *37*, 113.

repeated for each voltage. For measurement of currents during the mobilization step, CIEF buffer was loaded, a 25 kV focusing voltage was applied for 10 min, the capillary outlet was switched to 350 mM acetic acid, a 30 kV mobilization voltage was applied for 30 min, and measurements were taken for 15 s at each voltage. All measurements were made with the sample thermostatted at 4 °C and the capillary at 15 °C.

RESULTS AND DISCUSSION

Implications of Protein Complex Purification Methods. In recent years biological studies have emphasized the identification and analysis of protein complexes involved in physiological processes. Methods and strategies have evolved, for example, for the large-scale analysis of protein complexes from different model organisms. Commonly, protein complexes are isolated using genetically integrated purification tags or antibodies,[54] as illustrated in Figure 1A. The two complexes analyzed herein were purified using the His-tagged Spc34 protein from *E. coli* (Dam1 complex) and the FLAG-tagged mLST8 from HEK-293T cells (mTORC1 and 2). For comparison, most native mass spectrometry experiments of complexes have been performed on overexpressed proteins from *E. coli* with well know purification strategies.[15,16,21] Recent advances in stabilization of soluble[17,55] and membrane bound[56,57] protein complexes are quite promising, yet it is likely there will always be protein complexes which will not be compatible with native mass spectrometry. Isolation of an endogenous protein complex using a particular protein as "bait" will yield a variety of protein isoforms or subcomplexes to which the protein belongs. To sort out the physiological roles of each of the protein complex forms and subcomplexes, methods to purify and study the complexes are needed. The versatility of native CIEF, similar to MudPIT analysis of protein complexes,[25] should complement other methods for protein complex analysis.

Separation Temperature Control during Native CIEF. Essential to protein complex isoform separation and analysis is maintenance of protein complex integrity prior to detection of the separated complexes. Traditional biochemical separations and purifications of protein complexes are often performed at 4 °C to maintain the complex integrity and stability.[26] Our current instrument configuration limited capillary cooling to 15 °C. To properly thermostat the capillary during separations even with active cooling, Joule heating must be avoided. Joule heating in capillary electrophoresis is the resistive heating of buffer in the capillary by the current generated from the high voltages applied during the separation. Joule heating is best known for its adverse effects on separation efficiency,[58] but can have many other detrimental effects.[59] In this case, we were concerned that internal heating of the buffer may cause dissociation of native complexes.

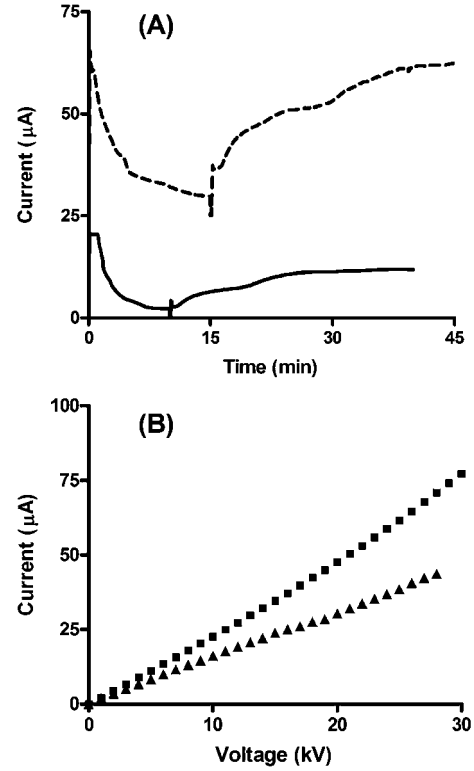

Figure 2. (A) CIEF current traces for 50 μm (—) and 100 μm (- - -) ID capillaries. The current trace for the 100 μm ID capillary was offset 25 μA for clarity. (B) Ω plot for the focusing (■) and mobilization (▲) steps using a 100 μm ID capillary.

Often this is not an issue with CIEF since viscosity increasing additives decrease the current and small inner diameter capillaries adequately disperse heat.[51,60] We eliminated viscosity additives for native conditions and tested both 50 and 100 μm inner diameter capillaries in the interest of preparative fractionation. The highest voltage in capillary isoelectric focusing yields the best isoelectric point resolution,[61] so we determined the conditions which yielded the best possibility for resolving protein complex isoforms and subcomplexes. We tested the acceptable voltages and currents for focusing and mobilization because the current varies dramatically during CIEF runs, particularly with cathodic mobilization.[62] As shown in Figure 2A, the maximum voltages during CIEF occur at the beginning of the focusing step and the end of the mobilization step. Plotting the current generated at different voltages yields an Ω plot. A positive inflection from linearity indicates the onset of Joule heating conditions. Figure 2B illustrates that Joule heating occurs during the focusing at a voltage of 25 kV and current of 50 μA. Thus, 50 μA was set as the maximum current allowable for the two step process.

Protein Complex Stability during Native CIEF. Little is known about the stability of protein complexes during CIEF. CIEF profiling of *E. coli* protein complexes using UV detection indicated a few unknown ~550 kDa protein complexes were stable during the course of separations, but not after 8 h.[47] Thus, we investigated the effects of separation temperature on the stability of a known

(54) Monti, M.; Cozzolino, M.; Cozzolino, F.; Vitiello, G.; Tedesco, R.; Flagiello, A.; Pucci, P. *Expert Rev. Proteomics* **2009**, *6*, 159–169.
(55) Bagal, D.; Kitova, E. N.; Liu, L.; El-Hawiet, A.; Schnier, P. D.; Klassen, J. S. *Anal. Chem.* **2009**, *81*, 7801–7806.
(56) Barrera, N. P.; Di Bartolo, N.; Booth, P. J.; Robinson, C. V. *Science* **2008**, *321*, 243–246.
(57) Barrera, N. P.; Isaacson, S. C.; Zhou, M.; Bavro, V. N.; Welch, A.; Schaedler, T. A.; Seeger, M. A.; Miguel, R. N.; Korkhov, V. M.; van Veen, H. W.; Venter, H.; Walmsley, A. R.; Tate, C. G.; Robinson, C. V. *Nat. Methods* **2009**, *6*, 585–587.
(58) Foret, F.; Deml, M.; Bocek, P. *J. Chromatogr.* **1988**, *452*, 601–613.
(59) Evenhuis, C. J.; Haddad, P. R. *Electrophoresis* **2009**, *30*, 897–909.
(60) Thormann, W.; Tsai, A.; Michaud, J. P.; Mosher, R. A.; Bier, M. *J. Chromatogr.* **1987**, *389*, 75–86.
(61) Wang, Y.; Balgley, B. M.; Lee, C. S. *Expert Rev. Proteomics* **2005**, *2*, 659–667.
(62) Manabe, T.; Miyamoto, H.; Iwasaki, A. *Electrophoresis* **1997**, *18*, 92–97.

protein complex, Dam1. The 10-mer Dam1 complex is part of the outer kinetochore in yeast, an arrangement of at least 65 proteins, which is responsible for attachment of sister chromatids to microtubules for segregation during mitosis.[63] Phosphorylation of the protein Dam1 within the complex by Mps1 kinase is required for coupling of the kinetochore to the plus-ends of microtubules.[64] The purification and kinase assay developed for characterization of the Dam1 complex make it an excellent protein complex model to generally evaluate protein complex stabilization and separation using native CIEF.

Dam1 is a stable complex, but in order to confirm the association of the Dam1 complex at 15 °C, we used increasing capillary temperature to monitor the dissociation of the complex. The results are illustrated in Figure 3A. Comparison of the native CIEF electropherograms from increased separation temperatures appear to show a general trend of increased dissociation of the Dam1 complex to its components. From 20 to 30 °C, the large broad peak completely disappears and the small sharp peak intensities increase, indicative of thermal dissociation of the complex to its components. Thus, the largest broad peak, most prominent in the 15 and 20 °C electropherograms, can be indirectly identified as the intact Dam1 complex. Small sharp peaks in the separation at 15 °C indicate a minor amount of dissociation of the Dam1 complex to its components.

The Dam1 complex peak is unusually broad for CIEF. This was likely due to aggregation since sample was overloaded (1.2 μg) to adequately detect the complex dissociation components. Aggregation of antibodies during CIEF yield similar results.[51] To test the possibility that Dam1 dissociates upon focusing from capillary overloading, a separation of Dam1 under normal loading conditions (120 ng) was performed (Figure 4A). An extremely sharp peak with a few other small peaks was observed. These results indicate that either the Dam1 complex remains completely intact when not overloaded or that the dissociated protein signals are below the limit of detection.

Dam1 Subcomplex Separation. One might expect that as the separation temperature was increased, the Dam1 complex would lose individual proteins one at a time until it was fully dissociated into its 10 components (listed in Table 1). With each increase in separation temperature an increasing number of peaks should have been detected until a maximum was reached. However, after close examination of the number of peaks from dissociation of the Dam1 complex at different temperatures it became obvious that the electropherogram from separations performed at 25 °C, and not 30 °C, had the most peaks. This is clearly illustrated in the viscosity corrected and expanded separations in Figure 3B. This counterintuitive trend was likely due to the partial dissociation of the complex into subcomplexes with higher thermodynamic stability than the complex itself. Peaks present at 25 °C, but not 30 °C, were marked (●) as likely subcomplexes. At 30 °C, the Dam1 complex and its subcomplexes appear to be completely dissociated into their component proteins which were then focused individually to their isoelectric points.

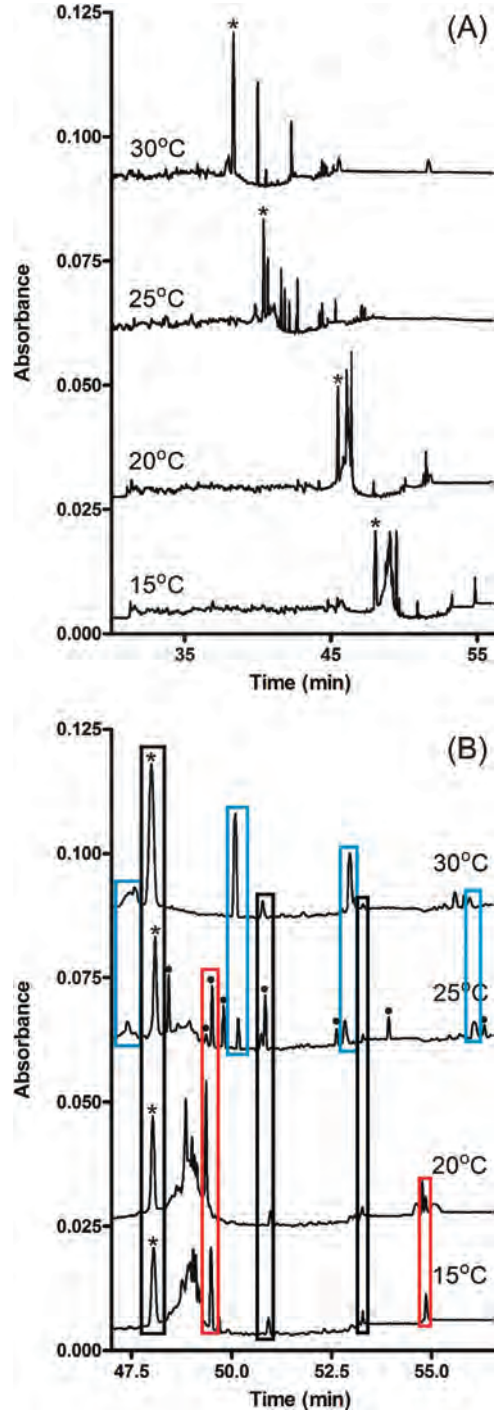

Figure 3. Thermal dissociation studies of the Dam1 complex. (A) CIEF separations of 500 μg/mL Dam1 complex at different separation temperatures using a 100 μm HPC coated capillary. The peaks marked with (*) were used as a mobilization marker for viscosity corrections. (B) The same CIEF separations from (A) viscosity corrected and expanded in the region of Dam1 complex peaks. Potential subcomplex peaks were marked with (●) in the 25 °C separation. Peaks that were common to specific separation temperatures were enclosed with a box, marking individual proteins (blue), subcomplexes (red), and potentially individual proteins, system peaks, or impurities (black).

Note there are fewer than 10 protein peaks in the 30 °C separation. This was likely a detection issue since only 7 of the 10 Dam1 components have tryptophan (see Table 1), the highest adsorbing residue at 280 nm. Tyrosine is present in all Dam1 complex

(63) McAinsh, A. D.; Tytell, J. D.; Sorger, P. K. *Annu. Rev. Cell Dev. Biol.* **2003**, *19*, 519–539.

(64) Shimogawa, M. M.; Graczyk, B.; Gardner, M. K.; Francis, S. E.; White, E. A.; Ess, M.; Molk, J. N.; Ruse, C.; Niessen, S.; Yates, J. R., 3rd; Muller, E. G.; Bloom, K.; Odde, D. J.; Davis, T. N. *Curr. Biol.* **2006**, *16*, 1489–1501.

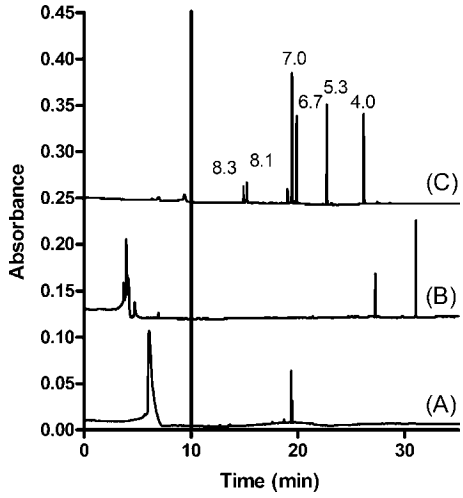

Figure 4. Dam1 complex phosphorylation analysis. CIEF separations of (A) 50 μg/mL purified Dam1 complex, (B) 50 μg/mL Dam1 with ~1 μg/mL Mps1 kinase, and (C) 10 μM pI markers for monitoring pI shift in Dam1 using a 100 μm HPC coated capillary. The focusing and mobilization steps were differentiated using a solid vertical line at 10 min.

Table 1. Known, Confirmed Protein Components Making up the Dam1 Complex with Their Theoretical Molecular Weights and Isoelectric Points, Calculated Using ExPASy (www.expasy.org) with Sequences From the *Saccharomyces* Genome Database (http://www.yeastgenome.org/)[a]

Protein	MW (kDa)	pI	No. of W's	No. of Y's
Dam1	38.4	9.2	1	6
Spc34−6XHis	34.9	8.3	1	9
Duo1	27.5	10.0	2	4
Dad1	10.5	4.2	2	13
Dad2	15.1	4.1	2	2
Dad3	10.8	5.3	0	3
Dad4	8.2	6.7	0	1
Spc19	18.9	4.8	0	3
Ask1	32.1	4.6	1	2
Hsk3	8.1	7.9	1	4
total	**204.5**		**10**	**47**
average		**6.5**	**1**	**4.7**

[a] Note that post-translational modifications are not accounted for in the calculations. The number of tryptophan (W) and tyrosine (Y) residues, necessary for UV detection at 280 nm, were counted from their protein sequences.

components, but has a ~5-fold lower extinction coefficient.[65] Three of the peaks present at all separation temperatures, indicated by the black boxes spanning all separation temperatures, were categorized as either individual proteins which do not interact with the Dam1 complex under the given conditions, system peaks from separations under overloading conditions, or impurities. Four other component proteins are only detected individually at 25 and 30 °C, indicated by blue rectangles spanning only those temperatures. The red boxes designate subcomplexes that are present at temperatures lower than 25 °C and thus bound to the Dam1 complex less tightly.

The direct observation of subcomplexes was not new and has been shown for the well-studied RNA polymerase III using traditional molecular biology techniques[66] and native mass spectrometry.[21] Similarly, a bioinformatic analysis of four global protein complex data sets from yeast identified statistically probable subcomplexes.[24] However, by performing the native CIEF separations at different temperatures in solution, we will be able to understand and quantify the thermodynamic characteristics of protein subcomplexes within a given protein complex. A similar strategy was used for native MS analysis of the solution-phase equilibria of a small heat shock protein.[22]

Dam1 Complex Phosphorylation State Separation. CIEF has proven useful for identification and quantification of protein phosphorylation due to the inherent isoelectric point shift associated with addition of a phosphate moiety to a serine, threonine, or tyrosine residue.[67,68] We were able to extend this analysis to protein complexes using native CIEF through detection of the isoelectric point shift of Dam1 phosphorylation in vitro by Mps1 kinase. The CIEF results are shown in Figure 4. Addition of purified Mps1 kinase causes an average stoichiometry of phosphorylation of 8.3 moles phosphate per mole of Dam1 complex from a radioactivity kinase assay (unpublished results). The Mps1 kinase was 50-fold lower in concentration than the Dam1 complex and thus below the limit of detection. Therefore we reason that both sharp peaks in Figure 4B are the Dam1 complex with different phosphorylation stoichiometries. Based on the peak height ratio (2:1), the close proximity of the peaks (similar pI and thus phosphorylation state), and the average stoichiometry of 8.3 from the radioactivity assay, we hypothesize that the two phosphorylation states of the Dam1 complex are either hepta- and nona-phosphorylated or penta- and deca-phosphorylated. However, further analysis with mass spectrometry will be necessary to elucidate the phosphorylation stoichiometry of the two states. Analysis of nonstoichiometric phosphorylation of proteins is a constant challenge using mass spectrometry.[69] The ability to differentiate and quantify different phosphorylation stoichiometries, particularly of protein complexes, their isoforms, and subcomplexes, will be highly beneficial in numerous biological studies.

The peak height ratio of the differentially phosphorylated Dam1 complex was used to estimate their phosphorylation states, yet there is a discrepancy in the peak heights of the phosphorylated and unphosphorylated Dam1 complexes (Figure 4A versus 4B). We believe this may have been due to loss of the unphosphorylated Dam1 complex during focusing due to EOF. For these separations, we used in-house hydroxypropyl cellulose-coated capillaries which may have inactivated the capillary surface to different degrees. Since the unphosphorylated Dam1 complex is nearer to the capillary outlet, a fraction of it could have been mobilized out of the capillary during the focusing step prior to detection. The slower focusing rate of the unphosphorylated Dam1 complex, illustrated in the 0−10 min region of Figure 4A and 4B, further supports this idea. Additionally, this explains the much shorter mobilization times for the Dam1 complex in Figure 4

(65) Holiday, E. R. *Biochem. J.* **1936**, *30*, 1795–1803.
(66) Myer, V. E.; Young, R. A. *J. Biol. Chem.* **1998**, *273*, 27757–27760.
(67) Shiraishi, M.; Loutzenhiser, R. D.; Walsh, M. P. *Electrophoresis* **2005**, *26*, 571–580.
(68) Wei, J.; Yang, L.; Harrata, A. K.; Lee, C. S. *Electrophoresis* **1998**, *19*, 2356–2360.
(69) Paradela, A.; Albar, J. P. *J. Proteome Res.* **2008**, *7*, 1809–1818.

Table 2. List of Viscosity Correction (ν) Values Based on Either Migration Time (t) or Average Mobilization Current (I)[a]

separation temperature (°C)	ν_t	ν_I
15	1	1
20	1.06	1.07
25	1.19	1.21
30	1.25	1.31

[a] Migration time corrections in Figure 3B were made using ν_t values.

relative to Figure 3. Thus, the peak heights of the phosphorylated Dam1 complex should be more accurate and comparable than the unphosphorylated Dam1 complex peak height.

mTORC1 and 2 Protein Complex Isoform Separation. The mammalian target of rapamycin (mTOR) is a serine/threonine protein kinase known to be involved in cell metabolism, growth, and survival. It has been implicated in cancer, type 2 diabetes, and neurodegenerative diseases.[70] mTOR participates in two distinct complexes, mTORC1 and mTORC2, making it an ideal model protein complex isoform. The rapamycin-sensitive mTOR signaling complex (mTORC1), composed of mTOR, Raptor, mLST8, PRAS40, and Deptor, regulates cell growth and translation through phosphorylation of eIF-4E binding protein 1 and S6 kinase.[71−75] The rapamycin-insensitive mTOR signaling complex (mTORC2), composed of mTOR, Rictor, mLST8, mSIN1, Protor, and Deptor, controls cell proliferation and survival by phosphorylating and activating the Akt/PKB kinase.[75–81] A method for separating mTORC1 and 2 for further biochemical characterization would improve our understanding of the function of each complex and its role in human diseases. Since both complexes exist in the same cellular environment[82] and are theoretically similar in size and isoelectric point (Table 3), their separation is a formidable challenge. Previous efforts to separate mTORC1 and 2 using conventional gel filtration chromatography had neither the resolution nor the short analysis time to maintain mTORC2 complex integrity.[83]

Using native CIEF we were able to resolve mTORC1 and 2, shown in Figure 5A. As expected, due to the similar components of the complexes the high efficiency CIEF separation technique was necessary to resolve the complex isoforms with very similar isoelectric points. Using isoelectric point markers, we estimate the isoelectric points of the complex isoforms are 5.88 (mTORC1) and 5.94 (mTORC2). Comparison of the peak areas for the two complexes in Figure 5A indicates that, under the conditions for isolation and separation, there is double the amount of mTORC1 present relative to mTORC2. Addition of a narrow range of

Table 3. The Known, Confirmed Protein Components Making up mTORC1 and 2 with Their Theoretical Molecular Weights and Isoelectric Points, Calculated Using ExPASy (www.expasy.org) from Human Protein Sequences Listed by NIH (www.ncbi.nlm.nih.gov/protein)[a]

mTORC1	MW (kDa)	pI	mTORC2	MW (kDa)	pI
mTOR	288.9	6.7	mTOR	288.9	6.7
mLST8	35.9	5.5	mLST8	35.9	5.5
Deptor	46.3	8.3	Deptor	46.3	8.3
Raptor	149.0	6.4	Rictor	192.2	7.2
PRAS40	27.4	4.7	Protor	40.9	6.3
			SIN1	59.1	7.2
total	**547.5**		**total**	**665.1**	
average		**6.3**	**average**		**7.2**

[a] Note that the theoretical molecular weight and pI may be inaccurate since some unknown proteins may have yet to be identified in the complexes and post-translational modifications are not accounted for in the calculations.

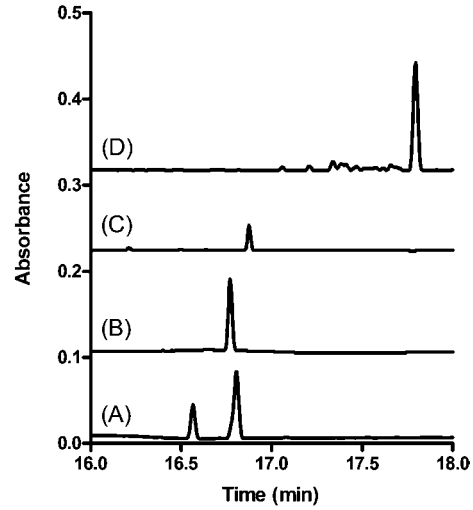

Figure 5. CIEF separations of 25 μg/mL mTORC1 and 2 with different conditions using a 50 μm PVA coated capillary. (A) Successful separation of mTORC1 and 2 upon immediate analysis with 1.7% w/v pI 3−10 and 2.1% w/v pI 4−6.5 ampholytes. (B) Replicate analysis of mTORC1 and 2 as in (A) after 5 h. (C) Separation of dissociated mTORC1 and 2 as in (A) after storage at 4 °C for one week. (D) Unsuccessful separation of mTORC1 and 2 using only 1.7% w/v pI 3−10 ampholytes.

(70) Goberdhan, D. C.; Boyd, C. A. *Biochem. Soc. Trans.* **2009**, *37*, 213–216.
(71) Hara, K.; Maruki, Y.; Long, X.; Yoshino, K.; Oshiro, N.; Hidayat, S.; Tokunaga, C.; Avruch, J.; Yonezawa, K. *Cell* **2002**, *110*, 177–189.
(72) Kim, D. H.; Sarbassov, D. D.; Ali, S. M.; King, J. E.; Latek, R. R.; Erdjument-Bromage, H.; Tempst, P.; Sabatini, D. M. *Cell* **2002**, *110*, 163–175.
(73) Kim, D. H.; Sarbassov, D. D.; Ali, S. M.; Latek, R. R.; Guntur, K. V.; Erdjument-Bromage, H.; Tempst, P.; Sabatini, D. M. *Mol. Cell* **2003**, *11*, 895–904.
(74) Vander Haar, E.; Lee, S. I.; Bandhakavi, S.; Griffin, T. J.; Kim, D. H. *Nat. Cell Biol.* **2007**, *9*, 316–323.
(75) Peterson, T. R.; Laplante, M.; Thoreen, C. C.; Sancak, Y.; Kang, S. A.; Kuehl, W. M.; Gray, N. S.; Sabatini, D. M. *Cell* **2009**, *137*, 873–886.
(76) Sarbassov, D. D.; Ali, S. M.; Kim, D. H.; Guertin, D. A.; Latek, R. R.; Erdjument-Bromage, H.; Tempst, P.; Sabatini, D. M. *Curr. Biol.* **2004**, *14*, 1296–1302.
(77) Frias, M. A.; Thoreen, C. C.; Jaffe, J. D.; Schroder, W.; Sculley, T.; Carr, S. A.; Sabatini, D. M. *Curr. Biol.* **2006**, *16*, 1865–1870.
(78) Jacinto, E.; Facchinetti, V.; Liu, D.; Soto, N.; Wei, S.; Jung, S. Y.; Huang, Q.; Qin, J.; Su, B. *Cell* **2006**, *127*, 125–137.
(79) Yang, Q.; Inoki, K.; Ikenoue, T.; Guan, K. L. *Genes Dev.* **2006**, *20*, 2820–2832.
(80) Pearce, L. R.; Huang, X.; Boudeau, J.; Pawlowski, R.; Wullschleger, S.; Deak, M.; Ibrahim, A. F.; Gourlay, R.; Magnuson, M. A.; Alessi, D. R. *Biochem. J.* **2007**, *405*, 513–522.
(81) Sarbassov, D. D.; Guertin, D. A.; Ali, S. M.; Sabatini, D. M. *Science* **2005**, *307*, 1098–1101.
(82) Sarbassov, D. D.; Ali, S. M.; Sabatini, D. M. *Curr. Opin. Cell Biol.* **2005**, *17*, 596–603.
(83) Yip, C. K.; Murata, K.; Walz, T.; Sabatini, D. M.; Kang, S. A. *Mol. Cell* **2010**, *38*, 768–774.

ampholytes (pH 4−6.5) was necessary to achieve resolution and possibly maintain mTORC2 stability, illustrated by comparison of Figure 5A and D. We used the narrow range ampholytes to decrease the slope of the pH gradient in the pH 4−6.5 region and to increase resolution of the already established pH 3−10 gradient. CIEF separations have been performed with only small range ampholytes,[51] but the combination of ampholytes allows for monitoring a larger pH range while improving resolution in a region of interest.[84]

The native conditions and short analysis time of CIEF made separation and maintenance of the unstable mTORC2 possible. Upon replicate analysis after storage with carrier ampholytes at 4 °C for five hours, the mTORC2 peak completely disappeared as seen in Figure 5B. Similar results were found from CIEF separations of protein complexes from *E. coli* extracts stored in ampholytes for extended periods.[47] mTORC1 was more stable and was still detectable in replicate runs well after 5 h in carrier ampholytes at 4 °C (data not shown). From electron microscopy experiments, the complexes were expected to have lifetimes of ca. four days at 4 °C in purification buffer.[83] Indeed, we were able to observe nearly complete dissociation of the complexes after seven days at 4 °C shown in Figure 5C. Thus, native CIEF may also be a cheap, fast, and automated method for characterization of protein complex stability.

CONCLUSIONS

We have demonstrated that native CIEF is a powerful technique for separating large protein complex isoforms and subcomplexes. The capability to resolve these complexes in solution instead of in the gas phase, as in native mass spectrometry, presents the possibility of performing numerous targeted analyses of protein complex composition, post-translational modification state, architecture, stability, equilibrium, and relative abundance under biologically relevant conditions. Further improvements to the CIEF instrumentation to lower separation temperatures and stabilize weakly associated protein complexes like mTORC2 will benefit the aforementioned experiments and allow for accurate quantification of protein complex isoform ratios. Utilization of a more sensitive and selective detector, such as native laser-induced fluorescence or mass spectrometry, would also expand the capabilities of native CIEF. In these experiments, proteins from the dissociated Dam1 complex were detected only when overloaded and mTORC1 and 2 component proteins were barely above the limit of detection at the purification concentration analyzed. Additionally, the coupling of native CIEF to a mass spectrometer would strengthen both native CIEF and native mass spectrometry. Most native mass spectrometry experiments have been performed on highly abundant, easily purified, stable complexes such as RNA polymerase III,[21] the 20S proteosome,[15] and GroEL.[16] Recent advances in stabilization of soluble[17,55] and membrane bound[56,57] protein complexes will surely expand the capabilities for analyzing biologically interesting, uncharacterized complexes. However, native CIEF could drastically simplify the need for structural maintenance of protein complexes during the electrospray and ion transmission processes; resolution of protein complex isoforms and subcomplexes could be achieved prior to mass spectrometric detection. Native CIEF could also expand the capabilities of native mass spectrometry from the added purification of protein complexes prior to the electrospray process.

Biochemical interactions are known to be dependent on pH.[26] Thus, it is possible that native CIEF separation may not be compatible with protein complexes that are sensitive to pH changes. To our knowledge, there have not been any studies which investigate the effect of the exposure of biochemical interactions to different pHs during CIEF. The point detector used for these CIEF experiments did not allow monitoring of complexes during the separation process. However, the stability of these interactions at different pHs could be probed using CE with different pH buffers or CIEF with whole-column detection. Additionally, analysis of other purified native complexes with different biochemical properties will shed further light on this phenomenon.

(84) Poitevin, M.; Morin, A.; Busnel, J. M.; Descroix, S.; Hennion, M. C.; Peltre, G. *J Chromatogr., A* **2007**, *1155*, 230–236.

ACKNOWLEDGMENT

We acknowledge funding from the National Institute of Health grants R01DK074798 (B.R.F), P41RR011823 (J.R.Y.), R01GM40506 (D.R.G., B.G., and T.N.D.), R01AI47389 (D.M.S.), and R01CA103866 (D.M.S), fellowships from the American Cancer Society and LAM Foundation (S.A.K.), and the Department of Defense grant W81XWH-07-1-0448 (D.M.S.). D.M.S is an investigator of the Howard Hughes Medical Institute. We thank Beckman Coulter for their donation of coated capillaries and isoelectric focusing reagents, Scott Mack for many useful conversations about CIEF, and James J. Moresco, Dwight R. Stoll, and Christopher R. Harrison for feedback on the manuscript.

Received for review May 11, 2010. Accepted June 15, 2010.

AC101235K

Molecular Cell
Short Article

Structure of the Human mTOR Complex I and Its Implications for Rapamycin Inhibition

Calvin K. Yip,[1] Kazuyoshi Murata,[3,7] Thomas Walz,[1,2] David M. Sabatini,[3,4,5,6] and Seong A. Kang[3,4,*]
[1]Department of Cell Biology
[2]Howard Hughes Medical Institute
Harvard Medical School, Boston, MA 02115, USA
[3]The Whitehead Institute for Biomedical Research, Nine Cambridge Center, Cambridge, MA 02142, USA
[4]Howard Hughes Medical Institute, Department of Biology, Massachusetts Institute of Technology, Cambridge, MA 02139, USA
[5]Koch Institute for Integrative Cancer Research at MIT, 77 Massachusetts Avenue, Cambridge, MA 02139, USA
[6]Broad Institute, Seven Cambridge Center, Cambridge, MA 02142, USA
[7]Present address: National Institute for Physiological Sciences, 38 Nishigonaka, Myodaiji, Okazaki, Aichi 444-8585, Japan
*Correspondence: skang@wi.mit.edu
DOI 10.1016/j.molcel.2010.05.017

SUMMARY

The mammalian target of rapamycin complex 1 (mTORC1) regulates cell growth in response to the nutrient and energy status of the cell, and its deregulation is common in human cancers. Little is known about the overall architecture and subunit organization of this essential signaling complex. We have determined the three-dimensional (3D) structure of the fully assembled human mTORC1 by cryo-electron microscopy (cryo-EM). Our analyses reveal that mTORC1 is an obligate dimer with an overall rhomboid shape and a central cavity. The dimeric interfaces are formed by interlocking interactions between the mTOR and raptor subunits. Extended incubation with FKBP12-rapamycin compromises the structural integrity of mTORC1 in a stepwise manner, leading us to propose a model in which rapamycin inhibits mTORC1-mediated phosphorylation of 4E-BP1 and S6K1 through different mechanisms.

INTRODUCTION

The mTOR serine/threonine kinase is a member of the phosphoinositide 3-kinase (PI3K)-related kinase (PIKK) family. This conserved protein integrates diverse upstream signals to regulate growth-related processes, including mRNA translation, ribosome biogenesis, autophagy, and metabolism (Sarbassov et al., 2005a). mTOR nucleates two large physically and functionally distinct signaling complexes: mTOR complex 1 (mTORC1) and mTOR complex 2 (mTORC2) (Guertin and Sabatini, 2007). mTORC1 consists of mTOR, raptor (regulatory associated protein of mTOR), PRAS40 (proline-rich AKT substrate 40 kDa), and mLST8 (mammalian lethal with sec-13). mTORC2, on the other hand, is composed of mTOR, mLST8, rictor (raptor independent companion of mTOR), mSIN1 (mammalian stress-activated protein kinase interacting protein 1), and Protor-1 (protein observed with rictor-1) and controls cell proliferation and survival by phosphorylating and activating the Akt/PKB kinase (Sarbassov et al., 2005b). The key structural features that differentiate the substrate specificity of mTORC1 and mTORC2 remain unclear.

Unlike mTORC2, mTORC1 appears to play critical roles in cell growth in response to nutrients. The mTOR protein, which consists of multiple HEAT repeats at its N-terminal half followed by the FKBP12-rapamycin-binding (FRB) and serine-threonine protein kinase domains near its C-terminal end, has no known enzymatic functions besides its kinase activity. PRAS40 has been characterized as a negative regulator of mTORC1 (Sancak et al., 2007; Vander Haar et al., 2007; Wang et al., 2007), but the functions of other mTOR-interacting proteins in mTORC1 are ambiguous. Previous studies indicate that raptor may have roles in mediating mTORC1 assembly, recruiting substrates, and regulating mTORC1 activity and subcellular localization (Hara et al., 2002; Kim et al., 2002; Sancak et al., 2008). The strength of the interaction between mTOR and raptor can be modified by nutrients and other signals that regulate the mTORC1 pathway, but how this translates into regulation of the mTORC1 pathway remains elusive. The role of mLST8 in mTORC1 function is also unclear, as the chronic loss of this protein does not affect mTORC1 activity in vivo (Guertin et al., 2006). However, the loss of mLST8 can perturb the assembly of mTORC2 and its function. The small GTP-binding protein Rheb (Ras homolog enriched in brain) binds near the mTOR kinase domain (Long et al., 2005) and seems to have a key role in stimulating the kinase activity of mTORC1 (Long et al., 2005; Sancak et al., 2007).

mTORC1 can be hyperactivated by oncogenic phosphoinositide 3-kinase signaling and promotes cellular growth in cancer (Guertin and Sabatini, 2007; Shaw and Cantley, 2006). mTORC1 drives growth through at least two downstream substrates, S6 kinase 1 (S6K1) and eIF-4E-binding protein 1 (4E-BP1) (Richter and Sonenberg, 2005; Ma and Blenis, 2009). The regulation of the activity of mTORC1 toward these and yet unidentified substrates appears to be complex and is likely to be dependent on the organization of the various subunits in the mTORC1 complex. The study of mTORC1 phosphorylation of substrate sites has been greatly aided by pharmacological inhibitors of mTORC1, in particular rapamycin. Rapamycin, in complex with its intracellular receptor FKBP12 (FK506-binding protein of

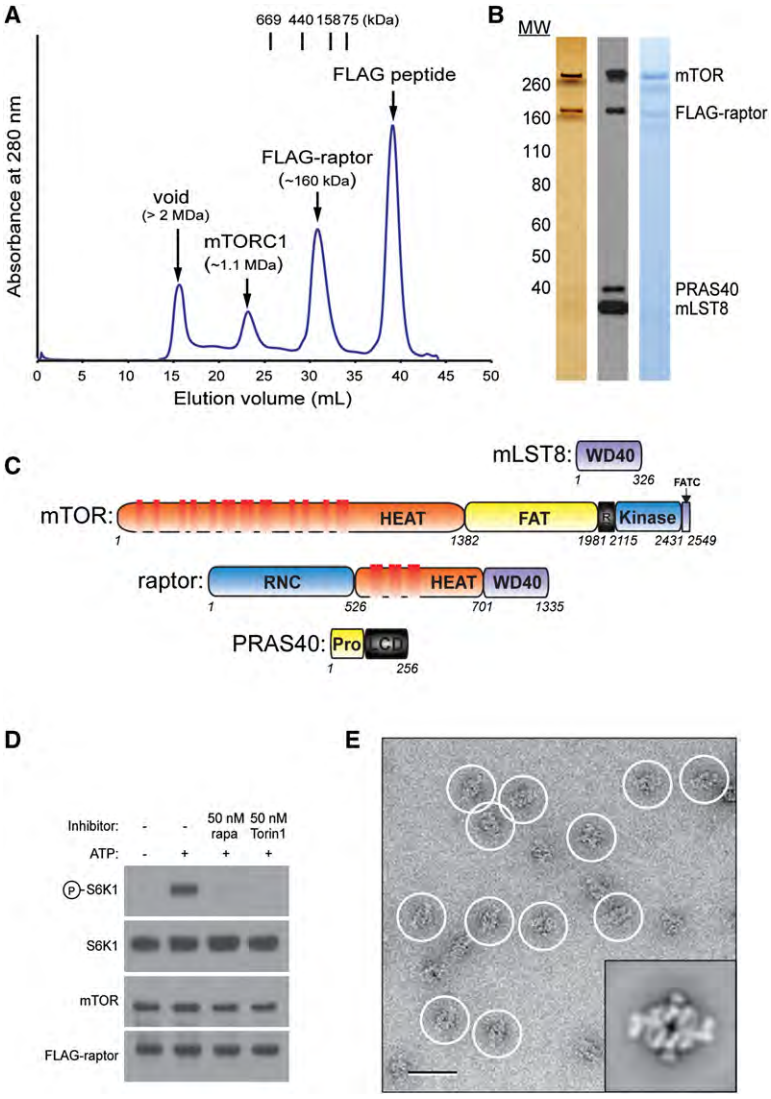

Figure 1. mTORC1 Purification

(A) mTORC1 and FLAG-raptor were purified by tandem gel filtration chromatography. Their masses were estimated based on known molecular weight standards as indicated (Thyroglobulin [669 kDa], Ferritin [440 kDa], Aldolase [158 kDa], and Conalbumin [75 kDa]).

(B) The gel filtration fraction corresponding to mTORC1 was analyzed by SDS-PAGE followed by silver and Coomassie staining as well as immunoblotting for indicated proteins.

(C) Schematics of mTORC1 components illustrating the various predicted domains.

(D) In vitro kinase assay showing that purified mTORC1 phosphorylates S6K1 and is inhibited by both rapamycin-FKBP12 (rapa) and Torin1.

(E) EM of negatively stained mTORC1. A raw image of mTORC1 particles (circled) and a representative class average from the classification of 10,080 particles (inset). The scale bar represents 50 nm, and the side length of the panel showing the class average is 45 nm.

See also Figure S1.

12 kDa), acutely inhibits mTORC1 by binding to the FRB domain of mTOR (Sarbassov et al., 2005a). Yet, the molecular mechanism of how this high-affinity interaction perturbs mTOR kinase activity and the fully assembled mTORC1 is currently unknown. Although there have been attempts to model the N-terminal domain of mTOR based on the low-resolution structure of human DNA-PK (Sibanda et al., 2010), these efforts have failed to provide insights into the function and regulation of the mTOR kinase. Thus, a detailed knowledge of mTORC1 structure, including the organization of its components, has the potential to help understand the regulation of its kinase activity and to aid in the development of more effective mTORC1 inhibitors. We report the three-dimensional (3D) structure of human mTORC1 as determined by cryo-EM. This structure, together with labeling and biochemical studies, reveals the intricate organization of the components within mTORC1 and provides structural insights into the mechanism of its inhibition by FKBP12-rapamycin.

RESULTS AND DISCUSSION

Purification of Human mTORC1

The large size (~1 MDa) and instability of mTORC1 make it difficult to obtain the purified complex for structural analysis. To address this issue, we devised a method to purify microgram quantities of intact and active human mTORC1. Keys to the successful purification of mTORC1 were (1) the development of a human cell line stably expressing a tagged raptor subunit that incorporates into endogenous mTORC1, (2) the identification of buffer conditions that minimize mTORC1 disintegration and/or aggregation during purification, and (3) the implementation of tandem gel filtration chromatography steps to separate mTORC1 from other large contaminants (Figure 1A). Purified mTORC1 consists of equimolar quantities of mTOR, raptor, and mLST8 and of PRAS40 at substoichiometric level (Figures 1B and 1C). The kinase activity of purified mTORC1 toward S6K1 was sensitive to FKBP12-rapamycin and Torin1, an ATP-competitive inhibitor of mTOR (Thoreen et al., 2009) (Figure 1D). Negative-stain EM analysis of the purified complex revealed particles that were homogeneous in size and shape (Figure 1E). Projection averages calculated from the classification of 10,080 particle images illustrated that mTORC1 has an elongated, rhomboid shape with a central, stain-filled cavity and "feet-like" protrusions emanating from both ends of the molecule (Figure 1E, inset, and Figure S1 available online). The averages displayed a 2-fold symmetry. This observation, together with the mass estimated from gel filtration, provides evidence for the obligate dimeric organization of mTORC1 that had been previously suggested by genetic and coimmunoprecipitation studies (Zhang et al., 2006; Takahara et al., 2006; Urano et al., 2007; Wang et al., 2006). Although PRAS40 was present in substoichiometric amounts in our purified mTORC1 sample, the fact that all averages show particles

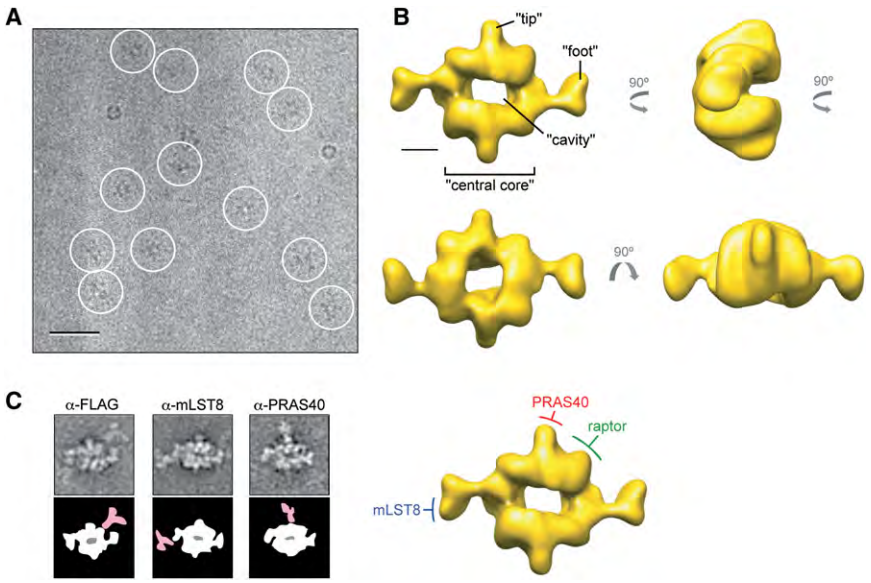

Figure 2. Cryo-EM Reconstruction of mTORC1 and Its Molecular Organization

(A) Image of a vitrified specimen showing individual mTORC1 particles (circled). The scale bar represents 50 nm.

(B) Different views of the 3D reconstruction of mTORC1 filtered to 26 Å, with the main structural features denoted. The scale bar represents 5 nm.

(C) Molecular organization of mTORC1. (Left) Representative class averages from antibody labeling experiments of mTORC1 (top) and schematic representations showing mTORC1 in white and the antibody in pale red (bottom). The side length of each panel is 45 nm. (Right) Location of raptor, mLST8, and PRAS40 in the cryo-EM density map of mTORC1.

See also Figure S2.

with identical overall shape suggests that PRAS40 contributes little to the density of the complex and is not required for proper assembly and stability of mTORC1. Our projection structure does not resemble the monomeric structure obtained from the recent negative-stain EM analysis of *Saccharomyces cerevisiae* TOR in complex with KOG1 (the raptor homolog in yeast) (Adami et al., 2007). These striking differences may be due to the differences in composition and stoichiometry of known components within the two TOR complexes. The sample used in the EM study of the yeast complex may not reflect a fully assembled TORC1 complex but, rather, a subassembly. For example, LST8, a bona fide yeast TORC1 component, is missing in the analyzed sample of the yeast study. In addition, human mTOR and raptor are only conserved over limited regions compared to their yeast orthologs, TOR1 and KOG1, respectively. Therefore, it is conceivable that human mTORC1 and yeast TORC1 could adopt different quaternary structures.

Cryo-EM Structure of mTORC1

To determine the 3D structure of mTORC1 by cryo-EM, we first produced a reliable initial model by calculating a random conical tilt (RCT) reconstruction with 50°/0° tilt pair images of cryo-negatively stained specimens (Figure S2). Collecting images of vitrified mTORC1 specimens proved difficult due to low protein concentration (attempts to concentrate mTORC1 samples were unsuccessful) and a strong tendency of mTORC1 to dissociate upon contact with the air-water interface. We overcame these difficulties by adsorbing mTORC1 to a thin carbon film prior to vitrification. Even so, only a few particles were present (Figure 2A), requiring us to collect many images to obtain a sufficient number of particles for structure determination. The carbon film also induced mTORC1 to adsorb to the grid in a preferred orientation, making it necessary to collect images of tilted specimens to obtain the multiple views needed for 3D reconstruction. The final data set contained 28,325 particle images, including 3,905 from 45° tilted specimens. A 3D reconstruction was calculated by aligning these individual images of the vitrified complex to the initial model produced with the cryo-negatively stained sample, followed by iterative refinement of their orientation parameters. The estimated resolution of the final reconstruction is 26 Å according to the Fourier shell correlation = 0.5 criterion (Figure S2). However, the resolution is clearly anisotropic, with lower resolution in the direction perpendicular to the carbon film, a result of the limited number of views other than the face-on view (Figure S2). mTORC1 has overall dimensions of ~290 Å × 210 Å × 135 Å and an estimated volume of 1.4×10^6 Å^3 at the contour level of the displayed map, which was chosen to be consistent with the calculated molecular mass of dimeric mTORC1 (Figure 2B).

The cryo-EM structure reveals a central cavity that has an oval shape when viewed from one face but a rectangular shape from the opposite face, with two troughs located at the extensions linking the central core to the "feet-like" structures. Though the biological relevance of this cavity remains elusive, its location between the two "monomeric" complexes may enable substrates with multiple phosphorylation sites, such as 4E-BP1 (Gingras et al., 1999), to shuttle between the two mTOR active sites within the complex. Another, albeit less likely, possibility is that the cavity may serve as a docking platform for nucleic acids because its size (~40 Å × 28 Å) is large enough to accommodate double-stranded DNA (dsDNA). Though mTORC1 has not yet been shown to interact with dsDNA or other macromolecules, several members of the PIKK family (Keith and Schreiber, 1995), most notably DNA-PK, are known to mediate DNA repair by directly binding to DNA (Gottlieb and Jackson, 1993; Spagnolo et al., 2006).

Subunit Organization of mTORC1 and EM Structure of Raptor

Whereas the cryo-EM structure revealed the overall shape of mTORC1, at the current resolution, it was not possible to define intermolecular and intersubunit boundaries. Therefore,

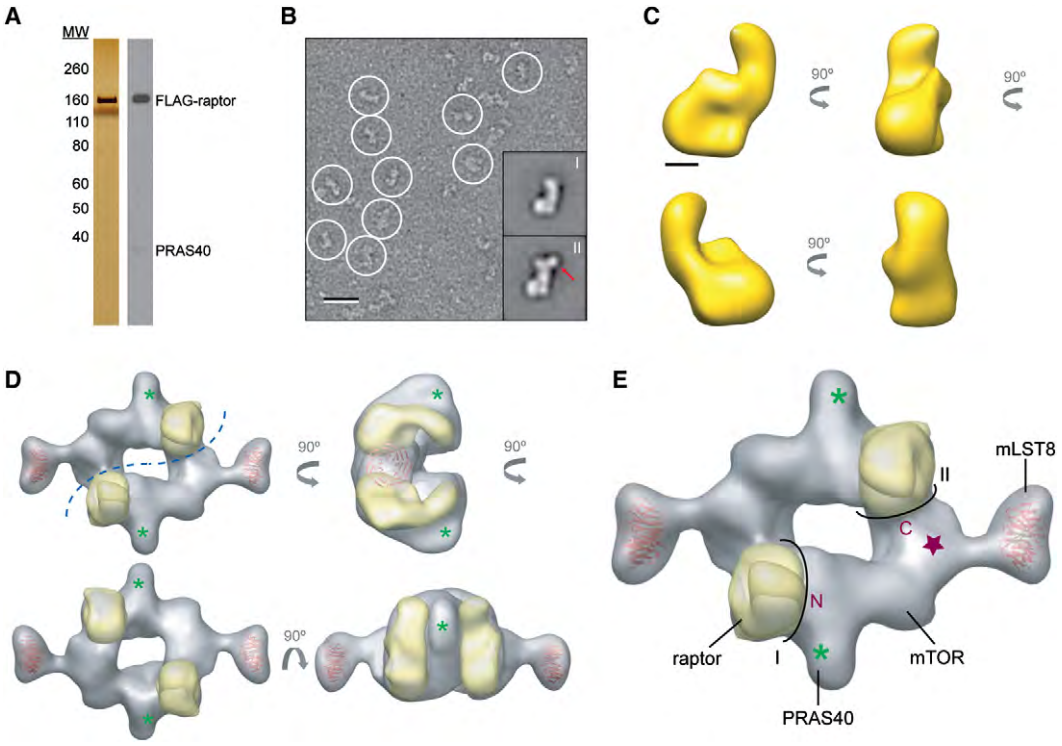

Figure 3. Three-Dimensional Reconstruction of Raptor and Molecular Docking

(A) Silver-stained gel and immunoblot of the gel filtration fraction containing free raptor detected the presence of PRAS40.

(B) EM image of negatively stained raptor (circled) and two representative class averages from the classification of 12,216 particles (bottom-right insets). Class II particles contain an additional density (red arrow) compared to class I particles, which likely represents PRAS40. The scale bar represents 25 nm, and the side length of the panels showing the class averages is 27 nm.

(C) Different views of the raptor 3D reconstruction. The scale bar represents 2.5 nm.

(D) Two copies of the raptor 3D reconstruction (gold) and two models of a representative WD40 domain (PDB code 3EMH, red) were placed into the cryo-EM density map (gray). The green asterisk depicts the location of PRAS40 as determined by antibody labeling. The blue dotted line represents the dimer interface.

(E) The proposed locations of the N- and C-terminal domains (marked "N" and "C") and the kinase domain of mTOR (purple star). The black lines labeled "I" and "II" delineate the two interaction interfaces formed by each mTOR molecule with the two raptor subunits.

See also Figure S3.

we performed antibody labeling experiments to localize individual subunits within mTORC1, including raptor (detected through its FLAG tag), mLST8, and PRAS40. The labeled particles were imaged by negative-stain EM and analyzed by classification and image averaging. We discovered that mLST8 localizes to the distal foot-like structures, PRAS40 to the small tips in the midsection of the central core, and the N terminus of raptor to the corner of the core (Figure 2C). The occasional observation of double-labeled particles provided further assurance for the dimeric organization of mTORC1 (Figure S2).

In addition, we determined the EM structure of raptor. FLAG-tagged raptor that did not incorporate into mTORC1 eluted as a separate peak from gel filtration (Figures 1A and 3A). Purified raptor was homogeneous in size and shape according to negative-stain EM analysis (Figures 3B and S3). The 3D reconstruction of raptor, determined by the RCT approach using 60°/0° image pairs of negatively stained specimens (Figure S3), revealed that its overall shape resembles a "comma" with the circular lobe likely representing the predicted C-terminal WD40 domain (Kim et al., 2002) (Figure 3C). Utilizing the antibody labeling data as a guide, the structure of mTORC1 provides an adequate framework in which the EM reconstruction of raptor can be meaningfully fitted (gold surface in Figure 3D). Because mLST8 is solely composed of a seven-bladed β-propeller (Kim et al., 2003), we next docked two β-propeller models (PDB code 3EMH) into the "foot" substructures (Figure 3D). By subtracting two copies of raptor and mLST8, the densities occupied by two mTOR subunits can be predicted while accounting for minor contributions by the two small PRAS40 subunits (Figure 3D). It has been shown that the C-terminal kinase domain of mTOR associates with mLST8 (Kim et al., 2003), suggesting that this domain is likely positioned adjacent to the "foot" (purple star in Figure 3E). From the position of the kinase domain, we deduced that the N terminus of mTOR interacts with the flat face of one raptor molecule (bottom-left view in Figure 3C), forming interface I, whereas the C terminus interacts with the side of the second raptor molecule (top-right view in Figure 3C), forming interface II. The interlocking raptor-mTOR interactions within the central core provide an understanding of the basis of dimerization and illustrate the crucial function of raptor in mediating and maintaining the higher-order organization of mTORC1 (Figure 3E). In contrast, each mLST8 contacts only one mTOR within the complex. Its localization to

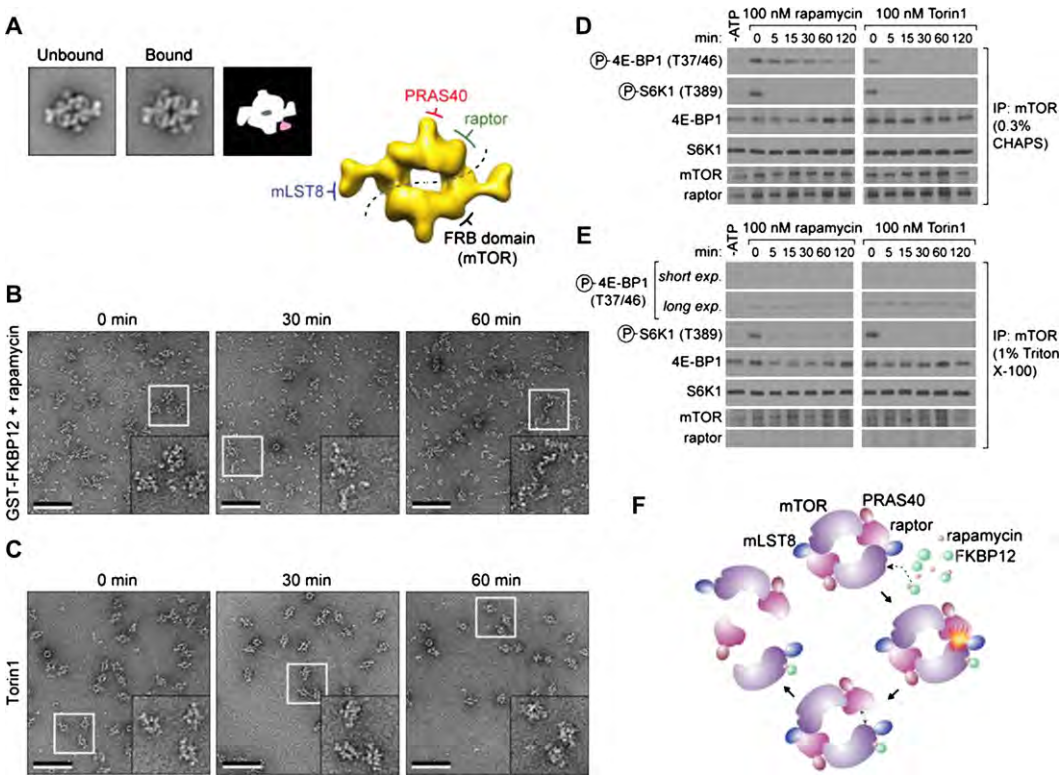

Figure 4. Effects of Rapamycin-FKBP12 on mTORC1

(A) Representative class averages of untreated mTORC1 (left) and mTORC1 treated with 50 nM of rapamycin and 0.02 μg/μl GST-FKBP12 (middle) and a schematic representation showing the additional density in pale red (right). The side length of each panel is 45 nm. To the right, the location of the FRB domain with respect to the other components in the cryo-EM map of mTORC1 is shown.

(B and C) Purified mTORC1 was treated with 50 nM of rapamycin and 0.02 μg/μl GST-FKBP12 or 100 nM Torin1. EM images of negatively stained samples were taken at the indicated time points. The inset in each image shows an enlarged view of the area marked by the white square. The scale bars represent 100 nm.

(D and E) mTOR immunoprecipitates, prepared in lysis buffers containing 0.3% CHAPS or 1% Triton X-100, were subjected to in vitro kinase assays using 4E-BP1 or S6K1 as a substrate in the presence of 100 nM rapamycin and 0.02 μg/μl FKBP12 or 100 nM Torin1. Assays were then analyzed by immunoblotting for the indicated proteins and phosphorylation states.

(F) A model depicting a potential mechanism of mTORC1 inhibition by FKBP12-rapamycin.

See also Figure S4.

the distal "foot" structures suggests that it could potentially assist substrate entry into the catalytic site.

According to our data and composite model, PRAS40 localizes in close proximity to raptor (asterisk in Figure 3D), which is in agreement with the known binding of PRAS40 to raptor (Sancak et al., 2007; Wang et al., 2007). Of interest, some class averages of purified raptor showed an additional small density, which may represent bound PRAS40 (indicated by red arrow in Figures 3B and S3). This interpretation is supported by immunoblots that show PRAS40 to be present in the analyzed raptor fraction (Figure 3A). Thus, our structural data suggest that PRAS40 inhibition is not likely to be achieved through an interaction of PRAS40 with the mTOR kinase domain. Instead, it favors the model that PRAS40 acts as a competitive inhibitor for the binding of mTORC1 substrates to raptor (Wang et al., 2007).

FKBP12-Rapamycin Destabilizes mTORC1 in a Stepwise Manner

With a more detailed understanding of the subunit organization of mTORC1, we next investigated how rapamycin affects its structure. As an allosteric inhibitor of mTORC1, rapamycin requires the intracellular protein FKBP12 to form a gain-of-function complex, which directly interacts with the FKBP12-rapamycin-binding (FRB) domain of mTOR (Chen et al., 1995; Sabatini et al., 1994). The crystal structure of FKBP12-rapamycin in complex with the FRB domain did not reveal how this interaction prevents phosphorylation of direct mTORC1 substrates (Choi et al., 1996). Previous biochemical studies indicated that binding of FKBP12-rapamycin to mTORC1 induces a conformational change that weakens the mTOR-raptor interaction (Kim et al., 2002). To test this hypothesis, we incubated mTORC1 with N-terminal GST-tagged FKBP12 in the presence of 50 nM rapamycin for 15 min and then visualized the particles by negative-stain EM (Figure S4). Although the raw images did not reveal any obvious structural changes (Figure S4), image classification showed that about 10% of the particles featured an additional density, likely constituting FKBP12-rapamycin, tethered to the region that we assigned to mTOR and directly opposite of raptor (Figure 4A). Of interest, we did not observe individual particles or averages of mTORC1 showing two extra densities, suggesting

that either mTORC1 cannot accommodate two FKBP12-rapamycin complexes or that this intermediate is short lived.

Whereas relatively short exposure to FKBP12-rapamycin did not affect the structural integrity of mTORC1, extended incubations resulted in a drastic reduction in the total number of intact mTORC1 particles. Many smaller fragments appeared in the background, suggesting that FKBP12-rapamycin may cause disassembly of mTORC1 (Figure 4B). Once initiated, this dissociation appears to be swift, as we were unable to detect intermediates with defined structures during the course of the reaction (data not shown). After 1 hr incubation, virtually no intact mTORC1 particles could be detected, and the sample contained only smaller fragments, likely representing free mTOR or its subcomplexes, and undefined aggregates (Figure 4B). In contrast, Torin1 did not affect mTORC1 stability even after extended incubation (Figure 4C).

The disruption of mTORC1 by FKBP12-rapamycin may play a role in the inhibition by rapamycin of mTORC1 kinase activity toward certain substrates. Consistent with the time-dependent effects of FKBP12-rapamycin on the structural integrity of mTORC1, FKBP12-rapamycin significantly inhibited the in vitro phosphorylation of 4E-BP1 by mTORC1 only after mTORC1 had been incubated with the drug for at least 60 min (Figure 4D). In contrast, FKBP12-rapamycin rapidly blocked the phosphorylation of S6K1 by mTORC1, and Torin1 quickly blocked the phosphorylation of both S6K1 and 4E-BP1. In close agreement with in vitro kinase assays, in vivo experiments produced similar time-dependent effects of rapamycin on endogenous 4E-BP1, but not S6K1 (Figure S4). To assess the importance of mTORC1 integrity in the phosphorylation of S6K1 and 4E-BP1, we prepared mTORC1 that lacked raptor (Kim et al., 2002). Though raptor-free mTORC1, as predicted (Hara et al., 2002), could not support 4E-BP1 phosphorylation, it was capable of phosphorylating full-length S6K1 (Figure 4E). Furthermore, the phosphorylation of S6K1 by raptor-free mTORC1 was still inhibited by FKBP12-rapamycin. Thus, contrary to previous assumptions, raptor is dispensable for mTORC1 to phosphorylate S6K1 in a rapamycin-sensitive fashion in vitro. Our results suggest an important role for the mTORC1 dimer in 4E-BP1 phosphorylation. Perhaps, 4E-BP1 binds to the raptor in one monomer but is phosphorylated by the kinase of the adjacent monomer, such that, in the absence of dimerization, 4E-BP1 is not in a position to be phosphorylated.

Based on these observations and our knowledge of the molecular organization of mTORC1, we propose the following model for rapamycin-mediated inhibition of mTORC1. The initial binding of one FKBP12-rapamycin to mTORC1 causes a subtle conformational change in mTOR that weakens the mTOR-raptor interaction but does not suffice to disrupt the dimeric architecture. Moreover, the bound FKBP12-rapamycin likely occludes the binding of or blocks access to the active site for larger-sized substrates, such as S6K1. Over time, either amplified structural strain caused by the first FKBP12-rapamycin or, perhaps, the binding of a second rapamycin complex leads to a fast disintegration of the already "weakened" mTORC1 and the complete abolishment of 4E-BP1 phosphorylation (Figure 4F). Therefore, our work suggests that in vitro rapamycin is an mTORC1 inhibitor that may work through at least two different modes. The fact that, within cells, rapamycin does not completely inhibit 4E-BP1 phosphorylation (Choo et al., 2008; Thoreen et al., 2009; Feldman et al., 2009) or mTORC1 stability (Kim et al., 2002) suggests that cells contain buffering mechanisms that counter the effects of rapamycin on mTORC1 and that these are lost when mTORC1 is purified.

EXPERIMENTAL PROCEDURES

Protein Expression and Purification

mTORC1 was purified from a HEK293T cell line that stably expresses N terminally FLAG-tagged raptor by FLAG-M2 monoclonal antibody-agarose and gel filtration. Details of the expression method and purification conditions are described in the Supplemental Experimental Procedures.

In Vitro Kinase Assay

Kinase assays were performed using immunoprecipitated mTORC1 and inactive 4E-BP1 or S6K1 as a substrate. Reactions were analyzed by SDS-PAGE and immunoblotting. Details of the assay conditions are described in the Supplemental Experimental Procedures.

Electron Microscopy

Negatively stained specimens were prepared as described (Ohi et al., 2004). Images were collected with a Tecnai T12 electron microscope (FEI) equipped with a LaB_6 filament and operated at an acceleration voltage of 120 kV. Images were recorded on imaging plates at a nominal magnification of 67,000 using a defocus value of –1.5 μm. Cryo-negatively stained specimens were prepared as described (Ohi et al., 2004). Grids used to collect image pairs of 50°/0° tilted specimens were loaded on an Oxford cryo-transfer holder. Images were taken under low-dose conditions at a nominal magnification of 50,000× and a defocus value of –2.5 μm using a Tecnai F20 electron microscope (FEI) equipped with a field emission electron source operated at an acceleration voltage of 200 kV. For vitrification, Quantifoil R1.2/1.3 400 mesh grids were overlaid with a thin layer of carbon film and glow discharged. 3 μl of mTORC1 (~0.02 mg/ml) was adsorbed to a grid, and the grid was blotted and frozen in liquid ethane using a Vitrobot (FEI). Specimens were examined using a Gatan 626 cryo-holder on a Tecnai F20 electron microscope equipped with a field emission electron source (FEI) operated at 200 kV. Additional details of specimen preparation and data collection are described in the Supplemental Experimental Procedures.

Image Processing

Details are described in the Supplemental Experimental Procedures.

SUPPLEMENTAL INFORMATION

Supplemental Information includes Supplemental Experimental Procedures and four figures and can be found with this article online at doi:10.1016/j.molcel.2010.05.017.

ACKNOWLEDGMENTS

This work was supported by fellowships from the American Cancer Society and LAM Foundation to S.A.K.; grants from the NIH (AI47389 and CA103866), Department of Defense (W81XWH-07-1-0448), and W.M. Keck Foundation to D.M.S.; and fellowships from the Jane Coffin-Childs Memorial Fund and the Canadian Institutes of Health Research to C.K.Y. D.M.S and T.W. are Investigators of the Howard Hughes Medical Institute. The molecular electron microscopy facility at Harvard Medical School was established with a generous donation from the Giovanni Armenise Harvard Center for Structural Biology. We thank Yasemin Sancak, Eric Spooner for technical assistance, Zongli Li for assistance in microscopy and image processing, and members of the Sabatini and Walz laboratories for support and discussions.

Received: January 22, 2010
Revised: March 25, 2010
Accepted: April 29, 2010
Published: June 10, 2010

REFERENCES

Adami, A., García-Alvarez, B., Arias-Palomo, E., Barford, D., and Llorca, O. (2007). Structure of TOR and its complex with KOG1. Mol. Cell *27*, 509–516.

Chen, J., Zheng, X.F., Brown, E.J., and Schreiber, S.L. (1995). Identification of an 11-kDa FKBP12-rapamycin-binding domain within the 289-kDa FKBP12-rapamycin-associated protein and characterization of a critical serine residue. Proc. Natl. Acad. Sci. USA *92*, 4947–4951.

Choi, J., Chen, J., Schreiber, S.L., and Clardy, J. (1996). Structure of the FKBP12-rapamycin complex interacting with the binding domain of human FRAP. Science *273*, 239–242.

Choo, A.Y., Yoon, S.O., Kim, S.G., Roux, P.P., and Blenis, J. (2008). Rapamycin differentially inhibits S6Ks and 4E-BP1 to mediate cell-type-specific repression of mRNA translation. Proc. Natl. Acad. Sci. USA *105*, 17414–17419.

Feldman, M.E., Apsel, B., Uotila, A., Loewith, R., Knight, Z.A., Ruggero, D., and Shokat, K.M. (2009). Active-site inhibitors of mTOR target rapamycin-resistant outputs of mTORC1 and mTORC2. PLoS Biol. *7*, e38.

Gingras, A.C., Gygi, S.P., Raught, B., Polakiewicz, R.D., Abraham, R.T., Hoekstra, M.F., Aebersold, R., and Sonenberg, N. (1999). Regulation of 4E-BP1 phosphorylation: a novel two-step mechanism. Genes Dev. *13*, 1422–1437.

Gottlieb, T.M., and Jackson, S.P. (1993). The DNA-dependent protein kinase: requirement for DNA ends and association with Ku antigen. Cell *72*, 131–142.

Guertin, D.A., and Sabatini, D.M. (2007). Defining the role of mTOR in cancer. Cancer Cell *12*, 9–22.

Guertin, D.A., Stevens, D.M., Thoreen, C.C., Burds, A.A., Kalaany, N.Y., Moffat, J., Brown, M., Fitzgerald, K.J., and Sabatini, D.M. (2006). Ablation in mice of the mTORC components raptor, rictor, or mLST8 reveals that mTORC2 is required for signaling to Akt-FOXO and PKCalpha, but not S6K1. Dev. Cell *11*, 859–871.

Hara, K., Maruki, Y., Long, X., Yoshino, K., Oshiro, N., Hidayat, S., Tokunaga, C., Avruch, J., and Yonezawa, K. (2002). Raptor, a binding partner of target of rapamycin (TOR), mediates TOR action. Cell *110*, 177–189.

Keith, C.T., and Schreiber, S.L. (1995). PIK-related kinases: DNA repair, recombination, and cell cycle checkpoints. Science *270*, 50–51.

Kim, D.H., Sarbassov, D.D., Ali, S.M., King, J.E., Latek, R.R., Erdjument-Bromage, H., Tempst, P., and Sabatini, D.M. (2002). mTOR interacts with raptor to form a nutrient-sensitive complex that signals to the cell growth machinery. Cell *110*, 163–175.

Kim, D.H., Sarbassov, D.D., Ali, S.M., Latek, R.R., Guntur, K.V., Erdjument-Bromage, H., Tempst, P., and Sabatini, D.M. (2003). GbetaL, a positive regulator of the rapamycin-sensitive pathway required for the nutrient-sensitive interaction between raptor and mTOR. Mol. Cell *11*, 895–904.

Long, X., Lin, Y., Ortiz-Vega, S., Yonezawa, K., and Avruch, J. (2005). Rheb binds and regulates the mTOR kinase. Curr. Biol. *15*, 702–713.

Ma, X.M., and Blenis, J. (2009). Molecular mechanisms of mTOR-mediated translational control. Nat. Rev. Mol. Cell Biol. *10*, 307–318.

Ohi, M., Li, Y., Cheng, Y., and Walz, T. (2004). Negative Staining and Image Classification - Powerful Tools in Modern Electron Microscopy. Biol. Proced. Online *6*, 23–34.

Richter, J.D., and Sonenberg, N. (2005). Regulation of cap-dependent translation by eIF4E inhibitory proteins. Nature *433*, 477–480.

Sabatini, D.M., Erdjument-Bromage, H., Lui, M., Tempst, P., and Snyder, S.H. (1994). RAFT1: a mammalian protein that binds to FKBP12 in a rapamycin-dependent fashion and is homologous to yeast TORs. Cell *78*, 35–43.

Sancak, Y., Thoreen, C.C., Peterson, T.R., Lindquist, R.A., Kang, S.A., Spooner, E., Carr, S.A., and Sabatini, D.M. (2007). PRAS40 is an insulin-regulated inhibitor of the mTORC1 protein kinase. Mol. Cell *25*, 903–915.

Sancak, Y., Peterson, T.R., Shaul, Y.D., Lindquist, R.A., Thoreen, C.C., Bar-Peled, L., and Sabatini, D.M. (2008). The Rag GTPases bind raptor and mediate amino acid signaling to mTORC1. Science *320*, 1496–1501.

Sarbassov, D.D., Ali, S.M., and Sabatini, D.M. (2005a). Growing roles for the mTOR pathway. Curr. Opin. Cell Biol. *17*, 596–603.

Sarbassov, D.D., Guertin, D.A., Ali, S.M., and Sabatini, D.M. (2005b). Phosphorylation and regulation of Akt/PKB by the rictor-mTOR complex. Science *307*, 1098–1101.

Shaw, R.J., and Cantley, L.C. (2006). Ras, PI(3)K and mTOR signalling controls tumour cell growth. Nature *441*, 424–430.

Sibanda, B.L., Chirgadze, D.Y., and Blundell, T.L. (2010). Crystal structure of DNA-PKcs reveals a large open-ring cradle comprised of HEAT repeats. Nature *463*, 118–121.

Spagnolo, L., Rivera-Calzada, A., Pearl, L.H., and Llorca, O. (2006). Three-dimensional structure of the human DNA-PKcs/Ku70/Ku80 complex assembled on DNA and its implications for DNA DSB repair. Mol. Cell *22*, 511–519.

Takahara, T., Hara, K., Yonezawa, K., Sorimachi, H., and Maeda, T. (2006). Nutrient-dependent multimerization of the mammalian target of rapamycin through the N-terminal HEAT repeat region. J. Biol. Chem. *281*, 28605–28614.

Thoreen, C.C., Kang, S.A., Chang, J.W., Liu, Q., Zhang, J., Gao, Y., Reichling, L.J., Sim, T., Sabatini, D.M., and Gray, N.S. (2009). An ATP-competitive mammalian target of rapamycin inhibitor reveals rapamycin-resistant functions of mTORC1. J. Biol. Chem. *284*, 8023–8032.

Urano, J., Sato, T., Matsuo, T., Otsubo, Y., Yamamoto, M., and Tamanoi, F. (2007). Point mutations in TOR confer Rheb-independent growth in fission yeast and nutrient-independent mammalian TOR signaling in mammalian cells. Proc. Natl. Acad. Sci. USA *104*, 3514–3519.

Vander Haar, E., Lee, S.I., Bandhakavi, S., Griffin, T.J., and Kim, D.H. (2007). Insulin signalling to mTOR mediated by the Akt/PKB substrate PRAS40. Nat. Cell Biol. *9*, 316–323.

Wang, L., Rhodes, C.J., and Lawrence, J.C., Jr. (2006). Activation of mammalian target of rapamycin (mTOR) by insulin is associated with stimulation of 4EBP1 binding to dimeric mTOR complex 1. J. Biol. Chem. *281*, 24293–24303.

Wang, L., Harris, T.E., Roth, R.A., and Lawrence, J.C., Jr. (2007). PRAS40 regulates mTORC1 kinase activity by functioning as a direct inhibitor of substrate binding. J. Biol. Chem. *282*, 20036–20044.

Zhang, Y., Billington, C.J., Jr., Pan, D., and Neufeld, T.P. (2006). Drosophila target of rapamycin kinase functions as a multimer. Genetics *172*, 355–362.

Cell

Ragulator-Rag Complex Targets mTORC1 to the Lysosomal Surface and Is Necessary for Its Activation by Amino Acids

Yasemin Sancak,[1,2,3,6] Liron Bar-Peled,[1,2,3,6] Roberto Zoncu,[1,2,3] Andrew L. Markhard,[1,2] Shigeyuki Nada,[4] and David M. Sabatini[1,2,3,5,*]

[1]Whitehead Institute for Biomedical Research, 9 Cambridge Center, Cambridge, MA 02142, USA
[2]Department of Biology, Massachusetts Institute of Technology, Cambridge, MA 02139, USA
[3]The David H. Koch Institute for Integrative Cancer Research at MIT, 77 Massachusetts Avenue, Cambridge, MA 02139, USA
[4]Department of Oncogene Research, Research Institute for Microbial Diseases, Osaka University, 3-1 Yamadaoka, Suita, Osaka 565-0871, Japan
[5]Howard Hughes Medical Institute
[6]These authors contributed equally to this work
*Correspondence: sabatini@wi.mit.edu
DOI 10.1016/j.cell.2010.02.024

SUMMARY

The mTORC1 kinase promotes growth in response to growth factors, energy levels, and amino acids, and its activity is often deregulated in disease. The Rag GTPases interact with mTORC1 and are proposed to activate it in response to amino acids by promoting mTORC1 translocation to a membrane-bound compartment that contains the mTORC1 activator, Rheb. We show that amino acids induce the movement of mTORC1 to lysosomal membranes, where the Rag proteins reside. A complex encoded by the *MAPKSP1*, *ROBLD3*, and *c11orf59* genes, which we term Ragulator, interacts with the Rag GTPases, recruits them to lysosomes, and is essential for mTORC1 activation. Constitutive targeting of mTORC1 to the lysosomal surface is sufficient to render the mTORC1 pathway amino acid insensitive and independent of Rag and Ragulator, but not Rheb, function. Thus, Rag-Ragulator-mediated translocation of mTORC1 to lysosomal membranes is the key event in amino acid signaling to mTORC1.

INTRODUCTION

The multicomponent kinase mTORC1 (mammalian target of rapamycin complex 1) regulates cell growth by coordinating upstream signals from growth factors, intracellular energy levels, and amino acid availability and is deregulated in diseases such as cancer and diabetes (reviewed in Guertin and Sabatini, 2007). The TSC1 and TSC2 proteins form a tumor suppressor complex that transmits growth factor and energy signals to mTORC1 by regulating the GTP-loading state of Rheb, a Ras-related GTP-binding protein. When bound to GTP, Rheb interacts with and activates mTORC1 (reviewed in Laplante and Sabatini, 2009) and appears to be necessary for the activation of mTORC1 by all signals, including amino acid availability. In contrast, TSC1-TSC2 is dispensable for the regulation of mTORC1 by amino acids, and, in cells lacking TSC2, the mTORC1 pathway is sensitive to amino acid starvation but resistant to growth factor withdrawal (Roccio et al., 2006; Smith et al., 2005).

Recently, the Rag GTPases, which are also members of the Ras family of GTP-binding proteins, were shown to be amino acid-specific regulators of the mTORC1 pathway (Kim et al., 2008; Sancak et al., 2008). Mammals express four Rag proteins—RagA, RagB, RagC, and RagD—that form heterodimers consisting of RagA or RagB with RagC or RagD. RagA and RagB, like RagC and RagD, are highly similar to each other and are functionally redundant (Hirose et al., 1998; Sancak et al., 2008; Schürmann et al., 1995; Sekiguchi et al., 2001). Rag heterodimers containing GTP-bound RagB interact with mTORC1, and amino acids induce the mTORC1-Rag interaction by promoting the loading of RagB with GTP, which enables it to directly interact with the raptor component of mTORC1 (Sancak et al., 2008). The activation of the mTORC1 pathway by amino acids correlates with the movement of mTORC1 from an undefined location to a compartment containing Rab7 (Sancak et al., 2008), a marker of both late endosomes and lysosomes (Chavrier et al., 1990; Luzio et al., 2007). How the Rag proteins regulate mTORC1 is unknown, but, in cells expressing a RagB mutant that is constitutively bound to GTP ($RagB^{GTP}$), the mTORC1 pathway is insensitive to amino acid starvation and mTORC1 resides in the Rab7-positive compartment even in the absence of amino acids (Sancak et al., 2008). We previously proposed that amino acids promote the translocation of mTORC1—in a Rag-dependent fashion—to the surface of an endomembrane compartment, where mTORC1 can find its well-known activator, Rheb. Here, we show that the lysosomal surface is the compartment where the Rag proteins reside and to which mTORC1 moves in response to amino acids. We identify the trimeric Ragulator protein complex as a new component of the mTORC1 pathway that interacts with the Rag GTPases, is

essential for localizing them and mTORC1 to the lysosomal surface, and is necessary for the activation of the mTORC1 pathway by amino acids. In addition, by expressing in cells a modified raptor protein that targets mTORC1 to the lysosomal surface, we provide evidence that supports our model of mTORC1 pathway activation by amino acids.

RESULTS

Amino Acids Cause the Translocation of mTORC1 to Lysosomal Membranes, Where the Rag GTPases Are Already Present

To better define the compartment to which mTORC1 moves upon amino acid stimulation, we costained human cells with antibodies to endogenous mTOR, raptor, or RagC, as well as to various endomembrane markers (data not shown). This revealed that in the presence, but not in the absence, of amino acids, mTOR and raptor colocalized with LAMP2 (Figures 1A and 1B), a well-characterized lysosomal marker (reviewed in Eskelinen, 2006). Amino acid stimulation also resulted in an appreciable increase in the average size of lysosomes, which, as determined by live-cell imaging, was most likely caused by lysosome-lysosome fusion (R.Z., unpublished data). The amino acid-induced movement of mTOR to the LAMP2-positive compartment depends on the Rag GTPases, as it was eliminated by the RNA interference (RNAi)-mediated coknockdown of RagA and RagB (Figures S1A and S1B available online). Endogenous RagC also colocalized extensively with LAMP2, but, unlike mTORC1, this colocalization was unaffected by amino acid availability (Figure 1C). Consistent with amino acids not regulating the interaction between RagC and RagA or RagB (Figure 1D), an antibody that recognizes RagA and RagB stained lysosomes in both amino acid-starved and replete cells (Figure 1E). Lastly, GFP-tagged wild-type and GTP-bound mutants of RagB ($RagB^{GTP}$) and RagD ($RagD^{GTP}$) behaved identically to their endogenous counterparts (Figures 1F and 1G). Thus, amino acids stimulate the translocation of mTORC1 to the lysosomal surface, where the Rag GTPases reside irrespective of their GTP-loaded states or amino acid availability. Given that mTORC1 interacts with the Rag heterodimers in an amino acid-dependent fashion (Sancak et al., 2008), the mTORC1 and Rag localization data are consistent with the Rag GTPases serving as an amino acid-regulated docking site for mTORC1 on lysosomes.

The Translocation of mTORC1 to Lysosomes Does Not Depend on Growth Factors, Rheb, or mTORC1 Activity

The movement of mTORC1 to lysosomes is a specific response to amino acids. In wild-type mouse embryonic fibroblasts (MEFs), amino acids promoted the translocation of mTORC1 to lysosomes even when cells were cultured in the absence of serum (Figure S1C), a condition in which mTORC1 signaling, as detected by phosphorylated S6K1, is not active (Figure S1D). Conversely, in the absence of amino acids, neither serum stimulation nor constitutive activation of Rheb caused by the loss of TSC2 led to the lysosomal translocation of mTORC1 (Figure S1C). In both wild-type and TSC2 null MEFs, RNAi-mediated suppression of Rheb1 expression inhibited mTORC1 activation by amino acids (Figure S1E) but did not interfere with the amino acid-induced movement of mTOR to lysosomes (Figure S1F). Thus, the amino acid-induced translocation of mTORC1 to the lysosomal surface occurs independently of mTORC1 activity and does not require TSC2, Rheb, or growth factors.

The Trimeric Ragulator Complex Interacts with the Rag GTPases and Colocalizes with Them on Lysosomal Membranes

Inspection of the amino acid sequence of the Rag GTPases did not reveal any obvious lipid modification signals that might mediate Rag recruitment to lysosomal membranes. Thus, we pursued the possibility that unknown Rag-interacting proteins are needed to localize the Rag GTPases to lysosomes and play a role in mTORC1 signaling. To identify such proteins, we used protein purification approaches that have led to the discovery of other mTOR pathway components (see the Extended Experimental Procedures). Mass spectrometric analysis of anti-FLAG immunoprecipitates prepared from human HEK293T cells stably expressing FLAG-RagB or FLAG-RagD, but not FLAG-Rap2a, consistently revealed the presence of proteins encoded by the *MAPKSP1*, *ROBLD3*, and *c11orf59* genes (Figure 2A). Furthermore, the same proteins were also detected in immunoprecipitates of endogenous RagC but not control proteins like p53 or tubulin. Previous work indicates that these three small proteins interact with each other, localize to endosomes and lysosomes, and play positive roles in the MAPK pathway (Lunin et al., 2004; Nada et al., 2009; Schaeffer et al., 1998; Teis et al., 2002, 2006; Wunderlich et al., 2001). The proteins encoded by *MAPKSP1*, *ROBLD3*, and *c11orf59* have been called MP1, p14, and p18, respectively, and we use these names throughout this study. For convenience and because MP1, p14, and p18 are Rag and mTORC1 regulators (see below), we refer to the trimeric complex as the "Ragulator."

Orthologs of MP1, p14, and p18 are readily detectable in vertebrates as well as in *Drosophila* (Figure 2A), but extensive database searches did not reveal any potential orthologs in budding or fission yeast. The amino acid sequences of MP1, p14, and p18 reveal little about their function, and other than p14, which has a roadblock domain of unknown function (Koonin and Aravind, 2000), the proteins do not share sequence homology among themselves or with any other proteins in the databases besides their direct orthologs. In particular, they do not share any sequence similarity with the Ego1p or Ego3p, proteins, which interact with Gtr1p and Gtr2p (Dubouloz et al., 2005; Gao and Kaiser, 2006), the orthologs of the Rag proteins in budding yeast (Gao and Kaiser, 2006; Schürmann et al., 1995). The lysosomal localization of p18 requires its lipidation through N-terminal myristoylation and palmitoylation sites, and p18 likely serves as a platform for keeping MP1 and p14 on the lysosomal surface (Nada et al., 2009).

In humans, a mutation that leads to a partial reduction in the expression of p14 causes a pronounced growth defect so that individuals carrying the mutation are below the third percentile in age-adjusted height (Bohn et al., 2007). Furthermore, mice engineered to lack either p14 or p18 die around embryonic day 7–8 and exhibit severe growth retardation (Nada et al., 2009; Teis et al., 2006). Given the major role of the mTORC1

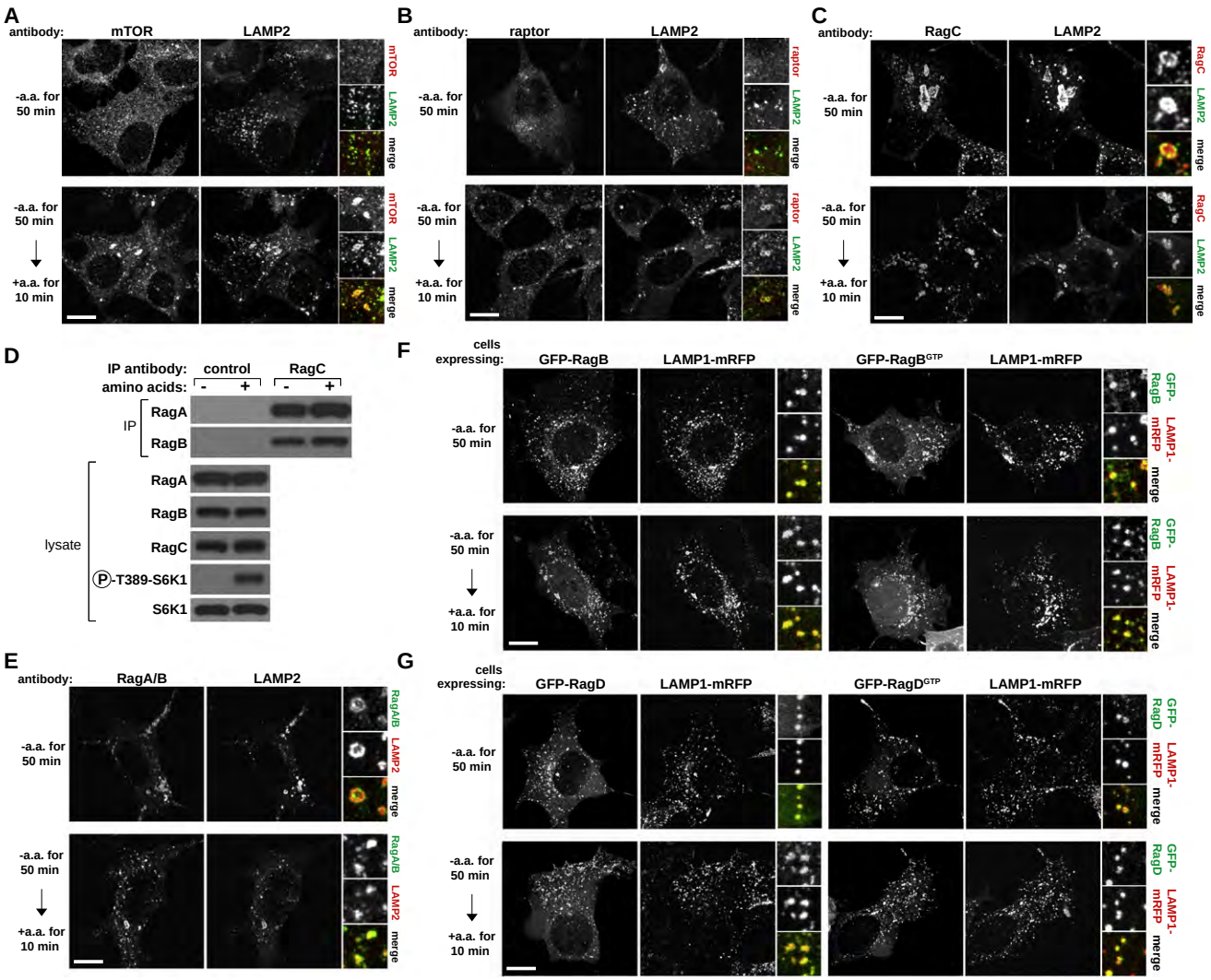

Figure 1. mTORC1 Localizes to Lysosomal Membranes in an Amino Acid-Dependent Fashion while the Rag GTPases Are Constitutively Localized to the Same Compartment

(A) Images of HEK293T cells coimmunostained for lysosomal protein LAMP2 (green) and mTOR (red). Cells were starved of and restimulated with amino acids for the indicated times before processing and imaging.

(B) Images of HEK293T cells coimmunostained for LAMP2 (green) and raptor (red). Cells were treated and processed as in (A).

(C) Images of HEK293T cells coimmunostained for LAMP2 (green) and RagC (red). Cells were treated and processed as in (A).

(D) RagC interacts with RagA and RagB independently of amino acid availability. RagC immunoprecipitates were prepared from HEK293T cells starved or stimulated with amino acids as in (A), and immunoprecipitates and lysates were analyzed by immunoblotting for the indicated proteins.

(E) Images of HEK293T cells coimmunostained for RagA/B (green) and LAMP2 (red). Cells were treated, processed, and imaged as in (A).

(F) GFP-RagB and GFP-RagB^{GTP} colocalize with coexpressed LAMP1-mRFP independently of amino acid availability. HEK293T cells transfected with the indicated cDNAs were treated and processed as in (A).

(G) GFP-RagD and GFP-RagD^{GTP} colocalize with coexpressed LAMP1-mRFP independently of amino acid availability. HEK293T cells transfected with the indicated cDNAs were treated and processed as in (A).

In all images, insets show selected fields that were magnified five times and their overlays. Scale bars represent 10 μm. See also Figure S1.

pathway in growth control, these loss-of-function phenotypes were of interest to us.

As an initial step in verifying our mass spectrometric identification of MP1, p14, and p18 as Rag-interacting proteins, we coexpressed them along with RagB and RagD in HEK293T cells and found that the Ragulator, but not the control Rap2A protein, coimmunoprecipitated both Rag GTPases but not the metap2 protein that has the same molecular weight as tagged RagB (Figure 2B). Furthermore, when coexpressed with a RagB mutant (RagB^{GTP}) that binds constitutively to GTP, the Ragulator coimmunoprecipitated the mTORC1 components raptor and mTOR (Figure 2C), consistent with the GTP-loading of RagB promoting the interaction of the Rag heterodimers with mTORC1 (Sancak et al., 2008). Furthermore, endogenous RagA, RagB, and RagC

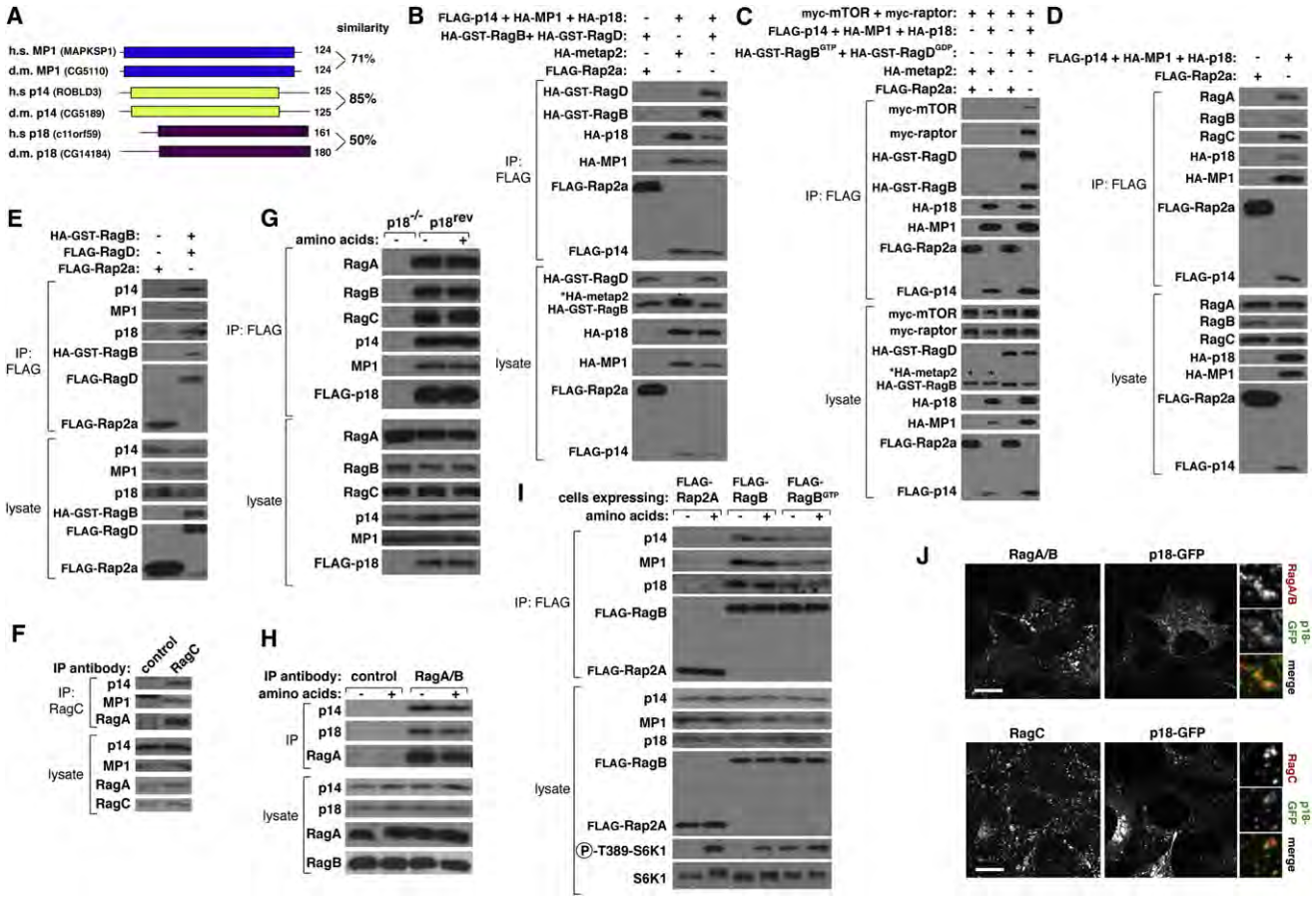

Figure 2. The Trimeric Ragulator Complex Interacts and Colocalizes with the Rag GTPases

(A) Schematic amino acid sequence alignment of human MP1, p14, and p18 and their corresponding *Drosophila* orthologs.

(B) Recombinant epitope-tagged Ragulator coimmunoprecipitates recombinant RagB and RagD. Anti-FLAG immunoprecipitates were prepared from HEK293T cells cotransfected with the indicated cDNAs in expression vectors and cell lysates and immunoprecipitates analyzed by immunoblotting for levels of indicated proteins. The * indicates the band corresponding to the metap2 protein as it has the same apparent molecular weight as HA-GST-RagB.

(C) Recombinant Ragulator coimmunoprecipitates mTORC1 when it is coexpressed with the GTP-bound mutant of RagB. HEK293T cells were cotransfected with the indicated cDNAs in expression vectors and analyzed as in (B). The * indicates the bands corresponding to metap2 as it has the same apparent molecular weight as HA-GST-RagB.

(D) Recombinant Ragulator co-immunoprecipitates endogenous RagA, RagB, and RagC. HEK293T cells were cotransfected with indicated cDNAs in expression vectors and anti-FLAG immunoprecipitates analyzed as in (B).

(E) Recombinant RagB-RagD heterodimers coimmunoprecipitate endogenous p14, MP1, and p18. HEK293T cells were cotransfected with indicated cDNAs in expression vectors and anti-FLAG immunoprecipitates analyzed as in (B).

(F) Endogenous RagC coimmunoprecipitates endogenous p14 and MP1. Anti-RagC immunoprecipitates were prepared from HEK293T cells and analyzed for the levels of the indicated proteins.

(G) Amino acids do not regulate the amounts of endogenous MP1, p14, RagA, or RagB that coimmunoprecipitate with recombinant p18. p18 null cells ($p18^{-/-}$) or p18 null cells stably expressing FLAG-p18 ($p18^{rev}$) were starved for amino acids for 50 min or starved and restimulated with amino acids for 10 min. After in-cell crosslinking, anti-FLAG immunoprecipitates were prepared from cell lysates and analyzed for the levels of the indicated proteins by immunoblotting.

(H) Amino acids do not affect the amounts of endogenous p14 and p18 that coimmunoprecipitate with endogenous RagA/B. HEK293T cells were treated as in (G), and anti-RagA/B immunoprecipitates were analyzed by immunoblotting for the indicated proteins.

(I) Endogenous Ragulator coimmunoprecipitates with FLAG-RagB independently of amino acid availability and GTP-loading of RagB. HEK293T cells stably expressing FLAG-RagB or FLAG-$RagB^{GTP}$ were starved and restimulated with amino acids as in (G), and anti-FLAG immunoprecipitates were analyzed for the levels of indicated proteins.

(J) The Rag GTPases colocalize with GFP-tagged p18. HEK293T cells were transfected with a cDNA encoding p18-GFP, processed for immunostaining for endogenous RagA/B or RagC, and imaged for the RagA/B (red) or RagC (red) signal as well as for p18-GFP fluorescence (green). Note that not all cells express p18-GFP. In all images, insets show selected fields that were magnified five times and their overlays. Scale bars represent 10 μm.

See also Figure S2.

copurified with recombinant Ragulator (Figure 2D), and endogenous Ragulator components copurified with the recombinant RagB-RagD heterodimer (Figure 2E). Lastly, endogenous p14 and MP1 were present in immunoprecipitates prepared with an antibody directed against endogenous RagC that readily coimmunoprecipitates RagA (Figure 2F).

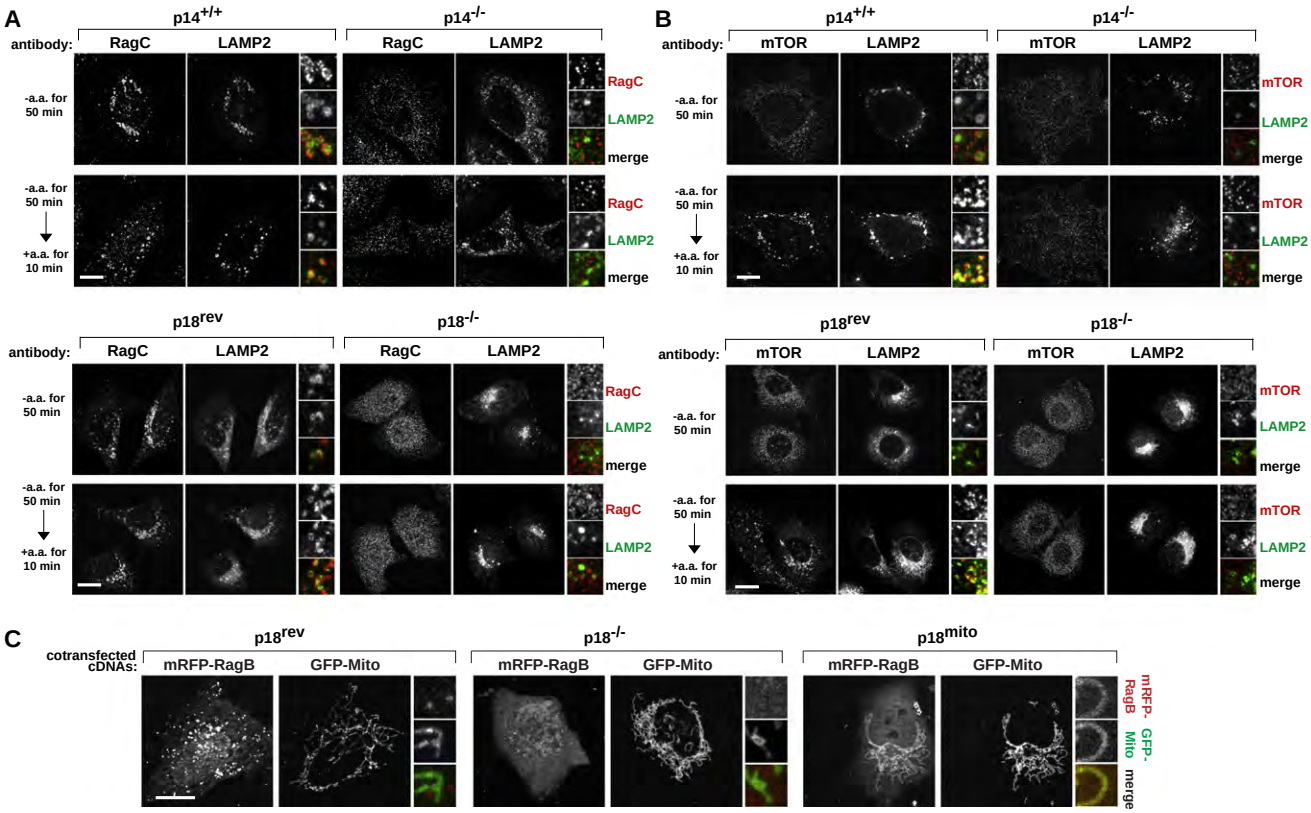

Figure 3. The Ragulator Is Necessary to Localize the Rag GTPases and mTORC1 to Lysosomal Membranes

(A) Images of p14 null or p18 null cells or their respective controls coimmunostained for RagC (red) and LAMP2 (green). Cells were starved of and restimulated with amino acids for the indicated times before processing for the immunofluorescence assay and imaging.

(B) Images of p14 null or p18 null cells or their respective controls coimmunostained for mTOR (red) and LAMP2 (green). Cells were treated and processed as in (A).

(C) Colocalization of mRFP-RagB (red) with GFP-Mito (green) in cells expressing mitochondrially localized p18. p18 null cells ($p18^{-/-}$), or p18 null cells expressing wild-type p18 ($p18^{rev}$) or mitochondrially localized p18 ($p18^{mito}$), were transiently transfected with the indicated cDNAs in expression plasmids and imaged.

In all images, insets show selected fields that were magnified five times and their overlays. Scale bars represent 10 μm. See also Figure S3.

Amino acids did not appreciably regulate the interaction of recombinant p18 with endogenous p14, MP1, or the Rag GTPases (Figure 2G). Similarly, amino acids did not affect the interaction of endogenous Ragulator with endogenous Rag A/B (Figure 2H). The amounts of p14, p18, and MP1 that coimmunoprecipitated with the GTP-bound RagB mutant ($RagB^{GTP}$) were slightly less than with wild-type RagB (Figure 2I). Because mTORC1 pathway activity is high in cells expressing $RagB^{GTP}$ (Sancak et al., 2008), the reduced Ragulator-Rag interaction in these cells may reflect a compensatory mechanism to reduce mTORC1 activity. To test whether the Rag GTPases interact with one or more Ragulator components directly, we performed in vitro binding assays between purified RagB-RagD heterodimers and individual Ragulator proteins. p18 interacted with RagB-RagD in vitro, but not with the Rap2a control protein (Figure S2A). In contrast, we did not detect a direct interaction between either p14 or MP1 and the Rag GTPases (data not shown), suggesting that p18 is the principal Rag-binding subunit of the Ragulator. Lastly, within HEK293T cells, GFP-tagged p18 colocalized with endogenous RagA/B and RagC (Figure 2J). Collectively, these results show that the Ragulator interacts with the Rag GTPases and that a supercomplex consisting of Ragulator, a Rag heterodimer, and mTORC1 can exist within cells.

Ragulator Localizes the Rag Proteins to the Lysosomal Surface and Is Necessary for the Amino Acid-Dependent Recruitment of mTORC1

Because the Rag GTPases interact with Ragulator and given the function of p18 in localizing MP1 and p14 to lysosomes (Nada et al., 2009), it seemed possible that the Ragulator is necessary for localizing the Rag proteins to the lysosomal surface. Indeed, in cells lacking p14 or p18 (Nada et al., 2009; Teis et al., 2006), endogenous RagC was localized in small puncta throughout the cytoplasm of the cells rather than to lysosomes (Figure 3A), the morphology of which was not obviously affected by the loss of either protein. In contrast, in $p14^{+/+}$ cells or p18 null cells reconstituted with wild-type p18 ($p18^{rev}$), RagC constitutively colocalized with the LAMP2 lysosomal marker (Figure 3A). Analogous results were obtained in HEK293T cells with an RNAi-mediated reduction in MP1 expression (Figure S3A). Consistent

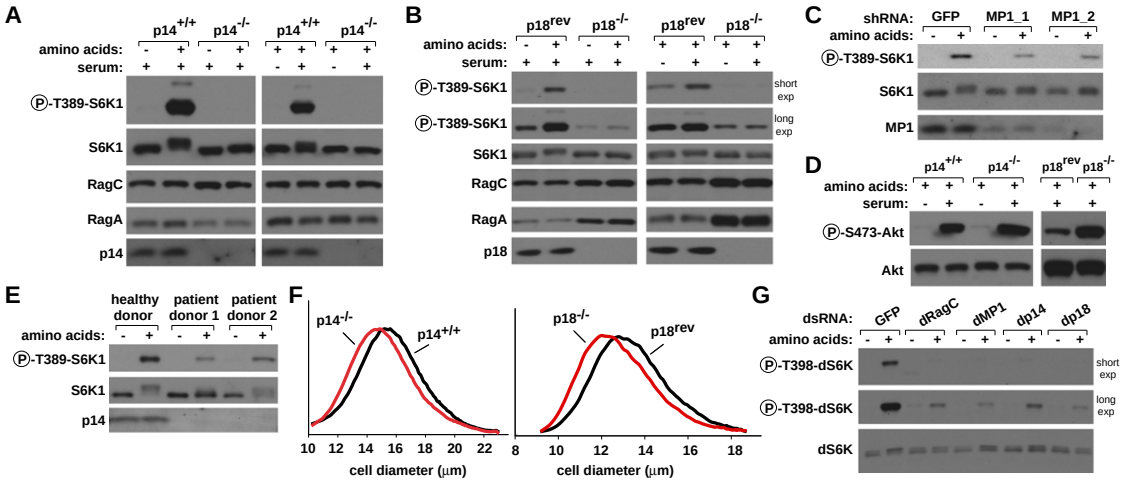

Figure 4. Ragulator Null and -Depleted Cells are Highly Deficient in the Activation of mTORC1 Signaling by Amino Acids

(A) p14 is necessary for the activation of the mTORC1 pathway by amino acids and serum. p14 null or control cells were starved of amino acids or serum for 50 min, or starved and restimulated with amino acids or serum for 10 min. Immunoblot analyses were used to measure the levels of the indicated proteins and phosphorylation states.

(B) p18 is necessary for the activation of the mTORC1 pathway by amino acids and serum. p18 null or control cells were treated and analyzed as in (A).

(C) Partial knockdown of MP1 blunts mTORC1 pathway activation by amino acids. HEK293T cells expressing a control shRNA or two distinct shRNAs targeting MP1 were starved for amino acids for 50 min, or starved and stimulated with amino acids for 10 min and analyzed as in (A).

(D) p14 and p18 are not necessary for mTORC2 pathway activity. p14 null or control cells were starved for serum, or starved and then restimulated with serum as in (A). p18 null or control cells were grown in complete media. Cell lysates were prepared and analyzed by immunobloting for the levels of Akt1 and Akt phosphorylation at the S473 site phosphorylated by mTORC2.

(E) Decreased p14 expression impairs amino acid-induced mTORC1 activation in human cells. Cells derived from patients with lower p14 expression or healthy individuals were treated and analyzed as in (A).

(F) Cells lacking Ragulator are smaller than control cells. Cell size distributions of p14 null or p18 null cells are overlaid with those from corresponding control cells.

(G) Ragulator function is conserved in *Drosophila* cells. *Drosophila* S2 cells were transfected with a control dsRNA, or dsRNAs targeting dRagC, dMP1, dp14, or dp18, starved of amino acids for 90 min, or starved and restimulated with amino acids for 30 min. Levels of indicated proteins and phosphorylation states were analyzed by immunobloting.

See also Figure S4.

with the essential role of the Rag proteins in the translocation of mTORC1 to the lysosomal surface (Figure S1), in cells lacking p14 or p18 or in HEK293T cells with p14, p18, or MP1 knockdowns, amino acids failed to induce lysosomal recruitment of mTOR, which was found throughout the cytoplasm in both amino acid-starved and -stimulated cells (Figure 3B, Figures S3B and S3D). Thus, all Ragulator subunits are required for lysosomal targeting of the Rag GTPases and mTORC1.

To determine whether Ragulator is sufficient to control the intracellular localization of the Rag proteins, it was necessary to target Ragulator to a location that is distinct from the lysosomal surface. As p18 binds both p14 and MP1 and is necessary for targeting them to the lysosomal surface (Nada et al., 2009), we chose to manipulate the intracellular localization of p18. To accomplish this, we generated a variant of p18, called $p18^{mito}$, which lacks its N-terminal lipidation sites but is fused at its C terminus to the transmembrane region of OMP25, which is sufficient to target heterologous proteins to the mitochondrial surface (Nemoto and De Camilli, 1999). When expressed in p18 null cells, $p18^{mito}$ was associated with mitochondria, as verified by colocalization with the established mitochondrial protein Cytochrome c (Figure S3E). Remarkably, in the p18 null cells expressing $p18^{mito}$, RFP-tagged RagB colocalized with the mitochondrial marker GFP-mito (Figure 3C). In contrast, RFP-RagB did not colocalize with GFP-mito in p18 null cells ($p18^{-/-}$) or $p18^{rev}$ cells and instead was present in a cytoplasmic or lysosomal pattern, respectively (Figure 3C). In cells expressing $p18^{mito}$, mTORC1 activity remained very low and mTOR was not recruited to the mitochondria (Figures S3E and S3F), likely because the mitochondrial surface does not contain the machinery necessary to load the Rag GTPases with the appropriate nucleotides. These results indicate that the location of p18 is sufficient to define that of the Rag proteins and are consistent with Ragulator serving as a constitutive docking site on lysosomes for the Rag heterodimers, which, in amino acid-replete cells, have an analogous function for mTORC1.

Ragulator Is Necessary for TORC1 Activation by Amino Acids in Mammalian and *Drosophila* Cells

We employed the cells lacking p14 or p18 to determine whether Ragulator is necessary for mTORC1 activation by amino acids. Strikingly, in both p14 and p18 null cells, but not in control cells, amino acids were incapable of activating the mTORC1 pathway as detected by the phosphorylation of S6K1 (Figures 4A and 4B) and 4E-BP1 (Figure S4A). Similarly, cells derived from patients with a homozygous mutation in the p14 gene that causes a reduction in p14 expression (Bohn et al., 2007) showed a defect in amino acid-induced mTORC1 activation compared to cells

derived from a healthy donor (Figure 4E). In addition, autophagy, a process normally inhibited by mTORC1, was activated in p14 null cells, as detected by an increase compared to in control cells in the size and number of GFP-LC3-II puncta (Figures S4B and S4C). mTORC1 activity was also suppressed in HEK293T cells with RNAi-induced reductions in p14, p18, or MP1 levels (Figure 4C, Figure S3C). Consistent with the known requirement of amino acids and Rag function for growth factors to activate mTORC1 (Sancak et al., 2008), serum was also incapable of activating the mTORC1 pathway in cells null for p14 or p18 (Figures 4A and 4B). In contrast, no defect was observed in the level of S473 phosphorylation of Akt (Figure 4D). In fact, Akt phosphoylation was slightly higher in the p14 null and p18 null cells than in controls cells, which likely results from the lack of the well-appreciated inhibitory input from mTORC1 to the PI3K pathway in these cells (reviewed in Manning, 2004). As mTORC2 is the growth factor-regulated S473 kinase of Akt (Sarbassov et al., 2005), these results also indicate that the Ragulator does not play a detectable positive role in mTORC2 signaling. Interestingly, in the p18 null cells the expression of RagA and RagC was higher than in control cells (Figure 4B), suggesting that feedback signals in these cells may be trying to overcome the defect in mTORC1 activity by boosting Rag expression or that Ragulator also negatively controls Rag GTPase levels. Consistent with p18, p14, and MP1 forming a complex, the expression or stability of the Ragulator proteins seems to be coregulated because in cells that lack p14, p18 protein levels are also reduced, and, similarly, in cells that lack p18, p14 protein levels are also low (Figure S2B). A well-known function of the mTORC1 pathway is the positive regulation of cell growth, so that inhibition of the pathway leads to a reduction in cell size (reviewed in Laplante and Sabatini, 2009). Consistent with Ragulator being a positive component of the mTORC1 pathway, the p14 and p18 null cells were smaller in size than their respective controls (Figure 4F).

Many components of the TORC1 pathway, such as the Rag proteins, have conserved roles in mammalian and *Drosophila* cells (Kim et al., 2008; Sancak et al., 2008). RNAi-inducing double-stranded RNAs (dsRNAs) that target the *Drosophila* orthologs of MP1 (CG5110), p14 (CG5189), and p18 (CG14184) were as effective at blocking amino acid-stimulated activation of dTORC1 in *Drosophila* S2 cells as dsRNAs targeting dRagC (Figure 4G). Our loss-of-function experiments indicate that Ragulator is a component of the TORC1 pathway that, like the Rag GTPases, is essential for amino acids to activate TORC1 signaling in mammalian and *Drosophila* cells.

Forced Targeting of mTORC1 to the Lysosomal Surface Eliminates the Amino Acid Sensitivity of the mTORC1 Pathway

The findings we have presented so far are consistent with the amino acid-induced movement of mTORC1 to the lysosomal surface being necessary for the activation of mTORC1 by amino acids. To test whether the placement of mTORC1 on lysosomal membranes is sufficient to mimic the amino acid input to mTORC1, it was necessary to force mTORC1 onto these membranes in the absence of amino acids. To accomplish this, we expressed in HEK293T cells modified raptor proteins that consist of epitope-tagged raptor fused to the intracellular targeting signals of Rheb1 or Rap1b, small GTPases that localize, in part, to the lysosomal surface (Pizon et al., 1994; Saito et al., 2005; Sancak et al., 2008). Because the targeting signals of these proteins are in their C-terminal tails, we added the last 15 or 17 amino acids of Rheb1 or Rap1b, respectively, to the C terminus of raptor (Figure 5A). For simplicity, we refer to these fusion proteins as raptor-Rheb15 and raptor-Rap1b17. As a control, we generated a raptor fusion protein that lacks the CAAX box of the Rheb1 targeting signal (raptor-Rheb15ΔCAAX) and so cannot associate with membranes (Buerger et al., 2006; Clark et al., 1997; Takahashi et al., 2005).

When expressed in cells together with myc-mTOR, raptor-Rheb15 and raptor-Rap1b17 localized to lysosomes in the presence or absence of amino acids, as judged by costaining with LAMP2 (Figure 5B). In contrast, raptor-Rheb15ΔCAAX behaved like wild-type raptor and localized to lysosomes only upon amino acid stimulation (Figure 5B). In all cases, the localization of the coexpressed myc-mTOR mirrored that of the wild-type or altered forms of raptor, indicating that C-terminal modifications of raptor do not perturb its interaction with mTOR (Figure 5C), which was confirmed in coimmunoprecipitation experiments (Figure S5A).

Remarkably, transient expression of raptor-Rheb15 or raptor-Rap1b17 in HEK293T cells was sufficient to render the mTORC1 pathway, as judged by the phosphorylation of S6K1, resistant to amino acid starvation (Figure 6A). In contrast, the expression of wild-type raptor or raptor-Rheb15ΔCAAX did not affect the amino acid sensitivity of the pathway (Figure 6A). In HEK293E cells, the expression of raptor-Rheb15 made S6K1 phosphorylation insensitive to amino acid starvation but did not affect its regulation by insulin (Figure 6B). Thus, lysosomal targeting of mTORC1 can substitute for the amino acid, but not growth factor, input to mTORC1. This is consistent with previous work showing that growth factors signal to mTORC1 in large part through the TSC1-TSC2-Rheb axis (reviewed in Laplante and Sabatini, 2009), and not through the Rag GTPases (Sancak et al., 2008).

To verify the effects of lysosomally targeted mTORC1 in a more physiological setting than that achieved by transient complementary DNA (cDNA) expression, we generated HEK293T cell lines stably expressing FLAG-tagged raptor-Rheb15 or wild-type raptor. In cells expressing the lysosomally targeted but not wild-type raptor, mTOR was always associated with lysosomes, irrespective of amino acids (Figure 6C). As with the transient expression of raptor-Rheb15, its stable expression rendered the mTORC1 pathway fully resistant to amino acid starvation (Figure 6D). Furthermore, under normal growth conditions, these cells had an increase in mTORC1 activity and were larger than controls (Figure 6E).

We next examined whether the targeting of mTORC1 to membranes other than lysosomal membranes could also eliminate the amino acid sensitivity of the mTORC1 pathway. This was not the case because although the stable expression of a raptor variant consisting of raptor fused to the last 25 amino acids of H-Ras (raptor-HRas25) (Figure 5A, Figure S5B) was sufficient to target a fraction of cellular mTOR to the plasma membrane (Figure 6C), it did not render the mTORC1 pathway resistant to amino acid starvation (Figure 6D).

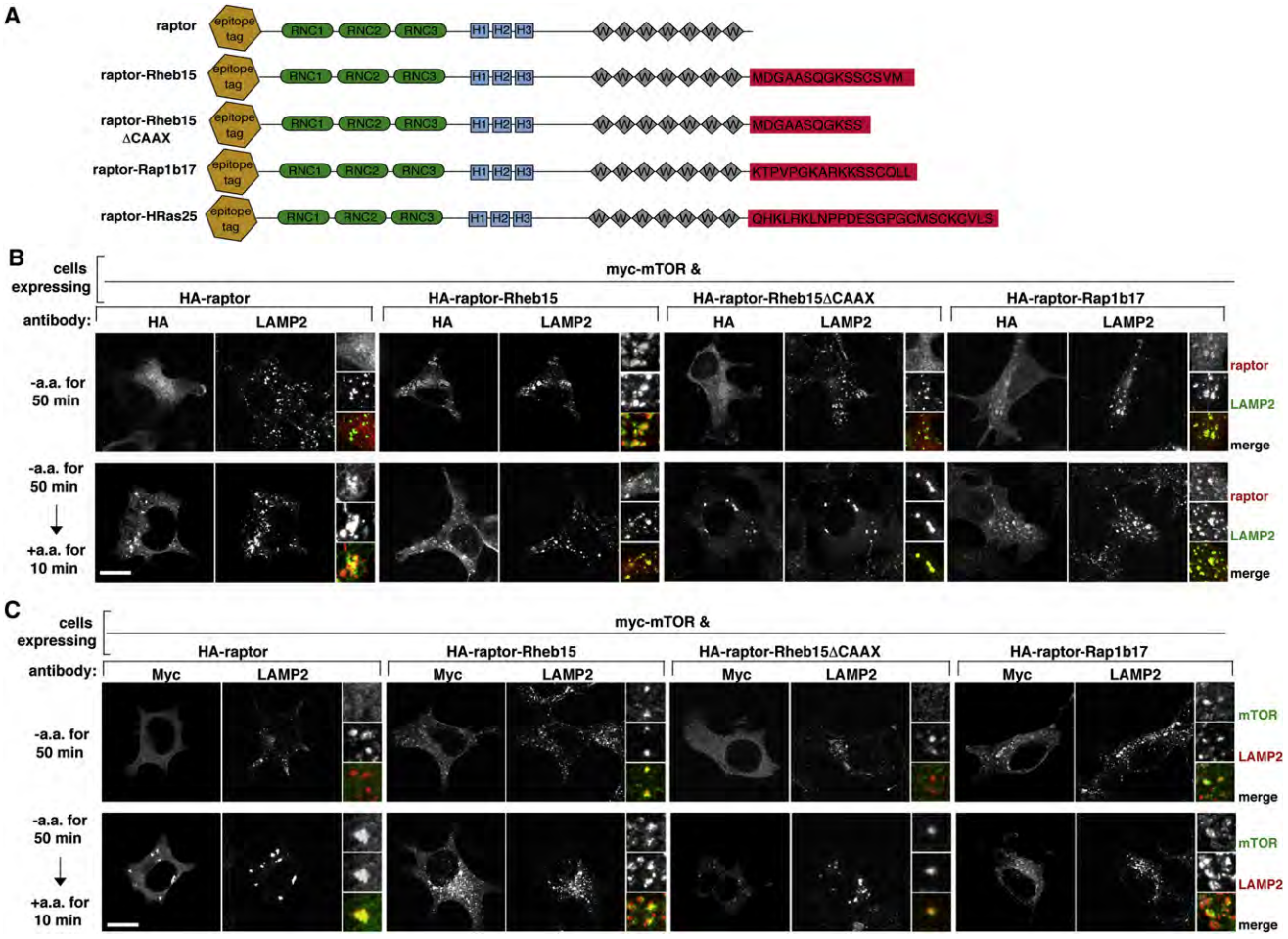

Figure 5. In Cells Expressing Raptor Variants Fused to the Targeting Signals of Rheb1 or Rap1b, mTORC1 Localizes to Lysosomal Membranes in an Amino Acid-Independent Fashion

(A) Schematic of raptor fusion proteins that target mTORC1 to lysosomal membranes (raptor-Rheb15; raptor-Rap1b17) or to the plasma membrane (Raptor-HRas25) as well as proteins used as controls (wild-type raptor; raptor-Rheb15ΔCAAX).

(B) Images of amino acid starved or replete cells expressing lysosomally targeted or control HA-tagged raptor proteins and coimmunostained for the HA epitope (red) and endogenous LAMP2 (green). HEK293T cells were transfected with the indicated cDNAs, starved of and restimulated with amino acids for the indicated times, and processed in the immunofluorescence assay.

(C) Images of amino acid starved or replete cells coexpressing myc-mTOR and the indicated raptor fusion proteins and coimmunostained for the myc epitope (green) and endogenous LAMP2 (red). HEK293T cells were co-transfected with the indicated cDNAs and treated and processed as in (B).

In all images, insets show selected fields that were magnified five times and their overlays. Scale bars represent 10 μm.

Forced Targeting of mTORC1 to the Lysosomal Surface Eliminates the Requirement in mTORC1 Signaling for Rag and Ragulator, but Not Rheb, Function

The ability to constitutively localize mTORC1 to lysosomal membranes enabled us to probe in more detail the role of the Rag and Rheb GTPases, as well as Ragulator, in the activation of mTORC1 by amino acids. We hypothesized that if the major role of the Rag GTPases is to allow mTORC1 to localize to lysosomes, then in cells that express raptor-Rheb15, mTORC1 activity should be independent of Rag function. Indeed, while in control cells the RNAi-mediated knockdown of both RagA and RagB strongly blunted the activation of mTORC1 by amino acids, it did not reduce the amino acid-insensitive mTORC1 activity observed in raptor-Rheb15-expressing cells (Figure 7A). As an additional approach to inhibit Rag function, we exploited the fact that coexpression of a GDP-bound RagB mutant ($RagB^{GDP}$) and a GTP-bound RagD mutant ($RagD^{GTP}$) eliminates mTORC1 pathway activity within cells (Kim et al., 2008; Sancak et al., 2008). Expression of $RagB^{GDP}$-$RagD^{GTP}$ completely prevented mTORC1 activation by amino acids in control cells but had no effect on the amino acid-insensitive mTORC1 activity of cells expressing raptor-Rheb15 (Figure 7B).

If the main function of Ragulator in the mTORC1 pathway is to localize the Rag GTPases to the lysosomes, then it should be possible to reactivate the mTORC1 pathway in Ragulator null cells by expressing raptor-Rheb15. Remarkably, the stable expression of raptor-Rheb15, but not wild-type raptor, in p14 or p18 null cells reactivated mTORC1 signaling and made it

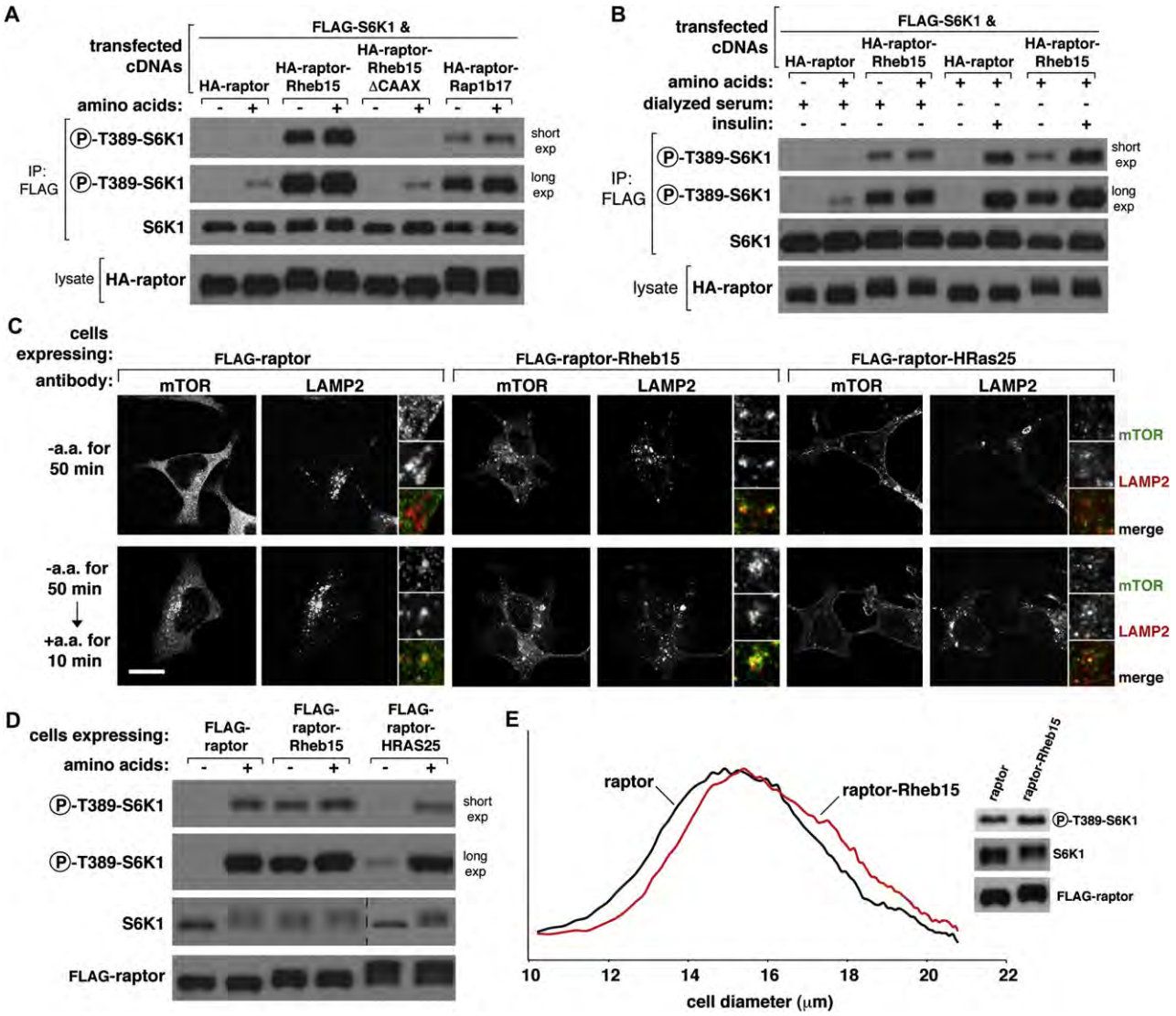

Figure 6. Constitutive Association of Raptor with Lysosomal Membranes, but Not the Plasma Membrane, Is Sufficient to Make the mTORC1 Pathway Insensitive to Amino Acid Starvation

(A) The mTORC1 pathway is not sensitive to amino acid starvation in cells that express lysosomally targeted but not control raptor proteins. HEK293T cells were cotransfected with the indicated cDNA expression plasmids and starved of amino acids for 50 min or starved and restimulated with amino acids for 10 min. Cell lysates and anti-FLAG-S6K1 immunoprecipitates were analyzed by immunobloting for the levels of the indicated proteins and phosphorylation states.

(B) The mTORC1 pathway is sensitive to serum starvation and insulin stimulation in cells that express lysosomally targeted as well as control raptor proteins. HEK293E cells were cotransfected with the indicated cDNA expression plasmids, starved of amino acids for 50 min, or starved and restimulated with amino acids for 10 min. Duplicate cultures were starved of serum for 50 min or starved and stimulated with insulin for 10 min. Cell lysates and anti-FLAG-S6K1 immunoprecipitates were analyzed by immunobloting for the levels of the indicated proteins and phosphorylation states.

(C) Images of cells stably expressing FLAG-raptor, FLAG-raptor-Rheb15, or FLAG-raptor-HRas25 and coimmunostained for endogenous mTOR (green) and endogenous LAMP2 (red). HEK293T cells stably expressing the indicated proteins were treated as in (A) for the indicated times before processing in the immunofluorescence assay. In all images, insets show selected fields that were magnified five times and their overlays. The scale bar represents 10 μm.

(D) Targeting of mTORC1 to the lysosomal but not the plasma membrane makes the mTORC1 pathway insensitive to amino acid starvation. HEK293T cells stably expressing FLAG-raptor, FLAG-raptor-Rheb15, or FLAG-raptor-HRas25 were treated as in (A) and analyzed by immunoblotting for the levels of the indicated proteins and phosphorylation states.

(E) Targeting of mTORC1 to the lysosomal membrane increases cell size and pathway activity in cells under normal growth conditions. Cell size distributions of cells that stably express FLAG-raptor or FLAG-raptor-rheb15 as well as immunoblot analyses of the mTORC1 pathway in the same cells are shown.

insensitive to amino acid deprivation (Figures 7C and 7D). Furthermore, expression of raptor-Rheb15 in the p18 null cells was sufficient to increase their size (Figure 7E). In contrast to the results observed with the Rag GTPases and Ragulator, RNAi-mediated suppression of Rheb1 blocked amino acid-induced mTORC1 activation in cells expressing raptor-Rheb15 to the same extent as it did in control cells (Figure 7F).

To test whether the presence of mTORC1 and Rheb on the same membrane compartment is sufficient to render the mTORC1 pathway insensitive to amino acid levels, we generated cells in which mTORC1 and Rheb are both present on the plasma membrane. To accomplish this, we prepared a Rheb1 variant, called Rheb1-HRas25, that localizes to the plasma-membrane (Figure S5C) because it contains the C-terminal 25 amino acids of H-Ras instead of the normal Rheb1 localization signal. When Rheb1-HRas25 was stably coexpressed with raptor-HRas25, but not wild-type raptor, the mTORC1 pathway became insensitive to amino acid starvation (Figure 7G). Importantly, mTORC1 signaling remained amino acid-sensitive in cells in which either Rheb or mTORC1, but not both, was targeted to the plasma membrane (Figure 7G).

DISCUSSION

Our findings, together with previous work showing that Rheb is required for amino acids to activate the mTORC1 pathway (Roccio et al., 2006; Smith et al., 2005) and can localize to late endosomes/lysosomes (Saito et al., 2005; Sancak et al., 2008), is consistent with a model in which amino acids induce mTORC1 to associate with the endomembrane system of the cell and thus allow it to encounter its activator Rheb. In this model, the essential role of the Ragulator-Rag complex is to serve as an amino acid-regulated docking site for mTORC1 on lysosomal membranes (see schematic in Figure 7H). The proposed link between the Rag and Rheb GTPases in the regulation of the mTORC1 pathway provides an explanation for why activation of mTORC1 occurs only when activators of both Rheb (e.g., growth factors and energy) and the Rags (i.e., amino acids) are available. For technical reasons (Buerger et al., 2006; Sancak et al., 2008), it has not been possible to determine the intracellular localization of endogenous Rheb, and work using overexpressed GFP-tagged Rheb1 has placed it on various endomembrane compartments, including endosomes and lysosomes (Buerger et al., 2006; Saito et al., 2005; Sancak et al., 2008; Takahashi et al., 2005). Our results suggest that at some point in its life cycle, Rheb must traverse the lysosomal surface in order to encounter mTORC1, and so in our model we have chosen to place Rheb on this compartment (Figure 7H). However, at any given time only a small fraction of cellular Rheb may actually be on the lysosomal surface, or, alternatively, some of the mTORC1 within the cell may move to a nonlysosomal endomembrane compartment that also contains Rheb. These issues will only be answered once a definitive location for endogenous Rheb can be determined.

The trimeric p14, p18, and MP1 protein complex, which we call Ragulator, is a Rag-interacting complex that is essential for amino acid signaling to mTORC1 and represents an additional critical component of the TORC1 signaling pathway in mammals and flies. p18 directly interacts with the Rag GTPases (Figure S2A) as well as with p14 and MP1 (Nada et al., 2009) and so may serve as a scaffold to bring the Rag GTPases and MP1-p14 next to each other. In vitro we have not detected a direct interaction between the Rag GTPases and either MP1 or p14, but both proteins are, like p18, necessary for localizing the Rag GTPases to the lysosomal surface. p14 is required to maintain normal p18 expression levels (Figure S2B), suggesting that within cells p14 and MP1 form a crucial part of the Ragulator structure. Given the nonspecific nature of the p14 and p18 names, in the future it may be best to rename these proteins, perhaps to names that reflect their essential roles in the mTORC1 pathway.

The location of the Rag GTPases, the Ragulator, and mTORC1 on the lysosomal surface implicates this organelle as the site of a yet to be discovered sensing system that signals amino acid availability to the Ragulator-Rag complex. The lysosomal location of the amino acid sensing branch of the mTORC1 pathway is consistent with increasing evidence that lysosomes, and their yeast counterparts, vacuoles, are at the nexus of amino acid metabolism within cells. Lysosomes are a major site of protein degradation and amino acid recycling, and vacuoles store amino acids at high concentrations (reviewed in Li and Kane, 2009). Thus, mTORC1 and its regulators may reside on the lysosomal surface so as to sense a currently unknown aspect of lysosomal function that reflects the intracellular pools of amino acids.

It is interesting to consider the differences and similarities between the still poorly understood amino acid signaling mechanisms employed by the mTORC1 and yeast TORC1 pathways. Consistent with previous work in mammalian cells (Sancak et al., 2008), the Gtr1p-Gtr2p heterodimer that is orthologous to RagA/B-RagC/D interacts with yeast TORC1 when Gtr1p is GTP loaded (Binda et al., 2009). TORC1 and the Gtr proteins are located on the surface of the vacuole (Berchtold and Walther, 2009; Binda et al., 2009), the yeast equivalent of lysosomes, but, unlike in mammals, yeast TORC1 does not leave the vacuolar surface upon amino acid deprivation although amino acids do control the interaction of TORC1 with Gtr1p-Gtr2p (Binda et al., 2009). This finding suggests that there must be a distinct mechanism for retaining TORC1 at the vacuolar surface and that in yeast the interaction between TORC1 and Gtr1p-Gtr2p serves other purposes besides controlling the intracellular location of TORC1. In contrast, our current work argues that in mammals, the main role of the Rag GTPase and the associated Ragulator complex is to control the association of mTORC1 with the cellular endomembrane system, in particular, lysosomes. Rheb, which is essential for the activation of mTORC1 by all upstream signals, does not appear to be part of the TORC1 pathway in yeast (reviewed in Berchtold and Walther, 2009). As we suggest that the Rag-dependent and amino acid-regulated translocation of mTORC1 to the lysosomal surface may ultimately be a mechanism for controlling the access of mTORC1 to Rheb, the absence of Rheb in the yeast TORC1 pathway may make regulation of TORC1 localization unnecessary. That known Rag- and Gtr-interacting proteins share no sequence homology also suggests that the mechanisms through which the Rag and Gtr GTPases regulate mTORC1 and yeast TORC1, respectively, have diverged. Although it is clear that

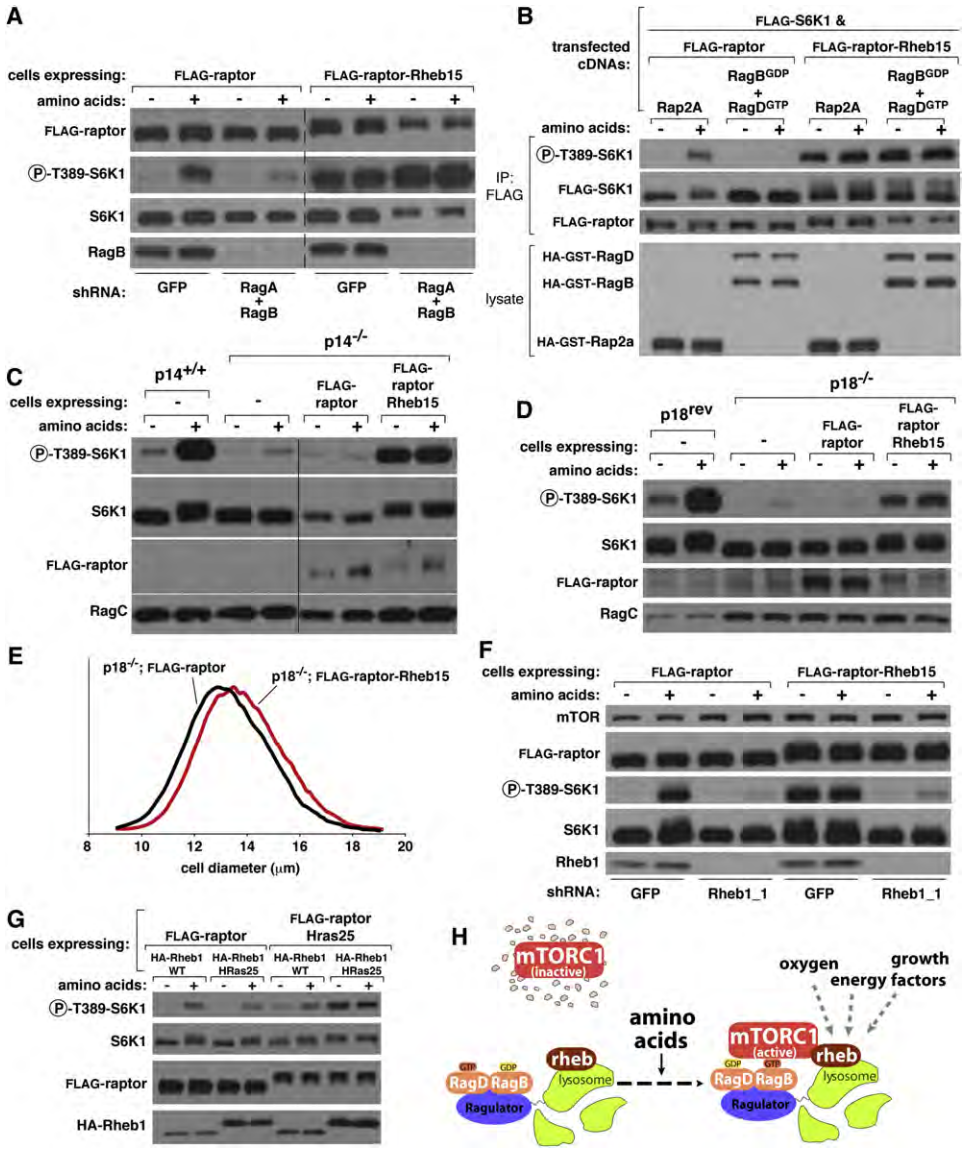

Figure 7. Targeting of mTORC1 to the Lysosomal Surface Makes the Activity of the mTORC1 Pathway Independent of Rag and Ragulator, but Not Rheb, Function

(A) In cells that express FLAG-raptor-Rheb15, mTORC1 pathway activity is independent of Rag GTPase function. Lysates of HEK293T cells expressing FLAG-raptor or FLAG-raptor-Rheb15 were analyzed by immunoblotting for the indicated proteins and phosphorylation states after disruption of Rag function by RNAi-mediated coknockdown of RagA and RagB. Cells were starved of amino acids for 50 min or starved and restimulated with amino acids for 10 min before lysis.

(B) In cells that express FLAG-raptor-Rheb15, mTORC1 pathway activity is independent of Rag GTPase function. Lysates of HEK293T cells expressing FLAG-raptor or FLAG-raptor-Rheb15 were analyzed as in (A) after disruption of Rag function by expression of the dominant negative $RagB^{GDP}$-$RagD^{GTP}$ heterodimer. Cells were treated and processed as in (A).

(C) Stable expression of FLAG-raptor-Rheb15 but not FLAG-raptor in p14 null cells is sufficient to reactivate the mTORC1 pathway and make it insensitive to amino acid starvation. Cells stably expressing the indicated proteins were treated and analyzed as in (A).

(D) Stable expression of FLAG-raptor-Rheb15 but not FLAG-raptor in p18 null cells is sufficient to reactivate the mTORC1 pathway and make it insensitive to amino acid starvation. Cells stably expressing the indicated proteins were treated and analyzed as in (A).

(E) In p18 null cells expression of raptor-Rheb15, but not wild-type raptor, increases cell size. Cell size distributions of p18 null cells that stably express FLAG-raptor or FLAG-raptor-Rheb15 are shown.

(F) In cells that express FLAG-raptor-Rheb15, the activity of the mTORC1 pathway is still Rheb dependent. Lysates of HEK293T cells that stably express FLAG-raptor or FLAG-raptor-Rheb15 were analyzed by immunoblotting for the indicated proteins and phosphorylation states after disruption of Rheb function by an RNAi-mediated knockdown of Rheb1. Cells were treated as in (A).

(G) Coexpression of plasma membrane-targeted raptor and plasma membrane-targeted Rheb1 renders the mTORC1 pathway insensitive to amino acid starvation. HEK293T cells stably expressing the indicated proteins were treated and analyzed as in (A).

the Ragulator and EGO complexes both control the intracellular localization of the Rag (this paper) and Gtr (Gao and Kaiser, 2006) GTPases, respectively, whether these complexes have additional functions remains to be determined.

Previous studies suggest that MP1-p14-p18 complex plays an adaptor role in the MAP kinase (MAPK) pathway (reviewed in Dard and Peter, 2006), and our current findings do not contradict these results. However, considering the very strong inhibition of the mTORC1 pathway that occurs in cells lacking p14 or p18, it seems possible that some of the impairment in MAPK signaling observed in those cells reflects an altered feedback signaling from Akt to the MAPK pathway. For example, in Ragulator null cells, Akt is slightly activated, almost certainly because the well-known inhibitory signal from mTORC1 to PI3K is absent. As Akt suppresses MAPK signaling by phosphorylating and inhibiting Raf (Zimmermann and Moelling, 1999), it is conceivable that the activation of Akt that occurs in Ragulator null cells could account, at least in part, for the inhibition of MAPK signaling that has been observed in these cells.

Mice lacking either p14 or p18 die around embryonic day 7.5–8 and have obvious growth defects (Nada et al., 2009; Teis et al., 2006). We would not be surprised if, when generated, mice lacking the Rag proteins die at around the same age and present similar defects. On the other hand, mice lacking the core mTORC1 component raptor die earlier (before embryonic day 6.5) than p14 and p18 null mice (Guertin et al., 2006). This may be expected because although loss of p14 or p18 completely blocks mTORC1 activation by amino acids, cells lacking the Ragulator proteins are likely to retain a low residual level of mTORC1 activity that may be sufficient to support development further than in embryos completely lacking mTORC1 function. Lastly, our results suggest that the strong growth retardation observed in humans with a mutation that reduces p14 expression (Bohn et al., 2007) is a result of partial suppression of the mTORC1 pathway. If this turns out to be the case, it would represent the first human example of a loss-of-function mutation in a positive component of the mTORC1 pathway.

EXPERIMENTAL PROCEDURES

Cell Lines and Tissue Culture

HEK293E cells, HEK293T cells, and TSC2$^{+/+}$, TSC2$^{-/-}$, p14$^{+/+}$, and p14$^{-/-}$ MEFs were cultured in Dulbecco's modified Eagle's medium (DMEM) with 10% inactivated fetal calf serum. p18^{rev}, p18^{mito}, and p18$^{-/-}$ cells were cultured in DMEM with 10% fetal bovine serum. HEK293E and HEK293T cells express E1a and SV40 large T antigen, respectively. In HEK293E, but not HEK293T, cells the mTORC1 pathway is strongly regulated by serum and insulin (Sancak et al., 2007). TSC2$^{-/-}$, p53$^{-/-}$, and TSC2$^{+/+}$, p53$^{-/-}$ MEFs were kindly provided by David Kwiatkowski (Harvard Medical School). The HEK293E cell line was kindly provided by John Blenis (Harvard Medical School). p14$^{-/-}$ and control MEFs were kindly provided by Lukas A. Huber (Innsbruck Medical University) and described are in Teis et al. (2006). p18$^{-/-}$ cells are epithelial in nature, and p18^{rev} cells are p18$^{-/-}$ cells in which wild-type p18 has been re-expressed (Nada et al., 2009). Patient-derived cells with a homozygous mutation in the *ROBLD3* (p14) gene 3′ untranslated region and control healthy donor-derived cells were kindly provided by Christoph Klein (Universität München) and have been described in Bohn et al. (2007)

Amino Acid and Serum Starvation and Stimulation of Cells

Serum and/or amino acid starvation of HEK293T cells, HEK293E cells, p14 null and control cells, p18 null and control cells, MEFs, and patient-derived and healthy donor-derived cells were performed essentially as described (Sancak et al., 2008). Serum was dialyzed against phosphate-buffered saline (PBS) in dialysis cassettes (Thermo Scientific) having a 3500 molecular weight cutoff.

Preparation of Cell Lysates and Immunoprecipitations

Cell lysate preparation, cell lysis, and immunoprecipitations were done as described in the Extended Experimental Procedures.

For cotransfection experiments, 2,000,000 HEK293T or HEK293E cells were plated in 10 cm culture dishes. Twenty-four hours later, cells were transfected with the indicated plasmids as follows: 50 ng or 1500 ng myc-mTOR in pRK5; 20 ng or 500 ng HA-, myc-, or FLAG-Raptor in pRK5 or pLJM1 with or without the targeting signals; 100 ng HA-GST-Rap2a in pRK5; 100 ng HA-GST-Rheb1 in pRK5; 100 ng HA-GST-RagB in pRK5; 100 ng HA-GST-RagD in pRK5; 1 ng FLAG-S6K1 in pRK7; 50 ng or 600 ng HA- or FLAG-p14 in pRK5; 75 ng or 600 ng HA-MP1 in pRK5; and 50 ng or 800 ng HA-p18 in pRK5. The total amount of plasmid DNA in each transfection was normalized to 2 μg with empty pRK5.

Cell Size Determinations

For measurement of cell size, 2,000,000 HEK293T cells or 200,000 of other cell types were plated into 10 cm culture dishes. Twenty-four hours later, the cells were harvested by trypsinization in a 4 ml volume and diluted 1:20 with counting solution (Isoton II Diluent, Beckman Coulter). Cell diameters were determined with a particle size counter (Coulter Z2, Beckman Coulter) running Coulter Z2 AccuComp software.

Mammalian Lentiviral shRNAs and cDNAs

Lentiviral short hairpin RNAs (shRNAs) targeting human Rheb1, RagB, and RagC have been described (Sancak et al., 2008). Lentiviral shRNAs targeting mouse Rheb1 and human p14 were obtained from Sigma-Aldrich. Lentiviral shRNAs targeting the messenger RNA for human MP1 and human p18 were cloned into pLKO.1 vector as described (Sarbassov et al., 2005). The target sequences are provided in the Extended Experimental Procedures. Virus generation and infection was done as previously described (Sancak et al., 2008).

Raptor was cloned into the AgeI and BamHI sites of a modified pLKO.1 vector (pLJM1) (Sancak et al., 2008) with or without the Rheb1, Rap1b, and HRas targeting signals or cloned into the pRK5 vector with or without the same localization signals. After sequence verification, pLJM1 based plasmids were used in transient cDNA transfections or to produce lentivirus needed to generate cell lines stably expressing these proteins. pRK5 based plasmids were also used for transient transfection experiments. The p18^{mito} expression plasmid was generated by cloning of a mutant p18 with amino acids 2–5 changed to alanines into a modified version of the pLKO.1 vector that added, to the C terminus of p18, the mitochondrial localization signal of OMP25 protein. This plasmid was used in transient cDNA transfections or to produce lentivirus needed to generate stable cell lines. HA-Rheb1 and HA-Rheb1-HRas25 were cloned into pLJM5, a derivative of pLJM1 carrying a hygromycin instead of puromycin resistance gene. The vectors were used as above for lentivirus production.

Immunofluorescence Assays

Fifty thousand HEK293T cells or 20,000 of other cell types were plated on fibronectin-coated glass coverslips in 12-well tissue culture plates. Twenty-four hours later, the slides were rinsed with PBS once and fixed for 15 min with 4% paraformaldehyde in PBS warmed to 37°C. The slides were rinsed

(H) Model for amino-acid induced mTORC1 activation. In the absence of amino acids, mTORC1 cannot associate with the endomembrane system and has no access to its activator Rheb. In the presence of amino acids, the Rag GTPases, which are tethered to the lysosomal surface by the Ragulator, serve as a docking site for mTORC1, allowing mTORC1 to associate with endomembranes and thus encounter and become activated by Rheb.
See also Figure S5.

twice with PBS and cells were permeabilized with 0.05% Triton X-100 in PBS for 30 s. After rinsing twice with PBS, the slides were incubated with primary antibody in 5% normal donkey serum for 2 hr at room temperature, rinsed four times with PBS, and incubated with secondary antibodies produced in donkey (diluted 1:1000 in 5% normal donkey serum) for 1 hr at room temperature in the dark, washed four times with PBS. Slides were mounted on glass coverslips using Vectashield (Vector Laboratories) and imaged. Transient transfections for immunofluorescence assays were performed as described in the Extended Experimental Procedures.

SUPPLEMENTAL INFORMATION

Supplemental Information includes Extended Experimental Procedures and Five Figures and can be found with this article online at doi:10.1016/j.cell.2010.02.024.

ACKNOWLEDGMENTS

We thank all members of the Sabatini Lab for helpful suggestions and Eric Spooner for the mass spectrometric analysis of samples. We thank Lukas A. Huber for providing p14 null and control cells and Christoph Klein for providing patient-derived and healthy donor-derived cells. This work was supported by grants from the National Institutes of Health (CA103866 and AI47389) and Department of Defense (W81XWH-07-0448) to D.M.S., awards from the W.M. Keck Foundation and LAM Foundation to D.M.S, and fellowship support from the LAM Foundation and from the Jane Coffin Childs Memorial Fund for Medical Research to R.Z. D.M.S. is an investigator of the Howard Hughes Medical Institute.

Received: October 16, 2009
Revised: December 28, 2009
Accepted: February 5, 2010
Published online: April 8, 2010

REFERENCES

Berchtold, D., and Walther, T.C. (2009). TORC2 plasma membrane localization is essential for cell viability and restricted to a distinct domain. Mol. Biol. Cell *20*, 1565–1575.

Binda, M., Péli-Gulli, M.P., Bonfils, G., Panchaud, N., Urban, J., Sturgill, T.W., Loewith, R., and De Virgilio, C. (2009). The Vam6 GEF controls TORC1 by activating the EGO complex. Mol. Cell *35*, 563–573.

Bohn, G., Allroth, A., Brandes, G., Thiel, J., Glocker, E., Schäffer, A.A., Rathinam, C., Taub, N., Teis, D., Zeidler, C., et al. (2007). A novel human primary immunodeficiency syndrome caused by deficiency of the endosomal adaptor protein p14. Nat. Med. *13*, 38–45.

Buerger, C., DeVries, B., and Stambolic, V. (2006). Localization of Rheb to the endomembrane is critical for its signaling function. Biochem. Biophys. Res. Commun. *344*, 869–880.

Chavrier, P., Parton, R.G., Hauri, H.P., Simons, K., and Zerial, M. (1990). Localization of low molecular weight GTP binding proteins to exocytic and endocytic compartments. Cell *62*, 317–329.

Clark, G.J., Kinch, M.S., Rogers-Graham, K., Sebti, S.M., Hamilton, A.D., and Der, C.J. (1997). The Ras-related protein Rheb is farnesylated and antagonizes Ras signaling and transformation. J. Biol. Chem. *272*, 10608–10615.

Dard, N., and Peter, M. (2006). Scaffold proteins in MAP kinase signaling: more than simple passive activating platforms. Bioessays *28*, 146–156.

Dubouloz, F., Deloche, O., Wanke, V., Cameroni, E., and De Virgilio, C. (2005). The TOR and EGO protein complexes orchestrate microautophagy in yeast. Mol. Cell *19*, 15–26.

Eskelinen, E.L. (2006). Roles of LAMP-1 and LAMP-2 in lysosome biogenesis and autophagy. Mol. Aspects Med. *27*, 495–502.

Gao, M., and Kaiser, C.A. (2006). A conserved GTPase-containing complex is required for intracellular sorting of the general amino-acid permease in yeast. Nat. Cell Biol. *8*, 657–667.

Guertin, D.A., and Sabatini, D.M. (2007). Defining the role of mTOR in cancer. Cancer Cell *12*, 9–22.

Guertin, D.A., Stevens, D.M., Thoreen, C.C., Burds, A.A., Kalaany, N.Y., Moffat, J., Brown, M., Fitzgerald, K.J., and Sabatini, D.M. (2006). Ablation in mice of the mTORC components raptor, rictor, or mLST8 reveals that mTORC2 is required for signaling to Akt-FOXO and PKCalpha, but not S6K1. Dev. Cell *11*, 859–871.

Hirose, E., Nakashima, N., Sekiguchi, T., and Nishimoto, T. (1998). RagA is a functional homologue of S. cerevisiae Gtr1p involved in the Ran/Gsp1-GTPase pathway. J. Cell Sci. *111*, 11–21.

Kim, E., Goraksha-Hicks, P., Li, L., Neufeld, T.P., and Guan, K.L. (2008). Regulation of TORC1 by Rag GTPases in nutrient response. Nat. Cell Biol. *10*, 935–945.

Koonin, E.V., and Aravind, L. (2000). Dynein light chains of the Roadblock/LC7 group belong to an ancient protein superfamily implicated in NTPase regulation. Curr. Biol. *10*, R774–R776.

Laplante, M., and Sabatini, D.M. (2009). mTOR signaling at a glance. J. Cell Sci. *122*, 3589–3594.

Li, S.C., and Kane, P.M. (2009). The yeast lysosome-like vacuole: endpoint and crossroads. Biochim. Biophys. Acta *1793*, 650–663.

Lunin, V.V., Munger, C., Wagner, J., Ye, Z., Cygler, M., and Sacher, M. (2004). The structure of the MAPK scaffold, MP1, bound to its partner, p14. A complex with a critical role in endosomal map kinase signaling. J. Biol. Chem. *279*, 23422–23430.

Luzio, J.P., Pryor, P.R., and Bright, N.A. (2007). Lysosomes: fusion and function. Nat. Rev. Mol. Cell Biol. *8*, 622–632.

Manning, B.D. (2004). Balancing Akt with S6K: implications for both metabolic diseases and tumorigenesis. J. Cell Biol. *167*, 399–403.

Nada, S., Hondo, A., Kasai, A., Koike, M., Saito, K., Uchiyama, Y., and Okada, M. (2009). The novel lipid raft adaptor p18 controls endosome dynamics by anchoring the MEK-ERK pathway to late endosomes. EMBO J. *28*, 477–489.

Nemoto, Y., and De Camilli, P. (1999). Recruitment of an alternatively spliced form of synaptojanin 2 to mitochondria by the interaction with the PDZ domain of a mitochondrial outer membrane protein. EMBO J. *18*, 2991–3006.

Pizon, V., Desjardins, M., Bucci, C., Parton, R.G., and Zerial, M. (1994). Association of Rap1a and Rap1b proteins with late endocytic/phagocytic compartments and Rap2a with the Golgi complex. J. Cell Sci. *107*, 1661–1670.

Roccio, M., Bos, J.L., and Zwartkruis, F.J.T. (2006). Regulation of the small GTPase Rheb by amino acids. Oncogene *25*, 657–664.

Saito, K., Araki, Y., Kontani, K., Nishina, H., and Katada, T. (2005). Novel role of the small GTPase Rheb: its implication in endocytic pathway independent of the activation of mammalian target of rapamycin. J. Biochem. *137*, 423–430.

Sancak, Y., Thoreen, C.C., Peterson, T.R., Lindquist, R.A., Kang, S.A., Spooner, E., Carr, S.A., and Sabatini, D.M. (2007). PRAS40 is an insulin-regulated inhibitor of the mTORC1 protein kinase. Mol. Cell *25*, 903–915.

Sancak, Y., Peterson, T.R., Shaul, Y.D., Lindquist, R.A., Thoreen, C.C., Bar-Peled, L., and Sabatini, D.M. (2008). The Rag GTPases bind raptor and mediate amino acid signaling to mTORC1. Science *320*, 1496–1501.

Sarbassov, D.D., Guertin, D.A., Ali, S.M., and Sabatini, D.M. (2005). Phosphorylation and regulation of Akt/PKB by the rictor-mTOR complex. Science *307*, 1098–1101.

Schaeffer, H.J., Catling, A.D., Eblen, S.T., Collier, L.S., Krauss, A., and Weber, M.J. (1998). MP1: a MEK binding partner that enhances enzymatic activation of the MAP kinase cascade. Science *281*, 1668–1671.

Schürmann, A., Brauers, A., Massmann, S., Becker, W., and Joost, H.G. (1995). Cloning of a novel family of mammalian GTP-binding proteins (RagA, RagBs, RagB1) with remote similarity to the Ras-related GTPases. J. Biol. Chem. *270*, 28982–28988.

Sekiguchi, T., Hirose, E., Nakashima, N., Ii, M., and Nishimoto, T. (2001). Novel G proteins, Rag C and Rag D, interact with GTP-binding proteins, Rag A and Rag B. J. Biol. Chem. *276*, 7246–7257.

Smith, E.M., Finn, S.G., Tee, A.R., Browne, G.J., and Proud, C.G. (2005). The tuberous sclerosis protein TSC2 is not required for the regulation of the mammalian target of rapamycin by amino acids and certain cellular stresses. J. Biol. Chem. *280*, 18717–18727.

Takahashi, K., Nakagawa, M., Young, S.G., and Yamanaka, S. (2005). Differential membrane localization of ERas and Rheb, two Ras-related proteins involved in the phosphatidylinositol 3-kinase/mTOR pathway. J. Biol. Chem. *280*, 32768–32774.

Teis, D., Wunderlich, W., and Huber, L.A. (2002). Localization of the MP1-MAPK scaffold complex to endosomes is mediated by p14 and required for signal transduction. Dev. Cell *3*, 803–814.

Teis, D., Taub, N., Kurzbauer, R., Hilber, D., de Araujo, M.E., Erlacher, M., Offterdinger, M., Villunger, A., Geley, S., Bohn, G., et al. (2006). p14-MP1-MEK1 signaling regulates endosomal traffic and cellular proliferation during tissue homeostasis. J. Cell Biol. *175*, 861–868.

Wunderlich, W., Fialka, I., Teis, D., Alpi, A., Pfeifer, A., Parton, R.G., Lottspeich, F., and Huber, L.A. (2001). A novel 14-kilodalton protein interacts with the mitogen-activated protein kinase scaffold mp1 on a late endosomal/lysosomal compartment. J. Cell Biol. *152*, 765–776.

Zimmermann, S., and Moelling, K. (1999). Phosphorylation and regulation of Raf by Akt (protein kinase B). Science *286*, 1741–1744.

EXTENDED EXPERIMENTAL PROCEDURES

Materials

Reagents were obtained from the following sources: antibodies to phospho-T389 S6K1, S6K1, mTOR, raptor, RagA/B, RagC, p14, p18, MP1, the myc epitope, the HA epitope, the FLAG epitope (unconjugated and alexa fluor conjugated), TSC2, phospho-T398 dS6K, phospho-S473 Akt, Akt1, phospho-T70 4E-BP1, 4E-BP1, and Rheb from Cell Signaling Technology; antibodies to LAMP2 from Abcam (ab25631 and ab13524); antibody to raptor (for immunostaining) from Millipore; antibody to Cytochrome c from BD Biosciences; HRP-labeled anti-mouse, anti-goat, and anti-rabbit secondary antibodies from Santa Cruz Biotechnology; FLAG M2 affinity gel, FLAG M2 antibody, human recombinant insulin, from Sigma Aldrich; protein G-sepharose and dialysis cassettes from Thermo Scientific; DMEM from SAFC Biosciences; FuGENE 6 and Complete Protease Cocktail from Roche; alexa fluor conjugated secondary antibodies from Invitrogen; 16% paraformaldehyde solution from Electron Microscopy Sciences; fibronectin from Jackson Immunoresearch Laboratories; 35 mm glass bottom dishes from Mattek Corporation; glass coverslips from Ted Pella, Inc; amino acid and glucose-free RPMI from United States Biological; Schneider's medium, *Drosophila*-SFM, and Inactivated Fetal Calf Serum (IFS) from Invitrogen. The dS6K antibody was a generous gift from Mary Stewart (North Dakota State University).

Preparation of Cell Lysates and Immunoprecipitations

Cells were rinsed once with ice-cold PBS and lysed in ice-cold lysis buffer (40 mM HEPES [pH 7.4], 2 mM EDTA or 5mM $MgCl_2$, 10 mM pyrophosphate, 10 mM glycerophosphate, 0.3% CHAPS, or 1% Trition X-100 and one tablet of EDTA-free protease inhibitors (Roche) per 25 ml). The soluble fractions of cell lysates were isolated by centrifugation at 13,000 rpm for 10 min by centrifugation. For immunoprecipitations, primary antibodies were added to the lysates and incubated with rotation for 1.5 hr at 4°C. 60 μl of a 50% slurry of protein G-sepharose was then added and the incubation continued for an additional 1 hr. Immunoprecipitates were washed three times with lysis buffer containing 150mM NaCl. Immunoprecipitated proteins were denatured by the addition of 20 μl of sample buffer and boiling for 5 min, resolved by 8%–16% SDS-PAGE, and analyzed by immunoblotting. For Flag purifications, Flag M2 affinity gel was washed with lysis buffer 3 times. 20 ul of beads in 50% slurry was then added to pre-cleared cell lysates and incubated with rotation for 2 hr at 4°C. Finally, The beads were washed 3 times with lysis buffer containing 150 mM NaCl. Immunoprecipitated proteins were denatured by the addition of 50 μl of sample buffer and boiling for 5 min.

Mammalian Lentiviral shRNAs and cDNAs

The sequences of shRNAs targeting human MP1 and p18 are as follows:

MP1_1: GAGATGGAGTACCTGTTATTA
MP1_2: ATATCAATCCAGCAATCTTTA
p18: AGACAGCCAGCAACATCATTG

Identification of Ragulator Components as Rag-Associated Proteins

Ragulator components (MP1, p14, and p18) were detected in anti-FLAG immunoprecipitates prepared from HEK293T cells stably expressing FLAG-RagB or FLAG-RagD as well as in immunoprecipitates of endogenous RagC prepared from HEK293T cells. Immunoprecipitates were prepared as described (Sancak et al., 2008). Proteins were eluted with the FLAG peptide from the anti-FLAG affinity matrix or recovered from the protein G-sepharose by boiling with sample buffer, resolved by SDS-PAGE, and stained with simply blue stain (Invitrogen). Each gel lane was sliced into 10-12 pieces and the proteins in each gel slice digested overnight with trypsin. The resulting digests were analyzed by mass spectrometry as described (Sancak et al., 2008). 2-3 peptides corresponding to each Ragulator component were identified in the FLAG-RagB and endogenous RagC immunoprecipitates, while no peptides corresponding to any of the proteins were ever found in the FLAG-Rap2a, p53, or α-tubulin immunoprecipitates that served as controls.

Amino Acid Starvation and Stimulation and dsRNA-Mediated Knockdowns in *Drosophila* Cells

Amino acid starvation and stimulation of *Drosophila* S2 cells was performed as described (Sancak et al., 2008). The design and synthesis of dsRNAs has also been described (Sancak et al., 2008).

Primer sequences used to amplify DNA templates for dsRNA synthesis for dp14, dp18, and dMP1, including underlined 5′ and 3′ T7 promoter sequences, are as follows:

dp14 (CG5189) dsRNA forward primer: GAATTAATACGACTCACTATAGGGAGACTCTATTGGCCTACTCCGGTTAT
dp14 (CG5189) dsRNA reverse primer: GAATTAATACGACTCACTATAGGGAGATATGAGGCCGAGATCTGCTTA
dp18 (CG14184) dsRNA forward primer: GAATTAATACGACTCACTATAGGGAGAGCAGAATACTGCGATAAACATGATA
dp18 (CG14184) dsRNA reverse primer: GAATTAATACGACTCACTATAGGGAGATGGATAGGTTGGCTTAGACAGATAG
dMP1 (CG5110) dsRNA forward primer: GAATTAATACGACTCACTATAGGGAGAGTCGGACGACATCAAGAAGTATTTA
dMP1 (CG5110) dsRNA reverse primer: GAATTAATACGACTCACTATAGGGAGAAGTACATGGAGATGATGGTCTTGTT

In Vitro Binding Assay

2 million HEK293T cells were transfected with 2 μg FLAG-p18 (lipidation mutant G2A), 2 μg HA-GST-Rap2a, or 2 μg HA-GST-RagB together with 2 μg of HA-GST-RagC. 2 days after transfection, the cells were lysed in lysis buffer containing 1% Triton X-100 as described (Sancak et al., 2007) and cleared lysates were incubated with glutathione- or FLAG-beads for 3 hr at 4°C with rotation. The beads were washed 3 times with lysis buffer and two times with lysis buffer containing 0.3% CHAPS. FLAG-p18 was eluted from FLAG beads with the FLAG peptide and 1/8 of the eluate was incubated with 1/4 of the Rag-containing glutathione beads in lysis buffer with 0.3% CHAPS for 45 min at 4°C. The glutathione beads were washed three times with lysis buffer containing 0.3% CHAPS and 150 mM NaCl. Proteins were denatured by the addition of 20 μl of sample buffer and boiling for 5 min and analyzed by SDS-PAGE and immunoblotting.

Transient Transfections for Immunofluorescence Assays

For myc-mTOR and HA-raptor co-transfection experiments, HEK293T cells were seeded in 60 mm culture plates. 24 hr later, cells were transfected with 500 ng myc-mTOR and 50 ng HA-Raptor. 24 hr after transfections, cells were split and plated on fibronectin coated glass coverslip in 12-well culture plates and processed as above.

For GFP-RagB, GFP-RagD, p18-GFP, GFP-Mito, RFP-RagB, and LAMP1-mRFP co-transfection experiments, HEK293T cells (250,000 cells/dish) or $p18^{-/-}$, $p18^{rev}$ or $p18^{mito}$ cells (50,000 cells/dish) were plated on 35 mm, glass-bottom Mattek dishes. The next day, each dish was transfected with 100 ng of GFP-RagB or GFP-RagD, p18-GFP, GFP-mito, RFP-RagB or LAMP1-mRFP using fugene. At 18-24 hr post transfections, cells were fixed and imaged. GFP-Mito has been described (Nemoto and De Camilli, 1999).

For GFP-LC3 localization experiments, 2 million cells were transfected by electroporation with 1 μg of GFP-LC3 plasmid, and plated on 35 mm glass-bottom Mattek dishes. The next day the cells were starved for 3 hr in serum- and amino acid-free RPMI to induce autophagy and processed for imaging as above.

All images were acquired with a spinning disk confocal microscope (Perkin Elmer) equipped with a Hamamatsu 1k X 1k EM-CCD camera. For each image, 8-10 optical slices were acquired and displayed as maximum projections.

Quantification of Number of Autophagosomes per Cell

After acquisition, the images were opened with Image J, made binary and the number of autophagosomes per cell was obtained using the "Analyze Particle" function.

SUPPLEMENTAL REFERENCES

Nemoto, Y., and De Camilli, P. (1999). Recruitment of an alternatively spliced form of synaptojanin 2 to mitochondria by the interaction with the PDZ domain of a mitochondrial outer membrane protein. EMBO J. *18*, 2991–3006.

Sancak, Y., Peterson, T.R., Shaul, Y.D., Lindquist, R.A., Thoreen, C.C., Bar-Peled, L., and Sabatini, D.M. (2008). The Rag GTPases bind raptor and mediate amino acid signaling to mTORC1. Science *320*, 1496–1501.

Sancak, Y., Thoreen, C.C., Peterson, T.R., Lindquist, R.A., Kang, S.A., Spooner, E., Carr, S.A., and Sabatini, D.M. (2007). PRAS40 is an insulin-regulated inhibitor of the mTORC1 protein kinase. Mol. Cell *25*, 903–915.

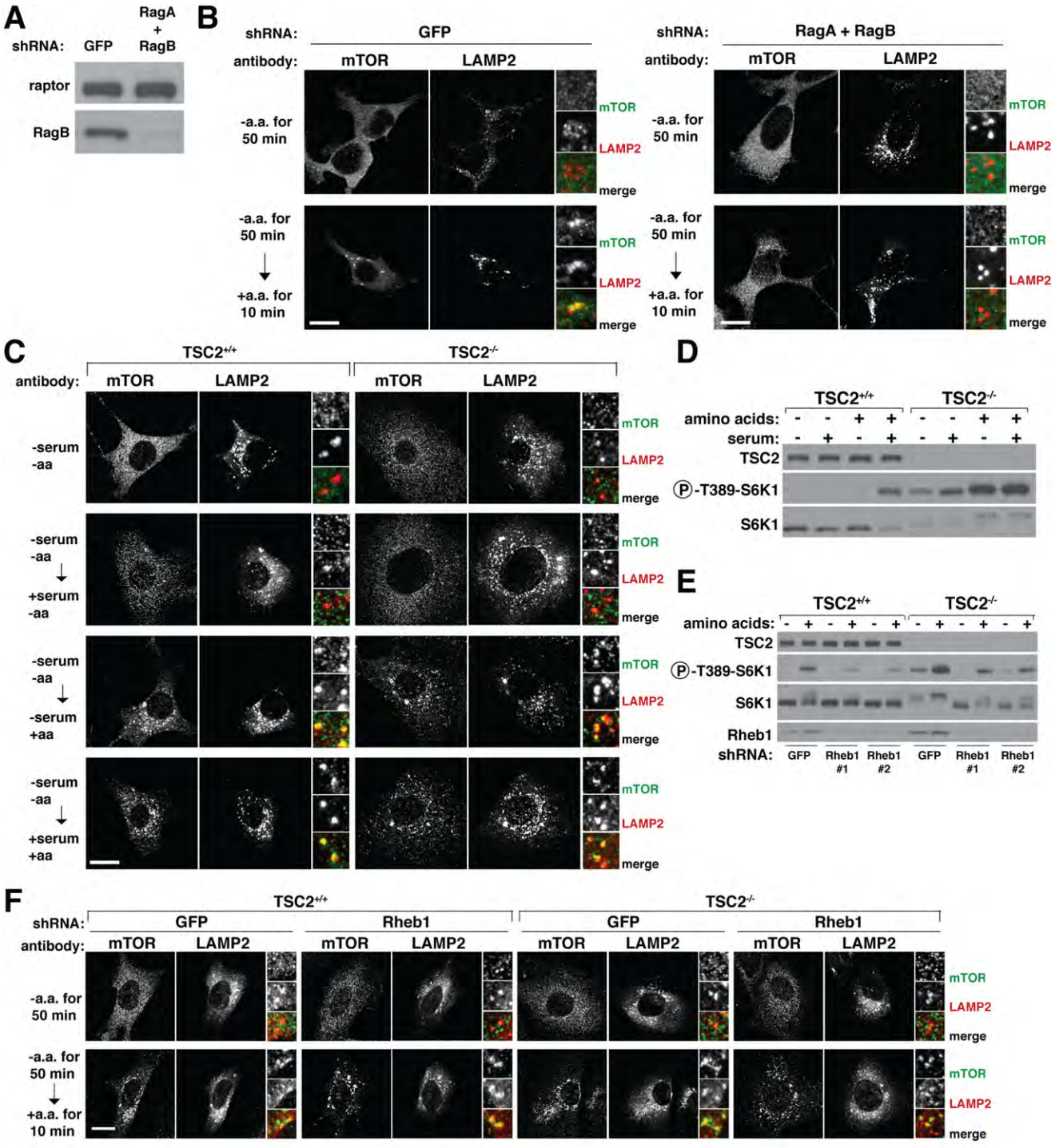

Figure S1. Movement of mTORC1 to Lysosomal Membranes in Response to Amino Acids Depends on the Rag GTPases and Is Independent of TSC1/2, Rheb, and Growth Factors, Related to Figure 1

(A) Immunoblot analysis of RagB and raptor protein levels in HEK293T cells with an RNAi-mediated knockdown of a control protein or RagA and RagB.

(B) Images of cells with knockdowns of RagA and RagB and co-immunostained for mTOR (green) and LAMP2 (red) after starvation and restimulation with amino acids for the indicated times. HEK293T cells expressing the indicated shRNAs were starved and restimulated with amino acids as indicated and processed in the immunofluorescence assay. In all images, insets show selected fields that were magnified five times and their overlay. Scale bar is 10 μm.

(C) mTOR co-localizes with LAMP2 only in the presence of amino acids and independently of serum stimulation. Images show co-immunostaining of mTOR (green) and LAMP2 (red) in $TSC2^{+/+}$ and $TSC2^{-/-}$ MEFs after indicated treatments. Cells were starved for serum and amino acids, and stimulated with dialyzed

serum, amino acids, or both before processing in the immunofluorescence assay.
(D) Lysates from $TSC2^{+/+}$ and $TSC2^{-/-}$ MEFs starved and stimulated as in (A) were analyzed by immunobloting for the activity of the mTORC1 pathway.
(E) Loss of Rheb expression inhibits mTORC1 signaling in $TSC2^{+/+}$ and $TSC2^{-/-}$ MEFs. Cells expressing the indicated shRNAs were starved for amino acids or starved and restimulated with amino acids and lysates analyzed by immunobloting for mTORC1 pathway activity and Rheb1 levels.
(F) mTOR co-localizes with LAMP2 only in the presence of amino acids and independently of Rheb or TSC2. Images show co-immunostaining of mTOR (green) and LAMP2 (red) in $TSC2^{+/+}$ and $TSC2^{-/-}$ MEFs treated as in (C).
In all images, insets show selected fields that were magnified five times and their overlays. Scale bar is 10 μm.

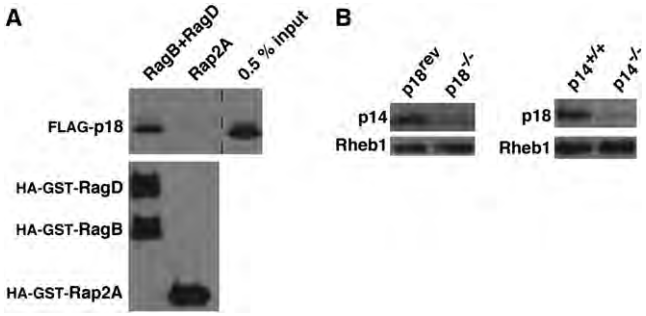

Figure S2. The Expression of Ragulator Proteins Is Coregulated and Purified FLAG-p18 Interacts with Purified HA-GST-RagB/HA-GST-RagD Dimer In Vitro, Related to Figure 2

(A) In vitro binding assay using purified soluble FLAG-p18 and HA-GST-RagB/HA-GST-RagD heterodimer bound to glutathione beads was performed as described in the Experimental Procedures.

(B) p14 protein levels are lower in p18 null cells than in p18 null cells expressing FLAG-p18 ($p18^{rev}$). Similarly, in cells that lack p14 ($p14^{-/-}$), p18 expression is reduced compared to control cells ($p14^{+/+}$). Cells were grown to confluency, lysates were prepared, and the levels of the indicated proteins analyzed by immunoblotting.

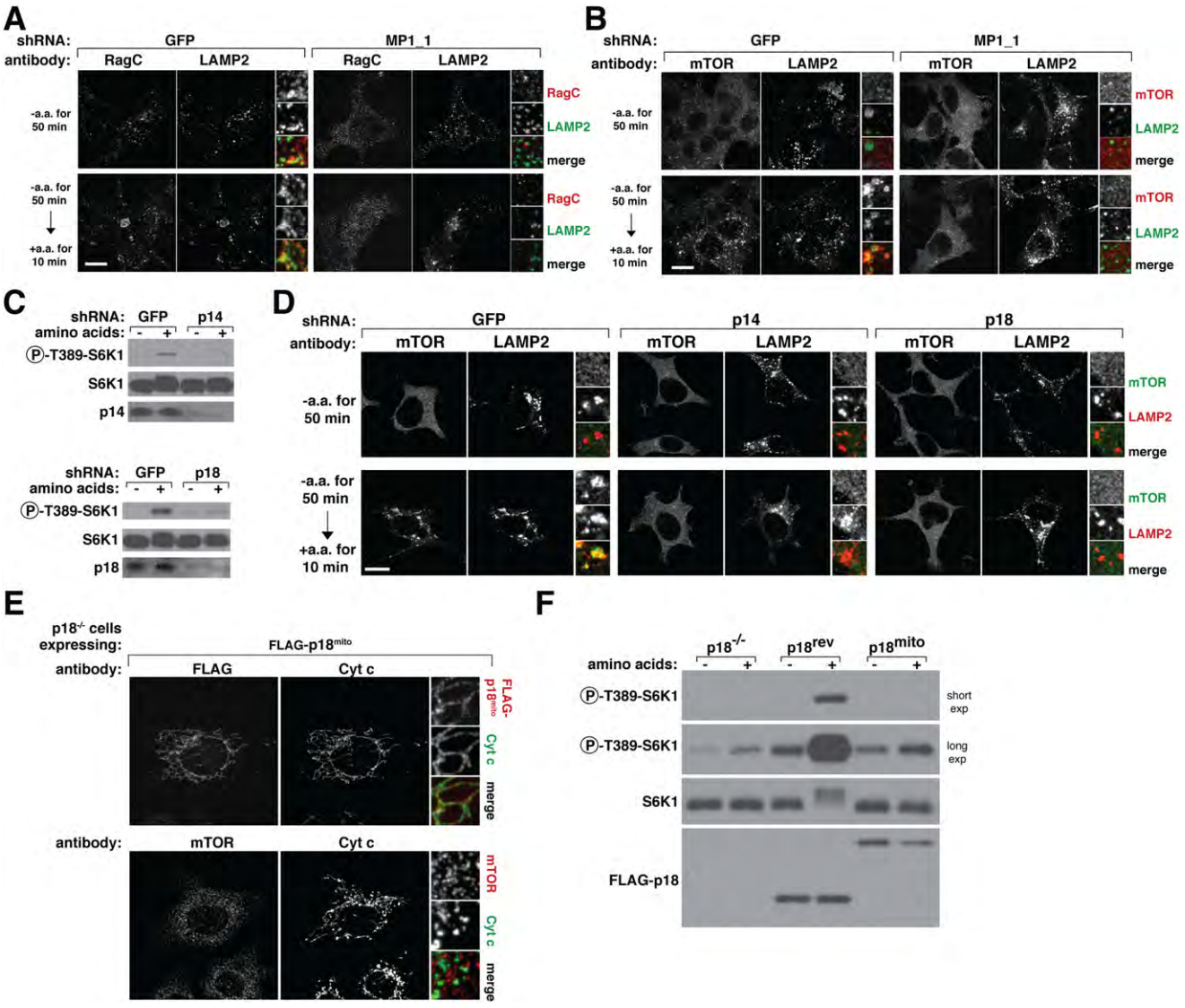

Figure S3. The Ragulator Is Required for RagC Localization to Lysosomal Membranes and Amino Acid-Induced mTOR Lysosomal Localization, Related to Figure 3

(A) An MP1 knockdown displaces RagC from the lysosomal surface. Images of cells with shRNA-mediated knockdowns of a control protein or MP1 and co-immunostained for RagC (red) and LAMP2 (green). HEK293T cells expressing the indicated shRNAs were starved of and restimulated with amino acids for the stated times and then processed in the immunofluorescence assay.

(B) An MP1 knockdown impairs the recruitment of mTOR to the lysosomal surface in response to amino acid stimulation. Images of cells with shRNA-mediated knockdowns of a control protein or MP1 and co-immunostained for mTOR (red) and LAMP2 (green). HEK293T cells expressing the indicated shRNAs were starved of and restimulated with amino acids for the stated times and then processed in the immunofluorescence assay.

(C) Knockdown of p18 or p14 in HEK293T cells impair amino acid-induced mTORC1 activation. HEK293T cells with RNAi-mediated knockdown of p14 or p18, or control cells, were starved for amino acids for 50 min or starved and restimulated with amino acid for 10 min. Cell lysates were prepared and analyzed by immunoblotting for the phosphorylation states and levels of indicated proteins.

(D) Knockdown of p18 or p14 in HEK293T cells impairs amino acid-induced lysosomal recruitment of mTOR. Control cells and cells with p14 or p18 knockdown were treated as in (C) and immunostained for mTOR (green) and LAMP2 (red). In all images, insets show selected fields that were magnified five times and their overlays. Scale bar is 10 μm.

(E) Images of $p18^{-/-}$ cells stably expressing FLAG-$p18^{mito}$ and co-immunostained for FLAG-$p18^{mito}$ or mTOR (red) and Cytochrome c (Cyt c) (green).

(F) The mTORC1 pathway can be activated by amino acids in p18 null cells expressing wild-type p18 ($p18^{rev}$), but not mitochondrially-targeted p18 ($p18^{mito}$). Cells were starved for amino acids in the presence of dialyzed serum for 50 min, or starved and restimulated with amino acids for 10 min. Lysates were prepared and phosphorylation states and levels of indicated proteins were analyzed by immunoblotting.

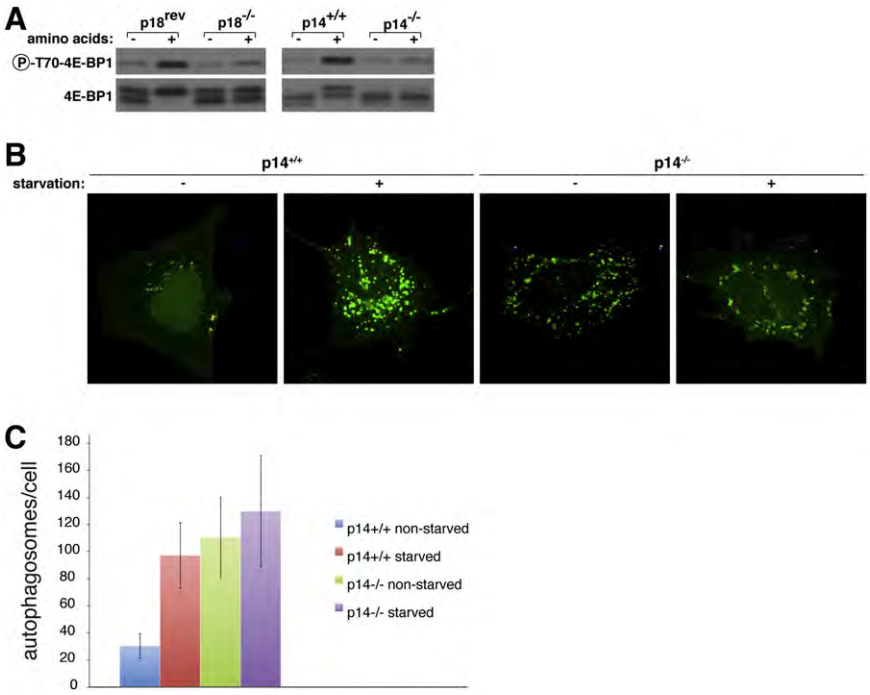

Figure S4. 4E-BP1 Phosphorylation Is Inhibited and Autophagy Is Induced in Cells Lacking Ragulator Components, Related to Figure 4

(A) Amino acids fail to stimulate 4E-BP1 phosphoryation in cells lacking p14 or p18. Cells were starved for amino acids in the presence of dialyzed serum for 50 min, or starved and restimulated with amino acids for 10 min. Lysates were prepared and 4E-BP1 phosphorylation and levels analyzed by immunoblotting.

(B) Autophagy is induced in p14 null cells. Images of cells transiently expressing GFP-LC3 and starved for amino acids and serum for 3 hr or growing in complete media. Accumulation of GFP-LC3 in large puncta in starved control cells and in the non-starved p14 null cells indicates increased levels of autophagy in these cells.

(C) Quantification of autophagosomes in wild-type or p14 null cells expressing GFP-LC3. Cells were treated as in (B), images were taken and the number of autophagosomes per cell was quantified using Image J. At least six cells were analyzed per sample. The data are represented as mean −/+ standard deviation. Starved wild-type cells, or p14 null cells, irrespective of being starved or not, show statistically significant increases in the number autophagosomes per cell compared to wild-type non-starved cells ($p < 0.000002$). There is no statistically significant difference between starved and non-starved p14 null cells ($p = 0.38$).

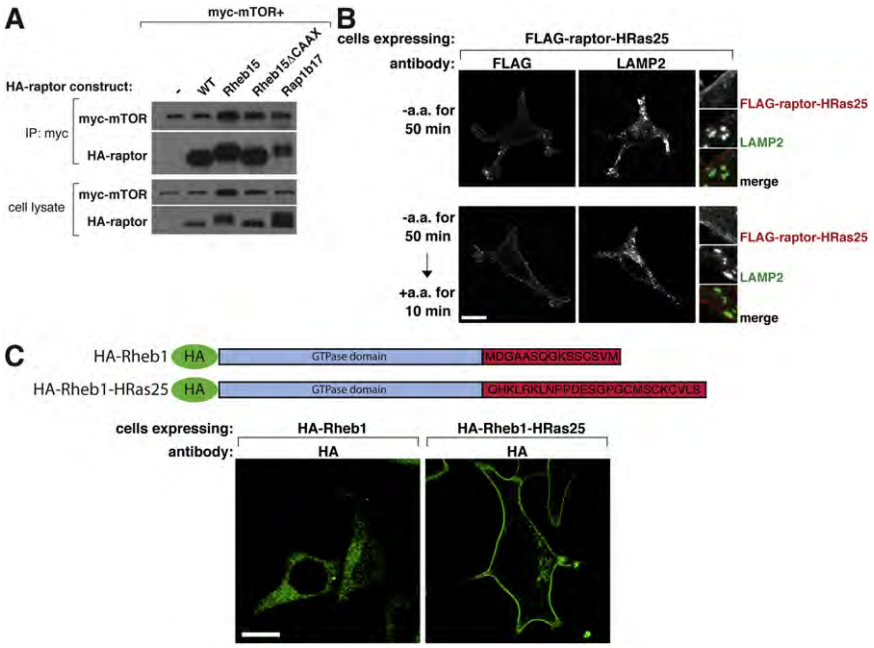

Figure S5. Addition of Rheb1 and Rap1b Targeting Signals to Raptor Does Not Interfere with Its Binding to mTOR and Raptor-HRas25 and Rheb-HRas25 Localize to the Plasma Membrane, Related to Figure 7

(A) HEK293T cells were co-transfected with plasmids encoding myc-mTOR and the indicated HA-raptor variants. Anti-myc immunoprecipitates as well as lysates were analyzed by immunobloting for the indicated proteins.

(B) Raptor fused at its C terminus with the localization signal of HRas localizes to the plasma membrane. Images of cells expressing FLAG-raptor-HRas25 and starved of and restimulated with amino acid for the indicated times and co-immunostained with antibodies to the FLAG epitope (red) and endogenous LAMP2 (green).

(C) Rheb1 localizes to the plasma membrane when its localization signal is swapped for that of HRas. Schematic shows composition of the HA-Rheb1-HRas25 variant. Images of cells expressing HA-Rheb1 or HA-Rheb1-HRas25 (green).

Cancer Cell
Article

Defective Regulation of Autophagy upon Leucine Deprivation Reveals a Targetable Liability of Human Melanoma Cells In Vitro and In Vivo

Joon-Ho Sheen,[1] Roberto Zoncu,[1] Dohoon Kim,[1] and David M. Sabatini[1,2,3,4,*]
[1]Whitehead Institute for Biomedical Research, 9 Cambridge Center, Cambridge, MA 02142, USA
[2]Department of Biology, Howard Hughes Medical Institute, Massachusetts Institute of Technology, Cambridge, MA 02139, USA
[3]David H. Koch Institute for Integrative Cancer Research, 500 Main Street, Cambridge, MA 02139, USA
[4]The Broad Institute, 7 Cambridge Center, Cambridge, MA 02142, USA
*Correspondence: sabatini@wi.mit.edu
DOI 10.1016/j.ccr.2011.03.012

SUMMARY

Autophagy is of increasing interest as a target for cancer therapy. We find that leucine deprivation causes the caspase-dependent apoptotic death of melanoma cells because it fails to appropriately activate autophagy. Hyperactivation of the RAS-MEK pathway, which is common in melanoma, prevents leucine deprivation from inhibiting mTORC1, the main repressor of autophagy under nutrient-rich conditions. In an in vivo tumor xenograft model, the combination of a leucine-free diet and an autophagy inhibitor synergistically suppresses the growth of human melanoma tumors and triggers widespread apoptosis of the cancer cells. Together, our study represents proof of principle that anticancer effects can be obtained with a combination of autophagy inhibition and strategies to deprive tumors of leucine.

INTRODUCTION

It is not completely understood how cancer cells survive and grow in nutrient-limiting conditions, but recent studies support a central role for autophagy (Klionsky, 2007; Kroemer and Levine, 2008; Levine and Kroemer, 2008; White et al., 2010). Autophagy is a lysosome-dependent cellular degradation pathway that is triggered by nutrient deprivation and requires the evolutionarily conserved ATG proteins. These proteins regulate the formation and expansion of a cup-shaped structure, termed the isolation membrane or phagophore, which eventually encloses a portion of cytoplasm in a double-membrane vesicle called an autophagosome. In the late stages of autophagy, the outer membrane of an autophagosome fuses with a lysosome to produce an autophagolysosome, which leads to the degradation of the enclosed cytoplasmic material by lysosomal enzymes and the recycling of metabolites that cannot be synthesized de novo, such as essential amino acids.

The development of the isolation membrane has two major steps: nucleation and elongation. The nucleation step requires the ATG1/ULK1 kinase and the type III phosphoinositide 3-kinase (PIK3C3)/VPS34 kinase complex, and the elongation step the ATG8/LC3- and ATG12-conjugation systems (Levine and Kroemer, 2008; Nakatogawa et al., 2009). A key regulator of the nucleation of the isolation membrane is the mTOR complex 1 (mTORC1) signaling pathway. Under nutrient-rich conditions, mTORC1 suppresses autophagy by inhibiting, in a poorly understood fashion, the ATG1/ULK1 kinase complex (Hosokawa et al., 2009; Jung et al., 2009). The mTORC1 pathway is sensitive to amino acid levels (Hara et al., 1998), and amino acid deprivation activates autophagy (Mortimore and Schworer, 1977; Schworer et al., 1981). How amino acids activate mTORC1 is not well understood, but recent work has revealed an essential role for the amino acid-stimulated translocation of mTORC1 to the lysosomal surface (Sancak et al., 2008; Sancak et al., 2010).

Cells can differ in which amino acids they require for survival, and oncogenic transformation may make them liable to the deficiency of a particular amino acid. For example, human fibroblasts with activated c-*MYC* depend on glutamine (Yuneva et al., 2007), lymphoblastic leukemia cells require tryptophan,

Significance

Melanoma is a highly aggressive cancer for which additional therapies are needed. Autophagy is a cytoprotective mechanism that may help cancer cells survive in nutrient-limiting conditions and is a potential target for anticancer therapies. However, in preclinical tumor models inhibition of autophagy alone has so far had relatively modest antitumor effects. Here, we show that the combination of leucine deprivation and autophagy inhibition induces the caspase-dependent death, in vitro and in vivo, of human melanoma cells driven by the RAS-MEK pathway, but not of nontransformed cells. The results represent a starting point for developing combination therapies involving autophagy inhibitors to target melanoma.

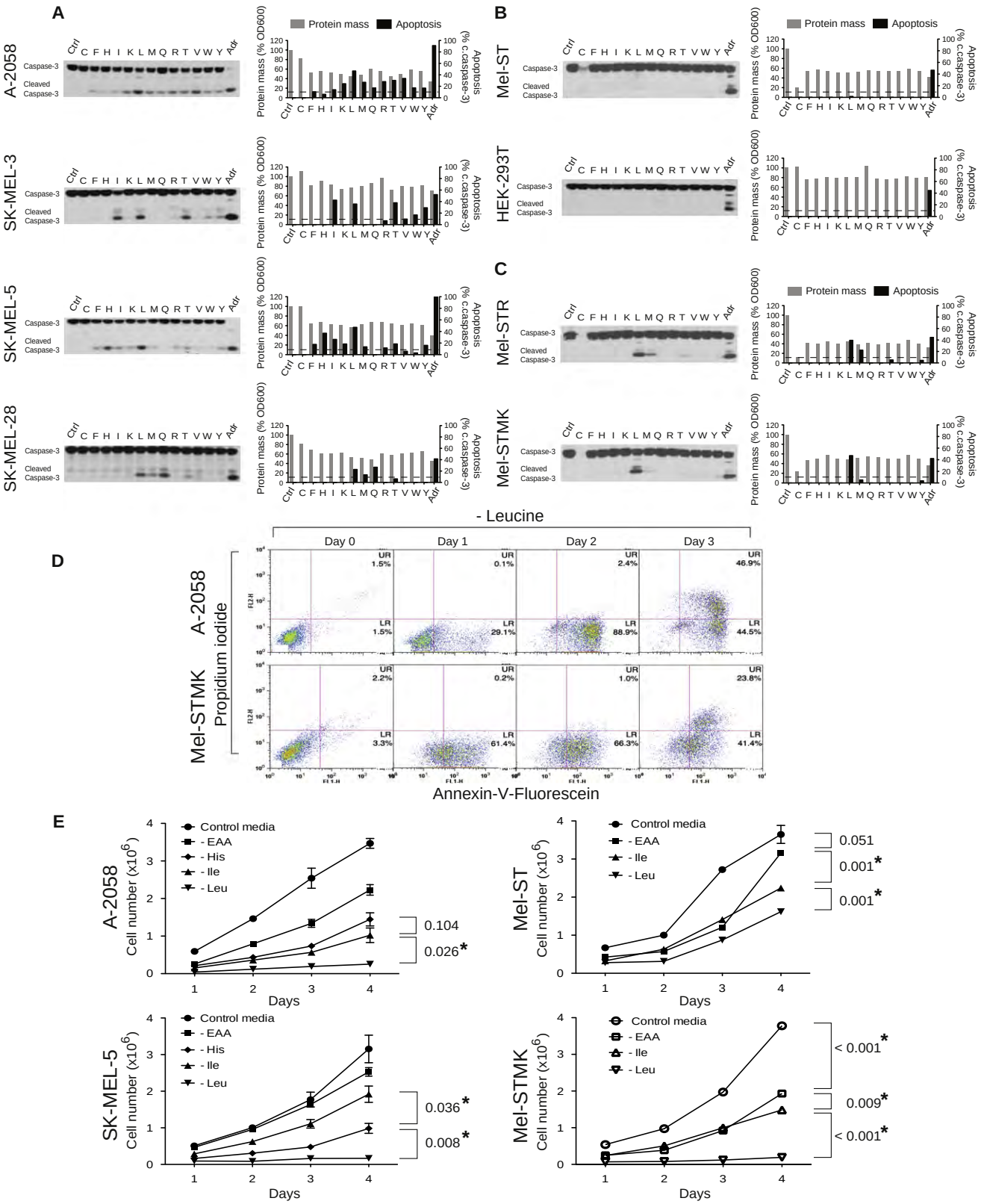

Figure 1. Leucine Deprivation Induces Apoptosis in Human Melanoma Cells

(A–C) Survey of patient-derived melanoma cells (A), immortalized human melanocytes and the nonmelanocyte-derived line (B), and transformed melanocytes (C). Immunoblot analyses for intact and cleaved caspase-3 of indicated cell lines following a 48-hr deprivation for individual essential amino acids. Bar graphs indicate

methionine, and valine (Gong et al., 2000; Kreis et al., 1980; Ohtawa et al., 1998; Woolley et al., 1974), and several types of solid tumor cells require arginine (Scott et al., 2000). However, in most cases the cellular underpinnings behind the particular amino acid requirements of a cancer cell type are largely unknown, making it difficult to exploit such information to implement anticancer therapeutics. Here, we investigated which essential amino acids are necessary for the survival of human melanoma cells and identified an oncogenic-signaling pathway that determines their sensitivity to leucine deprivation.

RESULTS

Leucine Deprivation Triggers the Apoptotic Cell Death of Human Melanoma Cells

We examined the survival of four patient-derived melanoma cell lines (A-2058, SK-MEL-3, SK-MEL-5, SK-MEL-28) as well as the nontransformed but immortalized human Mel-ST melanocyte line (Figures 1A and 1B). We used the cleavage of caspase-3 as a readout for the caspase-dependent apoptosis (Galluzzi et al., 2009; Kroemer et al., 2009; Taylor et al., 2008). Caspase-3 cleaves an array of apoptosis-related proteins, including PARP (see Figure S1A available online).

Cells were deprived, one amino acid at a time, of the 13 amino acids that are considered universally (F, I, K, L, M, T, V, W) or conditionally (C, H, Q, R, Y) essential in humans (Berg et al., 2007; Eagle, 1959). We deprived the melanoma cells of only essential amino acids because the cell lines could have differing capacities to synthesize nonessential amino acids, which would greatly confound the interpretation of the results. Unsurprisingly, upon the deprivation of any single essential amino acid, all cell lines halted proliferating and had a concomitant decrease in cyclin D1 levels and protein mass (Figures 1A and 1B; Figure S1A). In contrast the melanoma cell lines differed in which particular set of amino acids, when individually omitted from the media, trigger the cleavage of caspase-3 (Figure 1A). Interestingly, in all the melanoma lines, the only constant was that leucine deprivation triggered cleavage of caspase-3 and the corresponding caspase-dependent cleavage of PARP (Figure S1A). However, leucine deprivation did not induce caspase-3 cleavage in nontransformed Mel-ST melanocytes or nonmelanocyte-derived HEK293T cells (Figure 1B). The DNA-damaging agent Adriamycin did induce caspase-3 cleavage in these latter two lines, like in the patient-derived melanoma cells (Figures 1A and 1B).

Consistent with the caspase-3 cleavage results, an Annexin-V assay (Galluzzi et al., 2009; Kroemer et al., 2009) revealed, upon leucine deprivation, a time-dependent increase in phosphatidylserine (PS) on the outer leaflet of the plasma membrane of A-2058 cells (Figure 1D). The increase in Annexin-V staining preceded the eventual loss of plasma membrane integrity, which was detected by an increase in propidium iodide staining at the later time points (Figure 1D).

Hyperactivation of the RAS-MEK Pathway Renders Melanocytes Dependent on Leucine for Survival

Because all the melanoma lines in our study have activating mutations in the RAS-MAPK pathway (COSMIC database, Wellcome Trust Sanger Institute) (Bamford et al., 2004), we asked if Ras pathway hyperactivation could confer on melanocytes the capacity to induce caspase-3 activation upon leucine deprivation. Indeed, Mel-STR cells, an engineered melanoma line generated by transforming Mel-ST melanocyte with oncogenic *RAS-G12V* (Gupta et al., 2005), very strongly induced caspase-3 cleavage when deprived of leucine (Figure 1C). Mel-STMK cells, which are Mel-ST cells expressing an activated allele of *MEK1* (*MEK1-Q56P*) (Bottorff et al., 1995; Marks et al., 2008), behaved very similarly to Mel-STR cells in the caspase-3 cleavage assay and to A-2058 cells in the Annexin-V assay (Figures 1C and 1D). These data support the notion that the RAS-MEK pathway is responsible for the sensitivity of melanocytes to leucine deprivation. Consistent with this interpretation, U-0126 (a small molecule inhibitor of MEK1/2) (Davies et al., 2000; Favata et al., 1998), but not KT5720 (an inhibitor of PKA), prevented the cleavage of caspase-3 in Mel-STR cells deprived of leucine (Figure S1B).

Of the several components of the RAS-MAPK pathway found mutated in human cancers, *BRAF* is a critical oncogene in melanoma. Of disease cases, 50%–70% have activating mutations in it (Garnett and Marais, 2004; Gray-Schopfer et al., 2007), and all the patient-derived melanoma lines in our survey carry a mutant allele of *BRAF* (Bamford et al., 2004). Therefore, we asked if expression of oncogenic *BRAF-V600E*, the most common *BRAF* mutant allele found in melanoma (Davies et al., 2002), mimics the effects of *RAS-G12V* and *MEK1-Q56P* in sensitizing melanocytes to apoptosis upon leucine deprivation. Indeed, expression of *BRAF-V600E* as well as *BRAF-Δ3-V600E*, a variant that cannot interact with *CRAF* (Karreth et al., 2009), promoted the cleavage of caspase-3 upon leucine withdrawal (Figure S1C). Expression of wild-type *BRAF* or the *BRAF-Δ3* variant without the V600E mutation did not have the same effects (Figure S1C). Together, these results support a key role for the RAS-BRAF-MEK1 signaling axis in determining the liability of the cells to leucine deprivation.

We also determined the capacity of cells to resume proliferation upon reseeding equal number of cells at ~80% cell confluency into complete media after being deprived of leucine, isoleucine, or all amino acids. Mel-STMK, A-2058, and SK-MEL-5, but not Mel-ST, cells deprived of leucine failed to show proliferation when reseeded (Figure 1E). Just changing the media into complete media without reseeding also showed concordant results with those in which cells were reseeded, which excludes

relative changes in protein mass (a readout for cell growth and proliferation) and percent activation of caspase-3 (ratio of cleaved to full-length caspase-3). Dotted lines indicate 10% activation of caspase-3. Ctrl, control RPMI-1640 media; C-F-H-I-K-L-M-Q-R-T-V-W-Y, deprivation of the indicated single amino acid (single-letter code for amino acid); Adr, Adriamycin at 2 μg/ml.

(D) Annexin-V assay for apoptosis induction. FL1; Annexin-V-Fluorescein, FL2; Propidium Iodide, UR; upper-right quadrant, LR; lower-right quadrant.

(E) Cell survival assay. Cells were deprived of all essential amino acids (−EAA), histidine (−His), isoleucine (−Ile), or leucine (−Leu) for 2 days and reseeded into control RPMI-1640 media, and changes in cell number were measured at indicated time points. Data are represented as mean ± SD, and asterisk (*) indicates values that are significantly different from controls.

See also Figure S1.

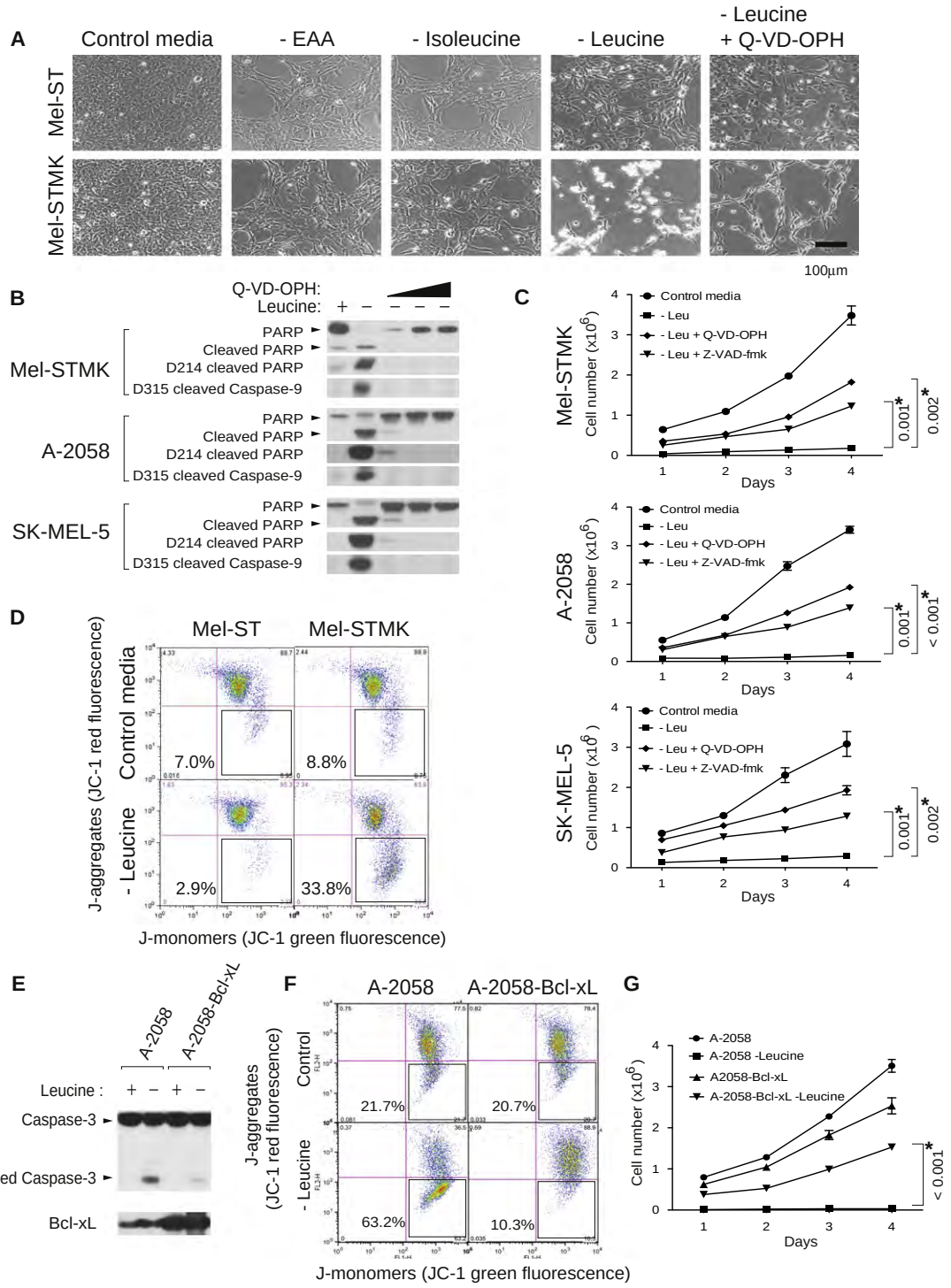

Figure 2. Activation of Caspase Cascade through the Mitochondrial Apoptotic Pathway Is Necessary for Leucine Deprivation-Induced Death

(A) Micrographs showing morphological changes following deprivations of all essential amino acids (−EAA), isoleucine, or leucine in the presence or absence of 20 μM Q-VD-OPH. Scale bar, 100 μm.

(B) Immunoblot analyses showing the dose-dependent inhibitory effect of increasing concentrations of Q-VD-OPH (0, 5, 20, and 100 μM) on caspase-mediated processes.

(C) Cell survival assay. Cells were deprived of leucine (−Leu) for 2 days in the presence or absence of pan-caspase inhibitors, 20 μM Q-VD-OPH, or 100 μM Z-VAD-fmk.

(D) Flow cytometric analyses showing changes in MOMP using JC-1 dye. FL1, green fluorescence of J-monomer; FL2, red fluorescence of J-aggregates.

(E) Immunoblot analyses show the effect of Bcl-xL expression on caspase-3 activation upon leucine deprivation.

the possibility of a change in plating efficiency accounting for the results observed (Figure S1D). In contrast to the results observed with leucine deprivation, all cell lines deprived of isoleucine or all essential amino acids successfully resumed proliferation (Figure 1E). In SK-MEL-5 and A-2058 cells deprived of histidine, the extent of cell survival inversely correlated with that of caspase-3 cleavage (Figures 1A and 1E).

Caspase Activity Regulated by the Mitochondrial Apoptotic Pathway Is Necessary for Cell Death Caused by Leucine Deprivation

To investigate if the apoptotic caspases are required for leucine deprivation to trigger cell death, we used the pan-caspase inhibitors Q-VD-OPH (Caserta et al., 2003; Chauvier et al., 2007) and Z-VAD-fmk (Slee et al., 1996). Q-VD-OPH inhibits a spectrum of caspases with high specificity, whereas Z-VAD-fmk may also inhibit other types of proteases, including calpains and lysosomal cathepsins (Caserta et al., 2003; Chauvier et al., 2007; Kroemer et al., 2009). Q-VD-OPH inhibited the morphological changes characteristic of apoptosing cells, as well the caspase-dependent cleavage of PARP in cells deprived of leucine (Figures 2A and 2B). Critically, Q-VD-OPH and Z-VAD-fmk greatly increased the survival of melanoma cells deprived of leucine (Figure 2C). Because Q-VD-OPH did not completely rescue cells from cell death induced by leucine deprivation, it is possible that other mechanisms in addition to caspase-dependent apoptosis may also contribute to the death of the cells.

The caspase inhibitor experiments also hinted at how leucine deprivation activates the caspase cascade. Not only did Q-VD-OPH inhibit the cleavage of PARP, a known substrate of caspase-3, but also the self-cleavage at Asp-315 of caspase-9. As an initiator caspase of the mitochondrial pathway, caspase-9 regulates executioner caspases, including caspase-3 (Figure 2B). Consistent with this finding, leucine deprivation increased the mitochondrial outer membrane permeabilization (MOMP) of A-2058 and Mel-STMK, but not Mel-ST, cells (Figures 2D and 2F). To determine if the increase in MOMP is necessary for the cell death caused by leucine deprivation, we established A-2058 cells overexpressing Bcl-xL (Figure 2E). In contrast to the parental line, Bcl-xL-overexpressing cells did not increase MOMP or trigger cleavage of caspase-3 when deprived of leucine (Figures 2E and 2F). The decrease in caspase-3 activation in Bcl-xL-overexpressing cells under no leucine conditions directly correlated with an increase in their survival (Figure 2G). These results support an important role for the mitochondrial apoptotic pathway in triggering cell death upon leucine deprivation.

Leucine Deprivation Does Not Activate Autophagy in Melanocyte-Derived Cells with Constitutively Active RAS-MEK Signaling

To investigate why the deprivation of leucine, but not other essential amino acids, is a universal inducer of apoptosis in melanoma cells, we examined the effects of leucine deprivation and RAS signaling on autophagy activity. It is increasingly appreciated that autophagy is critical for cells to survive nutrient deprivation and that amino acids are major regulators of this process (Klionsky, 2007; Levine and Kroemer, 2008).

We used a fluorescent protein-tagged LC3 reporter to quantitate autophagy activity. This dual-color DsRed-LC3-GFP reporter is a modified form of the classical GFP-tagged LC3 reporter (Kabeya et al., 2000), and provides two readouts for autophagy activity: the number of DsRed-LC3 puncta, and a flow cytometric measurement we call the autophagy index. Like previous results obtained using a GFP-LC3 reporter (Kabeya et al., 2000), our reporter showed an increase in the number of DsRed-LC3 puncta upon a phosphate-buffered saline (PBS) incubation or amino acid deprivation (Figure 3). The reporter has GFP separated from the C terminus of LC3 by a recognition site for the autophagic protease, ATG4, and loss of GFP fluorescence can be monitored by flow cytometry (see Figure S2 for details). As expected, deletion of the ATG4 recognition sequence abrogated the sensitivity of the reporter to low nutrient conditions (Figures S2C–S2E). In comparison to the control media condition, deprivation of all amino acids significantly decreased the levels of the full-length DsRed-LC3-GFP reporter as detected by immunoblotting (Figure S2B). To represent results obtained by flow cytometry, we introduced an autophagy index, which normalizes the change in GFP fluorescence to that in DsRed-LC3 fluorescence (see Experimental Procedures and Figure S2). With the autophagy index, potential changes in the synthesis of the reporter following amino acid deprivations can be normalized. Importantly, our autophagy index tightly correlated with the number of DsRed-LC3 puncta, an established measure of autophagy (Figures 3A–3D; Figure S2).

Mel-ST cells displayed a steady-state level of autophagic activity, with an ~40% autophagy index when growing in control media. As expected, the autophagy index increased (to 70%–80%) following deprivation of all amino acids or most single amino acids. In contrast, leucine deprivation failed to significantly activate autophagy (Figures 3A–3C). Immunoblot analyses also showed that deprivation of just leucine did not reduce the level of the full-length DsRed-LC3-GFP reporter, whereas deprivation of all amino acids or just isoleucine did (Figure S2B), indicating a defect in the regulation of autophagy upon leucine deprivation. This difference is unlikely due to a change in proteasomal activity because deprivation of all amino acids, isoleucine, or leucine equally affected the levels of Cyclin D1, a short-lived protein whose turnover is regulated by the ubiquitin-proteasome pathway (Figures S1A and S2B) (Alao, 2007; Diehl et al., 1997). In HEK293T cells the capacity of leucine deprivation to induce autophagy was indistinguishable from that of isoleucine, methionine, or all amino acids (Figure 3D). Thus, in a melanocyte-derived cell line, leucine is exceptional among the amino acids in that its deprivation does not activate autophagy.

It also quickly became apparent that, compared to the parental Mel-ST cells, the Mel-STR and Mel-STMK cells have a significant defect in autophagy upon nutrient withdrawal (Figures 3E and 3F). In these engineered melanoma cells, PBS incubation, complete amino acid deprivation, and isoleucine deprivation activated autophagy to smaller degrees than the same treatments did in parental Mel-ST cells (Figures 3E and

(F) Flow cytometric analyses showing changes in MOMP.
(G) Cell survival assay. Data are represented as mean ± SD, and asterisk (*) indicates values that are significantly different from controls.

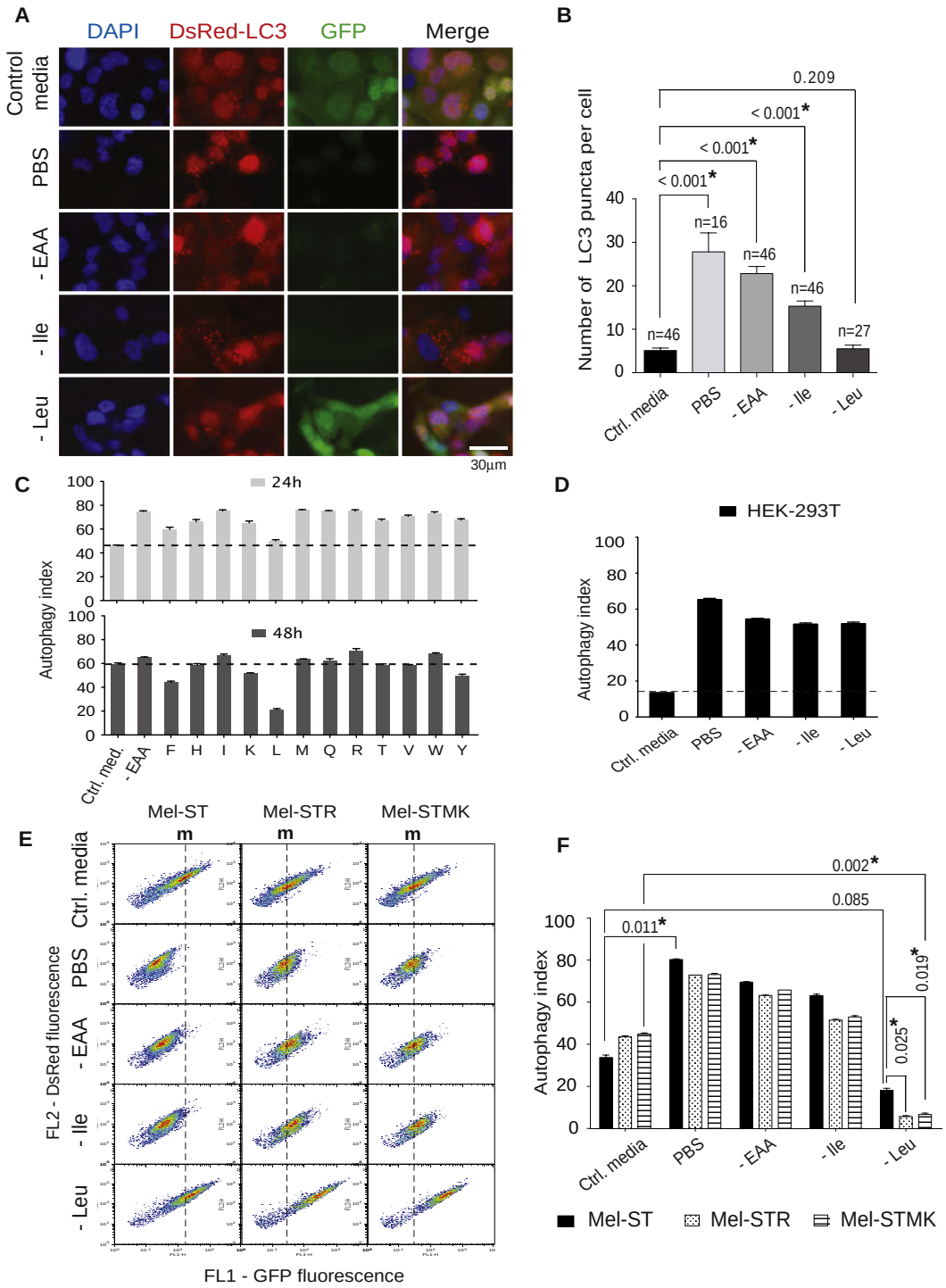

Figure 3. Deprivation of Leucine Does Not Activate Autophagy in Melanoma Cells with Activated Ras-MEK Signaling

(A) Fluorescent micrographs showing autophagy markers. Control, complete RPMI-1640 media control; −EAA, deprivation of all essential amino acids, −Ile, deprivation of isoleucine; −Leu, deprivation of leucine. DAPI, cell nuclei; DsRed-LC3, red fluorescence from DsRed-LC3 puncta; GFP, green fluorescence from the uncleaved DsRed-LC3-GFP reporter; Merge, merged image of DAPI, DsRed, and GFP signals.

(B) Quantitation of DsRed-LC3 puncta. Bar graphs display the mean ± SD of DsRed-LC3 puncta per cell following each type of nutrient starvation. The numbers of cells examined are indicated.

(C) Flow cytometric analyses of autophagic activity. The bar graphs show mean ± SD of autophagy indexes obtained after deprivation of single essential amino acids for 24 or 48 hr (n = 3). Dotted lines indicate the autophagy index of cells incubated in control media.

(D) Autophagy index in HEK293T cells following PBS incubation or indicated amino acid deprivations.

3F). Importantly, upon leucine deprivation, autophagy levels were even more greatly suppressed in the engineered melanoma cells, indicating that leucine deprivation has a profound impact on autophagy in the melanocyte-derived lines with activated RAS-MEK signaling (Figures 3E and 3F).

Constitutive Activation of MEK Renders the mTORC1 Pathway Resistant to Leucine Deprivation

Because mTORC1 suppresses autophagy (Kamada et al., 2000; Noda and Ohsumi, 1998) and amino acids activate mTORC1 (Hara et al., 1998), we asked if inappropriate regulation of mTORC1 might explain why leucine deprivation does not stimulate autophagy in cells with activated RAS-MEK signaling. We monitored mTORC1 activity by measuring the phosphorylation of S6K1 at Thr-389, a site that mTORC1 directly phosphorylates (Burnett et al., 1998). In the same cells we also monitored autophagy activity by examining endogenous LC3-I to LC3-II conversion and the eventual degradation of LC3 (Figure 4A). Deprivation of all amino acids acutely suppressed mTORC1 and activated autophagy in Mel-ST cells. Mel-STMK cells behaved similarly except that these cells maintained some residual mTORC1 activity, even after a long period of essential amino acid deprivation (Figure 4A). However, the more interesting findings were obtained upon leucine deprivation. In contrast to all amino acid deprivation, leucine deprivation was a much poorer inhibitor of mTORC1 and, consequently, inducer of autophagy (Figure 4A). Strikingly, in Mel-STMK cells, leucine deprivation barely inhibited mTORC1 activity. Consistent with the results obtained with the autophagy reporter, leucine deprivation did not cause substantial LC3-I to LC3-II conversion or loss of endogenous LC3 in Mel-STMK cells (Figure 4A).

To further investigate why leucine deprivation fails to suppress mTORC1 signaling in cells that have constitutively active MEK, we examined the amino acid-sensitive translocation of mTORC1 to the lysosomal surface (Figures 4B; see Figure S3 for high-resolution images and quantitation). Recent work indicates that the key event in amino acid signaling to mTORC1 is the amino acid-induced movement of mTORC1 to lysosomal membranes, where it can interact with its activator, Rheb, a small GTPase (Sancak et al., 2010). Constitutive targeting of mTORC1 to the lysosomal surface is sufficient to render the mTORC1 pathway insensitive to amino acid levels (Sancak et al., 2010). As expected, mTORC1 did not colocalize with the lysosomal marker LAMP2 in Mel-ST and Mel-STMK cells deprived of all amino acids for 50 min (Figure 4B). In contrast, in both lines the deprivation of just leucine for 50 min did not greatly affect the colocalization of mTORC1 with lysosomes. However, after depriving the cells of leucine for a longer period of time (4 hr), the two lines diverged in their behavior: in Mel-ST cells, mTORC1 no longer colocalized with lysosomes, whereas in Mel-STMK cells mTORC1 remained lysosome associated (Figure 4B). These findings are consistent with the RAS-MEK pathway impacting mTORC1 upstream of the leucine-sensitive machinery that regulates the subcellular localization of mTORC1.

Inappropriate Activation of the mTORC1 and RAS-MEK Pathways Confers Sensitivity to Apoptosis upon Leucine Deprivation

To determine if the failure to suppress the mTORC1 pathway in melanoma cells with activated RAS-MEK signaling causes cell death, we examined the effects of small molecule inhibitors of the signaling pathways. Mel-STR cells treated with rapamycin or U-0126 not only reactivated autophagy (Figure 5A) but also suppressed caspase-3 activation (Figure 5B). Moreover, across several patient-derived melanoma lines, rapamycin and U-0126 were equally effective at suppressing the cleavage of caspase-3 caused by leucine deprivation (Figures 5C–5E). Importantly, the mTORC1 or MEK inhibitor significantly increased the survival of leucine-deprived melanoma cells (Figures 5F–5H).

Autophagy Inhibition Mimics Activated RAS-MEK Signaling in Conferring Sensitivity to Leucine Deprivation

Upon leucine deprivation, autophagy is more strongly inhibited in Mel-STR than Mel-ST cells (Figures 3E and 3F). To determine if this difference is sufficient to confer on Mel-STR cells the capacity to trigger caspase-3 cleavage upon leucine withdrawal, we asked if the suppression of autophagy sensitizes, like RAS-MEK pathway activation, Mel-ST cells to leucine deprivation. To inhibit autophagy we employed two distinct shRNAs targeting *ATG1* (autophagy related gene 1, also known as *ULK1*) that greatly reduce ATG1 protein expression (Figure 5I). ATG1 is an evolutionarily conserved, Ser/Thr protein kinase that plays an essential role in the early stages of autophagy (Chan et al., 2007; Matsuura et al., 1997). Indeed, the knockdown of *ATG1* was as effective as the expression of *Ras-G12V* or *MEK1-Q56P* in sensitizing Mel-ST cells to leucine deprivation (Figure 5J). Similar results were obtained by knocking down *VPS34*, the class III PI3K (Figure S4A). These results confirm that a particular level of autophagy is necessary for cells to survive essential amino acid deprivation, and suggest that, when deprived of leucine, melanoma cells with activated RAS-MEK fall below this threshold.

A Small Molecule Inhibitor of Autophagy Sensitizes Melanoma Cells to Partial Leucine Deprivation In Vitro

To explore the potential therapeutic implications of the finding that melanoma cells die upon complete leucine deprivation, we needed to identify a way to sensitize melanoma cells to partial leucine deprivation because, to our knowledge, it is currently not possible to completely deprive, in vivo, cancer cells of extracellular leucine. Because all cells have a basal level of autophagy that likely contributes to the recycling of essential amino acids, we reasoned that if we partially suppressed autophagy with a small molecule inhibitor, the melanoma cells might induce apoptosis even if some leucine remained in the extracellular environment.

The feasibility of this idea was investigated using chloroquine, a small molecule inhibitor of autophagy. Chloroquine is

(E) Flow cytometric quantitation of the autophagy activity. "**m**" marks line indicating median fluorescence intensity of FL1 (GFP fluorescence) in cells in the control media.
(F) Bar graphs show mean ± SD of the autophagy index (n = 3), and asterisk (*) indicates values that are significantly different from controls.
See also Figure S2.

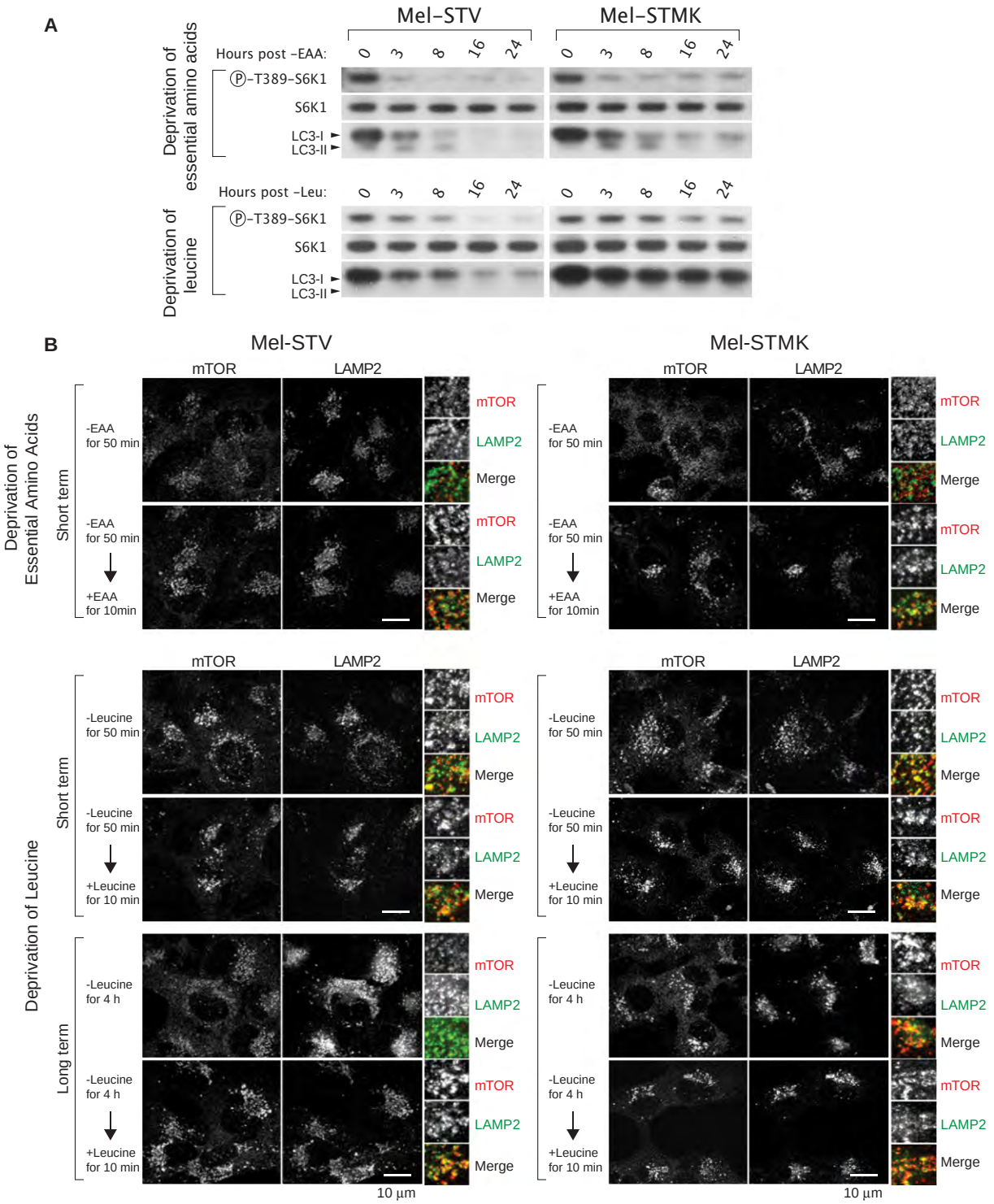

Figure 4. Deregulated Activation of the mTORC1 Pathway by Constitutively Active MEK Correlates with the Inappropriate Localization of mTOR to the Lysosomal Surface

(A) Immunoblot analyses showing time-dependent changes in mTORC1 and autophagy activity in indicated cell types following deprivation for all essential amino acids or leucine.

(B) Immunofluorescence analyses showing mTOR localization upon the deprivation of all essential amino acids (−EAA) or leucine (−Leu). Cells were deprived of indicated amino acids for short (50 min) or long (4 hr) periods of time, and refed with the amino acids for 10 min before processing for coimmunostaining for mTOR (red) and LAMP2 (green), and imaging. In all images, insets show selected fields that were magnified five times and their overlay. Scale bar, 10 μm.

See also Figure S3.

a lysosomotropic drug that inhibits the late stages of the autophagy pathway (Boya et al., 2005) and is currently in many clinical trials as an anticancer agent (http://www.clinicaltrials.gov). As expected, in A-2058 cells, chloroquine increased the levels of p62/SQSTM1/Sequestosome-1 and prevented loss of LC3-II (Figure S5A). By directly binding to LC3, p62 is incorporated onto autophagosomes and degraded (Bjorkoy et al., 2005) so that the level of p62 inversely correlates with autophagic activity (Mizushima et al., 2010).

To answer if chloroquine can induce apoptosis of melanoma cells upon a partial depletion of leucine, we first determined the greatest concentration of extracellular leucine that is still low enough to trigger apoptosis of the melanoma cells in culture (Figures 5K and 5L). We examined a range of leucine concentrations: 380 μM (the concentration of leucine in RPMI media); 120 μM (approximately the plasma leucine concentration of mice fed a normal diet); and 60 μM (approximately the plasma leucine concentration of mice fed an isocaloric, leucine-free synthetic diet; Anthony et al. [2004]). In the absence of chloroquine, only an extracellular leucine concentration of 30 μM or below was able to activate caspase-3 cleavage (Figures 5K and 5L). In contrast, when also treated with a moderate amount of chloroquine, A-2058 and Mel-STR cells triggered caspase-3 activation, even when cultured in media containing 60 μM leucine (Figures 5K and 5L). When completely deprived of leucine and treated with chloroquine, Mel-ST cells did cleave some caspase-3 (Figures 5K), consistent with the results obtained upon the knockdowns of *ATG1* and *VPS34* (Figures 5J; Figure S4A). Interestingly, the combination of chloroquine treatment with the deprivation of all amino acids or just methionine also promoted apoptosis, albeit to a smaller extent than that caused by chloroquine and leucine deprivation (Figure S4B). Most importantly, the combination of media containing 60 μM leucine and chloroquine synergistically decreased the survival of A-2058 cells (Figure 5M). Collectively, these results demonstrate that chloroquine-mediated suppression of autophagy sensitizes melanoma cells to the levels of plasma leucine that can be achieved by feeding animals a leucine-deficient diet (Anthony et al., 2004).

Dietary Leucine Deprivation and Autophagy Inhibition Synergistically Target Melanoma Xenografts In Vivo

To assess the potential of the combination strategy in vivo, A-2058 cells were injected subcutaneously into immunocompromised mice to establish tumor xenografts. When the tumors were ~100 mm^3 in volume, the host animals were fed: (1) a control diet, which consisted of a leucine-free diet supplemented with leucine; (2) an isocaloric leucine-free diet; (3) the control diet and treated with chloroquine; or (4) the leucine-free diet and treated with chloroquine (Figure 6). The amount of chloroquine used was 60 mg/kg body weight, which is similar to the dose employed by others (Amaravadi et al., 2007), and that in our hands caused no obvious toxicity to the animal. Chloroquine treatment did inhibit autophagy in vivo because an immunohistochemical assay revealed the expected increase in p62 levels in the tumors of chloroquine-treated mice (Figure S5B).

On its own, dietary leucine deprivation did not significantly affect tumor size. In contrast the tumors in the mice treated with a combination of dietary leucine deprivation and chloroquine were significantly smaller than those in mice in the control groups (Figures 6A and 6B). The inability of a leucine-free diet to reduce tumor growth on its own likely reflects the fact that a leucine-free diet decreases plasma leucine levels from ~133 to ~76 μM (Anthony et al., 2004), which our in vitro results show is not low enough on its own to induce significant death of melanoma cells (Figures 5L and 5M).

To determine if the synergistic effects on tumor size of dietary leucine deprivation and chloroquine treatment reflect the increased death of the melanoma cells, we stained the tumor sections with an in situ TUNEL assay (Figures 6C–6E). Analogous to the results in culture (Figures 5L and 5M), the combination treatment had a strong pro-death effect in vivo, so that extensive TUNEL-positive staining was observed in nearly all areas of the tumors (Figure 6C). Only cells in the outer shell of the tumors and in the immediate vicinity to the microcapillaries appeared to be spared (Figures 6D and 6E). This pattern of survival likely reflects that melanoma cells in cuffs surrounding the tumor vessels have access to greater amounts of leucine than cells farther away from the blood supply. Dietary leucine deprivation alone showed a significant, but less effective, induction of death of the melanoma cells in vivo, and chloroquine treatment alone promoted the death of the cells in only a few isolated areas of the tumor (Figures 6C and 6D).

Immunohistochemical analyses of the tumors with a site-specific (D175) cleaved caspase-3 antibody revealed that, like in vitro, partial leucine deprivation in combination with chloroquine treatment caused caspase-3 cleavage in vivo (Figures 7A and 7B). The cleaved caspase-3 signal was highest at the border between the viable cuffs surrounding capillaries and the large areas of strongly TUNEL-positive dead cells (Figure 7B). This pattern suggests that caspases likely initiate cell death, but as the apoptotic program progresses, the amount of cleaved caspase-3 drops, whereas the DNA fragments in the apoptotic bodies persist.

Most of the live cells within the tumors stained for the human-specific melanocyte marker, Melan-A, except for the murine endothelial cells of the capillaries and a thin layer of cells on the tumor surfaces (Figures 7A; Figure S5C). These Melan-A-negative murine cells did not stain for cleaved caspase-3, indicating that the combination of dietary leucine deprivation and chloroquine treatment did not affect the nontransformed cells of the tumors (Figure S5C).

DISCUSSION

There is mounting interest in the roles nutrient-sensing and metabolic pathways play in tumorigenesis and in the potential of these pathways to harbor targets for cancer therapies. Autophagy, for example, is increasingly recognized as important for eukaryotic cells and organisms to survive periods of nutrient withdrawal (Boya et al., 2005; Degenhardt et al., 2006; Kuma et al., 2004), and small molecule inhibitors of autophagy, such as chloroquine, are of interest for anticancer uses (reviewed in Rubinsztein et al., 2007).

In examining how cancer cells respond to deprivation of single essential amino acids, we made the observation that the deprivation of leucine, but not other essential amino acids, induces apoptosis in all the human melanoma lines studied. Substantial

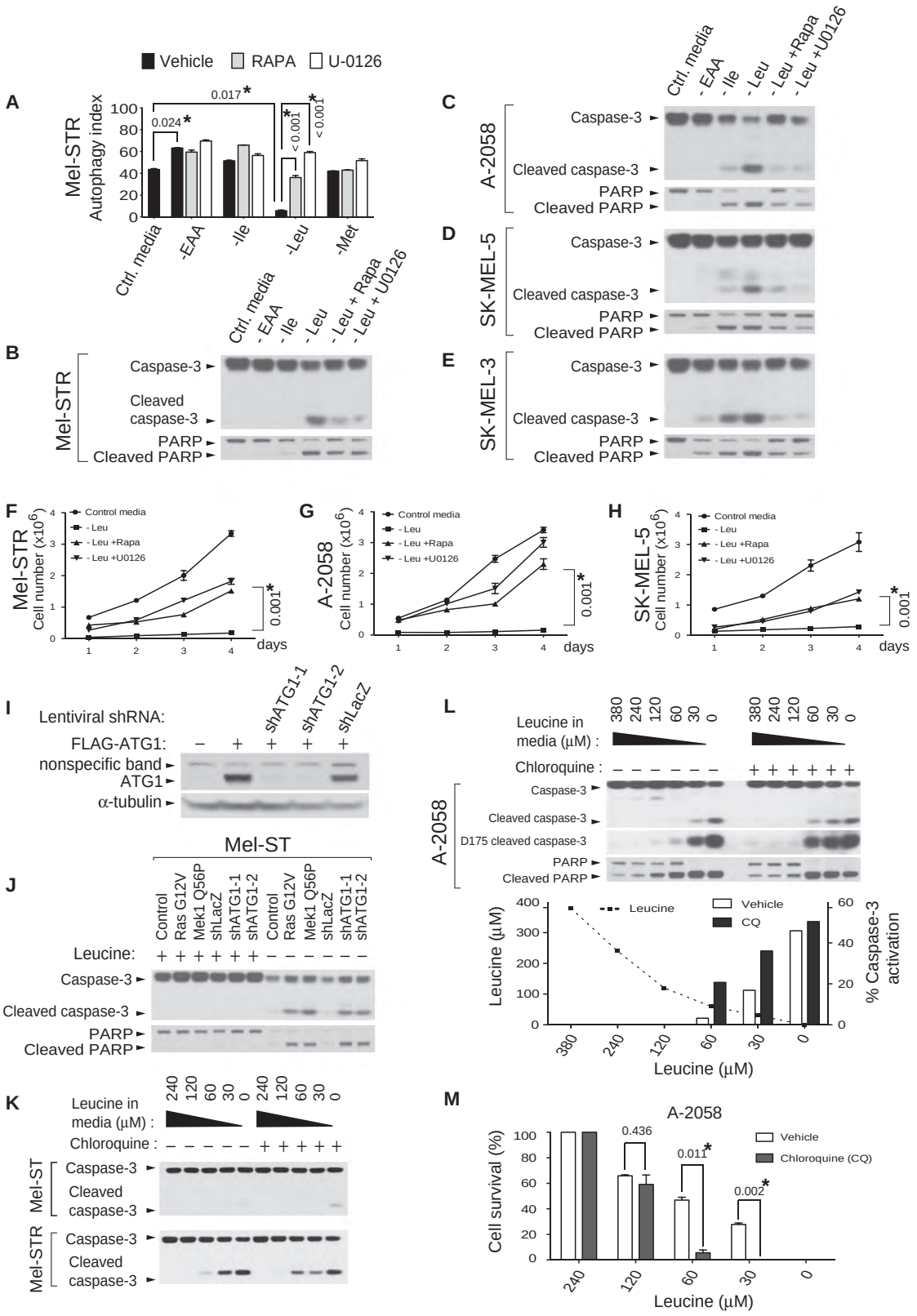

Figure 5. The Inhibition of Autophagy Synergizes with Low Leucine Concentrations in Inducing Apoptosis in Melanoma Cells

(A) Bar graphs displaying the autophagy index in the presence or absence of rapamycin (RAPA) or U-0126.

(B–E) Immunoblot analyses for cleavage and activation of caspase-3 and cleavage of PARP.

evidence suggests that leucine deprivation triggers apoptosis because, unlike in other cell types, it does not inhibit the mTORC1 pathway and, thus, does not activate autophagy. In fact the mTORC1 inhibitor rapamycin—normally thought of as an anticancer agent—reactivates autophagy in leucine-deprived melanoma cells and promotes their survival. It is odd that the mTORC1 pathway is so resistant to leucine withdrawal in melanoma cells because this amino acid is a canonical activator of the pathway, and its deprivation inhibits mTORC1 signaling in a wide variety of normal and transformed cells (Guertin and Sabatini, 2007). Amino acid signaling to mTORC1 is a subject of intense study, but the amino acid-sensing mechanism remains a mystery. It is possible that once the mechanism is understood, it will be found to be different in melanoma cells than in other cell types. The hyperactivation of the RAS-MAPK pathway that is a common occurrence in melanoma cells clearly contributes to the insensitivity of mTORC1 to leucine deprivation. So far, our work suggests that RAS-MEK signaling perturbs the normally leucine-sensitive localization of mTORC1 to the lysosomal surface. Kinases that are part of the MAPK pathway, such ERK and p90 RSK1, phosphorylate and repress the function of TSC2, a tumor suppressor that is a negative regulator of mTORC1 (Inoki et al., 2003; Ma et al., 2005; Roux et al., 2004; Tee et al., 2003). However, TSC2 does not appear to play a major role in amino acid signaling to mTORC1 (Byfield et al., 2005; Nobukuni et al., 2005; Smith et al., 2005), so it is likely that the MAPK pathway affects the leucine sensitivity of mTORC1 in melanoma cells through TSC2-independent mechanisms. Interestingly, the RAS pathway negatively regulates autophagy in budding yeast and in flies, but it is unclear if the TORC1 pathway is involved in autophagy repression in these organisms (Berry and Baehrecke, 2007; Budovskaya et al., 2004).

Autophagy inhibition alone did not trigger apoptosis in melanoma cells in vitro, and chloroquine treatment failed to show antitumor effects in mice fed a control diet in vivo. This is likely because most cells inside tumors have access to more than the minimal level of extracellular leucine required for survival. On the other hand, in animals fed a leucine-free diet, the inhibition of autophagy likely results in little leucine being liberated from internal sources so that cellular levels of this essential amino acid may fall below the threshold needed for survival. To implement this combination strategy in the current study, we used chloroquine to inhibit autophagy. However, one caveat of chloroquine is that as a lysosomotropic compound it may not only inhibit the autophagic process but also non-autophagy related functions of lysosomes. Inhibitors to proteins essential for autophagy, such as the protease, ATG4, and the kinases, ATG1/ULK1 and VPS34, are likely to be developed in the future. Using RNAi, we have shown that ATG1 and VPS34 are important for determining the sensitivity of melanoma cells to leucine deprivation.

To deprive the melanoma xenografts of leucine, we fed mice a leucine-free diet that is known to reduce the plasma-leucine concentration in rodents and humans without greatly affecting blood insulin levels (Anthony et al., 2004; Guo and Cavener, 2007; Hambraeus et al., 1976). A leucine-free diet is unlikely to be the ideal approach to deprive tumors of leucine in a clinical setting. In the future it may be possible to deliver, intravenously, enzymes that specifically degrade leucine or small molecule inhibitors of leucine uptake. As a model for the former, asparaginase (L-asparagine amidohydrolase) is an FDA-approved enzyme that hydrolyzes asparagine to aspartic acid and is a successful therapy for acute lymphocytic leukemia (ALL). Enzymes in the leucine catabolic pathway, such as branched chain aminotransferase (BCAT) (Berg et al., 2007), could be used in an analogous way if their substrate specificity could be engineered to be limited to leucine (Conway et al., 2003; Onuffer and Kirsch, 1995). There appear to be many transporters that mediate leucine uptake as well (Broer, 2008), and some of the better-characterized ones, such as LAT1, may be druggable. Alternatively, the easiest strategy to obtain synergistic effects with autophagy inhibition and nutrient deprivation on tumor cell survival may be to coadminister a drug that can deprive tumor cells of many nutrients, such as an angiogenesis blocker, along with a specific autophagy inhibitor. Our finding that in the presence of an autophagy inhibitor, melanoma cells trigger the activation of caspase-3 when deprived not only of leucine but also of all essential amino acids, supports the feasibility of this idea.

EXPERIMENTAL PROCEDURES

Materials

Reagents were obtained from the following sources: Adriamycin, Rapamycin, and U-0126 from Calbiochem and LC Laboratories; cell culture grade pure amino acids, glucose, and chloroquine from Sigma; JC-1 dye from Invitrogen; immunohistochemistry kits from Vector Laboratories and Dako; cDNA clones for MEK1, ATG1, and LC3 from Open Biosystems; cDNA clone for H-RAS-G12V from the Laboratory of Dr. Robert Weinberg (Whitehead Institute); cDNA clones for BRAF-WT, BRAF-Δ3, BRAF-V600E, and BRAF-Δ3-V600E from Dr. David Tuveson (Cancer Research UK) (Karreth et al., 2009); lentiviral shRNA constructs from The RNAi Consortium (TRC) (Broad Institute); antibodies to SQSTM1/p62 from American Research Products; antibodies to ATG1/ULK1, Bcl-xL, caspase-3, cyclin D1, LC3, Melan-A, PARP, phospho-T202/Y204-ERK, ERK, phopho-T389 S6K1, S6K1, VPS34, as well as HRP-conjugated anti-mouse, anti-rabbit secondary antibodies from Santa Cruz Biotechnology Inc., and Cell Signaling Technology.

Cell Lines and Tissue Culture

Cell lines were obtained from the American Type Culture Collection. Cell culture media powder and sera were purchased from the following sources: Dulbecco's

(F–H) Cell survival assay.
(I) Immunoblot analyses showing validation of shRNA-mediated knockdowns of ATG1.
(J) Knockdown of *ATG1* mimics effects of expressing *Ras-G12V* or *MEK1-Q56P* in sensitizing Mel-ST cells to caspase-3 activation upon leucine deprivation.
(K) Immunoblots show cleavage of caspase-3 and PARP in cells incubated with decreasing amounts of leucine in the presence or absence of chloroquine.
(L) Chloroquine (CQ) sensitizes A-2058 melanoma cells to partial leucine deprivation. Immunoblots show and graph quantitates activation of caspase-3 in relation to leucine concentration in media with or without chloroquine.
(M) Percent survival of A-2058 cells cultured under indicated conditions for 2 days. Data are represented as mean ± SD, and asterisk (*) indicates values that are significantly different from controls.
See also Figure S4.

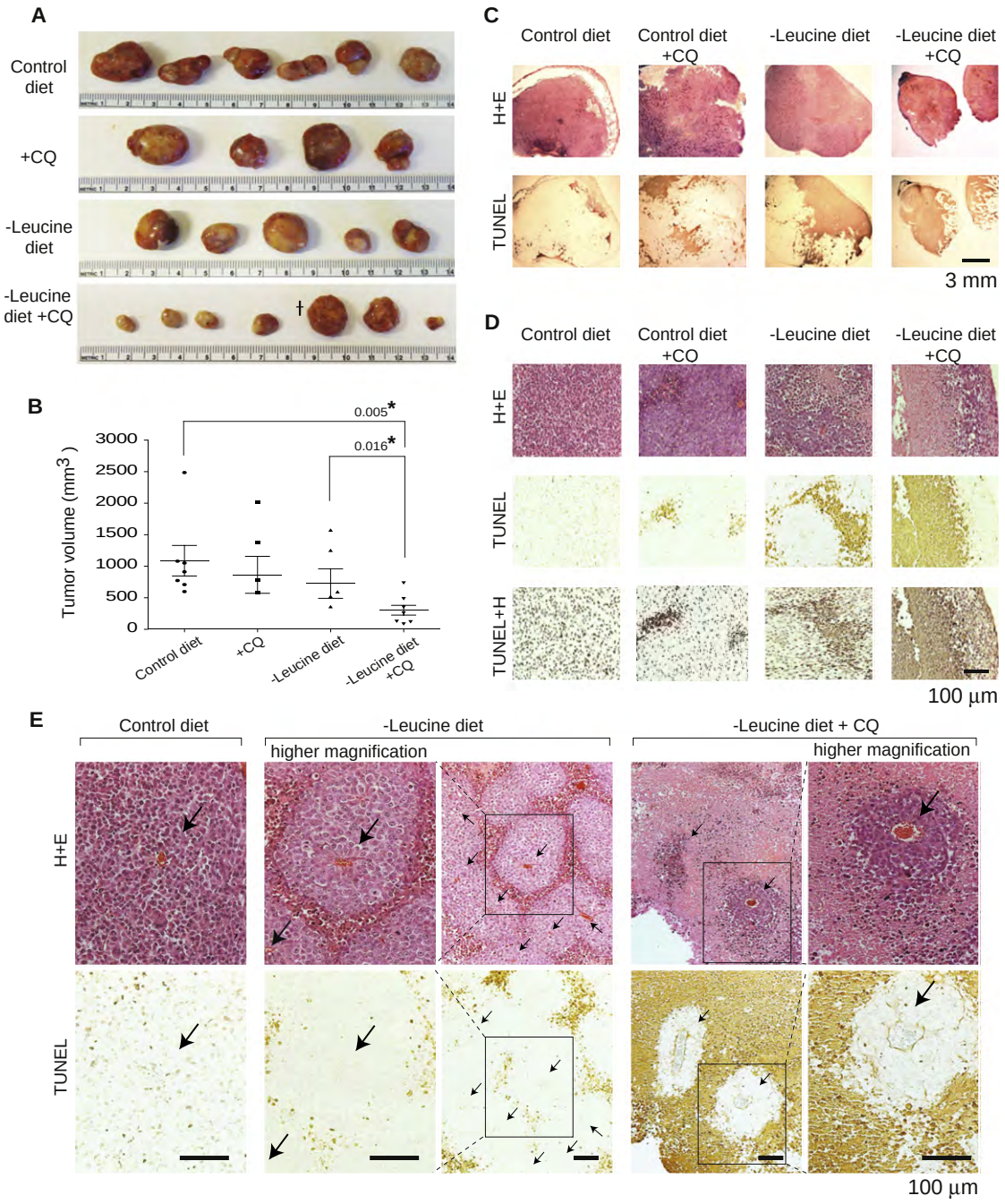

Figure 6. Synergistic Inhibition of Melanoma Tumor Growth in Mice Deprived of Dietary Leucine and Treated with an Autophagy Inhibitor

(A) Photographs of excised tumor xenografts following feeding for 14 days with an isocaloric control diet with added leucine (Control diet), control diet plus chloroquine (+CQ), leucine-free diet (−Leucine diet), or leucine-free diet plus chloroquine (−Leucine diet +CQ).

(B) Column scatter dot graph displays the mean ± SEM volume of the tumors. Asterisk (*) indicates volumes that are significantly different from controls. Note that the tumor that is third from the right in the −Leucine diet +CQ group had a flattened disc shape rather than the spherical shape of the large tumors obtained in the other groups. Thus, it appears deceptively large in the photograph.

(C) In situ TUNEL assay. H^+E, representative micrograph images of tumor sections stained with hematoxylin and eosin; TUNEL, representative images of tumor sections processed in the TUNEL assay; TUNEL+H, representative images of TUNEL results counterstained with hematoxylin. Scale bar, 3 mm.

(D) Representative high-magnification micrographs of tumor sections showing TUNEL-positive, apoptotic regions. Scale bar, 100 μm.

(E) Apoptosis of the melanoma cells inside tumors correlates with the distance from tumor capillaries, and inhibition of autophagy significantly shrinks the viable cuffs surrounding tumor capillaries. Micrographs show corresponding high and low-magnification images of tumor sections with capillaries indicated (with arrows) and TUNEL-positive, apoptotic regions. Scale bar, 100 μm.

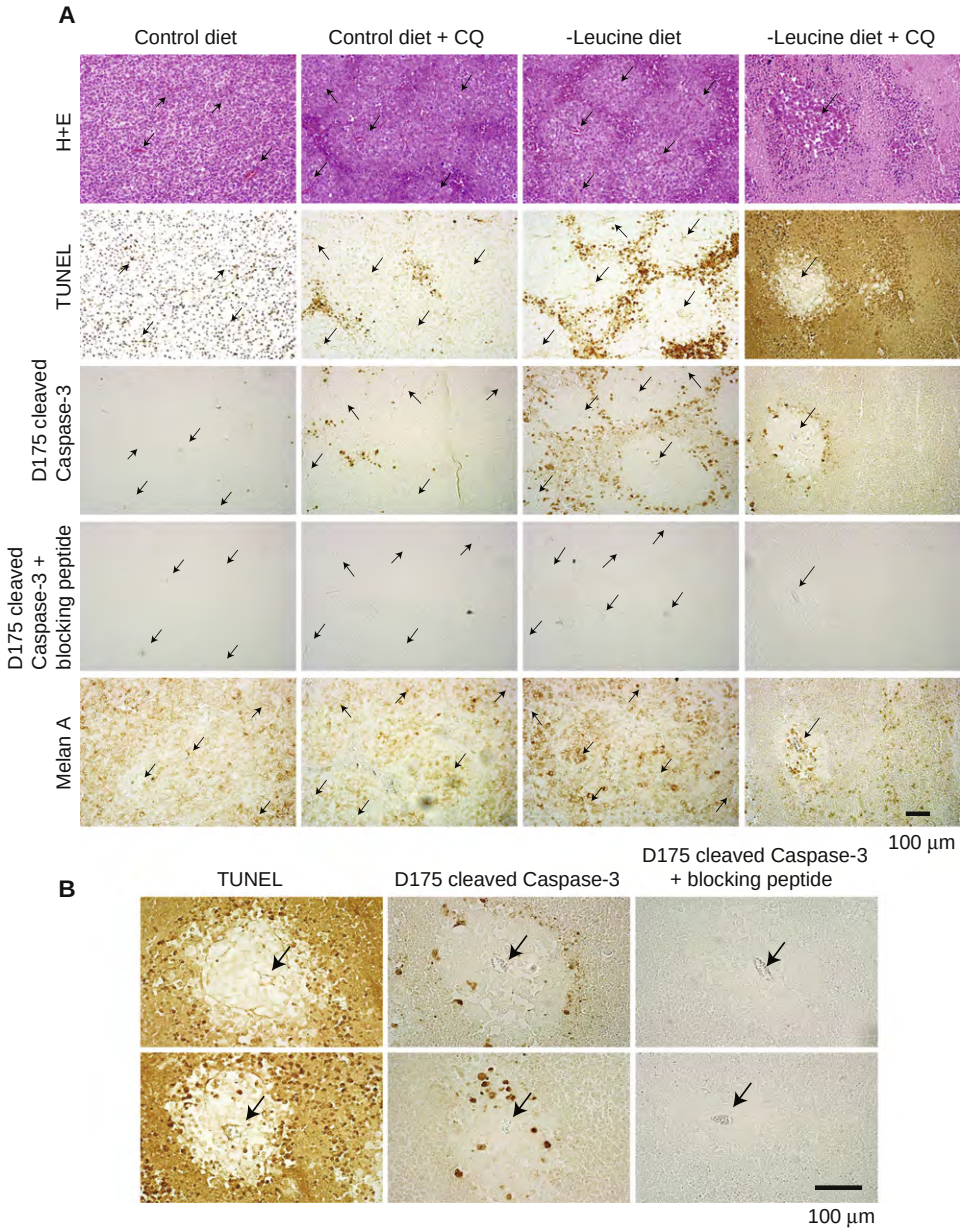

Figure 7. Combination of Dietary Leucine Deprivation and Autophagy Inhibition Induces Activation of Caspase-3 in Melanoma Tumors In Vivo

(A) Immunohistochemical analyses showing caspase-3 cleavage in vivo. H^+E, images of tumor sections stained with hematoxylin and eosin where capillaries are denoted with arrows; TUNEL, images of tumor sections processed for the TUNEL assay; D175 cleaved Caspase-3, images of tumor sections stained for active caspase-3 with the anti-Asp-175 site-specific cleaved caspase-3 antibody; D175 cleaved Caspase-3 + blocking peptide, images of tumor sections stained for active caspase-3 with the anti-Asp-175 site-specific cleaved caspase-3 antibody that was preincubated with the epitope-blocking peptide; Melan A, images of tumor sections stained with anti-Melan A, a human melanocyte-specific marker, antibodies. Scale bar, 100 μm.

(B) Representative high-magnification micrographs of tumor tissues showing geographic correlation between the TUNEL-positive signals and the D175 cleaved caspase-3 positive signals where capillaries are denoted with arrows. Scale bar, 100 μm.

See also Figure S5.

MEM (DMEM), RPMI-1640, fetal bovine serum (FBS), dialyzed fetal bovine serum (dFBS), heat-inactivated fetal bovine serum (IFS) from Invitrogen; amino acid-free, glucose-free RPMI-1640 from US Biological, Inc. Cells were cultured in the following media: HEK293T cells in DMEM with 10% IFS; A-2058, SK-MEL-3, SK-MEL-5, SK-MEL-28, Mel-ST, and Mel-ST-derivatives in DMEM with 10% FBS. For survival assay we treated cells with 20 μM Q-VD-OPH or 100 μM Z-VAD-fmk when depriving cells of essential amino acids.

Essential Amino Acid-Deprivation Protocol

To produce cell culture media deficient of single essential amino acids, we reconstituted the amino acid-free, glucose-free RPMI-1640 media by supplementing it with glucose and individual amino acids except the amino acid to be omitted. Cells were plated in the complete culture media 1 day prior to the amino acid-deprivation experiments so that the plated cells reached ~80% of confluency at the day of experiment. To deprive cells of single amino

acids, we replaced culture media twice with target amino acid-free RPMI-1640 media and incubated cells until sampling for analysis.

Autophagy Assay Using the DsRed-LC3-GFP Reporter

To develop a dual-color autophagy reporter, we inserted rat LC3 (also known as ATG8) cDNA in between the cDNAs for DsRed and EGFP so that the DsRed protein is fused with N terminus of LC3 protein and C terminus of the protein is connected to EGFP. When indicated, we introduced a deletion of five amino acids (TALAV) at the ATG4-recognition site near C terminus of LC3 to make a chimeric protein resistant to ATG4-mediated cleavage. To produce stable cell lines continuously reporting autophagy activity, recombinant retroviruses expressing the DsRed-LC3-GFP reporter were generated and used to infect target cells. The autophagy index is a measure of the relative change in median fluorescence intensity of GFP to that of DsRed and was calculated with the formula: autophagy index = 100 − (100 × (FL1/FL2)), where FL1 is Fluorescence 1 (the median fluorescence intensity of GFP fluorescence), and FL2 is Fluorescence 2 (the median fluorescence intensity of DsRed fluorescence). See Figure S2 for details on the development and validation of the autophagy reporter.

Flow Cytometric Analyses

Analysis of apoptosis induction using Annexin-V-fluorescein was carried out according to the assay kit manufacturer's instructions (Roche). Briefly, cultured cells were harvested and washed once in PBS, then incubated with the Ready-to-Use solution of Annexin-V-Fluorescein in a HEPES buffer containing Propidium Iodide. Samples were analyzed using a flow cytometer. Changes in MOMP were measured using the MOMP-sensitive cationic JC-1 dye according to the supplier's instruction (Roche). JC-1 exhibits membrane potential-dependent accumulation in mitochondria, indicated by a fluorescence emission shift from green (monomeric form in cytosol) to red (aggregates in mitochondria). Briefly, cultured cells were stained with 2 μM JC-1 for 15 min at the growth condition, washed with PBS, and analyzed using flow cytometry. When necessary, the concentration of JC-1 was optimized for different cell types using oligomycin as a control.

Immunofluorescence Assay

Mel-ST and Mel-STMK cells were plated on fibronectin-coated glass coverslips in 12-well tissue culture plates. Twenty-four hours later, the slides were rinsed with PBS once and fixed for 15 min with 4% paraformaldehyde in PBS warmed to 37°C. The slides were rinsed twice with PBS, and cells were permeabilized with 0.05% Triton X-100 in PBS for 5 min. After rinsing twice with PBS, the slides were incubated with primary antibodies for 2 hr at room temperature, rinsed four times with PBS, and incubated with secondary antibodies (1:400 in 5% normal donkey serum) for 1 hr at room temperature in the dark, washed four times with PBS. Slides were finally mounted on glass coverslips using VECTASHIELD (Vector Laboratories), and images were collected and analyzed on a PerkinElmer spinning disk confocal microscopy system.

Human Xenograft Tumor Model and Dietary Leucine Deprivation

Immunodeficient mice (NCR nude, nu/nu; Taconic Laboratories) were maintained in a pathogen-free facility and were given autoclaved food and water ad libitum, if not otherwise specified. A-2058 melanoma cells were xenografted into 6-week-old immunodeficient mice. Briefly, 1×10^6 melanoma cells were resuspended in 200 μl of media and injected subcutaneously in the upper flank region of mice that had been anesthetized with isoflurane. Tumors were allowed to grow to ~100 mm^3 in size, and the mice were then initiated on the dietary leucine restriction using an isocaloric leucine-free, synthetic diet alone or along with chloroquine treatment. Both the isocaloric control diet with added leucine and the leucine-free synthetic diet were obtained from Research Diet, Inc. Based on a series of preliminary experiments, chloroquine was injected intraperitoneally at 60 mg/kg body weight two times per week. Tumor volumes were estimated with the formula: volume = (2a × b)/2, where a = shortest and b = longest tumor lengths, respectively, in millimeters. When necessary, animals were sacrificed, and tumors were harvested and analyzed using standard histology and immunohistochemistry methods. Animal research protocols were approved by the MIT Committee on Animal Care, and all experiments were performed according to the official guidelines of the MIT Committee on Animal Care and the American Association of Laboratory Animal Care.

Lentiviral shRNA-Mediated RNAi

For the gene knockdown experiments, we obtained lentiviral shRNA constructs from TRC at the Broad Institute and produced recombinant lentiviruses using a transient transfection protocol. Briefly, we transfected HEK293T cells with the lentiviral shRNA plasmids and the packaging plasmids (pdeltaVPR and pVSVG) according to TRC standard protocols and used lentiviral supernatants to infect target cells (Moffat et al., 2006).

Statistical Analyses

Experimental results were analyzed with a Student's t test and graphed using Prism software (GraphPad Software, Inc.). In vitro data are expressed as mean ± SD and in vivo data as mean ± SEM. A p value <0.05 was considered statistically significant.

SUPPLEMENTAL INFORMATION

Supplemental Information includes Supplemental Experimental Procedures and five figures and can be found with this article online at doi:10.1016/j.ccr.2011.03.012.

ACKNOWLEDGMENTS

This work was supported by grants from the NIH (R01 CA103866 and CA1299105) to D.M.S., as well as postdoctoral fellowships from the U.S. Department of Defense (W81XWH-04-1-0496) to J.H.S., from the Jane Coffin Childs Memorial Fund for Medical Research to R.Z., and from the American Brain Tumor Association to D.K. We thank members of the Sabatini lab for helpful suggestions, Dr. Robert Weinberg (Whitehead Institute) for reagents and experimental protocols, Dr. David Tuveson (Cancer Research UK) for reagents, and the US Biological, Inc., Whitehead Institute FACS facility, MIT Division of Comparative Medicine, and Histology core facility at the MIT Koch Institute for Integrative Cancer Research for experimental advice.

Received: January 20, 2010
Revised: August 10, 2010
Accepted: March 15, 2011
Published: May 16, 2011

REFERENCES

Alao, J.P. (2007). The regulation of cyclin D1 degradation: roles in cancer development and the potential for therapeutic invention. Mol. Cancer *6*, 24.

Amaravadi, R.K., Yu, D., Lum, J.J., Bui, T., Christophorou, M.A., Evan, G.I., Thomas-Tikhonenko, A., and Thompson, C.B. (2007). Autophagy inhibition enhances therapy-induced apoptosis in a Myc-induced model of lymphoma. J. Clin. Invest. *117*, 326–336.

Anthony, T.G., McDaniel, B.J., Byerley, R.L., McGrath, B.C., Cavener, D.R., McNurlan, M.A., and Wek, R.C. (2004). Preservation of liver protein synthesis during dietary leucine deprivation occurs at the expense of skeletal muscle mass in mice deleted for eIF2 kinase GCN2. J. Biol. Chem. *279*, 36553–36561.

Bamford, S., Dawson, E., Forbes, S., Clements, J., Pettett, R., Dogan, A., Flanagan, A., Teague, J., Futreal, P.A., Stratton, M.R., and Wooster, R. (2004). The COSMIC (Catalogue of Somatic Mutations in Cancer) database and website. Br. J. Cancer *91*, 355–358.

Berg, J.M., Tymoczko, J.L., and Stryer, L. (2007). Biochemistry, Sixth Edition (New York: W.H.Freeman and Company).

Berry, D.L., and Baehrecke, E.H. (2007). Growth arrest and autophagy are required for salivary gland cell degradation in *Drosophila*. Cell *131*, 1137–1148.

Bjorkoy, G., Lamark, T., Brech, A., Outzen, H., Perander, M., Overvatn, A., Stenmark, H., and Johansen, T. (2005). p62/SQSTM1 forms protein aggregates degraded by autophagy and has a protective effect on huntingtin-induced cell death. J. Cell Biol. *171*, 603–614.

Bottorff, D., Stang, S., Agellon, S., and Stone, J.C. (1995). RAS signalling is abnormal in a c-raf1 MEK1 double mutant. Mol. Cell. Biol. *15*, 5113–5122.

Boya, P., Gonzalez-Polo, R.A., Casares, N., Perfettini, J.L., Dessen, P., Larochette, N., Metivier, D., Meley, D., Souquere, S., Yoshimori, T., et al. (2005). Inhibition of macroautophagy triggers apoptosis. Mol. Cell. Biol. *25*, 1025–1040.

Broer, S. (2008). Amino acid transport across mammalian intestinal and renal epithelia. Physiol. Rev. *88*, 249–286.

Budovskaya, Y.V., Stephan, J.S., Reggiori, F., Klionsky, D.J., and Herman, P.K. (2004). The Ras/cAMP-dependent protein kinase signaling pathway regulates an early step of the autophagy process in Saccharomyces cerevisiae. J. Biol. Chem. *279*, 20663–20671.

Burnett, P.E., Barrow, R.K., Cohen, N.A., Snyder, S.H., and Sabatini, D.M. (1998). RAFT1 phosphorylation of the translational regulators p70 S6 kinase and 4E-BP1. Proc. Natl. Acad. Sci. USA *95*, 1432–1437.

Byfield, M.P., Murray, J.T., and Backer, J.M. (2005). hVps34 is a nutrient-regulated lipid kinase required for activation of p70 S6 kinase. J. Biol. Chem. *280*, 33076–33082.

Caserta, T.M., Smith, A.N., Gultice, A.D., Reedy, M.A., and Brown, T.L. (2003). Q-VD-OPh, a broad spectrum caspase inhibitor with potent antiapoptotic properties. Apoptosis *8*, 345–352.

Chan, E.Y., Kir, S., and Tooze, S.A. (2007). siRNA screening of the kinome identifies ULK1 as a multidomain modulator of autophagy. J. Biol. Chem. *282*, 25464–25474.

Chauvier, D., Ankri, S., Charriaut-Marlangue, C., Casimir, R., and Jacotot, E. (2007). Broad-spectrum caspase inhibitors: from myth to reality? Cell Death Differ. *14*, 387–391.

Conway, M.E., Yennawar, N., Wallin, R., Poole, L.B., and Hutson, S.M. (2003). Human mitochondrial branched chain aminotransferase: structural basis for substrate specificity and role of redox active cysteines. Biochim. Biophys. Acta *1647*, 61–65.

Davies, H., Bignell, G.R., Cox, C., Stephens, P., Edkins, S., Clegg, S., Teague, J., Woffendin, H., Garnett, M.J., Bottomley, W., et al. (2002). Mutations of the BRAF gene in human cancer. Nature *417*, 949–954.

Davies, S.P., Reddy, H., Caivano, M., and Cohen, P. (2000). Specificity and mechanism of action of some commonly used protein kinase inhibitors. Biochem. J. *351*, 95–105.

Degenhardt, K., Mathew, R., Beaudoin, B., Bray, K., Anderson, D., Chen, G., Mukherjee, C., Shi, Y., Gelinas, C., Fan, Y., et al. (2006). Autophagy promotes tumor cell survival and restricts necrosis, inflammation, and tumorigenesis. Cancer Cell *10*, 51–64.

Diehl, J.A., Zindy, F., and Sherr, C.J. (1997). Inhibition of cyclin D1 phosphorylation on threonine-286 prevents its rapid degradation via the ubiquitin-proteasome pathway. Genes Dev. *11*, 957–972.

Eagle, H. (1959). Amino acid metabolism in mammalian cell cultures. Science *130*, 432–437.

Favata, M.F., Horiuchi, K.Y., Manos, E.J., Daulerio, A.J., Stradley, D.A., Feeser, W.S., Van Dyk, D.E., Pitts, W.J., Earl, R.A., Hobbs, F., et al. (1998). Identification of a novel inhibitor of mitogen-activated protein kinase kinase. J. Biol. Chem. *273*, 18623–18632.

Galluzzi, L., Aaronson, S.A., Abrams, J., Alnemri, E.S., Andrews, D.W., Baehrecke, E.H., Bazan, N.G., Blagosklonny, M.V., Blomgren, K., Borner, C., et al. (2009). Guidelines for the use and interpretation of assays for monitoring cell death in higher eukaryotes. Cell Death Differ. *16*, 1093–1107.

Garnett, M.J., and Marais, R. (2004). Guilty as charged: B-RAF is a human oncogene. Cancer Cell *6*, 313–319.

Gong, H., Zolzer, F., von Recklinghausen, G., Havers, W., and Schweigerer, L. (2000). Arginine deiminase inhibits proliferation of human leukemia cells more potently than asparaginase by inducing cell cycle arrest and apoptosis. Leukemia *14*, 826–829.

Gray-Schopfer, V., Wellbrock, C., and Marais, R. (2007). Melanoma biology and new targeted therapy. Nature *445*, 851–857.

Guertin, D.A., and Sabatini, D.M. (2007). Defining the role of mTOR in cancer. Cancer Cell *12*, 9–22.

Guo, F., and Cavener, D.R. (2007). The GCN2 eIF2alpha kinase regulates fatty-acid homeostasis in the liver during deprivation of an essential amino acid. Cell Metab. *5*, 103–114.

Gupta, P.B., Kuperwasser, C., Brunet, J.P., Ramaswamy, S., Kuo, W.L., Gray, J.W., Naber, S.P., and Weinberg, R.A. (2005). The melanocyte differentiation program predisposes to metastasis after neoplastic transformation. Nat. Genet. *37*, 1047–1054.

Hambraeus, L., Bilmazes, C., Dippel, C., Scrimshaw, N., and Young, V.R. (1976). Regulatory role of dietary leucine on plasma branched-chain amino acid levels in young men. J. Nutr. *106*, 230–240.

Hara, K., Yonezawa, K., Weng, Q.P., Kozlowski, M.T., Belham, C., and Avruch, J. (1998). Amino acid sufficiency and mTOR regulate p70 S6 kinase and eIF-4E BP1 through a common effector mechanism. J. Biol. Chem. *273*, 14484–14494.

Hosokawa, N., Hara, T., Kaizuka, T., Kishi, C., Takamura, A., Miura, Y., Iemura, S., Natsume, T., Takehana, K., Yamada, N., et al. (2009). Nutrient-dependent mTORC1 association with the ULK1-Atg13-FIP200 complex required for autophagy. Mol. Biol. Cell *20*, 1981–1991.

Inoki, K., Li, Y., Xu, T., and Guan, K.L. (2003). Rheb GTPase is a direct target of TSC2 GAP activity and regulates mTOR signaling. Genes Dev. *17*, 1829–1834.

Jung, C.H., Jun, C.B., Ro, S.H., Kim, Y.M., Otto, N.M., Cao, J., Kundu, M., and Kim, D.H. (2009). ULK-Atg13-FIP200 complexes mediate mTOR signaling to the autophagy machinery. Mol. Biol. Cell *20*, 1992–2003.

Kabeya, Y., Mizushima, N., Ueno, T., Yamamoto, A., Kirisako, T., Noda, T., Kominami, E., Ohsumi, Y., and Yoshimori, T. (2000). LC3, a mammalian homologue of yeast Apg8p, is localized in autophagosome membranes after processing. EMBO J. *19*, 5720–5728.

Kamada, Y., Funakoshi, T., Shintani, T., Nagano, K., Ohsumi, M., and Ohsumi, Y. (2000). Tor-mediated induction of autophagy via an Apg1 protein kinase complex. J. Cell Biol. *150*, 1507–1513.

Karreth, F.A., DeNicola, G.M., Winter, S.P., and Tuveson, D.A. (2009). C-Raf inhibits MAPK activation and transformation by B-Raf(V600E). Mol. Cell *36*, 477–486.

Klionsky, D.J. (2007). Autophagy: from phenomenology to molecular understanding in less than a decade. Nat. Rev. Mol. Cell Biol. *8*, 931–937.

Kreis, W., Baker, A., Ryan, V., and Bertasso, A. (1980). Effect of nutritional and enzymatic methionine deprivation upon human normal and malignant cells in tissue culture. Cancer Res. *40*, 634–641.

Kroemer, G., and Levine, B. (2008). Autophagic cell death: the story of a misnomer. Nat. Rev. Mol. Cell Biol. *9*, 1004–1010.

Kroemer, G., Galluzzi, L., Vandenabeele, P., Abrams, J., Alnemri, E.S., Baehrecke, E.H., Blagosklonny, M.V., El-Deiry, W.S., Golstein, P., Green, D.R., et al. (2009). Classification of cell death: recommendations of the Nomenclature Committee on Cell Death 2009. Cell Death Differ. *16*, 3–11.

Kuma, A., Hatano, M., Matsui, M., Yamamoto, A., Nakaya, H., Yoshimori, T., Ohsumi, Y., Tokuhisa, T., and Mizushima, N. (2004). The role of autophagy during the early neonatal starvation period. Nature *432*, 1032–1036.

Levine, B., and Kroemer, G. (2008). Autophagy in the pathogenesis of disease. Cell *132*, 27–42.

Ma, L., Chen, Z., Erdjument-Bromage, H., Tempst, P., and Pandolfi, P.P. (2005). Phosphorylation and functional inactivation of TSC2 by Erk implications for tuberous sclerosis and cancer pathogenesis. Cell *121*, 179–193.

Marks, J.L., Gong, Y., Chitale, D., Golas, B., McLellan, M.D., Kasai, Y., Ding, L., Mardis, E.R., Wilson, R.K., Solit, D., et al. (2008). Novel MEK1 mutation identified by mutational analysis of epidermal growth factor receptor signaling pathway genes in lung adenocarcinoma. Cancer Res. *68*, 5524–5528.

Matsuura, A., Tsukada, M., Wada, Y., and Ohsumi, Y. (1997). Apg1p, a novel protein kinase required for the autophagic process in Saccharomyces cerevisiae. Gene *192*, 245–250.

Mizushima, N., Yoshimori, T., and Levine, B. (2010). Methods in mammalian autophagy research. Cell *140*, 313–326.

Moffat, J., Grueneberg, D.A., Yang, X., Kim, S.Y., Kloepfer, A.M., Hinkle, G., Piqani, B., Eisenhaure, T.M., Luo, B., Grenier, J.K., et al. (2006). A lentiviral

RNAi library for human and mouse genes applied to an arrayed viral high-content screen. Cell *124*, 1283–1298.

Mortimore, G.E., and Schworer, C.M. (1977). Induction of autophagy by amino-acid deprivation in perfused rat liver. Nature *270*, 174–176.

Nakatogawa, H., Suzuki, K., Kamada, Y., and Ohsumi, Y. (2009). Dynamics and diversity in autophagy mechanisms: lessons from yeast. Nat. Rev. Mol. Cell Biol. *10*, 458–467.

Nobukuni, T., Joaquin, M., Roccio, M., Dann, S.G., Kim, S.Y., Gulati, P., Byfield, M.P., Backer, J.M., Natt, F., Bos, J.L., et al. (2005). Amino acids mediate mTOR/raptor signaling through activation of class 3 phosphatidylinositol 3OH-kinase. Proc. Natl. Acad. Sci. USA *102*, 14238–14243.

Noda, T., and Ohsumi, Y. (1998). Tor, a phosphatidylinositol kinase homologue, controls autophagy in yeast. J. Biol. Chem. *273*, 3963–3966.

Ohtawa, K., Ueno, T., Mitsui, K., Kodera, Y., Hiroto, M., Matsushima, A., Nishimura, H., and Inada, Y. (1998). Apoptosis of leukemia cells induced by valine-deficient medium. Leukemia *12*, 1651–1652.

Onuffer, J.J., and Kirsch, J.F. (1995). Redesign of the substrate specificity of *Escherichia coli* aspartate aminotransferase to that of *Escherichia coli* tyrosine aminotransferase by homology modeling and site-directed mutagenesis. Protein Sci. *4*, 1750–1757.

Roux, P.P., Ballif, B.A., Anjum, R., Gygi, S.P., and Blenis, J. (2004). Tumor-promoting phorbol esters and activated Ras inactivate the tuberous sclerosis tumor suppressor complex via p90 ribosomal S6 kinase. Proc. Natl. Acad. Sci. USA *101*, 13489–13494.

Rubinsztein, D.C., Gestwicki, J.E., Murphy, L.O., and Klionsky, D.J. (2007). Potential therapeutic applications of autophagy. Nat. Rev. Drug Discov. *6*, 304–312.

Sancak, Y., Peterson, T.R., Shaul, Y.D., Lindquist, R.A., Thoreen, C.C., Bar-Peled, L., and Sabatini, D.M. (2008). The Rag GTPases bind raptor and mediate amino acid signaling to mTORC1. Science *320*, 1496–1501.

Sancak, Y., Bar-Peled, L., Zoncu, R., Markhard, A.L., Nada, S., and Sabatini, D.M. (2010). Ragulator-Rag complex targets mTORC1 to the lysosomal surface and is necessary for its activation by amino acids. Cell *141*, 290–303.

Schworer, C.M., Shiffer, K.A., and Mortimore, G.E. (1981). Quantitative relationship between autophagy and proteolysis during graded amino acid deprivation in perfused rat liver. J. Biol. Chem. *256*, 7652–7658.

Scott, L., Lamb, J., Smith, S., and Wheatley, D.N. (2000). Single amino acid (arginine) deprivation: rapid and selective death of cultured transformed and malignant cells. Br. J. Cancer *83*, 800–810.

Slee, E.A., Zhu, H., Chow, S.C., MacFarlane, M., Nicholson, D.W., and Cohen, G.M. (1996). Benzyloxycarbonyl-Val-Ala-Asp (OMe) fluoromethylketone (Z-VAD.FMK) inhibits apoptosis by blocking the processing of CPP32. Biochem. J. *315*, 21–24.

Smith, E.M., Finn, S.G., Tee, A.R., Browne, G.J., and Proud, C.G. (2005). The tuberous sclerosis protein TSC2 is not required for the regulation of the mammalian target of rapamycin by amino acids and certain cellular stresses. J. Biol. Chem. *280*, 18717–18727.

Taylor, R.C., Cullen, S.P., and Martin, S.J. (2008). Apoptosis: controlled demolition at the cellular level. Nat. Rev. Mol. Cell Biol. *9*, 231–241.

Tee, A.R., Manning, B.D., Roux, P.P., Cantley, L.C., and Blenis, J. (2003). Tuberous sclerosis complex gene products, Tuberin and Hamartin, control mTOR signaling by acting as a GTPase-activating protein complex toward Rheb. Curr. Biol. *13*, 1259–1268.

White, E., Karp, C., Strohecker, A.M., Guo, Y., and Mathew, R. (2010). Role of autophagy in suppression of inflammation and cancer. Curr. Opin. Cell Biol. *22*, 212–217.

Woolley, P.V., Dion, R.L., and Bono, V.H., Jr. (1974). Effects of tryptophan deprivation on L1210 cells in culture. Cancer Res. *34*, 1010–1014.

Yuneva, M., Zamboni, N., Oefner, P., Sachidanandam, R., and Lazebnik, Y. (2007). Deficiency in glutamine but not glucose induces MYC-dependent apoptosis in human cells. J. Cell Biol. *178*, 93–105.

21. J. Lee, W. G. Dunphy, *Mol. Biol. Cell* **21**, 926 (2010).

Acknowledgments: We thank the Institute of Chemistry and Cell Biology-Longwood for screening assistance. We also thank K. Hofmann, A. Ciccia, A. Bredemeyer, B. Adamson, A. Burrows, A. Smogorzewska, and A. Brass for helpful discussions. This work was supported by NIH grants to S.J.E. and J.W.H. C.C.R. is the recipient of a long-term European Molecular Biology Organization fellowship. S.J.E. is a Howard Hughes Medical Institute investigator. W.H. is a paid consultant for Millennium Pharmaceuticals and its program in oncology.

Supporting Online Material
www.sciencemag.org/cgi/content/full/332/6035/1313/DC1
Materials and Methods
SOM Text
Figs. S1 to S15
Tables S1 to S4
References

27 January 2011; accepted 28 April 2011
10.1126/science.1203430

The mTOR-Regulated Phosphoproteome Reveals a Mechanism of mTORC1-Mediated Inhibition of Growth Factor Signaling

Peggy P. Hsu,[1,2] Seong A. Kang,[1] Jonathan Rameseder,[3,4] Yi Zhang,[5,6] Kathleen A. Ottina,[1,7] Daniel Lim,[4] Timothy R. Peterson,[1,2] Yongmun Choi,[5,8] Nathanael S. Gray,[5,8] Michael B. Yaffe,[2,4] Jarrod A. Marto,[5,6,8] David M. Sabatini[1,2,4,7]*

The mammalian target of rapamycin (mTOR) protein kinase is a master growth promoter that nucleates two complexes, mTORC1 and mTORC2. Despite the diverse processes controlled by mTOR, few substrates are known. We defined the mTOR-regulated phosphoproteome by quantitative mass spectrometry and characterized the primary sequence motif specificity of mTOR using positional scanning peptide libraries. We found that the phosphorylation response to insulin is largely mTOR dependent and that mTOR exhibits a unique preference for proline, hydrophobic, and aromatic residues at the +1 position. The adaptor protein Grb10 was identified as an mTORC1 substrate that mediates the inhibition of phosphoinositide 3-kinase typical of cells lacking tuberous sclerosis complex 2 (TSC2), a tumor suppressor and negative regulator of mTORC1. Our work clarifies how mTORC1 inhibits growth factor signaling and opens new areas of investigation in mTOR biology.

The serine-threonine kinase mammalian target of rapamycin (mTOR) is a major controller of growth that is deregulated in cancer and diabetes (*1*, *2*). mTOR is the catalytic subunit of two multiprotein complexes, mTORC1 and mTORC2. mTORC1 is activated by growth factors and nutrients through a pathway that involves the tuberous sclerosis complex (TSC1-TSC2) tumor suppressors as well as the Rag and Rheb guanosine triphosphatases (GTPases). mTORC1 phosphorylates the translational regulators S6 kinase 1 (S6K1) and the eukaryotic translation initiation factor 4E (eIF-4E) binding proteins (4E-BP1 and 4E-BP2), whereas mTORC2 activates Akt and serum- and glucocorticoid-regulated kinase 1 (SGK1) and is part of the growth factor–stimulated phosphoinositide 3-kinase (PI3K) pathway. Collectively, mTORC1 and mTORC2 regulate processes that control cell growth and proliferation, including protein synthesis, autophagy, and metabolism. mTOR inhibitors derived from rapamycin, an allosteric mTORC1 inhibitor, have been in trials for anticancer uses, but the feedback activation of the PI3K-Akt pathway that occurs with mTORC1 inhibition may lessen their clinical efficacy (*3*).

The few mTOR substrates with defined phosphorylation sites likely cannot explain all processes under the control of mTOR (*1*, *2*) (table S1). To discover additional substrates, we conducted a systematic investigation of the mTOR-regulated phosphoproteome using mass spectrometry and isobaric tags that permit four-way multiplexed relative and absolute quantification of phosphopeptide abundances (iTRAQ) (*4*). With duplicate analyses for each, we analyzed phosphopeptides from two sets of cells in which the pathway was hyperactivated and then inhibited with Torin1, a recently developed adenosine 5′-triphosphate (ATP)–competitive mTOR kinase domain inhibitor that blocks all known phosphorylations downstream of mTORC1 and mTORC2 (*5*). Human embryonic kidney (HEK)-293E cells were deprived of serum and then stimulated with insulin in the presence or absence of rapamycin or Torin1 (Fig. 1A). Wild-type ($TSC2^{+/+}$) and TSC2-null ($TSC2^{-/-}$) mouse embryonic fibroblasts (MEFs), which have increased mTORC1 signaling, were also treated with or without Torin1 (Fig. 1A). Under these conditions, phosphorylation events known to be downstream of mTORC1 (e.g., rapamycin-sensitive S6K1 T389 and rapamycin-insensitive 4E-BP1 T37 and T46) and mTORC2 (e.g., Akt S473, PRAS40/AKT1S1 T246, NDRG1 T346) behaved as expected (fig. S1).

From the HEK-293E cells, we identified 4256 unique phosphopeptides corresponding to 47 phosphotyrosine and 4204 phosphoserine-threonine sites on 1661 distinct proteins [false discovery rate (FDR) ~1%, table S2]. Using a cutoff of 2.5 median absolute deviations (MADs) below the median $\log_2$(Torin1/Insulin ratio) (robust *z*-score < −2.5), we identified 127 phosphopeptides from 93 proteins as sensitive to Torin1 and designated them as mTOR-regulated (Fig. 1B). From the MEFs, 7299 unique phosphopeptides corresponding to 110 phosphotyrosine and 7145 phosphoserine-threonine sites on 2406 distinct proteins were identified (FDR ~ 1%, table S2), of which 231 phosphopeptides from 174 proteins were regulated by mTOR [−2.5 MAD, $\log_2(TSC2^{-/-}$ Torin1/$TSC2^{-/-}$ vehicle] (Fig. 1C). By this −2.5 MAD cutoff for both the HEK-293E and MEF data sets, the mTOR-regulated sites were highly enriched in canonical mTOR pathway phosphorylations (Fisher's exact test $P = 5.2 \times 10^{-24}$ and 6.5×10^{-23}, respectively; Fig. 1, B and C, and table S1), an indication of the predictive potential of the data to identify mTOR pathway components. Additionally, we identified Torin1-sensitive sites on lesser or only recently characterized mTOR substrates [CAP-GLY domain containing linker protein 1 (CLIP1) S1158 (*6*), Unc-51–like kinase 1 (ULK1) S638 (*7*–*9*), and insulin receptor substrate 2 (IRS2) S616 (*10*)].

Global comparisons of the data sets revealed several interesting features. In the HEK-293E cells, phosphorylation changes resulting from Torin1 treatment were markedly similar to those observed under serum deprivation (Spearman's $\rho = 0.66$, $P \sim 0$, Fig. 1D), revealing that insulin-regulated phosphorylations (both down- and up-regulated) are largely mTOR dependent. The effects of rapamycin and Torin1 treatment were similar (Spearman's $\rho = 0.48$, $P \sim 0$, Fig. 1E), but a subset of Torin1-sensitive sites were not rapamycin sensitive (upper left quadrant, Fig. 1E), including 4E-BP1 and 4E-BP2 T37 and T46 (*5*, *11*, *12*) and the mTORC2-mediated Akt3 S472 and NDRG1 S330. Analysis of the MEF data set revealed that phosphorylations that increase with TSC2 loss are more likely to be inhibited by Torin1 (Spearman's $\rho = -0.25$, $P = 1.4 \times 10^{-130}$) (Fig. 1F). Heirarchical clustering of the conditions and sorting of the phosphopeptide abundances in the HEK-293E

[1]Whitehead Institute for Biomedical Research, Nine Cambridge Center, Cambridge, MA 02142, USA. [2]Department of Biology, Massachusetts Institute of Technology (MIT), Cambridge, MA 02139, USA. [3]Computational and Systems Biology Initiative, MIT, Cambridge, MA 02139, USA. [4]David H. Koch Institute for Integrative Cancer Research at MIT, 77 Massachusetts Avenue, Cambridge, MA 02139, USA. [5]Department of Cancer Biology, Dana-Farber Cancer Institute (DFCI), 250 Longwood Avenue, Boston, MA 02115, USA. [6]Blais Proteomics Center, DFCI, 250 Longwood Avenue, Boston, MA 02115, USA. [7]Howard Hughes Medical Institute, MIT, Cambridge, MA 02139, USA. [8]Department of Biological Chemistry and Molecular Pharmacology, Harvard Medical School, 250 Longwood Avenue, Boston, MA 02115, USA.

*To whom correspondence should be addressed. E-mail: sabatini@wi.mit.edu

cells also verified the similarity between serum starvation and Torin1 treatment (fig. S2) and our ability to discriminate between known rapamycin-sensitive (fig. S2, top) and -insensitive (fig. S2, bottom) sites, and showed that phosphorylations that are rapamycin sensitive tend to be inhibited by Torin1 treatment to a greater extent than those that are not (fig. S2).

Pathway analysis of the candidate mTOR-regulated proteins revealed enrichment (FDR < 10%) in processes downstream of mTOR, such as translation [Gene Ontology (GO):0006417] and regulation of cell size (GO:0008361), as well as some not generally considered to be under mTOR control (table S3). These include RNA splicing (GO:0008380), DNA replication (GO:0006260), vesicle-mediated transport (GO:0016192), and regulation of mRNA-processing bodies (GO:0000932), signifying a broader role for mTOR signaling than presently appreciated.

As the mTOR-regulated sites may be phosphorylated by mTOR or by downstream kinases, we sought to distinguish direct substrates from indirect effectors by determining a consensus phospho-acceptor motif for mTOR. An example of such a motif is the (R/K)X(R/K)XX(S*/T*) sequence [X, any amino acid; asterisk (*), phospho-acceptor] recognized by the mTOR substrates Akt, S6K1, and SGK1, all members of the AGC kinase family (*13*). Because mTOR phosphorylates hydrophobic motifs (HMs) of the AGC kinases as well as the distinct proline-directed sites of proteins such as 4E-BP1 and 4E-BP2 (fig. S3), it is unknown if the kinase exhibits any motif specificity or if the choice of sites is entirely determined by factors beyond the primary substrate sequence. We found that when combined with its activator, guanosine 5′-triphosphate (GTP)–bound Rheb, highly pure and intact mTORC1 (*14*) robustly phosphorylated an arrayed positional scanning peptide library (*15*) (fig. S4 and Fig. 2A). Although mTORC1 and mTORC2 phosphorylate distinct sets of substrates, they likely have similar motif preferences as they share the same catalytic domain. This unbiased assay revealed that mTOR possesses selectivity toward peptide substrates concordant with known mTOR sites (figs. S3 and S4 and Fig. 2, A and B), primarily at the +1 position at which mTOR prefers proline, hydrophobic residues (L, V), and aromatic residues (F, W, Y). This pattern of specificity at the +1 position is unique among all kinases previously profiled (*16*). mTOR also exhibits minor selectivity at other positions (fig. S4 and Fig. 2, A and B). These data suggest that within the HM of the AGC kinases (fig. S3) the −4 and −1 hydrophobic residues are dispensable for mTOR recognition.

Combining our two approaches, we classified the mTOR-regulated phosphorylation sites, first by rapamycin sensitivity [HEK-293E, −2.5 MAD $\log_2$(Rapamycin/Insulin)] or by increased phosphorylation in cells lacking TSC2 [MEFs, +2.5 MAD $\log_2$($TSC2^{-/-}$ vehicle/$TSC2^{+/+}$ vehicle)] (Fig. 2, C and D; figs. S5 and S6; and table S4). Rapamycin-sensitive sites or those up-regulated in $TSC2^{-/-}$

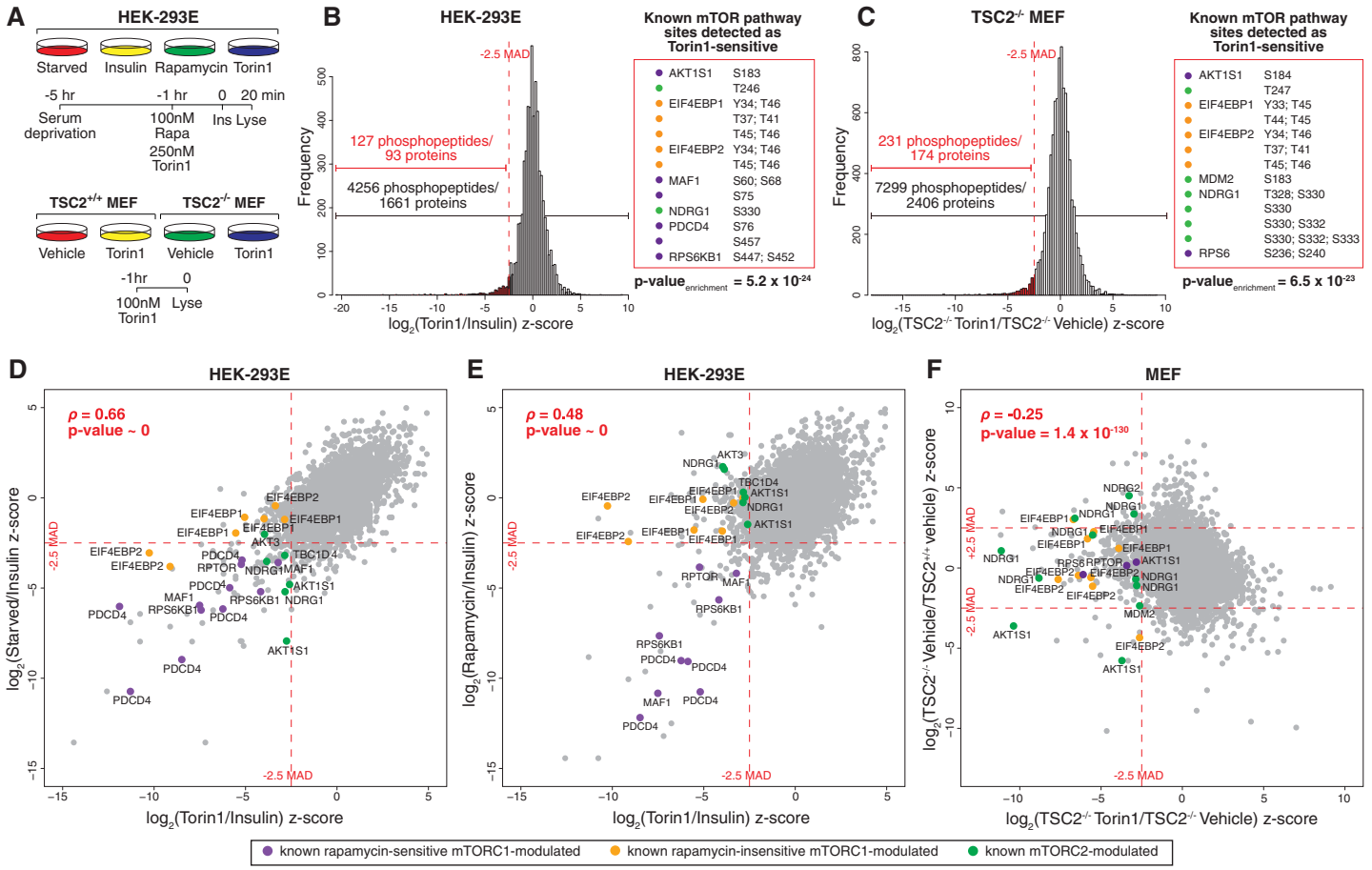

Fig. 1. Identification of the mTOR-regulated phosphoproteome. (**A**) Phosphopeptide abundances were determined from two sets of samples: HEK-293E cells serum starved for 4 hours, treated with 100 nM rapamycin, 250 nM Torin1, or vehicle control for 1 hour, and then stimulated with 150 nM insulin for 20 min and $TSC2^{+/+}$ and $TSC2^{-/-}$ MEFs treated with 100 nM Torin1 or vehicle control for 1 hour. (**B** and **C**) Distributions of robust *z*-scores [median absolute deviations (MADs) away from the median (B) $\log_2$(Torin1/Insulin) for HEK-293Es or (C) $\log_2$($TSC2^{-/-}$ Torin1/$TSC2^{-/-}$ vehicle) for MEFs] for both replicates. *P* values associated with enrichment for known mTOR-modulated sites among the −2.5 MAD Torin1-sensitive phosphopeptides were determined by Fisher's exact test. Phosphopeptides detected in both replicates had to meet the −2.5 MAD threshold both times to be considered mTOR-regulated. (**D** to **F**) Correspondence between (D) Torin1 treatment and serum deprivation in HEK-293Es, (E) Torin1 and rapamycin treatment in HEK-293Es, and (F) Torin1 treatment and up-regulation in $TSC2^{-/-}$ MEFs. The relevant robust *z*-scores for both replicates, phosphopeptides corresponding to known mTOR-modulated sites, Spearman's rank correlation coefficient (ρ), and associated *P* values are indicated. Axes were truncated to aid in visualization.

cells are likely mTORC1 regulated, whereas the remaining sites could be downstream of either complex. Second, we scored the sites by motif into the following categories: (i) candidate direct mTOR sites, (ii) candidate AGC kinase substrates, or (iii) mTOR-regulated but by an undetermined mechanism (Fig. 2, C and D; figs. S5 and S6; and table S4).

Several candidate substrates implicate mTOR in new aspects of cell growth regulation. WD repeat domain, phosphoinositide interacting 2 (WIPI2) (fig. S6), a sparsely characterized ortholog of the yeast Atg18p, is a potential substrate implicated in autophagosome formation (*17*). In addition, orthologs of the candidate substrates protein associated with topoisomerase II homolog 1 (PATL1) (fig. S5 and S6) and La ribonucleoprotein domain family member 1 (LARP1) (figs. S5 and S6) bind RNA, localize to P-bodies, and control mRNA stability (*18*, *19*). In yeast, Pat1p phosphorylation is sensitive to rapamycin (*20*), and contributes to repression of mRNA translation upon amino acid withdrawal (*21*), suggesting that regulation of mRNA degradation may be important for growth control. Other potential substrates point to nascent areas of mTOR biology. For example, mTOR putatively regulates the neural stem cell marker Nestin, the pleiotropic transcription factor c-Jun, and the myogenic stem cell transcription factor forkhead box K1 (FoxK1) (fig. S6).

One candidate of special interest was the adaptor protein growth factor receptor-bound protein 10 (Grb10) (Fig. 2D and fig. S6). The abundance of a Grb10 phosphopeptide with putative mTOR motif sites was increased in the absence of TSC2 and decreased after Torin1 treatment in both $TSC2^{+/+}$ and $TSC2^{-/-}$ MEFs (tables S2 and S4, Fig. 2D, and fig. S6), patterns consistent with being in the mTORC1 pathway. Conserved among vertebrates, Grb10 negatively regulates growth factor signaling (*22*). It binds the insulin and insulin-like growth factor 1 (IGF-1) receptors, and mice without Grb10 are larger and exhibit enhanced insulin sensitivity (*23*–*25*). Although the ubiquitin ligase neural precursor cell expressed, developmentally down-regulated 4 (Nedd4) does not directly ubiquitinate Grb10 (*26*), Nedd4-null mice have more Grb10 protein and are insulin and IGF resistant, a signaling phenotype reminiscent of cells lacking TSC1 or TSC2 (*27*). Therefore, we speculated that Grb10 might function downstream of mTORC1 to inhibit PI3K-Akt signaling.

In SDS–polyacrylamide gel electrophoresis analyses, Grb10 exhibited an insulin-stimulated mobility shift that is partially sensitive to rapamycin (Fig. 3A). In vitro phosphatase treatment eliminated the shift, as did Torin1, indicating that the shift results from phosphorylation and is dependent on mTOR activity (Fig. 3, A and B). Amino acids stimulated Grb10 phosphorylation and were required for its serum-dependent phosphorylation (Fig. 3C), and in $TSC2^{-/-}$ MEFs, Grb10 phosphorylation was retained in the absence of serum but lost upon acute rapamycin and Torin1 treatment (Fig. 3D). These data point to mTORC1, but not mTORC2, as the main regulator of Grb10. Consistent with this conclusion, the loss of rictor, a core component of mTORC2, did not affect Grb10 phosphorylation (fig. S7, A and B).

In cells lacking S6K1 and S6K2, Grb10 was still regulated in an mTOR-dependent manner (fig. S7C), suggesting that it might be a direct substrate. Indeed, Grb10 was phosphorylated in vitro by mTORC1 to an extent comparable with that of known substrates (Fig. 3E). The sites regulated by mTOR in vitro (Fig. 3G) and in cells (Fig. 3H) were mapped to S104, S150, T155, S428, and S476, which are located in or near the proline-rich region or between the pleckstrin homology (PH) and Src homology 2 (SH2) domains (BPS) of Grb10 (Fig. 3F). In cells, all sites were Torin1 sensitive, while S476 was also rapamycin sensitive (Fig. 3H). Grb10 is therefore similar to 4E-BP1, an mTORC1 substrate with both rapamycin-sensitive and -insensitive sites (Fig. 3I). We verified our characterization of these sites with phosphospecific antibodies against S150, S428, and S476 (Fig. 3J and fig. S8, A and B). Mutation of the identified sites along with a few neighboring residues eliminated the mobility shift (Fig. 3K), indicating that most if not all mTOR-regulated sites were localized.

mTORC1 inhibits PI3K-Akt signaling, but the molecular connections involved are poorly

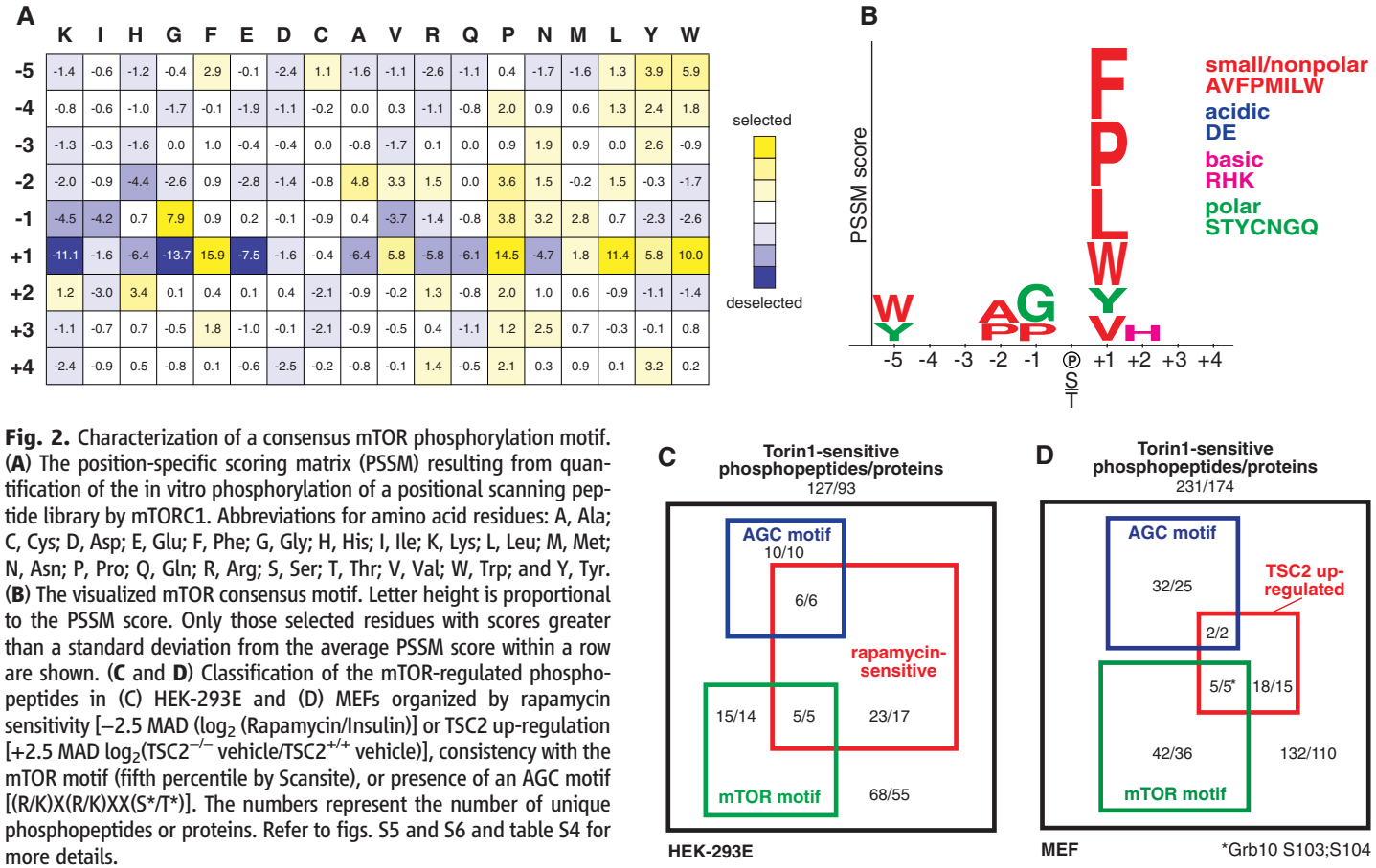

Fig. 2. Characterization of a consensus mTOR phosphorylation motif. (**A**) The position-specific scoring matrix (PSSM) resulting from quantification of the in vitro phosphorylation of a positional scanning peptide library by mTORC1. Abbreviations for amino acid residues: A, Ala; C, Cys; D, Asp; E, Glu; F, Phe; G, Gly; H, His; I, Ile; K, Lys; L, Leu; M, Met; N, Asn; P, Pro; Q, Gln; R, Arg; S, Ser; T, Thr; V, Val; W, Trp; and Y, Tyr. (**B**) The visualized mTOR consensus motif. Letter height is proportional to the PSSM score. Only those selected residues with scores greater than a standard deviation from the average PSSM score within a row are shown. (**C** and **D**) Classification of the mTOR-regulated phosphopeptides in (C) HEK-293E and (D) MEFs organized by rapamycin sensitivity [–2.5 MAD (log_2 (Rapamycin/Insulin)] or TSC2 up-regulation [+2.5 MAD log_2($TSC2^{-/-}$ vehicle/$TSC2^{+/+}$ vehicle)], consistency with the mTOR motif (fifth percentile by Scansite), or presence of an AGC motif [(R/K)X(R/K)XX(S*/T*)]. The numbers represent the number of unique phosphopeptides or proteins. Refer to figs. S5 and S6 and table S4 for more details.

understood. One mechanism is the destabilization of insulin receptor substrate 1 (IRS1) by S6K1 phosphorylation (*10*, *28*). However, other mechanisms likely exist because loss of raptor, an essential mTORC1 component, in S6K1$^{-/-}$S6K2$^{-/-}$ cells still activated Akt phosphorylation without affecting IRS1 abundance (Fig. 4A). Therefore, we tested whether mTORC1 might also inhibit the PI3K pathway through Grb10. Con-

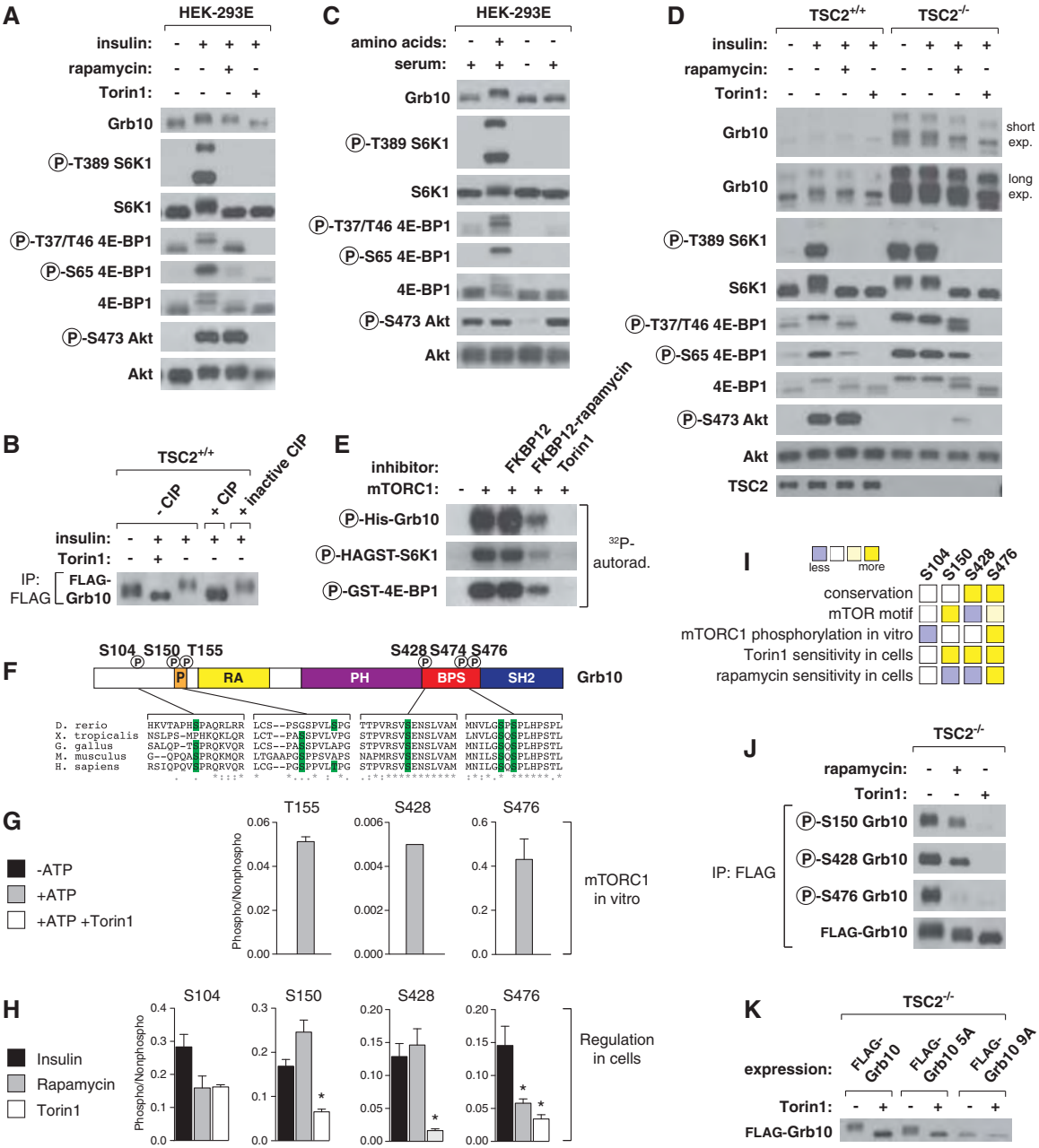

Fig. 3. Grb10 is an mTORC1 substrate with rapamycin-sensitive and -insensitive sites. (**A**) HEK-293E cells were deprived of serum for 4 hours, treated with 100 nM rapamycin or 250 nM Torin1 for 1 hour, and then stimulated with 150 nM insulin for 15 min. Cell lysates were analyzed by immunoblotting. (**B**) TSC2$^{+/+}$ MEFs stably expressing FLAG-Grb10 were serum deprived for 4 hours, treated with 250 nM Torin1 for 1 hour, and then stimulated with 150 nM insulin for 15 min. All FLAG-tagged Grb10 constructs correspond to isoform c of human Grb10. FLAG immunoprecipitates were incubated in buffer, calf intestinal phosphatase (CIP), or inactivated CIP and analyzed by immunoblotting. (**C**) HEK-293E cells were deprived of amino acids or both amino acids and serum for 50 min, and then stimulated with either amino acids or serum for 10 min and analyzed by immunoblotting. (**D**) TSC2$^{+/+}$ and TSC2$^{-/-}$ MEFs were treated and analyzed as in (A). (**E**) mTORC1 in vitro kinase assays with substrates in the presence of the indicated inhibitors and radiolabeled ATP were analyzed by autoradiography. (**F**) Schematic representation of Grb10 protein structure with the phosphorylation sites from vertebrate orthologs aligned below. Numbering is according to human isoform a. (**G**) The phosphorylation state of Grb10 from kinase assays performed similarly to (E) were analyzed by targeted mass spectrometry and phosphorylation ratios determined from chromatographic peak intensities. (**H**) FLAG immunoprecipitates from HEK-293E cells stably expressing FLAG-Grb10 treated as in (A) were analyzed as in (G). Data are means ± SEM (n = 2 to 6). *P < 0.05 for differences between stimulated and treated conditions (Mann-Whitney t test). (**I**) A summary of (F), (G), and (H) for each Grb10 phosphorylation site. (**J**) FLAG immunoprecipitates from TSC2$^{-/-}$ MEFs stably expressing FLAG-Grb10 treated with 100 nM rapamycin or 250 nM Torin1 for 1 hour were analyzed by immunoblotting with Grb10 phospho-specific antibodies. (**K**) TSC2$^{-/-}$ MEFs stably expressing FLAG-Grb10, 5A (S150A T155A S158A S474A S476A), or 9A (5A + S104A S426A S428A S431A) mutants treated with 250 nM Torin1 for 1 hour were analyzed by immunoblotting.

sistent with this possibility, the short hairpin RNA (shRNA)–mediated knockdown of Grb10 in HEK-293E and HeLa cells boosted Akt phosphorylation (fig. S9, A and B). This boost was increased with rapamycin treatment and, to a lesser extent, with S6K inhibition (*29*), suggesting that Grb10 is important for feedback but that other mTOR-dependent mechanisms are also at play (fig. S9, A and B). Loss of Grb10 in TSC2$^{-/-}$ MEFs also restored insulin sensitivity to Akt phosphorylation without affecting total IRS1 abundance or the phosphorylation of S636 and S639 on IRS1 (Fig. 4B and fig. S9C). Although in TSC2$^{-/-}$ cells Grb10 suppression or acute rapamycin treatment each did not rescue insulin signaling to the same extent as in wild-type cells, the two in combination approximated the wild-type level of Akt activation (fig. S9D). This restoration in growth factor sensitivity also applied to increased autophosphorylation of the insulin and IGF receptors, Erk1/2 activation, and IGF-1, but not epidermal growth factor (EGF) and platelet-derived growth factor (PDGF), stimulation (fig. S10, A and B). Suppression of Grb10 also increased tyrosine phosphorylation of IRS1 and IRS2 and p85 PI3K recruitment by IRS, again independently of IRS protein abundance (Fig. 4C). Compared to cells expressing wild-type Grb10, cells expressing an equivalent amount of nonphosphorylatable Grb10 had increased Akt phosphorylation, confirming that mTORC1 phosphorylation is necessary for its inhibitory function (Fig. 4D and fig. S10C).

We suspected that mTORC1-mediated phosphorylation of Grb10 might affect its stability, because the more sites we mutated to alanine, the more lentiviral expression construct was required to achieve expression levels equivalent to that of the wild-type protein. Grb10 is also highly abundant in the TSC2$^{-/-}$ cells with hyperactive mTORC1 signaling (Fig. 3D and fig. S11A), and chronic mTOR inhibition decreased Grb10 protein abundance (fig. S11A) without significantly affecting mRNA levels (fig. S11B). Indeed, determination of Grb10 half-life by pulse-chase experiments revealed at least a twofold decrease (~12 hours to ~5 hours) in stability with either mTOR inhibitor treatment (Fig. 4E) or mutation of the mTOR sites to alanines (Fig. 4F). Proteasome inhibition (fig. S11C), suppression of Nedd4 (fig. S11D), or phosphomimetic mutation of the mTOR sites (fig. S11E) rescued the decrease in Grb10 protein caused by mTOR inhibition. Therefore, mTORC1 inhibits and destabilizes IRS1 and simultaneously activates and stabilizes Grb10 (fig. S12).

These results confirm the importance of the mTORC1 pathway in regulating growth factor signaling and clarify the nature of the feedback loop to PI3K-Akt. Whereas acute mTORC1 inhibition leads to dephosphorylation of IRS1 and Grb10, chronic mTORC1 inhibition leads to changes in the abundance of IRS and Grb10

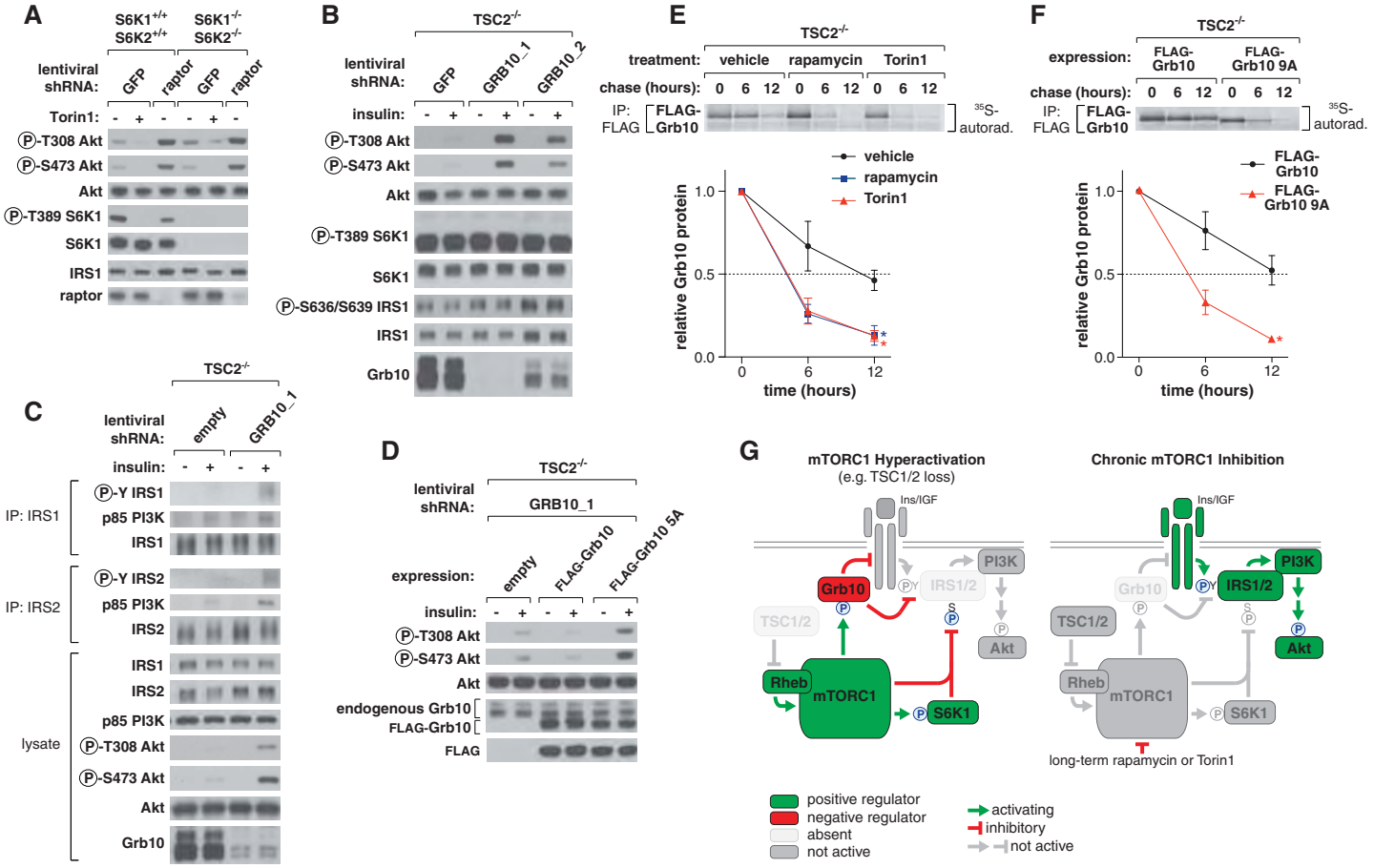

Fig. 4. mTORC1 inhibits PI3K-Akt signaling by regulating Grb10 function and stability. (**A**) S6K1$^{-/-}$ S6K2$^{-/-}$ or control cells expressing shRNA constructs against green fluorescent protein (GFP) or raptor were treated with 250 nM Torin1 or vehicle control for 1 hour, and lysates were analyzed by immunoblotting. (**B**) TSC2$^{-/-}$ MEFs expressing shRNAs against GFP or Grb10 were deprived of serum for 4 hours and then stimulated with 100 nM insulin for 15 min as indicated and analyzed by immunoblotting. (**C**) TSC2$^{-/-}$ MEFs expressing a control shRNA or shRNA against Grb10 were treated as in (B). IRS1 and IRS2 immunoprecipitates and cell lysates were analyzed by immunoblotting. (**D**) TSC2$^{-/-}$ MEFs coexpressing an shRNA against the mouse Grb10 3′ untranslated region and an empty vector, FLAG-Grb10 (human isoform c), or 5A cDNA expression construct were treated and analyzed as in (B). (**E**) TSC2$^{-/-}$ MEFs stably expressing FLAG-Grb10 were labeled for 2 hours with [^{35}S]cysteine and methionine and then chased for the indicated times in the presence of vehicle control, 100 nM rapamycin, or 100 nM Torin1. FLAG immunoprecipitates were analyzed by autoradiography. Data are means ± SEM (n = 3). *P < 0.05 for differences between vehicle and inhibitor treatment (two-way analysis of variance). (**F**) TSC2$^{-/-}$ MEFs stably expressing FLAG-Grb10 or 9A mutant were treated and analyzed as in (E) but without inhibitor treatment. (**G**) mTORC1 orchestrates feedback inhbition of PI3K-Akt signaling by activating and stabilizing Grb10 while inhibiting and destabilizing IRS proteins.

proteins, which are likely the most important effects of mTOR inhibitors to consider in their clinical use (Fig. 4G). Our findings also support the idea (*30*, *31*) that concomitant IGF-1 receptor inhibition may improve the anticancer efficacy of mTOR inhibitors. Finally, the discovery of Grb10 as an mTORC1 substrate validates our approach and suggests that the other potential downstream effectors that we identified may also serve as starting points for new areas of investigation in mTOR biology.

References and Notes

1. M. Laplante, D. M. Sabatini, *J. Cell Sci.* **122**, 3589 (2009).
2. R. Zoncu, A. Efeyan, D. M. Sabatini, *Nat. Rev. Mol. Cell Biol.* **12**, 21 (2011).
3. R. J. Dowling, I. Topisirovic, B. D. Fonseca, N. Sonenberg, *Biochim. Biophys. Acta* **1804**, 433 (2010).
4. P. L. Ross *et al.*, *Mol. Cell. Proteomics* **3**, 1154 (2004).
5. C. C. Thoreen *et al.*, *J. Biol. Chem.* **284**, 8023 (2009).
6. J. H. Choi *et al.*, *EMBO Rep.* **3**, 988 (2002).
7. C. H. Jung *et al.*, *Mol. Biol. Cell* **20**, 1992 (2009).
8. I. G. Ganley *et al.*, *J. Biol. Chem.* **284**, 12297 (2009).
9. N. Hosokawa *et al.*, *Mol. Biol. Cell* **20**, 1981 (2009).
10. O. J. Shah, Z. Wang, T. Hunter, *Curr. Biol.* **14**, 1650 (2004).
11. A. Y. Choo, S. O. Yoon, S. G. Kim, P. P. Roux, J. Blenis, *Proc. Natl. Acad. Sci. U.S.A.* **105**, 17414 (2008).
12. M. E. Feldman *et al.*, *PLoS Biol.* **7**, e38 (2009).
13. L. R. Pearce, D. Komander, D. R. Alessi, *Nat. Rev. Mol. Cell Biol.* **11**, 9 (2010).
14. C. K. Yip, K. Murata, T. Walz, D. M. Sabatini, S. A. Kang, *Mol. Cell* **38**, 768 (2010).
15. J. E. Hutti *et al.*, *Nat. Methods* **1**, 27 (2004).
16. J. Mok *et al.*, *Sci. Signal.* **3**, ra12 (2010).
17. H. E. Polson *et al.*, *Autophagy* **6**, 506 (2010).
18. R. Parker, U. Sheth, *Mol. Cell* **25**, 635 (2007).
19. K. Nykamp, M. H. Lee, J. Kimble, *RNA* **14**, 1378 (2008).
20. A. Huber *et al.*, *Genes Dev.* **23**, 1929 (2009).
21. J. Coller, R. Parker, *Cell* **122**, 875 (2005).
22. L. J. Holt, K. Siddle, *Biochem. J.* **388**, 393 (2005).
23. M. Charalambous *et al.*, *Proc. Natl. Acad. Sci. U.S.A.* **100**, 8292 (2003).
24. F. M. Smith *et al.*, *Mol. Cell. Biol.* **27**, 5871 (2007).
25. L. Wang *et al.*, *Mol. Cell. Biol.* **27**, 6497 (2007).
26. A. Morrione *et al.*, *J. Biol. Chem.* **274**, 24094 (1999).
27. X. R. Cao *et al.*, *Sci. Signal.* **1**, ra5 (2008).
28. L. S. Harrington *et al.*, *J. Cell Biol.* **166**, 213 (2004).
29. L. R. Pearce *et al.*, *Biochem. J.* **431**, 245 (2010).
30. K. E. O'Reilly *et al.*, *Cancer Res.* **66**, 1500 (2006).
31. X. Wan, B. Harkavy, N. Shen, P. Grohar, L. J. Helman, *Oncogene* **26**, 1932 (2007).

Acknowledgments: We thank members of the Sabatini Lab for helpful discussion, especially B. Joughin, G. Bell, H. Keys, K. Birsoy, N. Kory, C. Thoreen, J. Claessen, and D. Wagner for assistance with technical or conceptual aspects of this project. This work was supported by the National Institutes of Health (grants CA103866 and AI47389 to D.M.S.; ES015339, GM68762, and CA112967 to M.B.Y.), Department of Defense (W81XWH-07-0448 to D.M.S.), the W.M. Keck Foundation (D.M.S.), LAM Foundation (D.M.S.), Dana-Farber Cancer Institute (N.S.G, J.M), the International Fulbright Science and Technology Award (J.R.), and American Cancer Society (S.A.K.). D.M.S. is an investigator of the Howard Hughes Medical Institute. Torin1, the drug used in this paper, is part of a Whitehead-DFCI patent application on which N.S.G. and D.M.S. are inventors. Shared reagents are subject to a Materials Transfer Agreement.

Supporting Online Material

www.sciencemag.org/cgi/content/full/332/6035/1317/DC1
Materials and Methods
Figs. S1 to S12
Tables S1 to S4
References

25 October 2010; accepted 22 April 2011
10.1126/science.1199498

Phosphoproteomic Analysis Identifies Grb10 as an mTORC1 Substrate That Negatively Regulates Insulin Signaling

Yonghao Yu,[1] Sang-Oh Yoon,[1]* George Poulogiannis,[2] Qian Yang,[1,3] Xiaoju Max Ma,[1]† Judit Villén,[1]‡ Neil Kubica,[1]§ Gregory R. Hoffman,[1] Lewis C. Cantley,[2] Steven P. Gygi,[1]‖ John Blenis[1]‖

The evolutionarily conserved serine-threonine kinase mammalian target of rapamycin (mTOR) plays a critical role in regulating many pathophysiological processes. Functional characterization of the mTOR signaling pathways, however, has been hampered by the paucity of known substrates. We used large-scale quantitative phosphoproteomics experiments to define the signaling networks downstream of mTORC1 and mTORC2. Characterization of one mTORC1 substrate, the growth factor receptor–bound protein 10 (Grb10), showed that mTORC1-mediated phosphorylation stabilized Grb10, leading to feedback inhibition of the phosphatidylinositol 3-kinase (PI3K) and extracellular signal–regulated, mitogen-activated protein kinase (ERK-MAPK) pathways. Grb10 expression is frequently down-regulated in various cancers, and loss of Grb10 and loss of the well-established tumor suppressor phosphatase PTEN appear to be mutually exclusive events, suggesting that Grb10 might be a tumor suppressor regulated by mTORC1.

The evolutionarily conserved Ser-Thr protein kinase mammalian target of rapamycin (mTOR) functions as the core catalytic component of two structurally and functionally distinct signaling complexes. mTOR complex 1 (mTORC1) regulates protein translation, autophagy, and cell growth, whereas mTOR complex 2 (mTORC2) regulates the actin cytoskeleton and cell survival (*1*–*3*). mTORC1 and mTORC2 respond to upstream inputs such as growth factors, energetic status, and amino acid levels (*3*), but relatively few downstream targets of mTOR have been identified.

Misregulated mTOR activity is a common feature of most cancers (*1*), but clinical trials evaluating the mTORC1 selective inhibitor rapamycin as an anticancer agent have met with limited success (*2*). Rapamycin resistance has emerged as a major challenge to its clinical use (*4*) and is caused in part by feedback loops that activate the phosphatidylinositol 3-kinase (PI3K) and extracellular signal–regulated, mitogen-activated protein kinase (ERK-MAPK) signaling pathways in rapamycin-treated cells through poorly understood mechanisms (*5*, *6*). Identifying substrates of mTORC1 and mTORC2 will be important for understanding how mTOR signals downstream and for defining components of feedback loops involved in rapamycin resistance.

We performed two sets of large-scale, quantitative phosphoproteomics experiments to characterize the signaling network downstream of mTOR (Fig. 1 and figs. S1 to S3). The first stable isotope labeling with amino acids in cell culture (SILAC) experiment (Rapa screen) was performed using *Tsc2*$^{-/-}$ mouse embryonic fibroblasts (MEFs) [see supporting online material (SOM) text for detailed description of the screen]. We identified 4484 and 6832 unique phosphorylation sites on 1615 and 1866 proteins from two biological replicate experiments, respectively (table S1 and databases S1 and S2).

[1]Department of Cell Biology, Harvard Medical School, Boston, MA 02115, USA. [2]Division of Signal Transduction, Beth Israel Deaconess Medical Center, Boston, MA 02215, USA. [3]Harvard School of Dental Medicine, Boston, MA 02115, USA.

*Present address: Department of Cancer and Cell Biology, University of Cincinnati, College of Medicine, Cincinnati, OH 45267, USA.

†Present address: Department of Research Oncology Diagnostics, Genentech Inc., 1 DNA Way, South San Francisco, CA 94080, USA.

‡Present address: Department of Genome Sciences, University of Washington, Seattle, WA 98195, USA.

§Present address: Developmental and Molecular Pathways, Novartis Institutes for Biomedical Research, Cambridge, MA 02139, USA.

‖To whom correspondence should be addressed. E-mail: Steven_gygi@hms.harvard.edu (S.P.G); john_blenis@hms.harvard.edu (J.B.)